The Late Cretaceous to recent tectonic history of the Pacific Ocean basin

Nicky M. Wright*, Maria Seton, Simon E. Williams, R. Dietmar Müller

EarthByte Group, School of Geosciences, University of Sydney, NSW 2006, Sydney, Australia

* Corresponding author: nicky.wright@sydney.edu.au

Keywords: Pacific, relative plate motions, seafloor spreading, plate reconstruction, tectonics

Abstract

A vast ocean basin has spanned the region between the Americas, Asia and Australasia for well over 100 Myr, represented today by the Pacific Ocean. Its evolution includes a number of plate fragmentation and plate capture events, such as the formation of the Vancouver, Nazca, and Cocos plates from the break-up of the Farallon plate, and the incorporation of the Bellingshausen, Kula, and Aluk (Phoenix) plates, which have studied individually, but never been synthesised into one coherent model of ocean basin evolution. Previous regional tectonic models of the Pacific typically restrict their scope to either the North or South Pacific, and global kinematic models fail to incorporate some of the complexities in the Pacific plate evolution (e.g. Bellingshausen and Aluk independent motion), thereby limiting their usefulness for understanding tectonic events and processes occurring in the Pacific Ocean perimeter. We derive relative plate motions (with 95% uncertainties) for the Pacific-Farallon/Vancouver, Kula-Pacific, Bellingshausen-Pacific, and early Pacific-West Antarctic spreading systems, based on recent data including marine gravity anomalies, well-constrained fracture zone traces and a large compilation of magnetic anomaly identifications. We find our well-constrained relative plate motions result in a good match to the fracture zone traces and magnetic anomaly identifications in both the North and South Pacific. In conjunction with recently published and well-constrained relative plate motions for other Pacific spreading systems (e.g. Aluk-West Antarctic, Cocos-Pacific, recent Pacific-West Antarctic spreading), we explore variations in the age of the oceanic crust, seafloor spreading rates and crustal accretion and find considerable refinements have been made in the central and southern Pacific. Asymmetries in crustal accretion within the overall Pacific basin (where both flanks of the spreading system are preserved) have typically deviated less than 5% from symmetry, and large variations in crustal accretion along the southern East Pacific Rise (i.e. Pacific-Nazca/Farallon spreading) appear to be unique to this spreading corridor. Through a relative plate motion circuit, we explore the implied convergence history along the North and South Americas, where we find that the inclusion of small

tectonic plate fragments such as the Aluk plate along South America are critical for reconciling the history of convergence with onshore geological evidence.

1 Introduction

The circum-Pacific is the most geologically active region in the world with a long, episodic history of subduction, arc volcanism, continental and back-arc extension. The interpretation of these geological processes along the margins of the Pacific relies on a detailed plate tectonic history of the adjacent ocean floor to relate the onshore geological record with the offshore seafloor spreading record. The present day seafloor spreading record of the Pacific basin involves the Pacific, Antarctic, Nazca, Cocos and Juan De Fuca plates and the smaller Rivera, Galapagos, Easter and Juan Fernandez micro-plates along the East Pacific Rise (Bird, 2003) (Figure 1; Figure 2). Additionally, the Pacific basin preserves clear evidence in the seafloor spreading record and seafloor fabric that several now extinct plates (e.g. Farallon, Phoenix, Izanagi, Kula, Aluk, Mathematician and Bauer plates; Figure 2) operated within this area, revealing that the Pacific Ocean basin has undergone a complex fragmentation and subduction history throughout its Mesozoic-Cenozoic history.

Previous plate tectonic models of the Pacific Ocean basin have either focussed on identifying magnetic lineations and deriving relative plate motions between presently active plates (e.g. Juan De Fuca-Pacific, Pacific-(West) Antarctic, Pacific-Nazca, and Cocos-Nazca), or on identifying magnetic lineations in those areas where conjugate magnetic lineations no longer exist due to subduction (e.g. Kula-Pacific, Izanagi-Pacific, Pacific-Farallon and Phoenix-Pacific spreading). Another suite of plate tectonic models are regional in nature (e.g. Engebretson et al., 1985; Atwater, 1989), combining the seafloor spreading histories of the majority of these plates into one coherent study. These studies are hugely beneficial for deciphering the evolution of the largely continental circum-Pacific plates, including the subduction histories along these margins; the deep mantle structure beneath the Pacific and its margins; the evolution of the Hawaiian-Emperor Bend (HEB); and the effect of changing plate circuits on the motion of the Pacific plate. In addition, these models allow us to assess the validity of relative plate motion models of individual plate pairs by ensuring that the motion they imply is consistent with the geological evidence from the surrounding regions.

Several recent advances, such as the development of high-resolution satellite altimetry data (e.g. Sandwell et al., 2014); the establishment of a repository of magnetic anomaly identifications (Seton et al., 2014); and the development of plate reconstruction software *GPlates* (Boyden et al. 2011) have prompted a re-analysis of the seafloor spreading history of the Pacific Ocean basin. In particular, the recent satellite gravity anomaly data have greatly improved kinematic models by providing tight constraints on the direction of plate motion through the identification (with spatial confidence) of fracture zones and related features throughout the world's ocean basins (Matthews et al., 2011; Wessel et al., 2015).

Here, we revise the plate tectonic history of the Late Cretaceous (83 Ma) to present day Pacific Ocean in order to investigate the differences in the tectonic history of the Pacific basin (e.g. Pacific-West Antarctic, Pacific-Nazca/Farallon, Pacific-Vancouver/Farallon) and its influence on spreading rate and asymmetry and the implied convergence history along the North and South America margins. We provide relative plate motions with 95% uncertainties for the Pacific-West Antarctic, Bellingshausen-Pacific, Pacific-Farallon, and Kula-Pacific, based on recent fracture zone traces (Matthews et al., 2011) and a compilation of magnetic identifications (Seton et al., 2014). We refine the tectonic plate configuration of the plates in the Pacific basin since the Late Cretaceous (chron 34y; 83 Ma), to include tectonic plates omitted in Seton et al. (2012) and Müller et al. (2008) (e.g. Aluk and Bellingshausen plates) and to refine the extent and timing of tectonic plates (e.g. Kula, Vancouver, Rivera).

2 Methodology

2.1 Magnetic anomaly and fracture zone data

We utilise a synthesis of 481 published magnetic anomaly identifications (‘picks’) from the following studies: Atwater and Severinghaus (1989), Cande et al. (1995), Elvers et al. (1967), Granot et al. (2009), Larter et al. (2002), Lonsdale (1988), Munschy et al. (1996), Wobbe et al. (2012). These magnetic anomaly identifications were downloaded from the Global Seafloor Fabric and Magnetic Lineation (GSFML) repository (Seton et al., 2014). Metadata associated with the magnetic picks are preserved, including reference, chron, anomaly end (old [‘o’], young [‘y’], or center [‘c’]) and the confidence of the magnetic anomaly end assignment. Throughout our paper we cite the normal polarity of chrons, and ages assigned to magnetic identifications are given in the timescale of Cande and Kent (1995), except where noted. Full magnetic pick coverage of the south Pacific, southeast Pacific, and northeast Pacific used in this study can be seen in Figure 3. We rely on digitized fracture zone traces from the GSFML repository (Matthews et al., 2011; Wessel et al., 2015). These fracture zone traces are updated as new data, such as new marine gravity data (Sandwell et al., 2014) are available. The magnetic anomaly identifications and fracture zone traces are the primary constraints in refining the relative plate motions in our study region.

2.2 Relative plate motions

Relative plate motions were computed as finite rotations in regions where both flanks of the spreading system are preserved (Figure 4a). We calculate finite rotation parameters for the Pacific-West Antarctic (chron 34y–33y) and Bellingshausen-Pacific (chron 33o–28o) spreading systems, and rely on published finite rotation parameters for later times (Croon et al., 2008; Wright et al., 2015). In cases where the conjugate flank has been subducted, we derive half-stage rotation parameters by reconstructing the younger chron to the older (‘fixed) chron on the preserved spreading flank (Figure 4b). Stage rotations and finite rotations were subsequently calculated, based on assumed symmetrical spreading. We calculate half-stage rotations for Pacific-Farallon (chron

34y–31y), Kula-Pacific (chron 34y–25y), Vancouver-Pacific (chron 13y–4Ac), and Pacific-Aluk (chron 34y–27o) spreading systems, and use published rotations from Wright et al. (2015) and Müller et al. (2008) for other times. Relative plate motions and uncertainties were revised using magnetic picks and fracture zone identifications and the best fitting criteria of Hellinger (1981), as implemented using the methods described in Chang (1987); Chang (1988) and Royer and Chang (1991).

Uncertainties for magnetic anomaly identifications are primarily navigational uncertainties (Kirkwood et al., 1999), and dispersion analysis of data obtained through different navigation methods (e.g. celestial navigation, Transit, Global Positioning System [GPS]) suggests these errors range from 3.0 to 5.2 km (Royer et al., 1997). Since our magnetic identification compilation includes data from different navigation methods, we obtain our magnetic identification uncertainty using the method outlined in Gaina et al. (1998). We assign the 1-sigma standard error (σ) of the magnetic data as our magnetic uncertainty, based on $\sigma = \hat{\sigma}/\sqrt{\hat{\kappa}_{avg}}$, where $\hat{\sigma}$ is the estimated uncertainty (10 km), and $\hat{\kappa}_{avg}$ is the harmonic mean of the quality factor ($\hat{\kappa}$) for each magnetic anomaly crossing. For Pacific-West Antarctic/Bellingshausen finite rotations, we obtain $\hat{\kappa}_{avg}$ of 2.1 and σ of 6.9 km. For Pacific-Farallon/Vancouver/Kula rotations, we find $\hat{\kappa}_{avg}$ of 1.6 and σ of 7.8 km. We assign a 5 km uncertainty to fracture zone identifications, based on the average horizontal mismatch between topographic and gravity lows in the central North Atlantic (Müller et al., 1991). The quality factor $\hat{\kappa}$ indicates how well uncertainties have been estimated: uncertainties are closely estimated when $\hat{\kappa} \approx 1$, whilst when $\hat{\kappa} \ll 1$ errors are underestimated, and errors are overestimated when $\hat{\kappa} \gg 1$.

We derive rotations at times broadly similar to commonly identified seafloor spreading isochrons, e.g. chrons 21o, 25y, 31y, 34y. We rely on synthetic flowlines to assess our derived rotations, whereby our rotation parameters are considered suitable if a good spatial and temporal match is obtained between the synthetic flowline and corresponding fracture zone segment. Synthetic flowlines were created at reconstructed times, to avoid propagating complexities from recent spreading, such as known asymmetric spreading (e.g. Nazca-Pacific).

We embed our relative rotation parameters into a modified version of the Seton et al. (2012) global kinematic model. Key modifications to this kinematic model of relevance to the Pacific plate, include an update to the moving hotspot absolute reference frame to Torsvik et al. (2008); and an update to the relative motions of the West Antarctic Rift System (WARS) based on Matthews et al. (2015).

Seafloor spreading isochrons in the Pacific basin were created based on our rotation parameters and magnetic anomaly identifications. Seafloor spreading isochrons were constructed at chrons 5n.2o (10.9 Ma), 6o (20.1 Ma), 13y (33.1 Ma), 18n.2o (40.1 Ma), 21o (47.9 Ma), 25y (55.9 Ma), 31y (67.7 Ma), and 34y (83 Ma), in order to be consistent with the scheme developed by Müller et al. (2008) and to link the Pacific seafloor spreading history to the Atlantic and Indian Ocean realms. Additional isochrons were created at intermediate times to reflect major tectonic events, e.g. formation of the Bellingshausen plate at chron 33o (79.1 Ma), and formation and motion of the Bauer microplate. Through a set of seafloor spreading isochrons, seafloor spreading ridges (present day and extinct), and defined continent-ocean-boundaries (COB), grids showing the age-area distribution of oceanic crust were created between 83 Ma and present day, corresponding to the time period of revised rotation parameters.

2.3 Implied convergence history

We calculate the implied convergence history of the Pacific plates with respect to the Americas (North America, South America) between 83 Ma and present day. Points were chosen along the trench adjacent to North America (point 1: 48°N, 126.5°W; point 2: 38°N, 123.4°W; point 3: 28°N, 116°W) and South America (point 1: 5°S, 81°W; point 2: 20°S, 76°W, point 3: 45°S, 76°W) to capture differences in the plate configuration and tectonic regimes experienced by these margins. Convergence velocities were calculated orthogonal to the trench, whilst obliquity was calculated based on the difference between the strike of the trench and the true convergence angle (bearing from North), where an obliquity angle of 0° suggests strike slip motion. All convergence parameters were calculated in 5 Myr increments, except the stage from 80-83 Ma.

The convergence histories are calculated using a plate chain that involves relative rotations for North or South America-Africa, Africa-East Antarctica, East Antarctica-West Antarctica (from Matthews et al., 2015), and West Antarctica to the Pacific. We used the rotations from the compilation of Seton et al (2012) unless otherwise stated.

3 Pacific basin tectonics since chron 34y (83 Ma)

In the following section we describe the regional tectonic evolution of the Pacific basin. We present our derived relative rotation parameters within each section (section 3.1.1, section 3.1.2, section 3.1.3, section 3.2.1, section 3.2.2, section 3.2.3). For a comprehensive review of Pacific basin development prior to 83 Ma, see section 3.2 in Seton et al. (2012).

3.1 South Pacific spreading history

The evolution of the South Pacific is essential in reducing uncertainties in global circuit calculations, since the spreading history in this region links plate motions in the Pacific and Indo-Atlantic realms within the global plate circuit from the Late Cretaceous to present day (Cande et al., 1995; Larter et al., 2002; Matthews et al., 2015). The Antarctic and Pacific plates presently dominate spreading in this region, however the former Aluk plate (also known as the Phoenix or Drake plate), Bellingshausen, and Farallon plates have all contributed to the complex evolution of the region, observed in gravity anomalies and magnetic identifications (Figure 5). Prior to chron 34y (83 Ma), this region involved Aluk-Farallon, Pacific-Aluk and Pacific-Farallon spreading (Eagles et al., 2004a; Larter et al., 2002; Mayes et al., 1990; Weissel et al., 1977) and the early separation of Zealandia and West Antarctica (Larter et al., 2002).

The Aluk plate was initially named as a South Pacific analogue of the northern Pacific Kula Plate (Herron and Tucholke, 1976), however, it has since been noted that it is a fragment of the Mesozoic Phoenix plate (Barker, 1982). Although many publications describing the Late Cretaceous and Cenozoic history of the Aluk plate use the name ‘Phoenix’, we rely on the term ‘Aluk’ plate to distinguish this fragment’s spreading history since chron 34y (83 Ma) from the preceding Phoenix plate evolution and break-up history in the Cretaceous (i.e. Seton et al., 2012).

The final stages of Gondwana breakup and early stages of Zealandia-West Antarctic separation are not fully understood, with ambiguities in the oldest age of seafloor spreading, in the timing of independent West Antarctic and Bellingshausen motion, and the formation history of the Bounty Trough and Bollons Seamounts. The separation of Zealandia and West Antarctica is thought to initiate with rifting and crustal extension between the Chatham Rise (Figure 5) and West Antarctica around ~90 Ma (Eagles et al., 2004a; Larter et al., 2002). Seafloor spreading is believed to have started at ~85 Ma near the Bounty Trough (Davy, 2006), although the earliest magnetic identification in this region is a tentative chron 34y (83 Ma). Early seafloor spreading was highly asymmetric and involved a number of ridge jumps, including a ridge jump of the Bounty Trough rift to the Marie Byrd Land margin (Davy, 2006), and the initiation of seafloor spreading between Campbell Plateau and West Antarctica, during chron 33r (83–79.1 Ma) (Larter et al., 2002).

Mismatch in magnetic anomalies southeast of Zealandia and inferred Pacific-West Antarctic spreading led to the proposition of the independent Bellingshausen plate (Stock and Molnar, 1987). The Bellingshausen plate experienced independent motion from chron 33o (79.1 Ma) (Eagles et al., 2004b), with Bellingshausen-Pacific spreading forming seafloor west of the Bellingshausen gravity anomaly (BGA) (Figure 5). An additional fragment of the Aluk plate has been inferred in this region, known as the Charcot plate (McCarron and Larter, 1998): this plate forms the present-day triangular region of oceanic crust near Peter I Island, bounded by the BGA, southern De Gerlache gravity anomaly (DGGA), and Marie Byrd Land continental margin (Larter et al., 2002) (Figure 5). The Charcot plate was captured by the West Antarctic plate during Zealandia-West Antarctic breakup (by chron 34y), as subduction of the Charcot plate stalled (Larter et al., 2002; Cunningham et al., 2002).

By chron 34y (83 Ma), the West Pacific-Aluk spreading system was already established. Since chron 34y, the fast spreading Pacific-Aluk ridge has been replaced by slower spreading Pacific-

Antarctic and Antarctic-Aluk ridges (Cande et al., 1982). These ridge reorganisations are proposed to have occurred at chron 29 (~64 Ma), chron 28 (~63 Ma) and chron 21 (~47 Ma) (Cande et al., 1982), and are evident by the sequences of South Pacific magnetic lineations. However, re-interpretation and additional collection of magnetic lineations between the Tharp and Heezen Fracture zones indicates a north-westward younging trend in this area (Larter et al., 2002; Wobbe et al., 2012), suggesting this segment formed from Bellingshausen-Pacific spreading, rather than an earlier initiation of Aluk-Antarctic spreading at chron 29 (Cande et al., 1982; McCarron and Larter, 1998).

At chron 27 (~61 Ma), a tectonic reorganisation in the south Pacific (Eagles, 2004; Eagles et al., 2004b), led to the incorporation of the Bellingshausen plate into the West Antarctic plate (Eagles et al., 2004b), the initiation of Aluk-West Antarctic spreading (Eagles et al., 2004b), and changes in Australia, Antarctica and Zealandia relative motions (Eagles et al., 2004b). The timing of Bellingshausen plate incorporation has previously been suggested to be much later, at chron 18 (~39 Ma) (Stock and Molnar, 1987) or chron 24 (~53 Ma) (Mayes et al., 1990). At chron 27, Aluk-West Antarctic spreading initiated (Eagles and Scott, 2014), and was concurrently active with a Pacific-Aluk divergent boundary. The DGGA is thought to represent a 'scar' from the westward ridge jump of Bellingshausen-Aluk to West Antarctic-Aluk spreading at this time (Larter et al., 2002).

A number of right-stepping fracture zones developed at chron 27 along the Pacific-Antarctic ridge, including the right-stepping Pitman Fracture Zone (Cande et al., 1995). The trace of the Pacific-Farallon-Aluk triple junction between chron 27 and 21 is inferred by the Humboldt Fracture Zone (Cande et al., 1982), which formed as a transform fault connecting Pacific-Aluk and Farallon-Aluk spreading (Cande et al., 1982).

At chron 21 (~47 Ma), Pacific-Antarctic ridge propagation resulted in the Pacific flank of the final Pacific-Aluk spreading corridor (i.e. situated between the Tula and Humbuldt Fracture Zones) to be captured by the West Antarctic plate (Eagles, 2004). The propagation of the Pacific-Antarctic ridge is marked by the Hudson trough, a ‘scar’ on the West Antarctic plate as the ridge (Cande et al., 1982). The Henry Trough forms the conjugate feature on the Pacific plate (Cande et al., 1982). This propagating rift system led to the formation of the Menard Fracture Zone (Croon et al., 2008). At ~47 Ma, the West Antarctic-Aluk ridge replaced the former Pacific-Aluk ridge, as the Pacific-West Antarctic spreading center propagated eastward at chron 21 (Mayes et al., 1990).

Between chron 20 (~43 Ma) and chron 5, an overall 12° (Cande et al., 1995) to 15° (Lonsdale, 1986) counterclockwise change occurred in Pacific-West Antarctic spreading, based on observations along the Eltanin Fracture Zone. Additional changes in Pacific-West Antarctic spreading direction have been determined based on a detailed study of the Menard Fracture Zone, with a clockwise change at chron 13o (33.5 Ma) a counterclockwise change at chron 10y (28.3 Ma) (Croon et al., 2008). During this time period, the Pacific-Farallon ridge underwent a 5° clockwise change at chron 7 (~25 Ma), followed by Farallon plate fragmenation and Cocos and Nazca plate formation (see section 3.2) (Barckhausen et al., 2008). Since chron 5y (9.7 Ma), the Pacific-Antarctic ridge has undergone a clockwise change in spreading direction (Croon et al., 2008).

The Aluk plate was incorporated into the West Antarctic plate around chron 2A (~3.3 Ma) (Larter and Barker, 1991; Livermore et al., 2000), possibly as a result of ridge-trench collision SW of the Hero Fracture zone (along the Antarctic peninsular) (Larter and Barker, 1991) and the resultant reduction in slab width and slab pull (Livermore et al., 2000).

<u>East-West Antarctic motion</u>

Motion has been inferred between West and East Antarctica throughout the Cenozoic based on large misfits in southwest Pacific plate reconstructions (Cande et al., 2000), however reconstructions of the relative movement between East and West Antarctica (Marie Byrd Land) are generally poorly constrained. Anomalies from the Adare trough (a fossil rift valley) (Figure 5) indicate a former ridge-ridge-ridge triple junction in this area between chrons 20 and 8 (43–26 Ma) (Cande et al., 2000) and may be the site of the East-West Antarctic boundary during the Eocene and Oligocene (Cande et al., 2000; Müller et al., 2007). Due to the few data points useful for plate reconstructions that are confined to the short seafloor spreading portion of the East-West Antarctic plate boundary, most of which was a transform boundary straddling the Transantarctic Mountains, and ambiguities in magnetic anomaly identification (Cande et al., 2000), the few reconstructions of East Antarctica-West Antarctica result in uncertainties ranging from ~500 km (Granot et al., 2013) to ~5000 km (Cande et al., 2000). The type of motion described in East-West Antarctic models also differ: a recent study has indicated motion varied from east northeast-west southwest extension in the Adare Basin, to dextral transcurrent motion in the central parts of the rift zone, with predominant oblique convergence in the eastern parts of the West Antarctica Rift System (WARS) (Granot et al., 2013), whereas previous models indicated extensional motion throughout the WARS (Cande et al., 2000) and dextral transcurrent motion (Müller et al., 2007).

3.1.1 Relative Pacific-West Antarctic plate motion

Relative Pacific-West Antarctic plate rotations published within the last two decades are listed in Table 1.

Spreading velocities along the Pitman Fracture Zone suggest an increase in spreading rate between 83 Ma and ~70 Ma, followed by a ~40 mm/yr decrease in spreading rate until ~40 Ma (Figure 6). Little variation in spreading rate occurs until ~33 Ma, after which the spreading rate increases until present day. This is accompanied by a ~60° counterclockwise change in spreading direction between 83 Ma and 20 Ma, followed by a ~15° clockwise change until present day (Figure 6). We note differences arise between Eagles et al. (2004a) and Cande et al. (1995), due to a slight difference in anomaly end assignment. Whilst there is broad agreement in the Pacific-West Antarctic spreading velocities, notable variation is observed between Wobbe et al. (2012) and Cande et al. (1995), in particular, at 80 Ma and between 65–40 Ma. These variations can be attributed to the small stage intervals used in Wobbe et al. (2012) analysis, which increase rotation noise unless the rotations are smoothed (Iaffaldano et al., 2014). A large change in spreading velocity is observed in Eagles et al. (2004a) at 67 Ma, which may arise from merging the finite rotation parameters of Cande et al. (1995) and Stock et al (unpublished).

Our reconstruction of the Pacific-West Antarctic ridge since chron 34y (83 Ma) relies on a combination of published rotation parameters and derived finite rotations. We rely on the tightly constrained rotation parameters in Croon et al. (2008) between chrons 20o to 1o (43.79 Ma–0.78 Ma). Since kinematic models of the earlier Pacific-West Antarctic spreading history do not incorporate spatially constrained fracture zone identifications (e.g. Cande et al. 1995) or do not incorporate all available magnetic identifications (Wobbe et al., 2012), we derive finite rotations and uncertainties for chrons 33y to 21o (73.6–47.9 Ma) (Table 2; Figure 7). The rotation pole for chron 34y (83 Ma) is based on the spreading velocity of stage chron 33y–30o (73.6–67.7 Ma), due to the absence of reliable magnetic identifications for this time. Our $\hat{\kappa}$ values ranged between 0.87 and 4.94 (Table 2): chrons 27o and 30o have a high $\hat{\kappa}$ value (4.94 and 2.50, respectively), suggesting we overestimated the assigned magnetic identification or fracture zone uncertainties.

Our derived Pacific-West Antarctic rotations parameters exhibit a comparable trend to previous models (i.e. Cande et al., 1995; Eagles et al., 2004a; Müller et al., 2008; Wobbe et al., 2012) (Figure 8). The flowlines produced from this study demonstrate the best fit with the fracture zone interpretations (Matthews et al., 2011) and the marine gravity anomaly data (Figure 8), compared with other previously published models. For example, the relative plate motions from Wobbe et al. (2012) demonstrate a partial match with the fracture zone identifications during the earliest spreading history (83–75 Ma), and a large change in spreading direction between chrons 27–25, in contrast to the more gradual change during this time from this study (Figure 7). These differences may be attributed to the more limited dataset used in Wobbe et al. (2012) analysis.

3.1.2 Relative Bellingshausen-Pacific plate motion

Published rotations for the Bellingshausen-Pacific are listed in Table 3. Larter et al. (2002) and Eagles et al. (2004a) rely on common rotations, resulting in similar spreading velocities (Figure 9). Spreading rate and direction differs by up to 20 mm/yr and 10° between Wobbe et al. (2012) and other models of Bellingshausen-Pacific spreading, in particular, between chron 33o and chron 33y, and chron 31y-28o (Figure 9). There is little difference in the trend of spreading direction derived in the timescales of Cande and Kent (1995) and Ogg (2012), however, there is a difference in spreading rate: Cande and Kent (1995) results in a ~10 mm/yr larger increase in rate at chron 33y, whilst Ogg (2012) results in 5 mm/yr increase in spreading rate at chron 31y (Figure 9).

We reconstruct the Bellingshausen plate during its period of independent motion i.e. chron 33o to 27o. We derive well-constrained finite rotations, with up to 10° of uncertainty in the calculated 95% confidence ellipses (Figure 10). $\hat{\kappa}$ values ranged between 0.46 to 1.01 (Table 4), indicating the fracture zone and magnetic pick uncertainties were slightly underestimated.

Our Bellingshausen-Pacific rotations display similar spreading velocities to published models between chron 33y and chron 28o (Figure 9) and a good spatial match is observed between derived flowlines and preserved fracture zone geometries (Figure 11). A comparison of our Bellingshausen-Pacific flowlines and flowlines produced from Eagles et al. (2004a), Wobbe et al. (2012) and Larter et al. (2002) indicate a similar spreading history between all models for the period of 70–60 Ma

(Figure 11). Discrepancies arise in the modelled flowline and fracture zone geometries during the early Bellingshausen-Pacific spreading; whilst all models closely match the latter spreading history, our model results in a closer match to the early Bellingshausen-Pacific spreading history along the Udintsev Fracture Zone than Wobbe et al. (2012) and Eagles et al. (2004a). This is likely a result of different interpretation of the fracture zones in this area, which is hampered by magmatic overprinting (Gohl et al., 2007) present in the satellite gravity (Sandwell et al., 2014).

3.1.3 Relative Aluk (Phoenix)-West Antarctic plate motion

We rely on recently published Aluk-West Antarctic relative plate motions (Eagles and Scott, 2014) for the Aluk plate spreading history between chron 27o (61 Ma) and present day. Parameters describing Aluk spreading prior to the Aluk-West Antarctic ridge initiation at chron 27o suffer from great uncertainty, however we derive Pacific-Aluk rotations for chron 34y–27o (83–61 Ma) and compare our result to the Pacific-Aluk stage rotation parameter from Eagles et al., (2004a) (17.2°S, 126.5°W, 30.15°, for stage 34y–27o; Figure 12). The Pacific-Aluk ridge continued until chron 21o (47.9 Ma), inferred from trapped Pacific crust (formed from the Pacific-Aluk spreading system; Figure 2) on the West Antarctic plate. This latter portion of the Pacific-Aluk spreading system (chron 27o–21o; 61–47.9 Ma) can be derived from the better constrained Pacific-Antarctic (this study) and Antarctic-Aluk (Eagles and Scott, 2014) rotation parameters, as the limited magnetic identifications available (Cande et al., 1982) and lack of fracture zones preserving spreading direction (the Humboldt Fracture Zone is not indicative of Pacific-Aluk spreading direction; McCarron and Larter, 1998), greatly hinder independent kinematic analysis.

Due to the paucity of data available for the Pacific-Aluk spreading, we derive our half-stage rotation parameters based on a spatial fit of magnetic identifications and inferred fracture zone lineations in *GPlates* (Table 5). A major assumption to this approach is the age of the youngest preserved Pacific-Aluk crust on the Pacific plate, adjacent to the Henry Trough (Figure 5, Figure 12). Pacific-Aluk spreading is preserved on the Pacific plate (chron 34y–27o?) and the West

Antarctic plate (chron 27?–21o), and formed as a continuous segment (Cande et al., 1982; McCarron and Larter, 1998). At chron 21o (47.9 Ma), the younger portion of this spreading segment was captured onto the Antarctic plate by the propagation of the Pacific-Antarctic ridge, leading to the formation of the Henry Trough and Hudson Troughs (Cande et al., 1982; McCarron and Larter, 1998). Here, we assume the Henry Trough is approximately representative of chron 27 (~61 Ma) on the Pacific plate; however, there are little data available to validate this assumption.

Our synthetic flowline for Pacific-Aluk spreading suggest a relatively good match with the fabric observed in the gravity, and with some of the magnetic identifications in this region (Figure 12). Comparison of our flowline with one derived from Eagles et al. (2004a) demonstrates the large uncertainty in reconstructing the Pacific-Aluk spreading corridor, as there are little constraints (e.g. no clear fracture zones, ambiguous or conflicting magnetic identifications) to fully constrain this spreading. We also find our Pacific-Aluk rotation parameter allows for the derivation of a divergent Farallon-Aluk ridge in the Late Cretaceous, when combined with our Pacific-Farallon relative motion (see section 3.2.1). A Farallon-Aluk spreading ridge correlates with published schematics for this region (e.g. Cande et al., 1982), however the location of the Farallon-Aluk ridge is poorly constrained.

3.2 East Pacific spreading history

The eastern and northern Pacific basin formed from spreading between the Pacific and Farallon plates, including the Farallon subplates, e.g. Nazca, Cocos, and Vancouver. The seafloor spreading record suggests breakup and subduction of the Farallon plate since the Late Cretaceous. The present-day southeast Pacific basin is dominated by the Pacific, Nazca, and Cocos plates, which are separated by the north-south trending East Pacific Rise (i.e. Pacific and Nazca plates), and the east-west trending Galapagos Spreading Centre (i.e. Nazca and Cocos plates) (Hey, 1977; Mayes et al., 1990) (Figure 13). The northeast Pacific largely consists of the Pacific plate, with the Juan de Fuca plate subducting beneath North America (Figure 14). On the Pacific plate, C-sequence magnetic anomalies can be identified up to chron 34y (83 Ma) (Cande and Haxby, 1991; Munschy et al., 1996). Due to subduction along North and South America, no conjugate anomalies are available in the northern Pacific basin (Pacific plate), and conjugate magnetic anomalies on the Nazca plate are only available up to chron 23y (50.8 Ma) (Atwater, 1989; Cande and Haxby, 1991).

Prior to chron 34y (83 Ma), the East Pacific basin was dominated by spreading between the Pacific and Farallon plates, inferred from the Mesozoic sequence of magnetic anomalies (Nakanishi et al., 1989). During the Cretaceous Normal Superchron (CNS; M0-34y; 120.6–83 Ma), mismatches in fracture zone offsets suggest there was likely a number of ridge jumps (e.g. in the Murray-Mendocino segment) (Atwater, 1989), however due to the lack of magnetic anomalies, the timing of such events is hard to decipher.

The Kula plate, deceivingly named to mean “all gone” in Athapascan (Grow and Atwater, 1970), is presently preserved as a small fragment that was incorporated into the Pacific plate after Kula-Pacific spreading ceased during chron 18r (~41 Ma) (Lonsdale, 1988). However, it should be noted that this interpretation of a preserved Kula extinct ridge relies on a sparse dataset. Since the Kula plate has been mostly subducted into the Aleutian trench, its spreading history has been inferred from its conjugate spreading region on the Pacific plate. Consequently, many uncertainties remain in the tectonic history of the Kula plate, including its origin (e.g. whether it was originally part of Farallon or Izanagi), timing of independent spreading, paleoposition, and plate configuration with the Farallon and North American boundaries. The Kula plate is proposed to derive from the Farallon plate (Atwater, 1989; Mammerickx and Sharman, 1988; Woods and Davies, 1982) or the Izanagi plate (Hilde et al., 1977; Larson and Chase, 1972; Norton, 2007; Zonenshain et al., 1987). Reconstructions relying on an Izanagi plate derivative rely on a greatly different tectonic plate configuration in the Late Cretaceous. For example, Norton (2007) infer a Late Cretaceous subduction of the Pacific plate along Asia, however this scenario contrasts with the onshore geological record from east Asia and the preserved magnetic identifications from the NW Pacific basin, which suggest Izanagi-Pacific ridge subduction occurred at ~55 Ma (Whittaker et al., 2007; Seton et al., 2012). Additionally, there is no clear way to reconcile the M-sequence (and presumably CNS) spreading history of the Izanagi plate with the C-sequence spreading history of the Kula plate (Atwater, 1989), suggesting the Kula plate likely formed as a fragment of the Pacific or Farallon plate (Atwater, 1989; Rea and Dixon, 1983).

Magnetic lineations adjacent to the Chinook Trough (Figure 14) mark the first signs of the north-south Kula-Pacific spreading at chron 34y (83 Ma), where the Kula plate broke away from the Chinook Trough (Mammerickx and Sharman, 1988; Rea and Dixon, 1983; Woods and Davies, 1982). The initiation of Kula-Pacific spreading occurred progressively, propagating from west to east (Mammerickx and Sharman, 1988). Seafloor spreading accelerated during chron 33n (~75 Ma), inferred from a rough-smooth transition (Figure 14) in the seafloor topography near chron 33y (Mammerickx and Sharman, 1988), although Norton (2007) notes the rough-smooth transition may record ridge reorientation due to a change in spreading direction. The Emperor Trough (Figure 14) acts as a western boundary of the Kula plate, however its evolution is unclear: during the early stages of Kula plate formation, the Emperor Trough may have formed as a rift (Woods and Davies), although this feature has also been proposed to be a transform fault formed during the CNS (Hilde et al., 1977; Larson and Chase, 1972). An additional plate, the Chinook plate, has been proposed to have formed contemporaneously with the Kula plate during the Late Cretaceous (Mammerickx and Sharman, 1988; Rea and Dixon, 1983). This proposed plate is bounded by the Chinook Trough, Emperor Trough, and Mendocino Fracture Zone (Rea and Dixon, 1983) (Figure 14). However, based on their analysis of north Pacific fracture zones, Atwater et al. (1993) reject this idea as the proposed region of the Chinook plate implies the region north of the Mendocino Fracture Zone was not part of the Pacific plate, and this region does not contain any characteristics of a plate boundary reorganisation.

A counterclockwise change in Pacific-Farallon spreading occurred at chron 33r (~80 Ma), based on the distinct bends in the Mendocino, Pioneer, Murray, and Molokai fracture zones (Atwater et al., 1993; McCarthy et al., 1996) (Figure 14). This change in spreading direction is thought to be linked to the initiation of Kula-Pacific spreading, due to the removal of northward slab-pull forces on the Pacific plate (Atwater et al., 1993).

At chron 25y, a counterclockwise change in the Kula-Pacific spreading system occurred. This has previously been linked to a change in slab-pull forces at this time (Lonsdale, 1988) caused by the initiation of the Aleutian subduction zone at 55 Ma (Scholl et al., 1986), with recent radiometric dating suggesting fluctuating magmatism beginning at 45–50 Ma (Jicha et al., 2009). There is a mismatch in the spreading rate implied by the western and eastern Kula-Pacific magnetic identifications, between chron 25y (55.9 Ma) and chron 24n.3o (53.3 Ma): the eastern region of Kula-Pacific spreading implies spreading rates up to three times that of the western region, with only a very minor counterclockwise change in spreading direction. In the eastern region of the Kula-Pacific spreading, a three-armed chron 24r anomaly is observed ("T" anomaly) and is thought to represent a captured piece of the Pacific-Farallon-Kula triple junction (Atwater, 1989). Previously, this has been interpreted to indicate the cessation of Kula-Pacific spreading (Byrne, 1979), however it is conceivable that Kula-Pacific spreading underwent a counterclockwise change (Lonsdale, 1988) and reorganisation of the triple junction occurred at this time, considering that this coincides with the fragmentation of the Farallon plate to form the Vancouver plate.

Fragmentation of the Farallon plate occurred at chron 24 (52 Ma), based on magnetic identifications and the prominent bend in Pacific basin fracture zones (e.g. Surveyor, Mendocino, and Pioneer fracture zones) (Mayes et al., 1990). The northern fragment is known as the Vancouver plate (Menard, 1978; Rosa and Molnar, 1988), with the Vancouver-Farallon boundary occurring around the Murray Fracture Zone (McCarthy et al., 1996; Menard, 1978) or the Pioneer Fracture Zone (Rosa and Molnar, 1988) (Figure 14). During this break-up, the Pacific-Farallon spreading direction remained unchanged (Atwater, 1989) and the Vancouver-Pacific spreading diverged 20° south (Atwater, 1989; McCarthy et al., 1996) causing the former Mendocino transform fault (present-day Mendocino Fracture Zone) to break across and eliminate the former Pau transform fault (present-day Pau Fracture Zone) (Atwater and Severinghaus, 1989). By chron 21 (~48 Ma), this new system had 'settled' and spreading continued steadily until chron 15 (34 Ma): at this time a major propagator crossed the Surveyor Fracture Zone, and offsets of the Vancouver-Pacific ridge were reorganised by episodes of rift propagation (Atwater, 1989; Atwater and Severinghaus, 1989; McCarthy et al., 1996). The boundary for the Farallon and Vancouver plates varied between the Pioneer and Murray fracture zones, reflected in the set of 'toothlike disjunctures' between chrons 19 (41 Ma) to 13 (33 Ma) (Atwater, 1989). Since chron 22o, we have evidence (albeit sparse) of Kula-Pacific spreading asymmetry (Lonsdale, 1988; Vallier et al., 1996), roughly 35:65 per cent. At chron 18r (~41 Ma), the Pacific-Kula ridge ceased spreading and the Kula plate was incorporated into the Pacific plate (Lonsdale, 1988). The abrupt cessation of Pacific-Kula spreading was previously thought to be a consequence of the change in the absolute motion of the Pacific plate at 43 Ma (Atwater, 1989; Lonsdale, 1988), based on the previously thought timing of the Hawaiian-Emperor Bend (HEB) (Clague and Dalrymple, 1987) and the age of chron 18r in the timescale of Berggren et al. (1985) (~43 Ma). However, recent research does not support this interpretation: recent timescales place chron 18r at 40.13–41.257 Ma (Cande and Kent, 1995; Gee and Kent, 2007) or 40.145–41.154 Ma (Ogg, 2012), whilst the refined age of the HEB is now 47.5 Ma (O'Connor et al., 2013), and the change in hotspot and mantle dynamics is thought to play the major role in HEB formation (Tarduno et al., 2009).

Magnetic anomalies indicate many small ridge jumps or periods of large asymmetrical spreading throughout Farallon/Nazca-Pacific spreading history, in particular south of the Austral Fracture Zone between chron 20 (43 Ma) and 17 (37 Ma), based on the differences in the amount of preserved Pacific crust compared to Farallon crust and the resulting inconsistencies in reconstructions (Cande and Haxby, 1991). During this time, Pacific-Farallon spreading also underwent reorganisations: between chron 19 and 12 (~42 to 32 Ma), ridge jumps and/or propagating rifts caused several fragments of the Farallon plate to break off and be incorporated into the Pacific plate (Atwater, 1989).

A major reorganisation event occurred in the eastern Pacific during the Oligocene, after the first segment of the East Pacific Rise (Pacific-Farallon spreading centre) intersected with the North American subduction zone near Baja California. This is thought to have occurred as early as chron 13 (~33 Ma) (Engebretson et al., 1985), although more recent studies have placed it around chron 9 or 10y (~28 Ma) (Atwater, 1989). The Vancouver plate is referred to as the Juan de Fuca plate after the Farallon-Pacific spreading ridge reached the subduction zone along North America, around chron 10y (28 Ma), (Atwater and Stock, 1998). The Juan de Fuca plate moved in a more northerly direction to the former Vancouver plate (McCarthy et al., 1996), whilst the Pacific-Farallon ridge segments and Farallon spreading rotated clockwise. Magnetic lineations between the Pioneer and Murray fracture zones suggest Farallon plate fragmentation occurred at chron 10y (28 Ma), forming the Monterey and Arguello microplates (Atwater, 1989; Severinghaus and Atwater, 1990), although Stock and Lee (1994) suggest the independent motion of the Arguello plate began around ~20 Ma. Pacific-Monterey spreading was slower than Pacific-Arguello spreading, allowing for the formation of the right-lateral transform known as the Morro Fracture Zone (Nicholson et al., 1994) (Figure 14). The Arguello and Monterey plates experienced independent motion until after chron 6 (~18 Ma), when it was incorporated into the Pacific plate (Atwater, 1989; Lonsdale, 1991; Stock and Lee, 1994). The remnants of the Arguello plate have been subducted, and its spreading history is based on preserved lineations on the Pacific plate, however a remnant of the former Monterey plate is preserved between the Monterey and Morro fracture zones (Atwater, 1989).

Further south, the initial signs of a plate reorganisation began at chron 7 (~25 Ma), observed by a 5° clockwise change in the Pacific-Farallon ridge (Barckhausen et al., 2008). The break-up of the Farallon plate at chron 6B (22.7 Ma) (Barckhausen et al., 2001) resulted in the formation of the Nazca and Cocos plates (Barckhausen et al., 2008; Hey, 1977; Meschede and Barckhausen, 2000; Meschede et al., 2008) and the development of the Cocos-Nazca spreading system (Hey, 1977; Klitgord and Mammerickx, 1982; Mayes et al., 1990) (Figure 13). The break-up of the Farallon plate has been attributed to a combination of factors, including the changes in slab forces and plate strength, including increased northward pull after the earlier splits of the Farallon plate (from the Vancouver and Monterey plates) (Lonsdale, 2005), increased slab pull at the Middle America subduction zone due to the increased length of the Farallon plate, and a possible weakening of the plate along the break-up point due to the influence of the Galapagos Hotspot (Barckhausen et al., 2008; Hey, 1977; Lonsdale, 2005). The Farallon plate break-up is also attributed to changes in spreading direction, where the change in Pacific-Farallon to Pacific-Nazca motion can be observed in a 20° to 25° clockwise change in spreading direction (Eakins and Lonsdale, 2003; Lonsdale, 2005) and an increase in crustal accretion rates (Eakins and Lonsdale, 2003).

Spreading associated with the Cocos-Nazca ridge began at chron 6B (22.7 Ma), based on magnetic identifications near the Grijalva Scarp and its conjugate feature near Costa Rica (Barckhausen et al., 2001). Cocos-Nazca spreading can be divided into three systems: Cocos-Nazca spreading 1 (~23–19.5 Ma; NW-SE); Cocos-Nazca spreading 2 (19.5–14.7 Ma; ENE-WSW); and Cocos-Nazca spreading 3 (14.7 Ma–present; E-W) (Meschede and Barckhausen, 2000). Following this, a number of reorganisations can be observed, which are primarily associated with the evolution of microplates. By ~20 Ma, the Mendoza microplate was forming between the Mendana and Nazca fracture zones, however there is ambiguity in the timing of its incorporation into the Nazca plate, which varies from chron 5A (~12 Ma) (Liu, 1996) and chron 5Cn.2n (~16.3 Ma) (Eakins and Lonsdale, 2003). Around chron 5D and 5E (~18 Ma), the Bauer microplate formed near the Marquesas and Mendana fracture zones (Figure 13), and underwent independent motion until captured by the Nazca plate at 6 Ma (Eakins and Lonsdale, 2003). Around chron 5A (~12 Ma), the Mathematician microplate formed with dual spreading centers between the Mathematician Ridge and the East Pacific Rise, and transform boundaries at the Rivera and West O'Gorman fracture zones (Mammerickx et al., 1988) (Figure 13). This was followed by the formation of the Rivera plate above the Rivera Fracture Zone, at chron 5n.2n (~10 Ma) (DeMets and Traylen, 2000). The Mathematician paleoplate ceased with the failure of the Mathematician ridge around chron 2A (3.28 Ma) (DeMets and Traylen, 2000). A reorganisation at chron 3o (~5 Ma) resulted in the formation of the Juan Fernandez and Easter microplates (Tebbens and Cande, 1997).

3.2.1 Relative Pacific-Farallon plate motion

The Pacific-Farallon spreading history is crucial in understanding circum-Pacific tectonics and the events surrounding the formation of the HEB. The Nazca and Pacific plates preserve conjugate anomalies formed from Pacific-Nazca/Farallon spreading until chron 23y (50.8 Ma) (Atwater, 1989; Cande and Haxby, 1991), however no conjugate anomalies are available for earlier times due to the subduction of the Farallon plate. Since this hinders our ability to reconstruct the Farallon plate motion for earlier times, models of Pacific-Farallon seafloor spreading rely on the conjugate Pacific plate to derive 'half'-stage and 'full'-stage rotations by assuming spreading symmetry. This assumption is reasonable, as global present-day ocean crust displays <10% cumulative spreading asymmetry (Müller et al., 1998). It should be noted that there are limitations in this approach due to the observed Pacific-Nazca/Farallon asymmetries (e.g. Rowan and Rowley, 2014) (see Discussion).

Many published Pacific-Farallon rotations (Table 6) are limited in their extent, with the notable exception of Rowan and Rowley (2014), who cover the full Pacific-Farallon spreading history since chron 34y (end of the CNS) with accompanying 95% confidence ellipses. Pardo-Casas and Molnar (1987) and Rowan and Rowley (2014) suggest Pacific-Farallon seafloor spreading rates were over 200 mm/yr during the Eocene (Figure 15), though these fast speeds are likely model errors. Our models imply Pacific-Farallon spreading was around ~80–100 mm/yr during the Late Cretaceous and early Cenozoic, followed by an increase in spreading rate and clockwise change in spreading direction between chron 25y (~56 Ma) until chron 13y (~33 Ma) (Figure 15), regardless of the timescale used. However, the timing and magnitude of these events differs between all the models due to the stage intervals used and the dataset used in deriving stage intervals. For example, Wright et al. (2015) rely on relatively small (~1–2 Myr) stage intervals for the Paleocene, whereas all other models use larger (~7 Myr) stage intervals, resulting in large changes in spreading velocity between 66 and 33 Ma. Rowan and Rowley (2014) and Wright et al. (2015) both rely on magnetic identifications from the northern and southern Pacific plate, whereas Pardo-Casas and Molnar (1987) and Rosa and Molnar (1988) rely on magnetic identifications from the northern Pacific only, which further contributes to the variations in spreading velocity between the models.

We provide new relative Pacific-Farallon plate motions between chron 34y (83 Ma) and 31y (67.7 Ma). We combine these stages with the relative motions from Wright et al. (2015) to derive a Pacific-Farallon spreading history until chron 13y (33.1 Ma) (Table 7), which has well-constrained half-stage rotation parameters for all times (Figure 16). We incorporate a minor counterclockwise change in Pacific-Farallon spreading direction at chron 33o, as observed by Atwater et al. (1993). Following this change, spreading remained relatively constant until chron 28 in the North Pacific (Molokai Fracture Zone; Figure 15a). This was succeeded by a significant two-stage increase in Pacific-Farallon spreading rates, with an initial 26 mm/yr increase between chron 25y (55.9 Ma) and 24n.1y (52.4 Ma), followed by a 64 mm/yr increase between chron 22o (49.7 Ma) and chron

18n.2o (40.1 Ma) (Wright et al., 2015). The timing of the initial increase in spreading rate (i.e. at chron 25y) precedes the formation time of the Hawaiian-Emperor Bend (~47.5 Ma; O'Connor et al., 2013), and is thought to be a result of an increase in Farallon plate motion, rather than a change in the motion of the Pacific plate (Wright et al., 2015). We find a slightly different trend in spreading velocities in the South Pacific (Austral Fracture Zone; Figure 15b). Along the Austral Fracture Zone, there is an increase in spreading rate from chron 34y–31y (83–67.7 Ma), a significant 27 mm/yr decrease at chron 28y (62.5 Ma), and a further 93 mm/yr increase between chron 25y (55.9 Ma) and 20o (43.8 Ma).

The flowlines derived from Wright et al. (2015) and this study (Table 7) produce an overall good spatial fit to fracture zones in the North (e.g. Molokai Fracture Zone) and South (e.g. Marquesas Fracture Zone) Pacific and produces the best fit to the temporal progression suggested by the compilation of magnetic identifications (Atwater and Severginhause, 1989; Barckhausen et al., 2013; Cande and Haxby, 1991;; Munschy et al., 1996) (Figure 17). Since spreading varies within each fracture zone segment, e.g. due to rift propagation and/or changes in spreading direction, we do not expect all Pacific fracture zone corridors to match our flowlines for all stages. One example of this occurs within the Molokai-Clarion spreading segment, where a pseudofault results in an offset between chron 34y and 30o (Atwater and Severinghaus, 1989), and major propagating rifts have removed much of chron 18 and 19 (Atwater, 1989; Atwater and Severinghaus, 1989). Due to these events, our flowline within stage 31y–33o underestimates the spreading rate suggested by the magnetic identifications within the Molokai-Clarion segment, despite finding a good fit for this stage for other Pacific spreading corridors (e.g. Murray-Molokai, Marquesas-Austral) (Figure 17). Flowlines derived from the rotations of Rowan and Rowley (2014) demonstrate a good spatial fit to the fracture zones, and displays a good temporal fit for chron 34y–13y spreading within the Molokai-Clarion segment, however, they slightly overestimate the spreading within the Murray-Molokai and Marquesas-Austral fracture segments (Figure 17). Flowlines derived from Seton et al.

(2012) diverge from the Pacific fracture zones geometries, especially compared to Rowan and Rowley (2014), Wright et al. (2015) and this study. These flowlines also overestimate the total spreading between chron 34y and 13y for all fracture zone spreading segments (Figure 17).

3.2.2 Relative Juan de Fuca/Vancouver-Pacific plate motions

The reconstruction history of the former Vancouver plate has been poorly explored in the past, with published relative motions listed in Table 8. The half-stage rotation parameters in Rosa and Molnar (1988) were converted into stage and finite rotation parameters based on assumed symmetric spreading. Large differences arise in the clockwise spreading direction of Müller et al. (1997) and the counterclockwise motions suggested by all other models (Figure 18).

We derive Vancouver/Juan de Fuca-Pacific relative plate motions between chrons 24n.1y (52.4 Ma) and 5n.2y (9.9 Ma). An additional published Juan de Fuca-Pacific rotation pole is included at chron 4Ay (8.9 Ma), taken from Wilson (1993). However, we do not include the detailed spreading history of the Juan de Fuca ridge (e.g. Wilson, 1993) as incorporating the spreading history of a small plate at short time intervals is well beyond the scope of this study. We derive half-stage rotations for the Juan de Fuca-Pacific spreading history between chron 10.n1y (28.3 Ma) and chron 4Ac (8.9 Ma) (Table 9) using visual fitting in *GPlates* (Boyden et al., 2011).

We derive the Vancouver plate spreading history with uncertainties between chrons 24n.1y (52.4 Ma) and 10n.1y (28.3 Ma) as half-stage rotations (Table 10). We find a constrained uncertainty for all times (Figure 19), with slightly larger uncertainties for the early Vancouver-Pacific stages (e.g. chron 22o–24n.1y), likely due to the propagation of the Vancouver-Pacific ridge (Caress et al. 1988).

There is a large difference in Vancouver-Pacific relative plate motion between Müller et al. (1997) Rosa and Molnar (1988), and this study. There is a poor match between flowlines produced from Müller et al. (1997) and fracture zone identifications in the area (Figure 20). Flowlines derived from Rosa and Molnar (1988) suggests a similar geometry with the Surveyor Fracture Zone, however flowlines derived from this study closer resemble the geometries of the Sila and Sedna fracture zones (Figure 20). Vancouver-Pacific spreading rate is slightly overestimated by Wright et al. (2015), based on the spatial difference between chron 24n.1y (52.364 Ma) and the flowline endpoint (52.4 Ma).

3.2.3 Relative Kula-Pacific plate motion

The spreading history of the Kula plate has important implications for the northward transport of terranes across the Pacific basin (Atwater, 1989). However, there are few published rotation parameters for Kula-Pacific spreading (Table 11), despite the number of studies related to the formation and reconstruction history of the Kula plate. Nevertheless, we compare the spreading velocities of Rosa and Molnar (1988) and Seton et al. (2012) with derived rotation parameters and uncertainties from this study (Figure 21). Stage rates are calculated assuming symmetrical spreading. The stage rates are all broadly similar, however there is a large difference in spreading direction from chron 25y (55.9 Ma) between Seton et al. (2012) (counterclockwise change) and this study (clockwise change).

We derive Kula-Pacific half-stage rotation parameters and uncertaintaties between chron 34y (83 Ma) and chron 25y (55.9 Ma) (Table 12). We find well constrained half-stage rotation parameters, except for the stage 34y–33y (Figure 22), which is likely due to the sparse magnetic and fracture zone data for chron 34y, as the Kula-Pacific ridge propagated east. As the data for the remaining Kula-Pacific spreading history is sparse and the counterclockwise rotation at chron 25 has resulted in offsets and/or elimination of fracture zones (e.g. Rat and Adak fracture zone), we derive rotation parameters between chron 25y–19y based on visual fitting of magnetic identifications and fracutre zone traces using *GPlates*, where we implement a large counterclockwise change based on the Stalemate Fracture Zone. We calculate finite rotation parameters from chron 21y (47.9 Ma), as conjugate magnetic identifications are preserved on the remaining fragment of the Kula plate.

A comparison of flowlines depicting Kula-Pacific spreading before chron 25y (~56 Ma) demonstrates the misfit between the flowlines of Seton et al. (2012) and Rosa and Molnar (1988) and recognized fracture zones (e.g. Rat and Amlia fracture zones) (Figure 23), in particular, the slight counterclockwise change of Seton et al. (2012), compared to the clockwise change observed in this study between chron 34y and 25y. Rosa and Molnar (1988) and Seton et al. (2012) also underestimate the spreading rates, based on the mistmatch between the flowlines and magnetic identifications, in particular, during the stage chron 33y–31y.

3.3 Reconstruction Summary

We present reconstructions of the Pacific basin since chron 34y (83 Ma). Listed in Table 13 are the finite rotation parameters used in this study. As this is a rigid model focused on the seafloor spreading history of the Pacific basin, we do not incorporate any deformation of the West Antarctic margin, or the rifting history of the West Antarctic margin and Chatham rise.

Spreading between West Antarctica and Chatham plateau in the southern Pacific initially began at chron 34y (83 Ma), which was likely preceded by a period of continental rifting during east Gondwana break-up. This was contemporaneous with the initial stages of Kula plate formation in the northern-central Pacific. During this time, Aluk (Phoenix)-Pacific spreading was active including subduction along the Antarctic Peninsula and southern South American margin adjacent to the Aluk plate (Figure 24). Subduction of the Farallon plate was occurring along North and South America, whilst the newly formed Kula plate was subducting along the present-day Alaskan and

North American margin. Spreading between the West Antarctic and Pacific plates initiated with an almost north-south direction.

By chron 33o (79.1 Ma), Kula-Pacific spreading had established in the North Pacific, whilst northeast-southwest Bellingshausen-Pacific spreading initiation occurred in the South Pacific. By chron 27o (~61 Ma) the Bellingshausen plate had ceased independent motion and was incorporated into the West Antarctic plate, prompting the replacement of Bellingshausen-Aluk spreading with Aluk-West Antarctic spreading. As noted by Eagles et al. (2004b), this event correlates with a regional plate reorganisation. From chron 25y (55.9 Ma), there was a large counterclockwise change in Kula-Pacific spreading, and the beginning of a slow counterclockwise change in Pacific-West Antarctic spreading. This coincides with a large increase in Pacific-Farallon spreading rates and small clockwise change in Pacific-Farallon spreading. Following this change in Pacific-Farallon spreading, the Farallon plate fragmented at chron 24n1y to form the Vancouver plate in its north and this appears to correlate with the counterclockwise motion of the Kula plate at this time (Figure 24). At chron 21o (Figure 24), there was a further South Pacific reorganisation: a portion of the Pacific flank of Pacific-Aluk spreading was trapped onto the West Antarctic plate as the Pacific-Antarctic ridge propagated eastward. During chron 18r, the Kula-Pacific ridge ceased spreading, and the Kula plate was incorporated into the Pacific plate.

The initial arrival of the Pacific-Farallon ridge at the North American trench occurred at ~29 Ma, near the Pioneer Fracture Zone. Following this, the Farallon plate experienced a major fragmentation to form the Nazca and Cocos plates during chron 6B (22.7 Ma) (Figure 24). Further reorganisations occurred, including the formation of the Bauer microplate in the South Pacific around chron 5D, the Mathematician microplate at chron 5n.2o, and the Rivera microplate. As the Pacific-Farallon ridge was progressively subducted beneath North America, the extinct ridges and remnants of the paleoplates approached the margin.

4 Discussion

4.1 Age of the oceanic crust in the Pacific

Our refined tectonic model for the Pacific Ocean basin since chron 34y (83 Ma) allows for a comparison of the model-derived age of oceanic crust at present-day and throughout the Late Cretaceous and Cenozoic. Our refined present-day age grid (Figure 25) is largely similar to that of Seton et al. (2012), however we do find a number of differences. Throughout the Pacific basin, we find differences arising from recent magnetic anomaly identifications (i.e. Barckhausen et al., 2013; Wobbe et al., 2012) and the use of a large compilation of published magnetic identifications (Seton et al., 2014), resulting in over 10 Myr differences in the equatorial and south Pacific. The use of well-constrained fracture zone interpretations (Matthews et al., 2011) has also permitted the detailed mapping of oceanic crustal offsets (along fracture zone and small circles) that Seton et al. (2012) does not fully acknowledge, in particular, on the southern Pacific and West Antarctic plates. In the regions associated with Pacific, West Antarctic, and former Aluk and Bellingshausen spreading, we find variations over 10 Myr due to the incorporation of independent plates and their seafloor spreading isochrons (i.e. Bellingshausen, Aluk). Minor variations (up to 5 Myr) between our refined age grid and Seton et al. (2012) are found in the northeast Pacific (Figure 25), which is expected due to the dense coverage of magnetic interpretations in this region, and lack of conjugate spreading flank.

Our updated age grids of the Pacific allow us to derive half-spreading rate, crustal accretion, and age error grids. Comparison of our derived half-spreading rates (Figure 26a) and those from Müller et al. (2008) demonstrate large differences in estimates for the western Pacific. These reflect refinements to the Mesozoic spreading history of the Pacific basin made in Seton et al. (2012). Our spreading rate grid highlights the fast Pacific-Farallon spreading rates, in particular since ~50 Ma, compared to the remaining Pacific basin. Crustal accretion throughout the Pacific basin where both spreading flanks are preserved is largely more symmetric (50%) than Müller et al. (2008), who find a large area of excess accretion on the Pacific plate. We find a broadly similar trend in crustal accretion patterns along the East Pacific Rise, although our refined Cocos-Pacific seafloor isochrons suggest this system experienced more spreading symmetry than Müller et al. (2008) indicate. Our error grids, derived based on the difference between a compilation of magnetic identifications (Seton et al., 2014) and interpreted gridded age, indicate a large difference in error in the low-latitude Pacific and South Pacific, largely related to the improved coverage of these areas. Errors of ~10 Myr occur in regions where no magnetic identifications occur in both our study and Müller et al. (2008), due to the lack of coverage or the CNS.

We present new paleo-age grids in 10 Myr increments for the Pacific basin between 80 Ma and present day in the timescales of Gee and Kent (2007) and Ogg (2012) (Figure 27). There is little difference in the distribution of ocean floor age since 50 Ma, regardless of timescale used. This is expected, due to the similarity in C-sequence timescales (i.e. Gee and Kent, 2007; Ogg, 2012). A ~5–6 Myr difference is observed in oceanic crust produced prior to M0, due primarily to the large difference attributed to this chron (Gee and Kent, 2007: 120.6 Ma, vs. Ogg, 2012: 125.93 Ma).

4.2 Spreading asymmetry

Spreading asymmetry between the Pacific and Nazca plates can be determined based on the relative spacing of magnetic anomalies on conjugate ridge flanks and it has been suggested that since ~50 Ma the ridge crest has favoured accretion on the Nazca plate (56–60 per cent) over the Pacific plate (40–44 per cent) (Rowan and Rowley, 2014). The subduction of the Farallon plate makes it impossible to fully constrain Pacific-Farallon seafloor spreading (and hence, the history of crustal accretion) prior to ~50 Ma, with reconstructions of the Pacific-Farallon spreading derived from half-stage rotations (based on the Pacific plate) and assumed symmetric spreading. This assumption of symmetric spreading has been criticized, as observations of asymmetry since ~50 Ma suggests this approach underestimates the crustal accretion of the Farallon plate in the Mesozoic and early Cenozoic.

Recently, Rowan and Rowley (2014) highlighted the importance of asymmetric crustal accretion along the East Pacific Rise and inferred asymmetric crustal accretion along the entire Pacific-Farallon ridge until chron 34y (83 Ma) based on extrapolating their 'best-fit' crustal accretion fraction (Pacific:Farallon asymmetry of 44:56 per cent) for the past 50 Myr. However, this approach is still somewhat problematic. While there were likely minor asymmetries in Pacific-Farallon spreading prior to 50 Ma, it is arbitrary to infer continuous and systematic spreading asymmetry until chron 34y (83 Ma), and unreasonable to extrapolate such high values of spreading asymmetries to the entire Cenozoic-Mesozoic Pacific-Farallon spreading history. Further, the inferred Farallon Plate history in the Mesozoic and early Cenozoic (i.e. large Farallon plate, with the Pacific-Farallon ridge inferred to be much further from the North or South America subduction zones) differs greatly to its more recent history (i.e. multiple fragmentation events as the Pacific-Farallon ridge approached and intersected with the subduction zones).

We compare spreading crustal accretion for the major spreading systems in the Pacific basin with both spreading flanks preserved (Figure 28). We find the Pacific basin has largely experienced symmetric spreading, with over 60% of the oceanic crust experiencing less than 20% variation in crustal accretion, with asymmetries less than 5% most frequent (Figure 29). Crustal accretion has also varied from stages of symmetric spreading (e.g. 25y–21o; 55.9–47.9 Ma; 18n.2o–6Bn.1c; 40.1–23 Ma) to asymmetric spreading (i.e. 6o–present day; 20.1–0 Ma) along the southern East Pacific Rise (Challenger-Resolution fracture zone segment; Pacific-Nazca/Farallon spreading) (Figure 30). These large fluctuations in spreading asymmetry are not observed along any other major spreading system in the Pacific basin, including the Pacific-Antarctic ridge and northern East Pacific Rise (Clipperton-Galapagos fracture zone segment; Pacific-Cocos spreading) (Figure 30).

There are major differences in the mantle associated with regions of the Pacific basin. The South Pacific superswell (e.g. 10°N to 30°S; 130°W to 160°W; Adam et al., 2014) underlies the Pacific plate, and is associated with a large depth anomaly, that is the difference between the observed and theoretical oceanic basement depth based on thermal subsidence models. This mantle is hotter (Cochran, 1986), and has been found to have a lower resistivity to the mantle than that beneath the Nazca plate (Evans et al., 1999). Additionally, the mantle north and south of the Easter microplate (along the East Pacific Rise) can be divided into northern and southern domains due to the variation in axial depths (deep and shallow, respectively) and the distinct geochemical signatures of these domains (Vlastelic et al., 1999; Zhang et al., 2013). The southern East Pacific Rise has remained relatively “anchored’ throughout the past 100 Myr, due to the interaction of deep plumes and the mid-ocean ridge (Whittaker et al., 2015). We observe asymmetry along the southern East Pacific Rise (Pacific-Nazca/Farallon spreading) from ~48 Ma (chron 21o), with the East Pacific Rise successively jumping westwards towards the mantle upwelling associated with the South Pacific superswell. This behaviour has previously been identified in the Pacific and equivalently along spreading ridges in the Atlantic and Indian Ocean basins (Müller et al., 1998). The northern East Pacific Rise (Pacific-Cocos) spreading does not display this same pattern of westward ridge jumps (Figure 28). Asymmetry associated with Pacific-Cocos spreading is strongly driven by ridge-subduction zone interactions, where the large curvature of the subduction zone may induce an intraplate stress field on plate regions proximal to the subduction zone, resulting in ridge jumps and plate fragmentation. Contrary to the behaviour of the East Pacific Rise, the Pacific-Antarctic ridge demonstrates no major asymmetry in crustal accretion (Figure 30). Major driving forces such as upwelling (as underneath the southern East Pacific Rise) or a nearby subduction zone (as in the northern East Pacific Rise) are not located proximal to the Pacific-Antarctic Ridge. Rather, the Pacific-Antarctic ridge is likely influenced by small-scale mantle flow, causing random minor spreading asymmetry that varies between segments (Rouzo et al., 1995).

The variations in mantle dynamics along the East Pacific Rise indicate that this ridge cannot be treated as a continuous feature. Based on the largely symmetrical behaviour of the Pacific-Antarctic ridge and the northern East Pacific Rise (Cocos-Pacific), and the fluctuations in Pacific-Farallon spreading behaviour, we propose that Pacific-Nazca/Farallon spreading asymmetries since ~48 Ma (chron 21o) do not reflect the long-term behaviour of the entire Pacific-Farallon ridge. Rowan and Rowley (2014) observe a correlation between periods of high spreading rates and high spreading asymmetries since 40 Ma, and imply both high periods of spreading rate and asymmetry are causally linked to anomalous mantle flow beneath a mid-ocean ridge flank. There is little reason to expect high spreading asymmetries during periods of much slower Pacific-Farallon spreading rates, as is observed before ~50 Ma, contrary to the inferences by Rowan and Rowley (2014) (Figure 15).

4.3 Subduction along North and South America

4.3.1 Implied convergence history

We use our tectonic reconstructions to derive the convergence history along the western North and South American margins, by determining the relative motion of the Pacific plates and North/South Americas through the use of a plate circuit based on the seafloor spreading record preserved in the Pacific, Atlantic, and Indian oceans. This approach is relatively sensitive to changes in the relative motion of plates within the circuit and to the configuration of tectonic plates, in particular, the location of the Kula-Farallon ridge along the North American margin, and the Aluk-Farallon ridge location along the South American margin. Such discrepancies in the computed convergence history between kinematic models, such as our refined model and Seton et al. (2012), emphasize how such inferences are dependent on the kinematic model used. Despite this, there are also many similarities in the implied convergence history derived from Seton et al. (2012) and our refined model (i.e. since ~50 Ma), suggesting a robust trend for these times. Nevertheless, our model provides insights into the evolution of the North and South American convergent margins, and can provide a useful tectonic context when considering the geochemical and topographic evolution of these margins, particularly in relation to ridge subduction and slab window formation.

North America

The North American margin has been shaped by the convergence of Pacific basin plates, such as the Farallon, Kula, Vancouver, and Pacific plate. However, there are uncertainties in the extent of the paleoplates (e.g. Kula and Farallon plates) that bordered North America during most of the Late Cretaceous and Cenozoic. We model the Farallon-Kula ridge to coincide with southern British Columbia, which is broadly consistent with the tectonic configuration of Seton et al. (2012). This location is also consistent with the location of a slab window near Vancouver Island at 50 Ma, based on geochemical analysis of lavas from the Eocene Challis-Kamloops volcanic belt (Breitsprecher et al., 2003). The tectonic plate adjacent to the North American margin significantly affects the implied convergence velocity: after 60 Ma, there is a rapid increase in the Kula plate convergence velocity at point 1 (Vancouver Island), while there is little change in velocity if the Farallon/Vancouver plates are converging here (Figure 31). We derive similar implied convergence rates in the timescales of Cande and Kent (1995) and Ogg (2012) (Figure 31, Figure 32), and find no major differences in convergence velocity, suggesting our results are not strongly dependent on choice of timescale. Refinements to Pacific basin relative plate motions, such as Vancouver-Pacific and Pacific-Farallon, have a minor influence on the derived convergence history, in particular, at points 2 (San Francisico) and 3 (Baja California). The observed differences between Seton et al. (2012) and this study are likely due to the major influence of East-West Antarctica relative motion.

South America

The South American margin has experienced long-lived subduction since the Early Jurassic (Somoza and Ghidella, 2012). The configuration of the tectonic plates along the South American margin greatly influences the implied convergence history, especially along the southern Andean margin (e.g. Patagonia). We infer the Farallon-Aluk ridge to coincide with northern Chile in the Late Cretaceous and early Cenozoic (Figure 33), consistent with Somoza and Ghidella (2012), and broadly consistent with simplified schematics presented in Scalabrino et al. (2009). We implement a southward migrating Farallon-Aluk ridge, resulting in ridge intersection with Patagonia during the Eocene: this is consistent with alkali basalts suggesting a slab window occurred in this region at ~50 Ma (Breitsprecher and Thorkelson, 2009) and the location of the Farallon-Aluk paleo-ridge suggested by Eagles and Scott (2014). However, this contrasts with the scenario proposed by Scalabrino et al. (2009). We propose ridge subduction occurred in the vicinity of our point 3 (45°S, 76°W) at 53 Ma, after which the Farallon plate was subducted within this region. This correlates with Eagles and Scott (2014), who suggest ridge subduction in this region at 54 Ma. Our configuration of tectonic plates in the Late Cretaceous and early Cenozoic differs greatly from Seton et al. (2012), as their reconstruction does not incorporate the Aluk plate, and infers a Farallon-East Antarctica ridge intersecting the southern Andean margin (Figure 33).

Comparison with the implied convergence derived from Seton et al. (2012) (and their plate tectonic configuration) demonstrates little difference in rate and obliquity since 30 Ma (Figure 34, Figure 35). Prior to 30 Ma, minor differences in the convergence rate and obliquity are calculated along northern Peru (Point 1) and northern Chile (point 2). As the plate adjacent to the southern Andean margin (i.e. Patagonia; point 3) prior to 45 Ma differs between Seton et al. (2012) (Farallon plate) and this study (Aluk or Phoenix plate), the implied convergence history demonstrates significant differences in this region, with up to 150 mm/yr difference in convergence rate, and ~250° difference in convergence obliquity. Seton et al. (2012) proposes the Farallon and South American plates were diverging in the Patagonian region prior to 50 Ma (Figure 34, Figure 35), however Cretaceous and Cenozoic calcic/calc-alkaline rocks indicates this region has been influenced by subduction dynamics (Ramos, 2005), casting doubt on this interpretation.

4.3.2 Age of the subducting crust

The geological evolution of continental margins is further influenced by the age of subducting lithosphere through time. Due to its buoyancy, young lithosphere (<50 Myr old; Cross and Pilger, 1982) generally subducts at a shallower angle, and does not penetrate into the mantle as deeply as cold, older oceanic lithosphere (England and Wortel, 1980). Subduction of very young (≤ 20 Myr old) and relatively warm oceanic crust, including ridge subduction, is thought to result in dehydration of the slab and the release of volatiles at shallow depths (Harry and Green, 1999). Consequently, we expect a correlation in tectonic regimes and the age of the subducting oceanic lithosphere, where subduction of young lithosphere is linked to back-arc and intra-arc compression (Cross and Pilger, 1982), and cordilleran tectonics (Molnar and Atwater, 1978), whilst subduction of old lithosphere generally results in back-arc and intra-arc extension (Cross and Pilger, 1982). These broad relationships are not observed in all regions, with inconsistencies arising when we consider subduction of the older (e.g. ~60 Myr) Farallon and Nazca plate along the South American margin. The time-dependence of the age of oceanic lithosphere subducted beneath South America has important consequences for understanding changing spreading rates in the South Atlantic ocean, as discussed by Müller et al (in press).

North America

We find broadly similar trends in the age of oceanic crust at the North American trench through time, derived from Seton et al. (2012) and this study (Figure 36). We derive the age of oceanic crust at the trench based on a symmetrical spreading and 'best-fit' Farallon-Pacific asymmetrical spreading until chron 34y (83 Ma), based on the ratio described in Rowan and Rowley (2014). We do not incorporate any asymmetrical spreading into Vancouver-Pacific and Kula-Pacific relative motion. The incorporation of spreading asymmetry makes little difference in the age of subducting oceanic crust (Figure 36), with up to 15 Myr difference in the Late Cretaceous. Rather, the relative plate motions impart a larger influence on the age of oceanic crust at the trench, where there is up to a 40 Myr difference in the Late Cretaceous and early Cenozoic between Seton et al. (2012) and this study at point 2 (Figure 36). Point 1 shows little difference in the age of subducting oceanic crust derived from our models. This trend is expected, as this location records the subduction of the Kula and Vancouver plates, where we do not incorporate any spreading asymmetry into the 'asymmetric' model. Point 1 also shows a large decrease in the age of subducting oceanic crust at ~70 Ma in our model, which arises from the close proximity of point 1 to our modelled Kula-Farallon ridge. At ~60 Ma, our model records the subduction of the Kula-Farallon/Vancouver ridge along point 1, while Seton et al. (2012) record this event ~20 Myr later. This discrepancy highlights the dependence of such results on the kinematic model used in analysis. In this case, the age variation between our model and Seton et al. (2012) results from the slight change in the intersection of the Kula-Farallon ridge with the North American margin at this time, and is a consequence of the difference in Kula-Farallon relative motion (derived from Kula-Pacific and Farallon-Pacific relative motions). Since ~30 Ma, there is little difference in the age of subducting lithosphere, regardless of model choice. This is not unexpected; as for times younger than chron 13y (33.1 Ma) we incorporate the Farallon-Pacific relative motion from Seton et al. (2012).

South America

Comparison of the age of oceanic crust at the South American trench based on Seton et al. (2012) and this study indicates a relatively consistent 10–20 Myr age difference at all points. Despite the long-lived subduction of the Farallon plate, we find little difference in the age of oceanic crust when spreading asymmetry is incorporated, except for along northern Peru (point 1), where we observe up to 40 Myr differences in ocean crust age, at 30 Ma (Figure 37). The small difference in the age of subducting oceanic crust between our asymmetric and symmetric model is due to the orientation of the magnetic lineations on the subducting (e.g. Farallon) plate, and is a reflection on the earlier (pre-chron 34y; 83 Ma) tectonic history of the Pacific basin (i.e. Seton et al., 2012). At ~50 Ma, we observe ridge subduction at point 3, which is consistent with the proposed slab window in this region by Breitsprecher and Thorkelson (2009). This contrasts with the age derived from Seton et al. (2012), who suggest the subduction of ~20 Myr old oceanic crust (Figure 37).

4.4 Limitations

Uncertainties remain in our reconstruction of the Pacific Ocean basin due to the limited availability of data from preserved regions (e.g. central Nazca plate) and the subduction of former plates along the North and South American margins. The present-day age of oceanic lithosphere remains poorly constrained in regions where there is limited magnetic anomaly data available, in particular, areas associated with the CNS, and within the central Nazca plate. The age of oceanic lithosphere across the CNS is interpolated based on assuming no change in Pacific-Farallon spreading rate between M0 (120.6 Ma) and chron 34y (84 Ma), and further refinements to this region are beyond the scope of this study. The central Nazca Plate exhibits a large (~6 Myr) age error (Figure 26c), and is a region of relatively few magnetic identifications (Figure 3). This region is thought to preserve the remnants of transient microplates such as the Mendoza microplate (between the Mendana and Nazca fracture zones); however, we do not incorporate such events into our kinematic history due to large ambiguities in the limited data available. Additionally, we do not incorporate the independent motion of the Monterey or Arguello microplates. Uncertainty in the age of oceanic lithosphere also remains along the Marie Byrd Land margin, such as the age of the Charcot plate (McCarron and Larter, 1998). The age of oceanic lithosphere in such regions may be refined with the collection and provision of additional data.

As much of the record of Pacific basin seafloor spreading has been subducted (e.g. Farallon, Vancouver, Kula plates), our tectonic reconstruction represents the ‘simplest’ scenario, based on the preserved geophysical data from the Pacific plate, and onshore geochemical and geological data (e.g. locations of slab windows to infer ridge-trench interactions). Uncertainties in the plate configuration history are greatest during the earlier Pacific basin history, such as in the Cretaceous and early Cenozoic. In particular, the spreading history of the Kula plate remains poorly constrained, with concerns surrounding the tectonic history of the "T" anomaly, which has been proposed to represent a captured Kula-Farallon-Pacific triple junction (Atwater, 1989). The presence of a large Eocene-Oligoence aged turbidite body on the Aleutian Abyssal Plain, known as the Zodiac Fan (Stevenson et al., 1983), further suggests a gap in our understanding of the reconstruction history of the North Pacific. The Zodiac turbidite fan consists of granitic and metamorphic rocks, which are inferred to originate from southeastern Alaska and western Canada (Steward, 1976), and is thought to have contributed material to accretionary prisms along the eastern Aleutian trench (Suess et al., 1998). Eocene tectonic reconstructions place the Zodiac fan over ~2000 km away from its inferred source, and highlight the large uncertainty in the plate configuration of the North Pacific basin in parts of the Cenozoic.

It is possible that additional oceanic plates existed along the North and South American margins during the Late Cretaceous and early Cenozoic, contrary to our inferred configuration of large oceanic plates (e.g. the Farallon plate). Large uncertainties in the implied convergence history remain along northern North America, where the existence of an additional plate has been proposed (the Resurrection plate; Haeussler et al., 2003) based on the onshore geological record. We do not incorporate this plate into our model as there is little data to constrain its relative plate motion and plate boundary geometry and the geological evidence used to support a ridge-trench intersection event may be from an extinct rather than active mid-ocean ridge. The incorporation of the Resurrection plate, or any other tectonic plate within this region, would greatly alter the implied convergence history along northern North America and Alaska. The Late Cretaceous and early Cenozoic implied convergence history along central South America also has a large uncertainty, where variations in the age of subducting oceanic lithosphere are directly linked to the preceding events of the Farallon and Phoenix plates (e.g. Seton et al., 2012).

5 Conclusion

We have refined the plate tectonic model of the Pacific Ocean from the Late Cretaceous to present day, based on recent data including satellite marine gravity anomalies (Sandwell et al., 2014), well-constrained fracture zone traces (Matthews et al., 2011; Wessel et al., 2015) and a large compilation of magnetic anomaly identifications (Seton et al., 2014). Unlike many regional Pacific reviews that limit their scope to either the North (Atwater, 1989) or South Pacific (Mayes et al., 1990), we assess the seafloor spreading history for the entire Pacific basin and incorporate previously recognised tectonic plates, such as the Aluk (Phoenix) and Bellingshausen, which have so far been limited to regional studies. This approach allows for a comprehensive analysis of the Pacific-Farallon relative plate motion since the Late Cretaceous, as many previous studies have derived northern Farallon plate motions and extrapolated these to the entire Farallon plate. Our results show that this can result in skewed spreading velocities.

Where possible, we present 95% uncertainties for our relative plate motions, based on the best-fitting criteria of Hellinger (1981), allowing for the assessment of significance in tectonic changes. To eliminate any timescale bias in significant spreading events, we present all results in the timescale of Cande and Kent (1995) and Ogg (2012), and find similar trends regardless of timescale. Our relative plate motions result in a good match to both the fracture zone traces and magnetic pick data in both the North and South Pacific.

A comparison of our relative plate motions and published regional models demonstrates that while there are clear overall trends in spreading velocities, many publications do not conform with fracture zone traces observed in recent data (e.g. Vancouver-Pacific spreading based Seton et al. 2012), or do not incorporate changes in spreading rate indicated by the temporal progression of magnetic picks (e.g. Farallon-Pacific spreading based on Rowan and Rowley, 2014). Additionally, many regional studies do not provide any indication of uncertainties, or only provide spreading parameters for small portions of the spreading history of a plate (e.g. Rosa and Molnar, 1988).

Our refined reconstruction history of the Pacific allows for a comparison of Pacific basin oceanic age, spreading rates and asymmetries. Analysis of the error associated in the age grid demonstrates ~8 Myr errors between our refined age grids and Müller et al. (2008), in areas such as the central Pacific, where there is now improved magnetic pick coverage. Comparison of crustal accretion associated with the East Pacific Rise (i.e. Pacific-Farallon/Nazca and Pacific-Cocos) highlights how these systems have oscillated through periods of symmetrical and highly asymmetrical spreading, and varies greatly from the symmetrically spreading Pacific-Antarctic ridge. We attribute these differences to major differences in the Pacific mantle: the southern East Pacific Rise (Pacific-Farallon/Nazca) shows signs of successive westward ridge jumps towards mantle upwelling associated with the South Pacific superswell, however the northern East Pacific Rise (Pacific-Cocos) is strongly driven by the adjacent subduction zone, and underwent eastward ridge jumps. The Pacific-Antarctic ridge is not located near either of these major driving forces of asymmetry, and shows evidence of minor asymmetry due to small-scale changes in mantle flow. These regional differences in the Pacific mantle suggests that long-term Farallon-Pacific crustal accretion ratios cannot be extrapolated based on the ~50 Myr record of Farallon/Nazca-Pacific asymmetries.

Comparison of the implied convergence history of the Pacific plates along the western North and South American plates based on our refined model and Seton et al. (2012) highlights the importance of the Pacific plate tectonic configuration. In particular, the addition of the Aluk plate in the south Pacific significantly improves the implied convergence history in the Patagonian region of South America and correlates with a proposed ~50 Ma ridge subduction event (Breitsprecher and Thorkelson, 2009). Further, the incorporation of Farallon-Pacific spreading asymmetry (based on the 'best-fit' ratios of Rowan and Rowley, 2014) does not significantly influence the age of subducting oceanic lithosphere along the North and South American margin.

Our reconstruction provides a framework for understanding circum-Pacific tectonics, plate reorganisation events, and the evolution of seafloor spreading and asymmetry in the Pacific basin.

6 Acknowledgements

We thank Graeme Eagles and an anonymous reviewer for their detailed reviews, which greatly improved the manuscript. N.M.W. was supported by an Australian Postgraduate Award, M.S. by ARC grant FT130101564 and S.E.W. and R.D.M. by ARC grant FL0992245. Figures were constructed using Generic Mapping Tools.

Figure 1: Bathymetry (ETOPO1; Amante and Eakins (2009) of the present-day Pacific basin, showing the major tectonic plates and fracture zones. Plate boundaries (black) are from Bird (2003), and fracture zone (FZ) identifications (blue) are from Wessel et al. (2015). Coastlines (Wessel and Smith, 1996) are shown in grey. EA: Easter microplate; JDF: Juan de Fuca plate; JZ: Juan Fernandez microplate; R: Rivera microplate.

Figure 2: Overview of major spreading systems in the Pacific basin since chron 34y (83 Ma). The western Pacific basin formed prior to chron 34y. Uncertainties in the boundaries of spreading systems, including the Vancouver-Farallon boundary and the extinct of Pacific-Farallon spreading in the equatorial Pacific, are denoted with a “?”. Plate boundaries (black) are modified from Bird (2003) to denote subduction zones (toothed), and fracture zone (FZ) identifications (blue) are from Wessel et al. (2015). Present-day coastlines (Wessel and Smith, 1996) are in dark-grey, and non-oceanic regions are in light grey. Bellings.: Bellingshausen; EA: Easter microplate; JDF: Juan de Fuca plate; JZ: Juan Fernandez microplate; Math.: Mathematician microplate; MP: Microplate; R: Rivera microplate; Van.: Vancouver.

Figure 3: Overview of magnetic anomaly identifications in the Pacific basin, downloaded from the Global Seafloor Fabric and Magnetic Lineation (GSFML) repository (Seton et al. 2014) in April, 2015. C-sequence magnetic identifications are colored based on their age in Cande and Kent (1995), while M-sequence magnetic identifications are hollow. Plate boundaries (black) are modified from Bird (2003) to denote subduction zones (triangles), and fracture zone (FZ) identifications (blue) are from Wessel et al. (2015). Present-day coastlines (Wessel and Smith, 1996) are in dark-grey, and non-oceanic regions are in light grey. Legend for spreading regions as in Figure 2.

Figure 4: Schematic of Hellinger (1981)'s method. (a) Method to determine finite rotations, when both spreading flanks are preserved. The best-fit rotation pole is found by matching conjugate magnetic anomaly (black) and fracture zones (grey) of the same age (t_1) on both plates. (b) Method to determine half-stage rotations, when one of the plates has been subducted. The best-fit half-stage rotation pole is found by reconstructing a younger (t_1) magnetic anomaly and fracture zones segment onto an older (t_2) time. t_0 represents the present-day ridge. Modified from Rowan and Rowley (2014).

Figure 5: Overview of seafloor features in the South Pacific, observed in marine gravity anomalies (Sandwell et al., 2014). Plate boundaries (black) are from Bird (2003), fracture zones (FZ; white) are from Wessel et al. (2015) and coastlines (grey) are from Wessel and Smith (1996). Dashed outline refers to the region associated with Bellingshausen (BELL) independent motion. BGA: Bellingshausen gravity anomaly; DGGA: De Gerlache gravity anomaly; EA: East Antarctica; MBS: Marie Byrd Seamounts; NZ: New Zealand; SAM: South America.

Figure 6: Comparison of Pacific-West Antarctic spreading velocities in the timescales of Cande and Kent (1995) (CK95; left) and Ogg (2012) (GTS2012; right), with selected chrons labelled. 95% uncertainties (shaded blue) are for Wright et al. (2015) and this study. Full stage rates (mm/yr) and spreading directions (°) are calculated along the Pitman Fracture Zone.

Figure 7: Comparison of finite pole locations and 95% confidence ellipses from Wright et al. (2015) and this study. Finite rotation parameters are labelled based on their chron and reference (color).

Figure 8: Comparison of synthetic flowlines for Pacific-West Antarctic relative motion between chron 34y and 21y and the Erebus, Pitman and IX fracture zones (FZ) observed in the marine gravity anomaly (top; Sandwell et al., 2014) and in a cartoon schematic with fracture zone

identifications (black lines; Wessel et al., 2015; bottom) on the (a) Pacific plate and (b) Antarctic plate. Flowlines are colored based on reference (line, symbol outline). Wright et al. (2015) and this study have been combined into one flowline. Symbols along each flowline correspond to the age of plotted magnetic identifications (symbol fill). Magnetic identifications used in Hellinger's analysis in Wright et al. (2015) and this study are shown. Region associated with Bellingshausen (Bell.) spreading shown in dotted outline. EA: East Antarctica; MBL: Marie Byrd Land; NZ: New Zealand.

Figure 9: Comparison of Bellingshausen-Pacific spreading velocities in the timescales of Cande and Kent (1995) (CK95; left), and Ogg (2012) (GTS2012; right), with selected chrons labelled. 95% uncertainties (shaded blue) refer to this study only. Full stage rates (mm/yr) and spreading directions (°) are calculated along the Udintsev Fracture Zone.

Figure 10: Comparison of Bellingshausen-Pacific finite rotation pole locations and 95% confidence ellipses from this study. Finite rotation parameters are labelled based on their chron and reference (color).

Figure 11: Comparison of derived flowlines for Bellingshausen-Pacific relative motion and fracture zones observed in the marine gravity anomaly (Sandwell et al., 2014) (top) and as a cartoon schematic with fracture zone identifications (black lines; Wessel et al., 2015; middle). (a) Pacific plate. (b) Antarctic plate (former Bellingshausen region). Flowlines are colored based on reference, with divisions corresponding to chron times (labeled along the (a) Tharp and (b) Udintsev Fracture Zones [FZ]). Magnetic identifications used in this study's Hellinger analysis are shown (colored). EA: East Antarctica; MBL: Marie Byrd Land; NZ: New Zealand; SAM: South America

Figure 12: Comparison of synthetic flowlines for Pacific-Aluk (Phoenix) spreading observed in the marine gravity anomaly (Sandwell et al., 2014) (top) and as a cartoon schematic with fracture zone identifications (black lines; Wessel et al., 2015; middle panel). Interpreted isochrons (thin grey) and a compilation of magnetic identifications (Cande et al., 1995; Cande and Haxby, 1991; Croon et al., 2008; Eagles et al., 2004b; Larter et al., 2002; Wobbe et al., 2012) since chron 34y (colored circles) are shown. Regions of Aluk (Phoenix)-Pacific (Aluk-Pac), Bellingshausen-Pacific (Bell-Pac), and Pacific-Antarctic (Pac-Ant) are outlined. ANT: Antarctica

Figure 13: Overview of seafloor features in the south-central eastern Pacific, observed in marine gravity anomalies (Sandwell et al., 2014). Plate boundaries (black) are from Bird (2003), fracture zones (FZ; white) are from Matthews et al. (2011) and coastlines (grey) are from Wessel and Smith (1996). EA: Easter microplate; GP: Galapagos plate; JZ: Juan Fernandez microplate; R: Rivera plate; RSB: Rough-smooth boundary

Figure 14: Overview of seafloor features in the north-east Pacific, observed in marine gravity anomalies (Sandwell et al., 2014). Plate boundaries (black) are from Bird (2003), fracture zones (FZ; white) are from Wessel et al. (2015) and coastlines (grey) are from Wessel and Smith (1996). JDF: Juan de Fuca plate; RSB: Rough-smooth boundary

Figure 15: Comparison of Pacific-Farallon spreading velocities in Cande and Kent (1995) (left); and Ogg (2012) (right), with selected chrons labeled. 95% uncertainties (shaded blue) are for Wright et al. (2015) and this study. Large increases in spreading rate during ~50–40 Ma are likely artefacts of timescale conversion, rather than an actual increase in stage rates. Full stage rates (mm/yr) and spreading directions (°) are calculated along the (a) Molokai Fracture Zone (‘North Pacific’) and (b) Austral Fracture Zone (‘South Pacific).

Figure 16: 95% uncertainties for Pacific-Farallon half-stage rotations from Wright et al. (2015) (colored diamonds) and this study (black circles)

Figure 17: Comparison of synthetic flowlines for Pacific-Farallon spreading and fracture zones observed in the marine gravity anomaly (Sandwell et al., 2014) and as a cartoon schematic with fracture zone identifications (black lines; Wessel et al., 2015). A: North Pacific, with the Molokai and Clarion fracture zones (FZ). B: South Pacific, with the Marquesas and Austral FZs. Magnetic identifications (colored circles) on figure and inset are those used in the Hellinger's method for Wright et al. (2015) and this study. References compared include Seton et al. (2012) (inverted triangle, orange), Rowan and Rowley (2014) (star, red), and Wright et al. (2015) and this study (diamond, navy), where symbols along the flowlines are colored to match the timing of magnetic identifications used in Hellinger's analysis. Flowlines were constructed based on a common point, corresponding to chron 13y (Molokai FZ), chron 18n.2o (Clarion FZ), and chron 34y (Austral and Marquesas fracture zones). These chrons were chosen for easy comparison, as rift propagation has disturbed some regions within spreading corridors. CO: Cocos

Figure 18: Comparison of Vancouver-Pacific spreading velocities, in the timescales of Cande and Kent (1995) (left) and Ogg (2012) (right), with selected chrons labelled. 95% uncertainties (shaded blue) are for Wright et al. (2015) and this study. Full stage rates (mm/yr) and spreading direction (°) are calculated along the Mendocino Fracture Zone.

Figure 19: 95% uncertainty ellipses from Wright et al. (2015) and this study for Vancouver-Pacific spreading

Figure 20: Comparison of Vancouver-Pacific synthetic flowlines and North Pacific fracture zones, observed in marine gravity anomalies (left; Sandwell et al., 2014) and in a cartoon schematic

(middle), with fracture zone identifications (black lines; Wessel et al., 2015). References compared include Rosa and Molnar (1988) (star, green), Müller et al (1997) (inverted triangle, orange), McCrory and Wilson (triangle, red), Wright et al. (2015) (triangle: navy), and this study (diamond, blue), where symbols along the flowlines are colored to match the timing of magnetic identifications used in Hellinger's analysis (magnetic identifications shown). Flowlines for Müller et al. (1997) and this study were constructed based on a common point corresponding to chron 10n.1y, whereas other synthetic flowlines match the available rotations in each reference.

Figure 21: Comparison of Kula-Pacific spreading velocities in the timescales of Cande and Kent (1995) (CK95; left) and Ogg (2012) (GTS2012; right), with selected chrons labelled. 95% uncertainties (shaded blue) are for this study only. Full stage rates (mm/yr) and spreading directions (°N) are calculated along the Amlia Fracture Zone.

Figure 22: 95% confidence ellipses for Kula-Pacific half-stage rotation parameters

Figure 23: Comparison of Kula-Pacific synthetic flowlines observed in marine gravity anomalies (left; Sandwell et al., 2014) and in a cartoon schematic (middle), with fracture zone identifications (black lines; Wessel et al., 2015). Both Rosa and Molnar (1988) and Seton et al. (2012) have a poor geometric match with the Amlia and Rat fracture zones.

Figure 24: Reconstruction of the Pacific basin since chron 34y, shown at times corresponding to major seafloor spreading isochrons or major reorganization events within the Pacific basin. These ages are 83 Ma (34y), 79.1 Ma (33o), 67.7 Ma (31y), 55.9 Ma (25y), 52.4 Ma (24n.1y), 47.9 Ma (21o), 40.1 Ma (18n.2o), 33.1 Ma (13y), 22.7 Ma (6Bn.1c), 10.9 Ma (5n.2o), and present-day (0 Ma). Ages are in the timescale of Cande and Kent (1995). Marine gravity anomalies (Sandwell et al., 2014) are reconstructed, to highlight presently preserved oceanic crust. The compilation of

magnetic identifications from the GSFML repository (Seton et al., 2014) is shown as colored circles. Ant: Antarctica; B: Bauer microplate; Bell.: Bellingshausen; Coc: Cocos; IZ: Izanagi; JDF: Juan de Fuca; Van: Vancouver.

Figure 25: Refined present-day age grid and comparison with those from Seton et al. (2012). Residual age of the oceanic lithosphere is from the difference between our refined age grid and Seton et al. (2012).). Plate boundaries (white) for this study and residual are modified from Bird (2003), while those for Seton et al. (2012) are from their study. Coastlines (light grey) and non-oceanic regions (dark grey) are also shown.

Figure 26: Comparison of (a) half-spreading rate, (b) crustal accretion, and (c) error grids, based on this study and Müller et al. (2008). Residual is based on the difference between this study and Müller et al. (2008).

Figure 27: Paleo-age grid in 10 Myr increments. Left: Age grid in Gee and Kent (2007); Middle: Age grid in Ogg (2012); Left: Age difference between Gee and Kent (2007) and Ogg (2012).

Figure 28: Regions used in crustal accretion analysis within the Pacific basin. Some regions were excluded from analysis due to microplate formation (e.g. Bauer microplate). Regions that do not have a preserved conjugate flank are in white. Spreading regions used include Pacific-Nazca/Farallon (pink); Cocos-Pacific (dark green); Cocos-Nazca (light blue); Pacific-West Antarctic (blue); Bellingshausen-Pacific (gold); Antarctic-Nazca (light green); and Juan de Fuca-Pacific (maroon).

Figure 29: Variation in symmetric crustal accretion for the Pacific basin with preserved conjugate flanks (blue), and for spreading regions Pacific-Nazca/Farallon (pink), Pacific-West Antarctic (dark

blue), Bellingshausen-Pacific (gold), Cocos-Nazca (light blue), Cocos-Pacific (dark green); Juan de Fuca (JDF)-Pacific (maroon), and West Antarctic-Nazca (light green). Percentage (y-axes) refers to the percentage of the binned range of crustal asymmetry compared to all data points available for the spreading corridor.

Figure 30: Stage comparison of variations in crustal accretion for the Pacific-West Antarctic (blue; since chron 25y, 55.9 Ma), Pacific-Farallon/Nazca (pink) and Cocos-Pacific (green) spreading systems. Percentage (y-axes) refers to the percentage of the binned range of crustal asymmetry compared to all data points available for the spreading corridor.

Figure 31: Comparison of the implied convergence velocities along the North American margin, based on this study (filled: Cande and Kent, 1995; hollow: Ogg, 2012) and Seton et al. (2012). Van/JDF: Vancouver or Juan de Fuca plate.

Figure 32: Comparison of the implied convergence rate and obliquity from this study, in the timescales of Cande and Kent (1995; blue) and Ogg (2012; light blue), and Seton et al. (2012; orange) derived at three points along the North American margin. Convergence velocities are calculated in 5 Myr increments (except for the stage 83–80 Ma) based on the active plate at the time (labeled).

Figure 33: South Pacific plate configuration in the Early Cenozoic (~65 Ma). A: Plate boundaries from Seton et al. (2012). B: Plate boundaries from this study. Bellings: Bellingshausen

Figure 34: Comparison of the implied convergence velocities along the South American margin, based on this study (filled: Cande and Kent, 1995; hollow: Ogg, 2012) and Seton et al. (2012).

Figure 35: Comparison of the implied convergence rate and obliquity from this study, in the timescales of Cande and Kent (1995; blue) and Ogg (2012; light blue), and Seton et al. (2012; orange) derived at three points along the South American margin. Convergence velocities are calculated in 5 Myr increments (except for the stage 83–80 Ma) based on the active plate at the time (labeled). Since Seton et al. (2012) do not incorporate an Aluk plate, velocities between 83–20 Ma are based on their Farallon plate, and are compared with Farallon-South America relative motion derived from this model (red).

Figure 36: Age of the subducting oceanic crust at point 1 (48°N, 126.5°W), point 2 (38°N, 123°W), and point 3 (28°N, 116°W) along the North American trench. We derive the age of the subducting oceanic crust based on Farallon-Pacific symmetrical spreading (dark blue) and asymmetrical Farallon-Pacific spreading (light blue), based on the 'best-fit' ratio of Rowan and Rowley (2014). Age derived from Seton et al. (2012) is in orange. Grey regions refer to times where we rely on finite rotations for the down going plate (e.g. Pacific, Juan de Fuca).

Figure 37: Age of the subducting oceanic crust at point 1 (5°S, 81°W), point 2 (20°S, 76°W), and point 3 (45°S, 76°W) along the South American trench. We derive the age of the subducting oceanic crust based on Farallon-Pacific symmetrical spreading (dark blue) and asymmetrical Farallon-Pacific spreading (light blue), based on the 'best-fit' ratio of Rowan and Rowley (2014). Age of oceanic crust derived from Seton et al. (2012) is in orange. Grey regions refer to times where we rely on finite rotations for the down going plate (e.g. Nazca).

Table 1: Publications (with rotation parameters) for the Pacific plate relative to the West Antarctic plate. CNS: Cretaceous Normal Superchron

Source	Chrons	Age (Ma)	Comment
Cande et al. (1995)	31y–1o	67.7–0.8	Provides 95% confidence ellipses
Larter et al. (2002)	CNS–30r	90–67.7	Chrons 33y–30r are from Stock et al. (unpublished)
Eagles et al. (2004a)	33y–1c	73.6–0.4	Chron 31o and chrons 27o-1c are from Cande et al. (1995); chrons 33y, 32n1y, 30r, and 28r are from Stock et al. (unpublished)
Croon et al. (2008)	20o–1o	43.8–0.8	Provides 95% confidence ellipses
Müller et al. (2008)	34y–1o	83–0.8	Relies on the combination of Larter et al. (2002) (chrons 34y–31y) and Cande et al. (1995) (chrons 31y–1o)
Seton et al. (2012)	34y–1o	83–0.8	Same as Müller et al. (2008)
Wobbe et al. (2012)	CNS–20o	90–43.79	Relies only on new magnetic identifications presented within the study no uncertainties given
Wright et al. (2015)	30o–21o	67.6–47.9	Provides 95% confidence ellipses

Table 2: Finite rotations and covariance matrix for the Pacific plate relative to the West Antarctic plate

Chron	Age (Ma)	Lat (°N)	Lon (°E)	Angle (deg)	$\hat{\kappa}$	*dF*	*N*	*s*	*r*	*a*	*b*	*c*	*d*	*e*	*f*	*g*	Source
21o	47.9	74.431	-48.544	38.176	0.37	37	56	8	100.11	0.24	0.05	0.37	0.02	0.08	0.62	10^{-5}	(1)
24n.3o	53.3	73.474	-52.081	40.105	0.21	19	38	8	92.60	0.49	0.06	0.79	0.03	0.09	1.34	10^{-5}	(1)
25m	56.1	72.627	-54.727	41.142	0.36	18	35	7	49.40	0.87	0.16	1.21	0.06	0.22	1.76	10^{-5}	(1)
26o	57.9	72.317	-54.189	42.531	0.67	23	48	11	34.20	0.35	0.02	0.55	0.02	0.02	0.93	10^{-5}	(1)
27o	61.3	71.348	-54.157	45.498	1.25	31	44	5	24.78	1.84	-0.21	3.00	0.04	-0.33	5.00	10^{-5}	(1)
30o	67.6	68.941	-56.694	49.007	2.76	16	31	6	5.79	4.95	-0.26	7.47	0.06	-0.40	11.39	10^{-5}	(1)
33y	73.6	66.631	-57.357	52.776	0.35	39	52	5	112.32	1.67	0.00	2.24	0.02	0.02	3.09	10^{-5}	(2)

$\hat{\kappa}$ is the estimated quality factor, dF is the number of degrees of freedom, N is the number of datapoints, s is the number of great circle segments, and r is the total misfit. Variables $\hat{k}, a, b, c, d, e$ and f are in radians. The covariance matrix is defined as: $Cov(u) = \frac{g}{\hat{\kappa}} \begin{pmatrix} a & b & c \\ b & d & e \\ c & e & f \end{pmatrix}$ Sources: (1) Wright et al. (2015), (2) This study.

Table 3: Publications (with rotation parameters) for the Bellingshausen plate relative to the Pacific plate.

Source	Chrons	Age (Ma)	Comment
Stock and Molnar (1988)	30r–25c	67.7–56.1	Provides partial uncertainties
Larter et al. (2002)	33y–28r	73.6–63.8	Relies on Stock et al. (unpublished)
Eagles et al. (2004a)	33o–27o	79.08–61.3	Chrons 33y–28r are from Stock et al. (unpublished); chron 27o is from Cande et al. (2005)
Müller et al. (2008)	33y–27o	73.6–61.3	Same as Larter et al. (2002)
Seton et al. (2012)	33y–27o	73.6–61.2	Same as Müller et al. (2008)
Wobbe et al. (2012)	34y–27o	83–61.2	Relies only on new magnetic identifications presented within the study, and no uncertainties given

Table 4: Finite rotations and covariance matrix for the Bellingshausen plate relative to the Pacific plate.

Chron	Age (Ma)	Lat (°N)	Lon (°E)	Angle (deg)	$\hat{\kappa}$	*dF*	*N*	*s*	*r*	*a*	*b*	*c*	*d*	*e*	*f*	*g*
28o	63.63	-70.386	122.257	46.152	0.46	15	28	5	32.53	0.39	0.66	1.81	1.27	3.35	9.14	10^{-5}
30o	67.60	-71.101	129.504	52.623	1.01	7	20	5	6.94	0.18	0.43	0.98	1.35	2.92	6.60	10^{-5}
32n.1o	71.34	-71.655	137.499	59.611	0.55	9	18	3	16.29	0.51	0.91	2.41	1.87	4.80	12.84	10^{-5}
33y	73.60	-71.207	139.406	63.208	0.63	17	26	3	27.18	0.14	0.27	0.60	0.65	1.51	3.76	10^{-5}
33o	79.08	-70.107	144.208	70.971	0.54	27	36	3	49.98	0.07	0.16	0.32	0.74	1.56	3.65	10^{-5}

$\hat{\kappa}$ is the estimated quality factor, dF is the number of degrees of freedom, N is the number of datapoints, s is the number of great circle segments, and r is the total misfit. Variables $\hat{\kappa}, a, b, c, d, e$ and f are in radians. The covariance matrix is defined as: $Cov(u) = \frac{g}{\hat{\kappa}} \begin{pmatrix} a & b & c \\ b & d & e \\ c & e & f \end{pmatrix}$

Table 5: Pacific-Aluk spreading between chron 34y and 27o (83–61.3 Ma)

Stage		Half-stage			Full stage		
Chrons	Age (Ma)	Lat (°N)	Lon (°E)	Angle (°)	Lat (°N)	Lon (°E)	Angle (°)
27o–31y	61.3–67.7	-12.5	76.3	-6.13	-12.5	-76.3	-12.26
31y–34y	67.7–83	-53.9	132.0	-11.64	-53.9	132.0	-23.28

Table 6: Publications (with rotation parameters) for the Farallon plate relative to the Pacific plate between chron 34y and present-day

Source	Chrons	Age (Ma)	Comment
Pardo-Casas and Molnar (1987)	30r–5c	67.7–10.9	Finite rotations only
Rosa and Molnar (1988)	30r–13o	67.7–33.5	Half-stage rotations. Provides partial uncertainties
Stock and Molnar (1988)	30r–13o	67.7–33.5	From Rosa and Molnar (1988)
Müller et al. (2008)	34y–5n.2o	83–10.9	Finite rotations only. Provides rotations from 170 Ma
Seton et al. (2012)	34y–5n.2o	83–10.9	Same as Müller et al. (2008)
Rowan and Rowley (2014)	34y–10y	83–28.3	Half-stage rotations and finite rotations incorporating spreading asymmetry. Provides 95% confidence ellipses
Wright et al. (2015)	31y–13y	67.7–33.1	Half-stage rotations. Provides 95% confidence ellipses

Table 7: Half-stage rotations and covariance matrix for Farallon plate relative to the Pacific plate motion between chron 34y and 13y

Chron	Lat (°N)	Lon (°E)	Angle (deg.)	$\hat{\kappa}$	dF	*N*	*s*	*r*	*a*	*b*	*c*	*d*	*e*	*f*	*g*	Source
13y–18n.2o	-57.206	-119.683	5.796	0.24	51	76	11	208.82	8.49	8.83	0.24	11.90	0.27	1.90	10^{-7}	(1)

18n.2o–20o	-75.751	-90.302	2.765	0.30	51	74	10	172.34	10.45	9.08	-3.62	10.32	-3.58	2.94	10^{-7}	(1)
20o–21o	-59.482	-117.813	2.653	0.35	76	107	14	215.39	6.08	4.57	-1.72	4.95	-1.51	1.52	10^{-7}	(1)
21o–22o	-64.069	-111.485	0.954	0.99	105	138	15	105.87	3.20	2.11	-0.15	2.81	-0.24	0.68	10^{-7}	(1)
22o–24n.1y	-68.840	-104.776	1.147	3.19	57	80	10	17.86	6.18	3.79	-1.45	4.61	-1.30	1.61	10^{-7}	(1)
24n.1y–25y	-58.818	-119.609	1.591	0.60	71	96	11	118.99	6.58	4.17	-1.88	4.50	-1.51	1.65	10^{-7}	(1)
25y–26y	-61.494	-118.605	0.571	1.49	118	151	15	79.16	3.32	1.62	-1.70	2.15	-1.30	1.74	10^{-6}	(1)
26y–27o	-63.787	-117.523	1.177	0.87	87	114	12	99.97	6.28	3.34	-3.36	3.46	-2.31	2.87	10^{-7}	(1)
27o–28y	-52.581	-127.173	0.374	1.51	89	118	13	58.90	6.26	3.48	-3.34	3.36	-2.26	2.81	10^{-7}	(1)
28y–31y	-72.402	-102.630	1.881	0.61	122	145	10	198.70	4.84	2.05	-2.95	2.81	-2.01	2.82	10^{-7}	(1)
31y–33o	-60.674	-130.481	4.167	0.26	73	100	12	277.75	10.13	4.85	-6.11	3.98	-3.32	5.40	10^{-7}	(2)
33o–34y	-51.276	-140.757	1.493	0.28	77	102	11	271.81	4.45	1.47	-1.80	2.31	-0.87	1.79	10^{-7}	(2)

$\hat{\kappa}$ is the estimated quality factor, dF is the number of degrees of freedom, N is the number of datapoints, s is the number of great circle segments, and r is the total misfit. Variables $\hat{\kappa}, a, b, c, d, e$ and f are in radians. The covariance matrix is defined as: $Cov(u) = \frac{g}{\hat{\kappa}} \begin{pmatrix} a & b & c \\ b & d & e \\ c & e & f \end{pmatrix}$ Sources: (1) Wright et al. (2015), (2) This study.

Table 8: Publications (with rotation parameters) for the Vancouver plate relative to the Pacific plate

Source	Chrons	Age (Ma)	Comment
Rosa and Molnar (1988)	21y–13o	47.9–33.5	Half-stage rotations, includes partial uncertainties
Stock and Molnar (1988)	25c–13c	56.1–33.3	From Rosa and Molnar (1988), except for chron 21–25
Müller et al. (1997)	M21–5n.2o	147.7–10.9	Finite rotations
Seton et al. (2012)	24n.1y–5n.2o	52.4–10.9	Same as Müller et al. (1997)
McCrory and Wilson (2013)	24n.1y–18n.2o	52.4–40.1	Given as finite rotations
Wright et al. (2015)	24n.1y–13y	52.4–33.1	Half-stage rotations, includes 95% confidence ellipses

Table 9: Half-stage rotations for the Juan de Fuca plate relative to the Pacific plate between chron 10n.1y and 4Ac

Chron	Age (Ma)	Lat (+ °N)	Lon (+ °E)	Angle (deg)
4Ac–5n.2y	8.9–9.9	-65.32	50.03	1.91
5n.2y–6o	9.9–20.1	74.17	58.19	-3.11
6o–10n.1y	20.1–28.3	-70.34	39.23	8.58

Table 10: Half-stage rotations and covariance matrix for the Vancouver plate relative to the Pacific plate between 24n.1y and 10n.1y

Chron	Lat	Lon	Angle	$\hat{\kappa}$	dF	N	s	r	a	b	c	d	e	f	g	Source

	(°N)	(°E)	(deg.)													
10n.1y–13y	-75.414	35.037	5.135	1.92	79	100	9	41.14	1.96	1.59	-2.57	1.65	-2.33	3.76	10^{-6}	(2)
13y–18n.2o	-72.935	38.385	7.125	0.44	66	85	8	149.22	6.23	4.18	-8.02	3.10	-5.55	10.64	10^{-6}	(1)
18n.2o–21o	-71.865	39.600	6.217	1.41	49	66	7	34.78	5.06	2.94	-6.00	2.13	-3.72	7.50	10^{-6}	(1)
21o–22o	-71.145	37.555	1.319	2.32	35	52	7	15.06	7.80	3.91	-8.96	2.35	-4.72	10.72	10^{-6}	(1)
22o–24n.1y	-71.810	36.938	1.454	0.91	25	40	6	27.34	8.22	5.11	-9.40	3.65	-6.20	11.42	10^{-6}	(1)

$\hat{\kappa}$ is the estimated quality factor, dF is the number of degrees of freedom, N is the number of datapoints, s is the number of great circle segments, and r is the total misfit. Variables $\hat{\kappa}, a, b, c, d, e$ and f are in radians. The covariance matrix is defined as: $Cov(u) = \frac{g}{\hat{\kappa}} \begin{pmatrix} a & b & c \\ b & d & e \\ c & e & f \end{pmatrix}$ Sources: (1) Wright et al. (2015), (2) This study.

Table 11: Publications (with rotation parameters) for the Kula plate relative to the Pacific plate

Source	Chrons	Age (Ma)	Comment
Rosa and Molnar (1988)	30o–25m	67.6–56.1	Half-stage rotations. Provides partial uncertainties
Stock and Molnar (1988)	30o–25m	67.6–56.1	From Rosa and Molnar (1988)
Müller et al. (2008)	33o–18r	79.1–41	Finite rotations only
Seton et al. (2012)	33o–18r	79.1–41	From Müller et al. (2008)

Table 12: Half-stage rotation parameters and covariance matrix for the Kula plate relative to the Pacific plate motion.

Chron	Lat (°N)	Lon (°E)	Angle (deg.)	$\hat{\kappa}$	*dF*	*N*	*s*	*r*	*a*	*b*	*c*	*d*	*e*	*f*	*g*
25y–27o	-35.641	-48.924	1.373	2.65	75	90	6	28.26	4.15	0.89	-4.66	0.28	-1.02	5.94	10^{-6}
27o–31y	-30.598	-54.473	1.977	1.42	65	80	6	45.83	5.60	1.11	-6.29	0.32	-1.27	7.78	10^{-6}
31y–33y	-34.237	-47.824	3.744	0.25	41	58	7	162.27	1.37	0.15	-1.52	0.04	-0.17	1.73	10^{-5}
33y–34y	17.454	-105.400	2.253	3.39	13	28	6	3.84	16.55	0.98	-16.89	0.12	-0.99	17.28	10^{-5}

$\hat{\kappa}$ is the estimated quality factor, dF is the number of degrees of freedom, N is the number of datapoints, s is the number of great circle segments, and r is the total misfit. Variables $\hat{\kappa}, a, b, c, d, e$ and f are in radians. The covariance matrix is defined as: $Cov(u) = \frac{g}{\hat{\kappa}} \begin{pmatrix} a & b & c \\ b & d & e \\ c & e & f \end{pmatrix}$

Table 13: Summary of finite rotation parameters for the Pacifc basin since chron 34y

Chron	**Age**	**Latitude**	**Longitude**	**Angle**	**Source**
Pacific plate with respect to the West Antarctic plate					
5n.2o	10.9	70.36	-77.81	9.48	Croon et al. (2008)
6o	20.1	74.0	-70.16	16.73	Croon et al. (2008)
13y	33.1	74.5	-64.6	26.97	Derived from Croon et al. (2008)
18n.2o	40.1	74.87	-54.46	32.62	Croon et al. (2008)
21o	47.9	74.43	-48.54	38.18	Wright et al. (2015)

25y	55.9	73.0	-51.4	42.26	Derived from Wright et al. (2015)
31y	67.7	68.9	-56.7	49.07	Derived from Wright et al. (2015)
34y	83	63.6	-58.1	58.8	This study
Bellingshausen plate with respect to the Pacific plate					
27o	61.3	71.35	-54.16	-45.50	Crossover
31y	67.7	-71.07	129.93	52.72	This study
33o	79.1	-70.0441	144.3016	70.8871	This study
Aluk plate with respect to the West Antarctic plate					
5n.2o	10.9	-69.46	-89.6	12.4	Eagles and Scott (2014)
6o	20.1	-68.43	-89.45	32.3	Eagles and Scott (2014)
13y	33.1	-70.28	-106.31	40.72	Derived from Eagles and Scott (2014)
18n.2o	40.1	-70.77	-110.04	45.54	Eagles and Scott (2014)
21o	47.9	-71.67	-110.33	62.69	Derived from Eagles and Scott (2014)
25y	55.9	-71.82	-115.41	70.75	Derived from Eagles and Scott (2014)
27o	61.3	-71.48	-123.18	79.06	Eagles and Scott (2014)
Aluk plate with respect to the Pacific plate					
27o	61.3	70.3037	16.2941	-120.1011	Crossover
31y	67.7	66.2195	0.688	-120.9605	This study
34y	83	61.2364	-4.1952	-142.0441	This study
Farallon plate with respect to the Pacific plate					
5n.2o	10.9	60.11	-89.75	-14.88	Müller et al. (2008)
	23	73.53	-92.61	-31.08	Müller et al. (2008)
13y	33.1	76.1	-110.7	-45.27	Derived from Tebbens and Cande (1997)
18n.2o	40.1	84.45	-138.06	-53.87	Wright et al. (2015)
21o	47.9	85.5	168.93	-63.57	Wright et al. (2015)
25y	55.9	84.14	138.7	-70.14	Wright et al. (2015)
31y	67.7	82.43	124.34	-77.55	Wright et al. (2015)
33o	79.1	80.29	111.03	-84.97	This study
34y	83.0	79.29	106.41	-87.38	This study
Nazca plate with respect to the Pacific plate					
	5.0	60.08	-91.23	-7.13	Derived from Tebbens and Cande (1997) and Croon et al. (2008)
5n.2o	10.9	63.42	-91.82	-16.54	Derived from Tebbens and Cande (1997) and Croon et al. (2008)
	15.0	64.98	-91.73	-22.83	Derived from Tebbens and Cande (1997) and Croon et al. (2008)
6o	20.1	62.38	-93.02	-31.01	Tebbens and Cande (1997)
6Bn.1c	22.7	63.42	-94.11	-35.51	Derived from Tebbens and Cande (1997) and Croon et al. (2008)
Cocos plate with respect to the Pacific plate					
	5	39.13	-108.6	-10.25	Müller et al. (2008)
	10.0	35.3	-105.6	-25.08	Müller et al. (2008)
	11.9	36.0	-107.7	-30.27	Wilson (1996)
	13.0	36.7	-109.1	-32.66	Wilson (1996)
	14.8	38.3	-111.8	-36.33	Wilson (1996)
	17.3	39.3	-114.9	-42.45	Wilson (1996)
	20.0	40.42	-117.81	-47.44	Müller et al. (2008)
6Bn.1c	22.7	39.8	-119.7	-54.29	Müller et al. (2008)
Juan de Fuca/Vancouver plate with respect to the Pacific plate					
5n.2o	10.9	80.5	-38.8	-8.92	This study
6o	20.1	82.6	12.21	-14.34	This study
10n.1y	28.3	81.35	-117.91	-30.67	This study
13y	33.1	79.74	-125.38	-40.87	Wright et al. (2015)
18n.2o	40.1	77.74	-128.25	-55.02	Wright et al. (2015)
21o	47.9	76.45	-128.91	-67.38	Wright et al. (2015)
22o	49.7	76.2	-129.07	-70.0	Wright et al. (2015)
24n.1y	52.4	75.96	-129.3	-72.9	Wright et al. (2015)
Kula plate with respect to the Pacific plate					
19y	41.3	28.06	-56.8	0.11	This study

21o	47.9	27.14	-58.12	3.74	This study
25y	55.9	37.5205	153.3348	-24.1859	This study
27o	61.3	37.141	151.0921	-26.8115	This study
31y	67.7	35.9891	147.8721	-30.5089	This study
33y	73.6	35.1337	144.8728	-37.8426	This study
34y	83.0	30.2191	139.2524	-38.5042	This study
Bauer microplate with respect to the Pacific plate					
4n.1y	7.4	-28.0	-103.0	-3.9	Seton et al. (2012)
5n.2o	10.9	-27.25	-101.3	-19.3	Seton et al. (2012)
15.2	15.2	-24.86	-98.5	-40.63	Seton et al. (2012)
Mathematician microplate with respect to the Pacific plate					
3n.4c	5.1	27.7	-109.7	-6.29	DeMets and Traylen (2000)
5n.2o	10.9	-16.7	-115.6	9.39	DeMets and Traylen (2000)
Rivera microplate with respect to the Pacific plate					
1o	0.8	26.7	-105.2	-3.66	DeMets and Traylen (2000)
3n.4c	5.1	28.0	-105.7	-19.5	DeMets and Traylen (2000)
5n.2y	9.9	31.9	-106.0	-27.2	DeMets and Traylen (2000)

7 References

Adam, C., Yoshida, M., Suetsugu, D., Fakao, T. and Cadio, C., 2014. Geodynamic modeling of the South Pacific superswell. Physics of the Earth and Planetary Interiors, 229: 24-39

Amante, C. and Eakins, B., 2009. Arc-minute global relief model: procedures, data sources and analysis (ETOPO1). NOAA, National Geophysical Data Center, Colorado, USA.

Atwater, T., 1989. Plate tectonic history of the northeast Pacific and western North America. The eastern Pacific Ocean and Hawaii: Boulder, Colorado, Geological Society of America, Geology of North America, v. N: 21-72.

Atwater, T., Sclater, J., Sandwell, D., Severinghaus, J. and Marlow, M.S., 1993. Fracture zone traces across the North Pacific Cretaceous Quiet Zone and their tectonic implications. The Mesozoic Pacific: Geology, Tectonics, and Volcanism: 137-154.

Atwater, T. and Severinghaus, J., 1989. Tectonic maps of the northeast Pacific. The Geology of North America: 15-20.

Atwater, T. and Stock, J., 1998. Pacific-North America plate tectonics of the Neogene southwestern United States: an update. International Geology Review, 40(5): 375-402.

Barckhausen, U., Bagge, M. and Wilson, D.S., 2013. Seafloor spreading anomalies and crustal ages of the Clarion-Clipperton Zone. Marine Geophysical Research: 1-10.

Barckhausen, U., Ranero, C.R., Cande, S.C., Engels, M. and Weinrebe, W., 2008. Birth of an intraoceanic spreading center. Geology, 36(10): 767-770.

Barckhausen, U., Ranero, C.R., Huene, R.v., Cande, S.C. and Roeser, H.A., 2001. Revised tectonic boundaries in the Cocos Plate off Costa Rica: Implications for the segmentation of the convergent margin and for plate tectonic models. Journal of Geophysical Research: Solid Earth (1978–2012), 106(B9): 19207-19220.

Barker, P., 1982. The Cenozoic subduction history of the Pacific margin of the Antarctic Peninsula: ridge crest–trench interactions. Journal of the Geological Society, 139(6): 787-801.

Berggren, W.A., Kent, D.V., Flynn, J.J. and Van Couvering, J.A., 1985. Cenozoic geochronology.

Geological Society of America Bulletin, 96(11): 1407-1418.

Bird, P., 2003. An updated digital model of plate boundaries. Geochemistry, Geophysics, Geosystems, 4(3).

Bohannon, R.G. and Parsons, T., 1995. Tectonic implications of post–30 Ma Pacific and North American relative plate motions. Geological Society of America Bulletin, 107(8): 937-959.

Boyden, J.A., Müller, R.D., Gurnis, M., Torsvik, T.H., Clark, J.A., Turner, M., Ivey-Law, H., Watson, R.J. and Cannon, J.S., 2011. Next-generation plate-tectonic reconstructions using GPlates. Geoinformatics: cyberinfrastructure for the solid earth sciences: 95-114.

Breitsprecher, K., Thorkelson, D., Groome, W. and Dostal, J., 2003. Geochemical confirmation of the Kula-Farallon slab window beneath the Pacific Northwest in Eocene time. Geology, 31(4): 351-354.

Breitsprecher, K. and Thorkelson, D.J., 2009. Neogene kinematic history of Nazca–Antarctic–Phoenix slab windows beneath Patagonia and the Antarctic Peninsula. Tectonophysics, 464(1): 10-20.

Byrne, T., 1979. Late Paleocene demise of the Kula-Pacific spreading center. Geology, 7(7): 341-344.

Cande, S., Herron, E. and Hall, B., 1982. The early Cenozoic tectonic history of the southeast Pacific. Earth and Planetary Science Letters, 57(1): 63-74.

Cande, S.C. and Haxby, W.F., 1991. Eocene propagating rifts in the southwest Pacific and their conjugate features on the Nazca plate. Journal of Geophysical Research: Solid Earth (1978–2012), 96(B12): 19609-19622.

Cande, S.C. and Kent, D.V., 1995. Revised calibration of the geomagnetic polarity timescale for the Late Cretaceous and Cenozoic. Journal of Geophysical Research: Solid Earth, 100(B4): 6093-6095.

Cande, S.C., Raymond, C.A., Stock, J. and Haxby, W.F., 1995. Geophysics of the Pitman Fracture Zone and Pacific-Antarctic Plate. Science, 270: 10.

Cande, S.C., Stock, J.M., Müller, R.D. and Ishihara, T., 2000. Cenozoic motion between east and west Antarctica. Nature, 404(6774): 145-150.

Chang, T., 1987. On the statistical properties of estimated rotations. Journal of Geophysical Research: Solid Earth (1978–2012), 92(B7): 6319-6329.

Chang, T., 1988. Estimating the relative rotation of two tectonic plates from boundary crossings. Journal of the American Statistical Association, 83(404): 1178-1183.

Clague, D.A. and Dalrymple, G.B., 1987. The Hawaiian-Emperor volcanic chain. Part I. Geologic evolution. Volcanism in Hawaii, 1: 5-54.

Cochran, J.R., 1986. Variations in subsidence rates along intermediate and fast spreading mid-ocean ridges. Geophysical Journal International, 87(2): 421-454.

Conder, J.A., Forsyth, D.W. and Parmentier, E., 2002. Asthenospheric flow and asymmetry of the East Pacific Rise, MELT area. Journal of Geophysical Research: Solid Earth (1978–2012), 107(B12): ETG 8-1-ETG 8-13.

Croon, M.B., Cande, S.C. and Stock, J.M., 2008. Revised Pacific ‑ Antarctic plate motions and geophysics of the Menard Fracture Zone. Geochemistry, Geophysics, Geosystems, 9(7).

Cross, T.A. and Pilger, R.H., 1982. Controls of subduction geometry, location of magmatic arcs, and tectonics of arc and back-arc regions. Geological Society of America Bulletin, 93(6): 545-562.

Cunningham, A.P., Larter, R.D., Barker, P.F., Gohl, K. and Nitsche, F.O., 2002. Tectonic evolution of the Pacific margin of Antarctica 2. Structure of Late Cretaceous–early Tertiary plate boundaries in the Bellingshausen Sea from seismic reflection and gravity data. Journal of Geophysical Research: Solid Earth (1978–2012), 107(B12): EPM 6-1-EPM 6-20.

Davy, B., 2006. Bollons Seamount and early New Zealand–Antarctic seafloor spreading. Geochemistry, Geophysics, Geosystems, 7(6).

DeMets, C. and Traylen, S., 2000. Motion of the Rivera plate since 10 Ma relative to the Pacific and North American plates and the mantle. Tectonophysics, 318(1): 119-159.

Eagles, G., 2004. Tectonic evolution of the Antarctic–Phoenix plate system since 15 Ma. Earth and Planetary Science Letters, 217(1): 97-109.

Eagles, G., Gohl, K. and Larter, R.D., 2004a. High-resolution animated tectonic reconstruction of the South Pacific and West Antarctic margin. Geochemistry Geophysics Geosystems, 5(7): Q07002.

Eagles, G., Gohl, K. and Larter, R.D., 2004b. Life of the Bellingshausen plate. Geophysical research letters, 31(7).

Eagles, G. and Scott, B.G., 2014. Plate convergence west of Patagonia and the Antarctic Peninsula since 61Ma. Global and Planetary Change, 123: 189-198.

Eakins, B.W. and Lonsdale, P.F., 2003. Structural patterns and tectonic history of the Bauer microplate, Eastern Tropical Pacific. Marine Geophysical Researches, 24(3-4): 171-205.

Elvers, D., Peter, G. and Moses, R., 1967. Analysis of magnetic lineations in the North Pacific. Eos Trans. AGU, 48: 89.

Engebretson, D.C., Cox, A. and Gordon, R.G., 1985. Relative motions between oceanic and continental plates in the Pacific basin. Geological Society of America Special Papers, 206: 1-60.

England, P. and Wortel, R., 1980. Some consequences of the subduction of young slabs. Earth and Planetary Science Letters, 47(3): 403-415.

Evans, R., Tarits, P., Chave, A., White, A., Heinson, G., Filloux, J., Toh, H., Seama, N., Utada, H. and Booker, J., 1999. Asymmetric electrical structure in the mantle beneath the East Pacific Rise at 17 S. Science, 286(5440): 752-756.

Gaina, C., Müller, D.R., Royer, J.Y., Stock, J., Hardebeck, J. and Symonds, P., 1998. The tectonic history of the Tasman Sea: a puzzle with 13 pieces. Journal of Geophysical Research: Solid Earth (1978–2012), 103(B6): 12413-12433.

Gee, J.S. and Kent, D.V., 2007. Source of oceanic magnetic anomalies and the geomagnetic polarity timescale. Treatise on Geophysics, Vol. 5: Geomagnetism: 455-507.

Gohl, K., Teterin, D., Eagles, G., Netzeband, G., Grobys, J., Parsiegla, N., Schlüter, P., Leinweber, V.T., Larter, R.D. and Uenzelmann-Neben, G., 2007. Geophysical survey reveals tectonic structures in the Amundsen Sea embayment, West Antarctica. US Geological Survey Open-File Report, 2007-1047

Granot, R., Cande, S., Stock, J. and Damaske, D., 2013. Revised Eocene - Oligocene kinematics for the West Antarctic rift system. Geophysical research letters: 1-6.

Granot, R., Cande, S.C. and Gee, J.S., 2009. The implications of long-lived asymmetry of remanent magnetization across the North Pacific fracture zones. Earth and Planetary Science Letters, 288(3): 551-563.

Grow, J.A. and Atwater, T., 1970. Mid-Tertiary tectonic transition in the Aleutian Arc. Geological Society of America Bulletin, 81(12): 3715-3722.

Harry, D.L. and Green, N.L., 1999. Slab dehydration and basalt petrogenesis in subduction systems involving very young oceanic lithosphere. Chemical Geology, 160(4): 309-333.

Haeussler, P.J, Bradley, D.C., Wells, R.E. & Miller, M.L. 2003. 'Life and death of the Resurrection plate: Evidence for its existence and subduction in the northeastern Pacific in Paleocene–Eocene time.' Geological Society of America Bulletin, 115(7): 867-880.

Hellinger, S., 1981. The uncertainties of finite rotations in plate tectonics. Journal of Geophysical Research: Solid Earth (1978–2012), 86(B10): 9312-9318.

Herron, E. and Tucholke, B., 1976. Sea-floor magnetic patterns and basement structure in the southeastern Pacific. Initial Reports of the Deep Sea Drilling Project, 35: 263-278.

Hey, R., 1977. Tectonic evolution of the Cocos-Nazca spreading center. Geological Society of America Bulletin, 88(10): 1404-1420.

Hilde, T.W., Uyeda, S. and Kroenke, L., 1977. Evolution of the western Pacific and its margin. Tectonophysics, 38(1): 145-165.

Iaffaldano, G., Hawkins, R., Bodin, T., Sambridge, M., 2014. REDBACK: open-source software for efficient noise-reduction in plate kinematic reconstructions. Geochemistry Geophysics

Geosystems, v. 15, p. 1663-1670

Jicha, B. R., Scholl, D. W., and Rea, D. K. 2009. Circum-Pacific arc flare-ups and global cooling near the Eocene-Oligocene boundary. Geology, 37(4), 303-306.

Kirkwood, B.H., Royer, J.-Y., Chang, T.C. and Gordon, R.G., 1999. Statistical tools for estimating and combining finite rotations and their uncertainties. Geophysical Journal International, 137(2): 408-428.

Klitgord, K.D. and Mammerickx, J., 1982. Northern East Pacific Rise: magnetic anomaly and bathymetric framework. Journal of Geophysical Research: Solid Earth (1978–2012), 87(B8): 6725-6750.

Larson, R.L. and Chase, C.G., 1972. Late Mesozoic evolution of the western Pacific Ocean. Geological Society of America Bulletin, 83(12): 3627-3644.

Larter, R.D. and Barker, P.F., 1991. Effects of ridge crest ‐ trench interaction on Antarctic ‐ Phoenix Spreading: Forces on a young subducting plate. Journal of Geophysical Research: Solid Earth (1978ety of America Bulletin, 83(1

Larter, R.D., Cunningham, A.P., Barker, P.F., Gohl, K. and Nitsche, F.O., 2002. Tectonic evolution of the Pacific margin of Antarctica 1. Late Cretaceous tectonic reconstructions. Journal of Geophysical Research, 107(B12): 2345.

Liu, Z., 1996, The Origin and Evolution of the Easter Seamount Chain, Doctoral thesis, University of South Florida, St. Petersburg, 266 pp.

Livermore, R., Balanyá, J.C., Maldonado, A., Martínez, J.M., Rodríguez-Fernández, J., de Galdeano, C.S., Zaldívar, J.G., Jabaloy, A., Barnolas, A. and Somoza, L., 2000. Autopsy on a dead spreading center: the Phoenix Ridge, Drake Passage, Antarctica. Geology, 28(7): 607-610.

Lonsdale, P., 1986. Tectonic and magmatic ridges in the Eltanin fault system, South Pacific. Marine geophysical researches, 8(3): 203-242.

Lonsdale, P., 1988. Paleogene history of the Kula plate: Offshore evidence and onshore implications. Geological Society of America Bulletin, 100(5): 733-754.

Lonsdale, P., 1991. Structural patterns of the Pacific floor offshore of peninsular California. The gulf and peninsular province of the Californias, 47: 87-125.

Lonsdale, P., 2005. Creation of the Cocos and Nazca plates by fission of the Farallon plate. Tectonophysics, 404(3): 237-264.

Mammerickx, J., Naar, D. and Tyce, R., 1988. The mathematician paleoplate. Journal of Geophysical Research: Solid Earth (1978–2012), 93(B4): 3025-3040.

Mammerickx, J. and Sharman, G., 1988. Tectonic evolution of the North Pacific during the Cretaceous quiet period. Journal of Geophysical Research: Solid Earth (1978–2012), 93(B4): 3009-3024.

Matthews, K.J., Müller, R.D., Wessel, P. and Whittaker, J.M., 2011. The tectonic fabric of the ocean basins. Journal of Geophysical Research: Solid Earth (1978–2012), 116(B12).

Matthews, K.J., Williams, S.E., Whittaker, J.M., Müller, R.D., Seton, M. and Clarke, G.L., 2015. Geologic and kinematic constraints on Late Cretaceous to mid Eocene plate boundaries in the southwest Pacific. Earth-Science Reviews, 140: 72-107.

Mayes, C.L., Lawver, L.A. and Sandwell, D.T., 1990. Tectonic history and new isochron chart of the South Pacific. Journal of Geophysical Research: Solid Earth (1978–2012), 95(B6): 8543-8567.

McCarron, J.J. and Larter, R.D., 1998. Late Cretaceous to early Tertiary subduction history of the Antarctic Peninsula. Journal of the Geological Society, 155(2): 255-268.

McCarthy, M.C., Kruse, S.E., Brudzinski, M.R. and Ranieri, M.E., 1996. Changes in plate motions and the shape of Pacific fracture zones. Journal of Geophysical Research: Solid Earth (1978–2012), 101(B6): 13715-13730.

McCrory, P.A. and Wilson, D.S., 2013. A kinematic model for the formation of the Siletz‐Crescent forearc terrane by capture of coherent fragments of the Farallon and Resurrection plates. Tectonics, 32(3): 718-736.

Menard, H., 1978. Fragmentation of the Farallon plate by pivoting subduction. The Journal of Geology: 99-110.

Meschede, M. and Barckhausen, U., 2000. 7. Plate Tectonic Evolution of the Cocos-Nazca Spreading Center.

Meschede, M., Barckhausen, U., Engels, M. and Weinrebe, W., 2008. The trace of the Pacific – Cocos – Nazca triple junction in the Central Pacific and the formation of an overlapping spreading centre. Terra Nova, 20(3): 246-251.

Molnar, P. and Atwater, T., 1978. Interarc spreading and Cordilleran tectonics as alternates related to the age of subducted oceanic lithosphere. Earth and Planetary Science Letters, 41(3): 330-340.

Molnar, P., Atwater, T., Mammerickx, J. and Smith, S.M., 1975. Magnetic anomalies, bathymetry and the tectonic evolution of the South Pacific since the Late Cretaceous. Geophysical Journal International, 40(3): 383-420.

Müller, R.D, Gohl, K., Cande, S., Goncharov, A. and Golynsky, A., 2007. Eocene to Miocene geometry of the West Antarctic rift system. Australian Journal of Earth Sciences, 54(8): 1033-1045.

Müller, R.D., Roest, W.R. and Royer, J.-Y., 1998. Asymmetric sea-floor spreading caused by ridge–plume interactions. Nature, 396(6710): 455-459.

Müller, R.D., Roest, W.R., Royer, J.Y., Gahagan, L.M. and Sclater, J.G., 1997. Digital isochrons of the world's ocean floor. Journal of Geophysical Research: Solid Earth (1978–2012), 102(B2): 3211-3214.

Müller, R.D., Sandwell, D.T., Tucholke, B.E., Sclater, J.G. and Shaw, P.R., 1991. Depth to basement and geoid expression of the Kane Fracture Zone: A comparison. Marine geophysical researches, 13(2): 105-129.

Müller, R.D., Sdrolias, M., Gaina, C. and Roest, W.R., 2008. Age, spreading rates, and spreading asymmetry of the world's ocean crust. Geochemistry, Geophysics, Geosystems, 9(4).

Müller, R.D., Seton, M., Zahirovic, S., Williams, S.E., Matthews, K.J., Wright, N.M., Shephard, G.E., Maloney, K.T., Barnett-Moore, N., Hosseinpour, M., Bower, D.J., and Cannon, J. In press. Ocean basin evolution and global-scale plate reorganization events since Pangea breakup. Annual Review of Earth and Planetary Sciences.

Munschy, M., Antoine, C. and Gachon, A., 1996. Evolution tectonique de la région des Tuamotu, océan Pacifique Central. Comptes rendus de l'Académie des sciences. Série 2. Sciences de la terre et des planètes, 323(11): 941-948.

Nakanishi, M., Tamaki, K. and Kobayashi, K., 1989. Mesozoic magnetic anomaly lineations and seafloor spreading history of the northwestern Pacific. Journal of Geophysical Research: Solid Earth (1978–2012), 94(B11): 15437-15462.

Nicholson, C., Sorlien, C.C., Atwater, T., Crowell, J.C. and Luyendyk, B.P., 1994. Microplate capture, rotation of the western Transverse Ranges, and initiation of the San Andreas transform as a low-angle fault system. Geology, 22(6): 491-495.

Norton, I.O., 2007. Speculations on Cretaceous tectonic history of the northwest Pacific and a tectonic origin for the Hawaii hotspot. Geological Society of America Special Papers, 430: 451-470.

O'Connor, J.M., Steinberger, B., Regelous, M., Koppers, A.A., Wijbrans, J.R., Haase, K.M., Stoffers, P., Jokat, W. and Garbe-Schönberg, D., 2013. Constraints on past plate and mantle motion from new ages for the Hawaiian-Emperor Seamount Chain. Geochemistry, Geophysics, Geosystems, 14(10): 4564-4584.

Ogg, J.G., 2012. Chapter 5 - Geomagnetic Polarity Time Scale. In: F.M. Gradstein, J.G.O.D. Schmitz and G.M. Ogg (Editors), The Geologic Time Scale. Elsevier, Boston, pp. 85-113.

Pardo-Casas, F. and Molnar, P., 1987. Relative motion of the Nazca (Farallon) and South American plates since Late Cretaceous time. Tectonics, 6(3): 233-248.

Pitman, W.C., Herron, E. and Heirtzler, J., 1968. Magnetic anomalies in the Pacific and sea floor spreading. Journal of Geophysical Research, 73(6): 2069-2085.

Ramos, V.A., 2005. Seismic ridge subduction and topography: Foreland deformation in the Patagonian Andes. Tectonophysics, 399(1): 73-86.

Rea, D.K. and Dixon, J.M., 1983. Late Cretaceous and Paleogene tectonic evolution of the north Pacific Ocean. Earth and Planetary Science Letters, 65(1): 145-166.

Rosa, J.W.C. and Molnar, P., 1988. Uncertainties in reconstructions of the Pacific, Farallon, Vancouver, and Kula plates and constraints on the rigidity of the Pacific and Farallon (and Vancouver) plates between 72 and 35 Ma. Journal of Geophysical Research: Solid Earth (1978–2012), 93(B4): 2997-3008.

Rouzo, S., Rabinowicz, M. and Briais, A., 1995. Segmentation of mid-ocean ridges with an axial valley induced by small-scale mantle convection. Nature, 374(6525): 795–798.

Rowan, C.J. and Rowley, D.B., 2014. Spreading behaviour of the Pacific-Farallon ridge system since 83 Ma. Geophysical Journal International: ggu056.

Royer, J.-Y., Gordon, R.G., DeMets, C. and Vogt, P., 1997. New limits on India/Australia motion since Chron5 (11 Ma) and implications for the lithospheric deformation in the Equatorial Indian Ocean. Geophysical Journal International, 128: 41-74.

Royer, J.Y. and Chang, T., 1991. Evidence for relative motions between the Indian and Australian plates during the last 20 my from plate tectonic reconstructions: Implications for the deformation of the Indo‐Australian plate. Journal of Geophysical Research: Solid Earth (1978–2012), 96(B7): 11779-11802.

Sandwell, D.T., Müller, R.D., Smith, W.H., Garcia, E. and Francis, R., 2014. New global marine gravity model from CryoSat-2 and Jason-1 reveals buried tectonic structure. science, 346(6205): 65-67.

Sandwell, D.T. and Smith, W.H., 2009. Global marine gravity from retracked Geosat and ERS-1 altimetry: Ridge segmentation versus spreading rate. Journal of Geophysical Research: Solid Earth (1978del from CryoSat

Scalabrino, B., Lagabrielle, Y., de la Rupelle, A., Malavieille, J., Polvé, M., Espinoza, F., Morata,

D. and Suarez, M., 2009. Subduction of an active spreading ridge beneath southern South America: A review of the Cenozoic geological records from the Andean foreland, central Patagonia (46–47 S), Subduction Zone Geodynamics. Springer, pp. 227-246.

Scholl, D.W., Vallier, T.L. and Stevenson, A.J., 1986. Terrane accretion, production, and continental growth: A perspective based on the origin and tectonic fate of the Aleutian–Bering Sea region. Geology, 14(1): 43-47.

Seton, M., Müller, R.D., Zahirovic, S., Gaina, C., Torsvik, T., Shephard, G., Talsma, A., Gurnis, M., Turner, M. and Chandler, M., 2012. Global continental and ocean basin reconstructions since 200 Ma. Earth-Science Reviews.

Seton, M., Whittaker, J.M., Wessel, P., Müller, R.D., DeMets, C., Merkouriev, S., Cande, S., Gaina, C., Eagles, G., Granot, R., Stock, J., Wright, N. and Williams, S.E., 2014. Community infrastructure and repository for marine magnetic identifications. Geochemistry, Geophysics, Geosystems, 15(4): 1629-1641.

Severinghaus, J. and Atwater, T., 1990. Cenozoic geometry and thermal state of the subducting slabs beneath western North America. Geological Society of America Memoirs, 176: 1-22.

Somoza, R. and Ghidella, M.E., 2012. Late Cretaceous to recent plate motions in western South America revisited. Earth and Planetary Science Letters, 331: 152-163.

Stevenson, A.J., Scholl, D.W. and Vallier, T.L., 1983. Tectonic and geologic implications of the Zodiac fan, Aleutian Abyssal Plain, northeast Pacific. Geological Society of America Bulletin, 94(2): 259–273.

Stewart, R.J., 1976. Turbidites of the Aleutian abyssal plain: Mineralogy, provenance, and constraints for Cenozoic motion of the Pacific plate. Geological Society of America Bulletin, 87:793-808

Stock, J. and Lee, J., 1994. Do microplates in subduction zones leave a geological record? Tectonics, 13(6): 1472-1487

Stock, J. and Molnar, P., 1987. Revised history of early Tertiary plate motion in the south-west

Pacific. Nature, 325(6104): 495-499.

Stock, J. and Molnar, P., 1988. Uncertainties and implications of the Late Cretaceous and Tertiary position of North America relative to the Farallon, Kula, and Pacific plates. Tectonics, 7(6): 1339-1384.

Suess, E., Bohrmann, G., Huene, R., Linke, P., Wallmann, K., Lammers, S., ... & Orange, D. (1998). Fluid venting in the eastern Aleutian subduction zone. Journal of Geophysical Research: Solid Earth (1978–2012), 103(B2), 2597-2614.

Tarduno, J., Bunge, H.-P., Sleep, N. and Hansen, U., 2009. The bent Hawaiian-Emperor hotspot track: Inheriting the mantle wind. Science, 324(5923): 50-53.

Tebbens, S. and Cande, S., 1997. Southeast Pacific tectonic evolution from early Oligocene to Present. Journal of Geophysical Research, 102(B6): 12061-12,084.

Torsvik, T.H., Müller, R.D., Van der Voo, R., Steinberger, B. and Gaina, C., 2008. Global plate motion frames: toward a unified model. Reviews of Geophysics, 46(3).

Vallier, T.L., Mortera-Gutierrez, C.A., Karl, H.A., Masson, D.G., Prueher, L. and Chase, T.E., 1996. 18 Geology of the Kula Paleo-Plate, North Pacific Ocean. Geology of the United States' seafloor: the view from GLORIA: 333.

Vlastelic, I., Aslanian, D., Dosso, L., Bougault, H., Olivet, J. L., & Geli, L. (1999). Large-scale chemical and thermal division of the Pacific mantle. *Nature*, *399*(6734), 345-350.

Weissel, J.K., Hayes, D.E. and Herron, E.M., 1977. Plate tectonics synthesis: the displacements between Australia, New Zealand, and Antarctica since the Late Cretaceous. Marine geology, 25(1): 231-277.

Wessel, P., Matthews, K.J., Müller, R.D., Mazzoni, A., Whittaker, J.M., Myhill, R., and Chandler, M.T., 2015. Semiautomatic fracture zone tracking, Geochemistry, Geophysics, Geosystems, doi: 10.1002/2015GC005853

Wessel, P. and Smith, W.H., 1996. A global, self‐consistent, hierarchical, high-resolution shoreline database. Journal of Geophysical Research: Solid Earth (1978y, Geophysics, Geosystemsys

Whittaker, J.M., Afonso, J.C., Masterston, S., Müller, R.D. Wessel, P., Williams, S.E., and Seton, M. 2015. Long-term interaction between mid-ocean ridges and mantle plumes. Nature Geoscience, doi:10.1038/NGEO2437

Whittaker, J., Müller, R., Leitchenkov, G., Stagg, H., Sdrolias, M., Gaina, C. and Goncharov, A., 2007. Major Australian-Antarctic plate reorganization at Hawaiian-Emperor bend time. Science, 318(5847): 83-86.

Wilson, D.S., 1993. Confidence intervals for motion and deformation of the Juan de Fuca plate. Journal of Geophysical Research: Solid Earth (1978–2012), 98(B9): 16053-16071.

Wobbe, F., Gohl, K., Chambord, A. and Sutherland, R., 2012. Structure and breakup history of the rifted margin of West Antarctica in relation to Cretaceous separation from Zealandia and Bellingshausen plate motion. Geochemistry, Geophysics, Geosystems, 13(4).

Woods, M.T. and Davies, G.F., 1982. Late Cretaceous genesis of the Kula plate. Earth and Planetary Science Letters, 58(2): 161-166.

Wright, N.M., Müller, R.D., Seton, M. and Williams, S.E., 2015. Revision of Paleogene plate motions in the Pacific and implications for the Hawaiian-Emperor bend. Geology, 43(5): 455-458.

Zhang, G.-L., Chen, L.-H. and Li, S.-Z., 2013. Mantle dynamics and generation of a geochemical mantle boundary along the East Pacific Rise–Pacific/Antarctic ridge. Earth and Planetary Science Letters, 383: 153-163.

Zonenshain, L., Kononov, M. and Savostin, L., 1987. Pacific and Kula/Eurasia relative motions during the last 130 Ma and their bearing on orogenesis in northeast Asia. Circum-Pacific orogenic belts and evolution of the Pacific Ocean basin: 29-47.

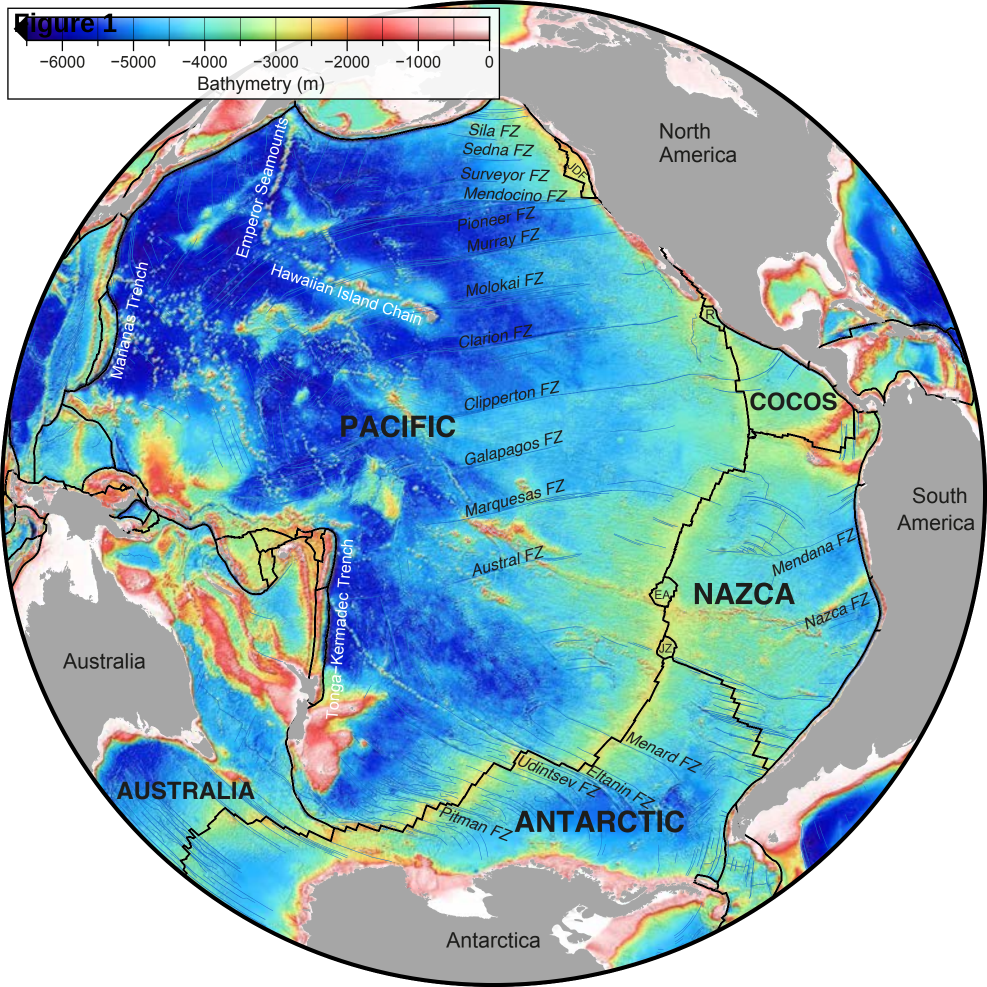
Figure 1
−6000
−5000
−4000
−3000
−2000
−1000
0
Bathymetry (m)
North America
South America
Australia
Antarctica
PACIFIC
COCOS
NAZCA
AUSTRALIA
ANTARCTIC
JDF
R
EA
JZ
Sila FZ
Sedna FZ
Surveyor FZ
Mendocino FZ
Pioneer FZ
Murray FZ
Molokai FZ
Clarion FZ
Clipperton FZ
Galapagos FZ
Marquesas FZ
Austral FZ
Mendana FZ
Nazca FZ
Menard FZ
Eltanin FZ
Udintsev FZ
Pitman FZ
Emperor Seamounts
Hawaiian Island Chain
Marianas Trench
Tonga–Kermadec Trench

Figure 2

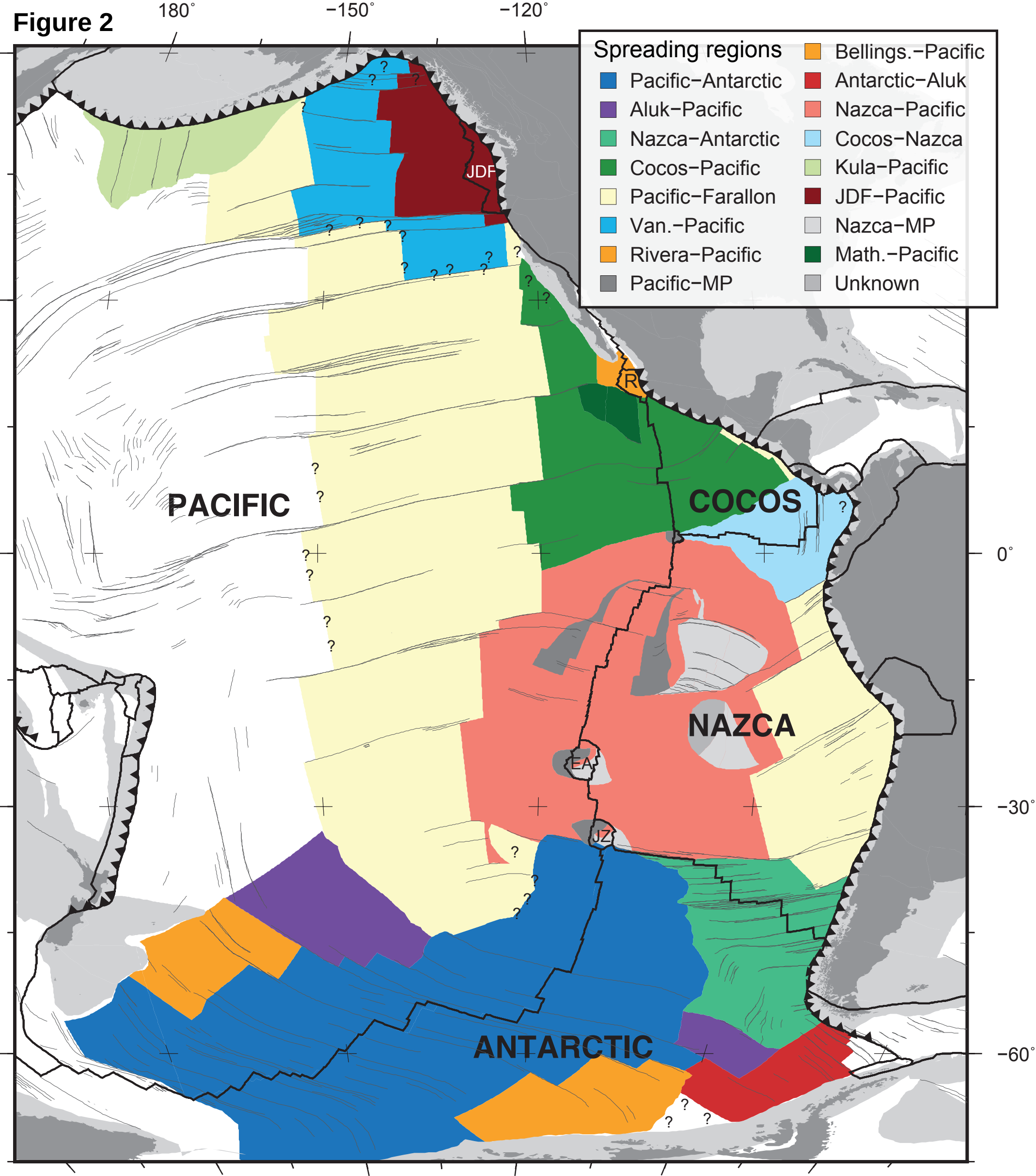
180°
−150°
−120°
0°
−30°
−60°
Spreading regions
Pacific−Antarctic
Aluk−Pacific
Nazca−Antarctic
Cocos−Pacific
Pacific−Farallon
Van.−Pacific
Rivera−Pacific
Pacific−MP
Bellings.−Pacific
Antarctic−Aluk
Nazca−Pacific
Cocos−Nazca
Kula−Pacific
JDF−Pacific
Nazca−MP
Math.−Pacific
Unknown
JDF
R
PACIFIC
COCOS
NAZCA
EA
JZ
ANTARCTIC

Figure 3

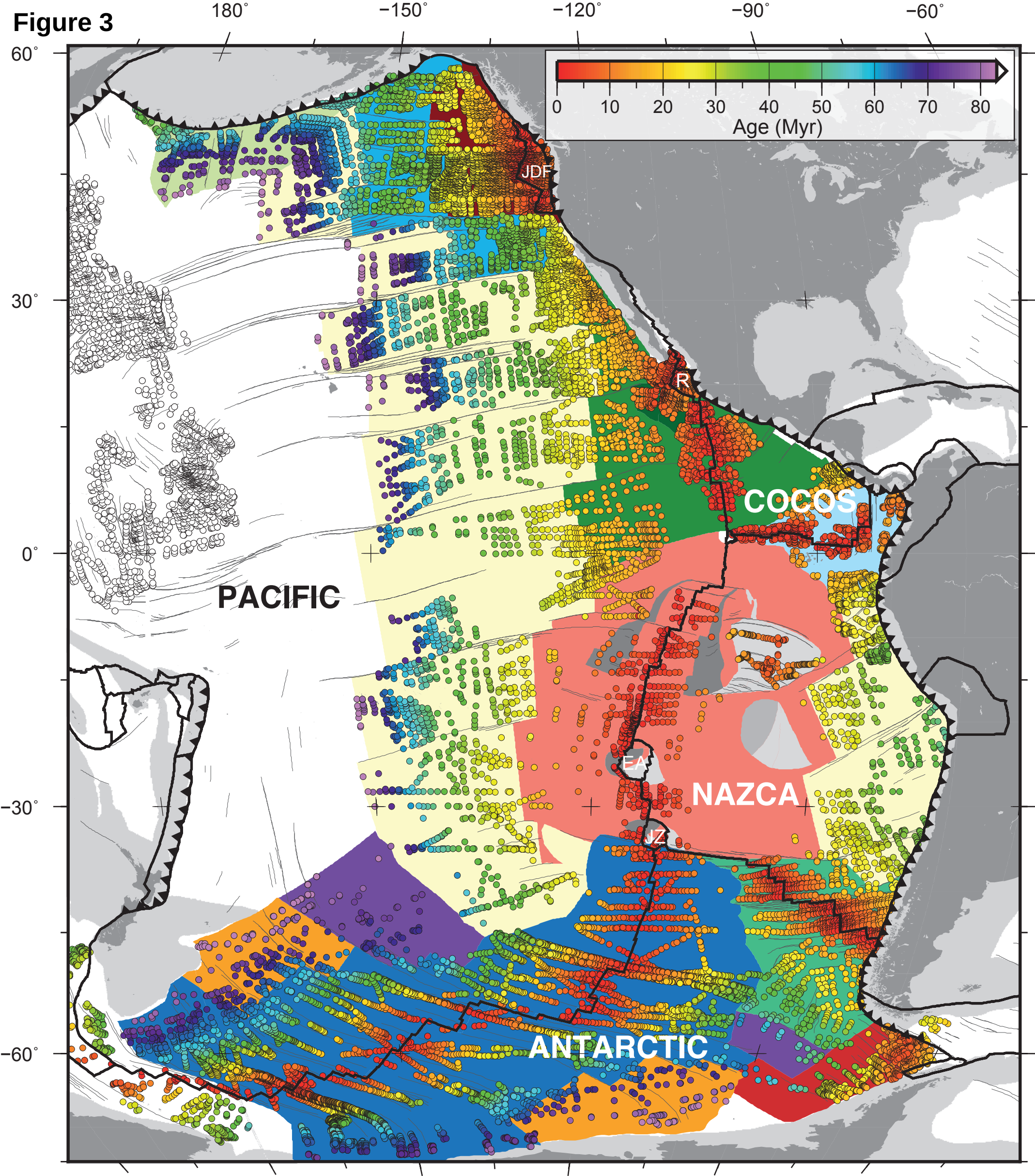

180°
−150°
−120°
−90°
−60°
60°
30°
0°
−30°
−60°
0
10
20
30
40
50
60
70
80
Age (Myr)
JDF
R
COCOS
PACIFIC
EA
NAZCA
JZ
ANTARCTIC

Figure 4

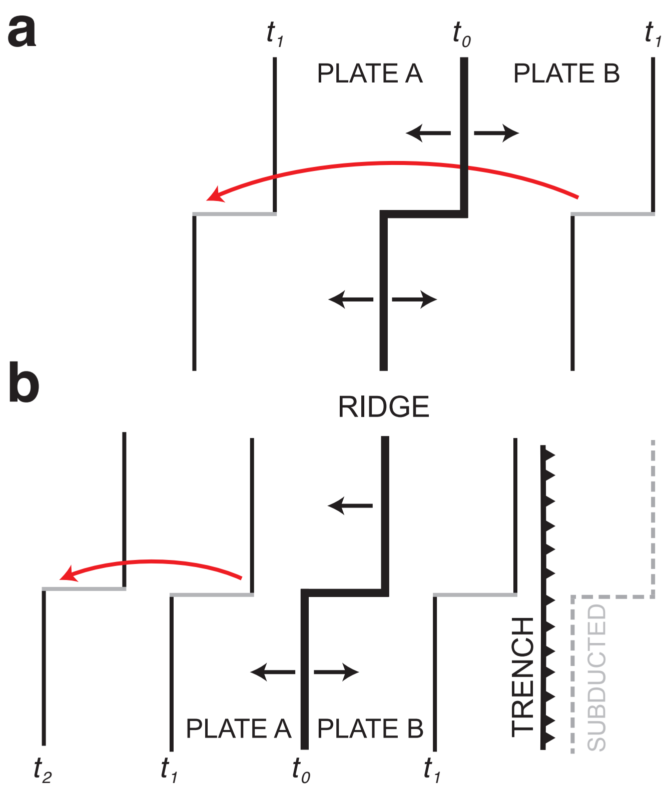

a
t_1
t_0
t_1
PLATE A
PLATE B
b
RIDGE
TRENCH
SUBDUCTED
PLATE A
PLATE B
t_2
t_1
t_0
t_1

Figure 5

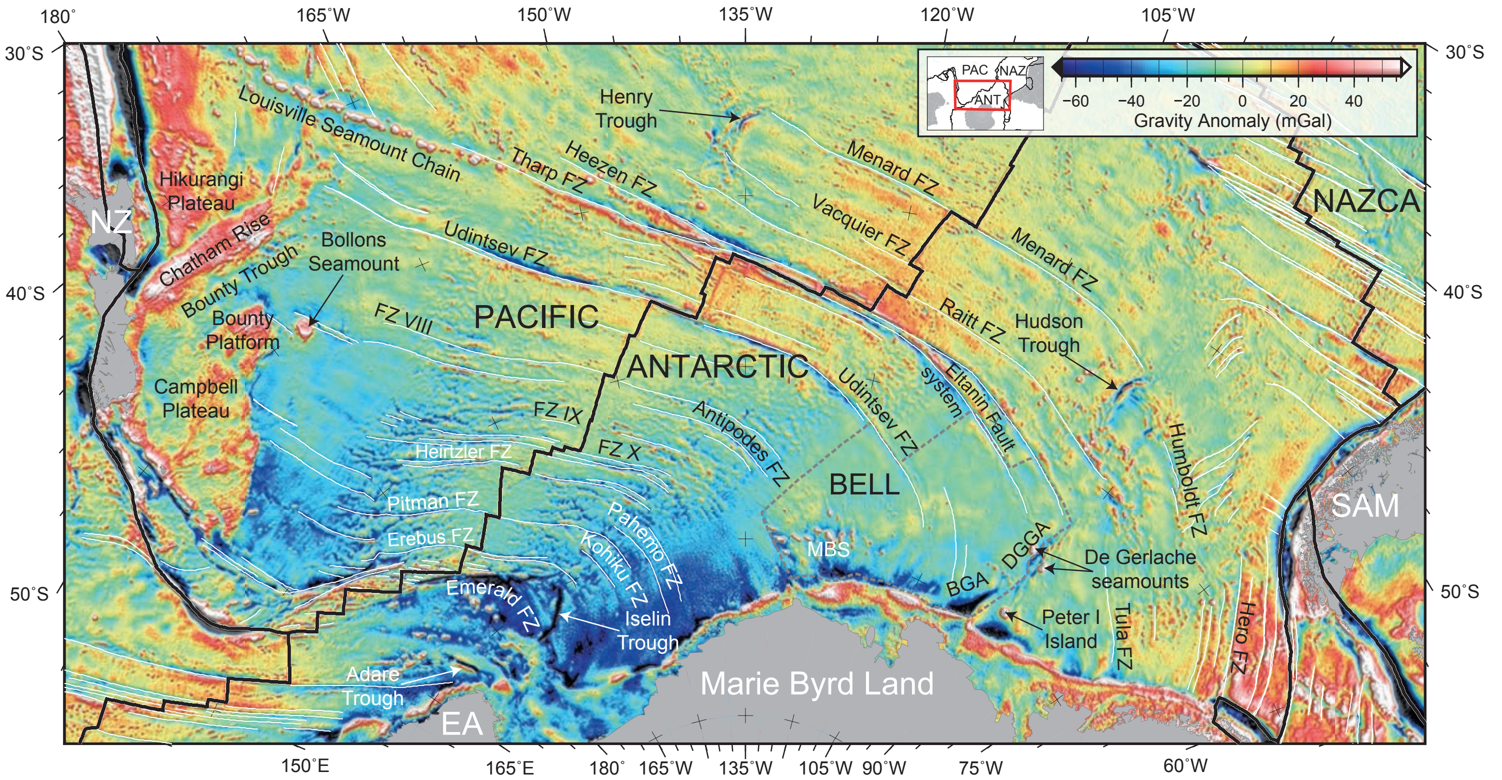
180°
165°W
150°W
135°W
120°W
105°W
30°S
40°S
50°S
PAC
NAZ
ANT
−60
−40
−20
0
20
40
Gravity Anomaly (mGal)
Henry Trough
Louisville Seamount Chain
Tharp FZ
Heezen FZ
Menard FZ
Vacquier FZ
Menard FZ
NAZCA
Hikurangi Plateau
NZ
Chatham Rise
Bounty Trough
Bollons Seamount
Udintsev FZ
Bounty Platform
Campbell Plateau
FZ VIII
PACIFIC
ANTARCTIC
Raitt FZ
Hudson Trough
Udintsev FZ
system
Eltanin Fault
FZ IX
Antipodes FZ
Heirtzler FZ
FZ X
BELL
Humboldt FZ
SAM
Pitman FZ
Pahemo FZ
Erebus FZ
Kohiku FZ
MBS
DGGA
De Gerlache seamounts
BGA
Emerald FZ
Iselin Trough
Peter I Island
Tula FZ
Hero FZ
Adare Trough
Marie Byrd Land
EA
150°E
165°E
180°
165°W
135°W
105°W
90°W
75°W
60°W

Figure 6

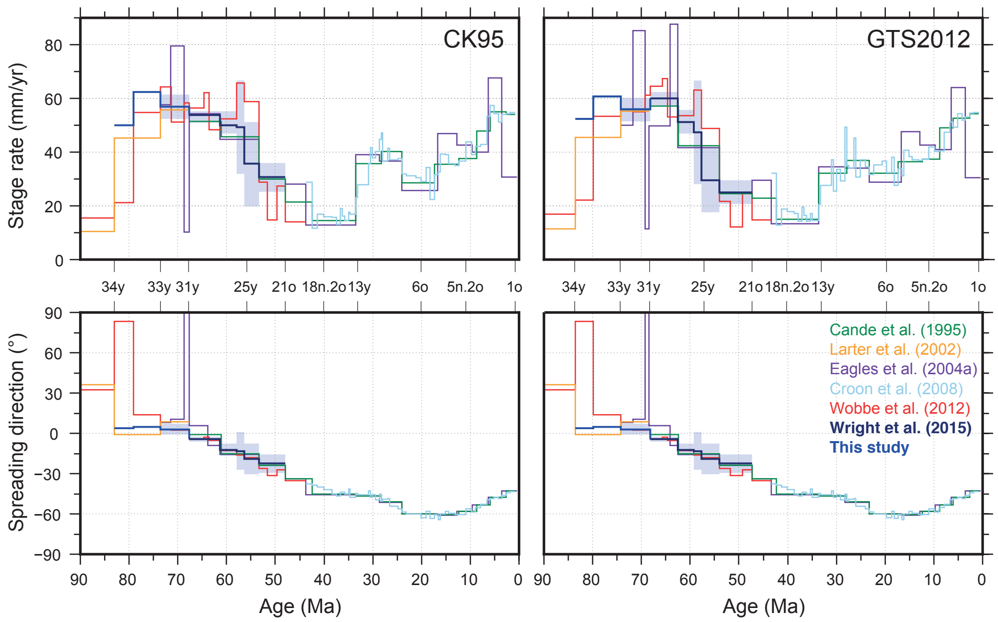
CK95
GTS2012
Stage rate (mm/yr)
Spreading direction (°)
Age (Ma)
34y
33y
31y
25y
21o
18n.2o
13y
6o
5n.2o
1o
Cande et al. (1995)
Larter et al. (2002)
Eagles et al. (2004a)
Croon et al. (2008)
Wobbe et al. (2012)
Wright et al. (2015)
This study

Figure 7

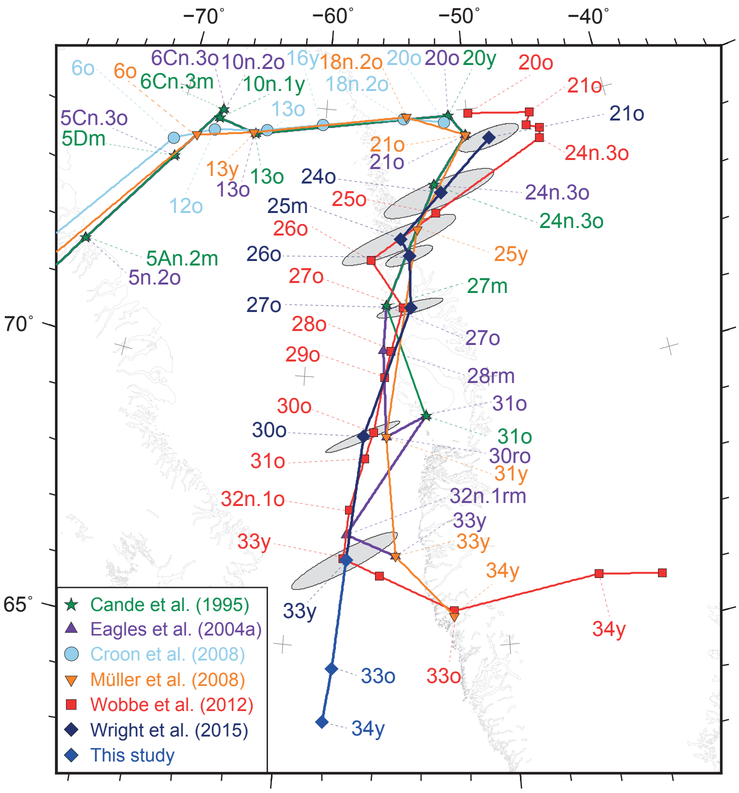

−70˚
−60˚
−50˚
−40˚
70˚
65˚
6o
6o
6Cn.3o
6Cn.3m
10n.2o
10n.1y
16y
18n.2o
18n.2o
20o
20o
20y
20o
21o
21o
13o
5Cn.3o
5Dm
21o
21o
24n.3o
13y
13o
13o
12o
24o
24n.3o
24n.3o
25m
25o
26o
25y
26o
5An.2m
5n.2o
27o
27m
27o
28o
27o
29o
28rm
30o
31o
30o
31o
30ro
31o
31y
32n.1o
32n.1rm
33y
33y
33y
34y
33y
34y
33o
33o
34y
Cande et al. (1995)
Eagles et al. (2004a)
Croon et al. (2008)
Müller et al. (2008)
Wobbe et al. (2012)
Wright et al. (2015)
This study

Figure 8

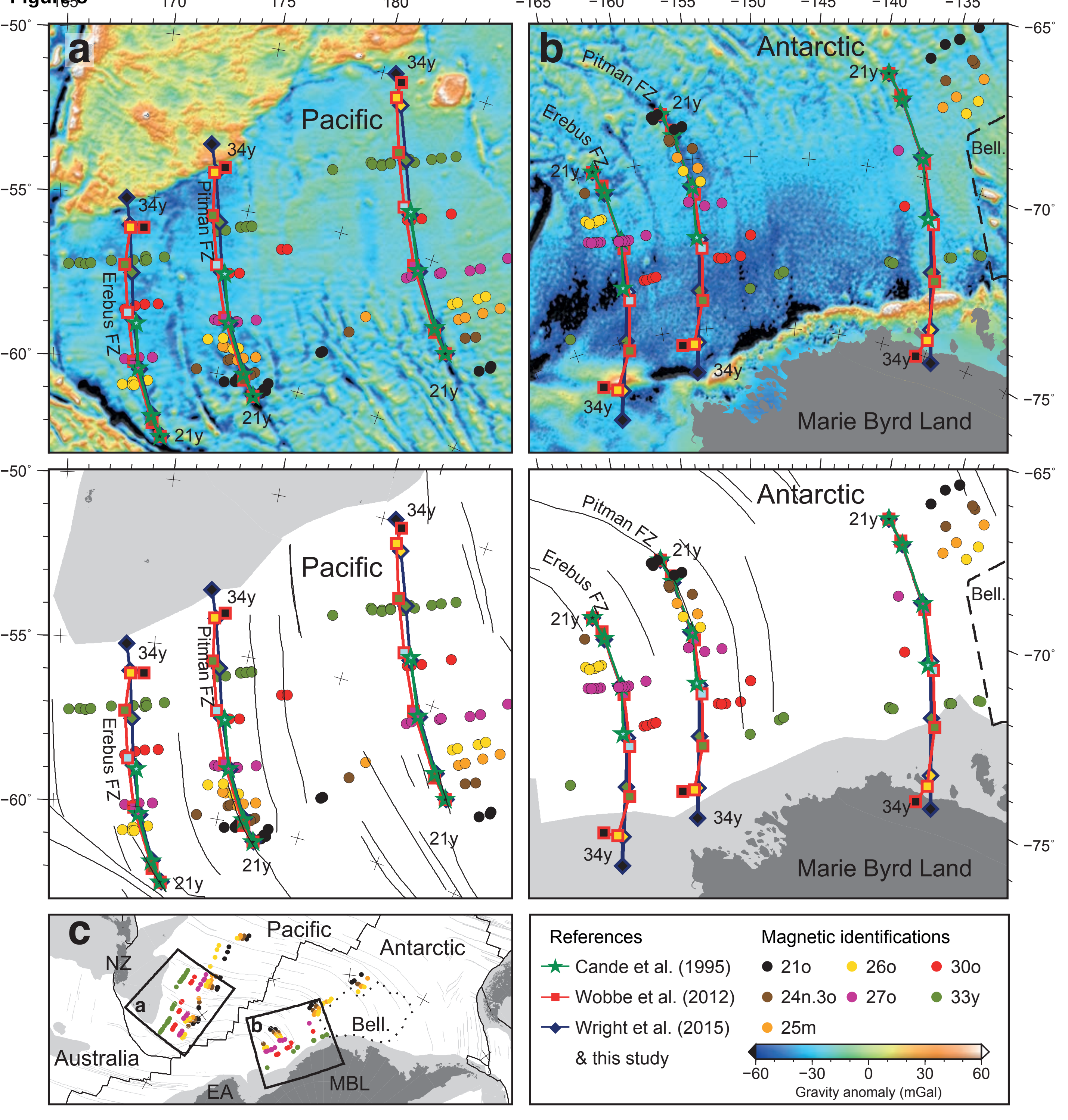
a
b
c
165°
170°
175°
180°
−165°
−160°
−155°
−150°
−145°
−140°
−135°
−50°
−55°
−60°
−65°
−70°
−75°
Pacific
Antarctic
Pitman FZ
Erebus FZ
34y
21y
Bell.
Marie Byrd Land
NZ
Australia
EA
MBL
References
Cande et al. (1995)
Wobbe et al. (2012)
Wright et al. (2015)
& this study
Magnetic identifications
21o
24n.3o
25m
26o
27o
30o
33y
−60
−30
0
30
60
Gravity anomaly (mGal)

Figure 9

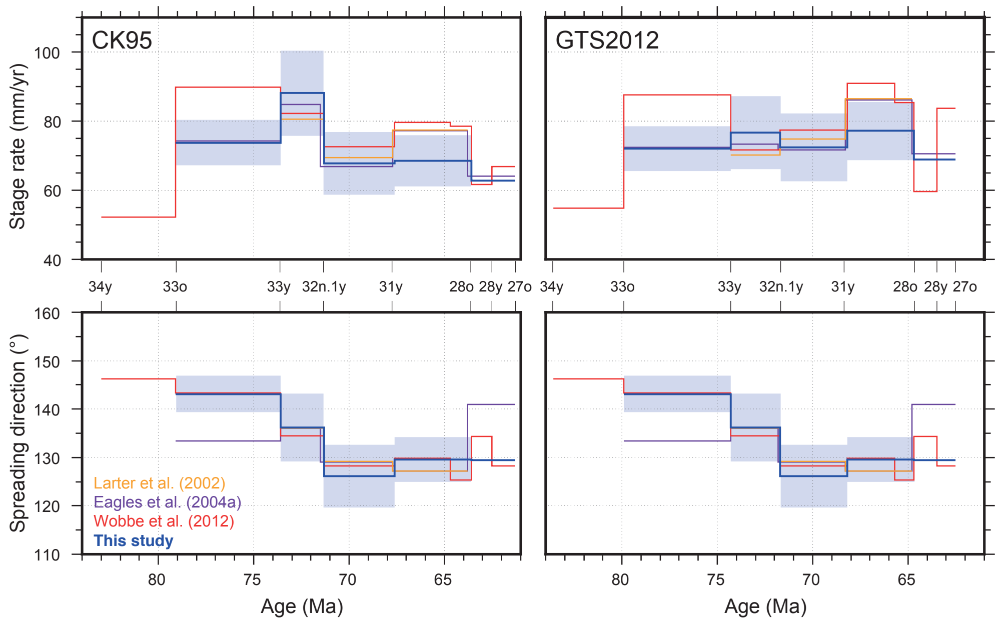
CK95
GTS2012
Stage rate (mm/yr)
100
80
60
40
34y
33o
33y
32n.1y
31y
28o
28y
27o
Spreading direction (°)
160
150
140
130
120
110
Larter et al. (2002)
Eagles et al. (2004a)
Wobbe et al. (2012)
This study
80
75
70
65
Age (Ma)

Figure 10

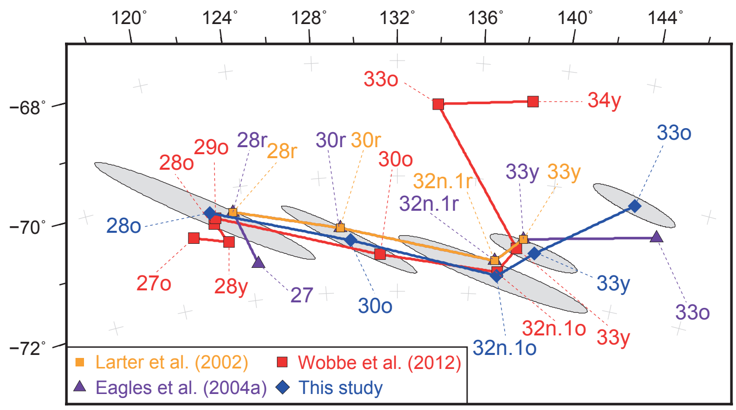

120°
124°
128°
132°
136°
140°
144°
−68°
−70°
−72°
33o
34y
33o
29o
28r
28r
30r
30r
28o
30o
32n.1r
33y
33y
32n.1r
28o
33y
27o
28y
27
30o
33o
32n.1o
33y
32n.1o
Larter et al. (2002)
Wobbe et al. (2012)
Eagles et al. (2004a)
This study

Figure 11

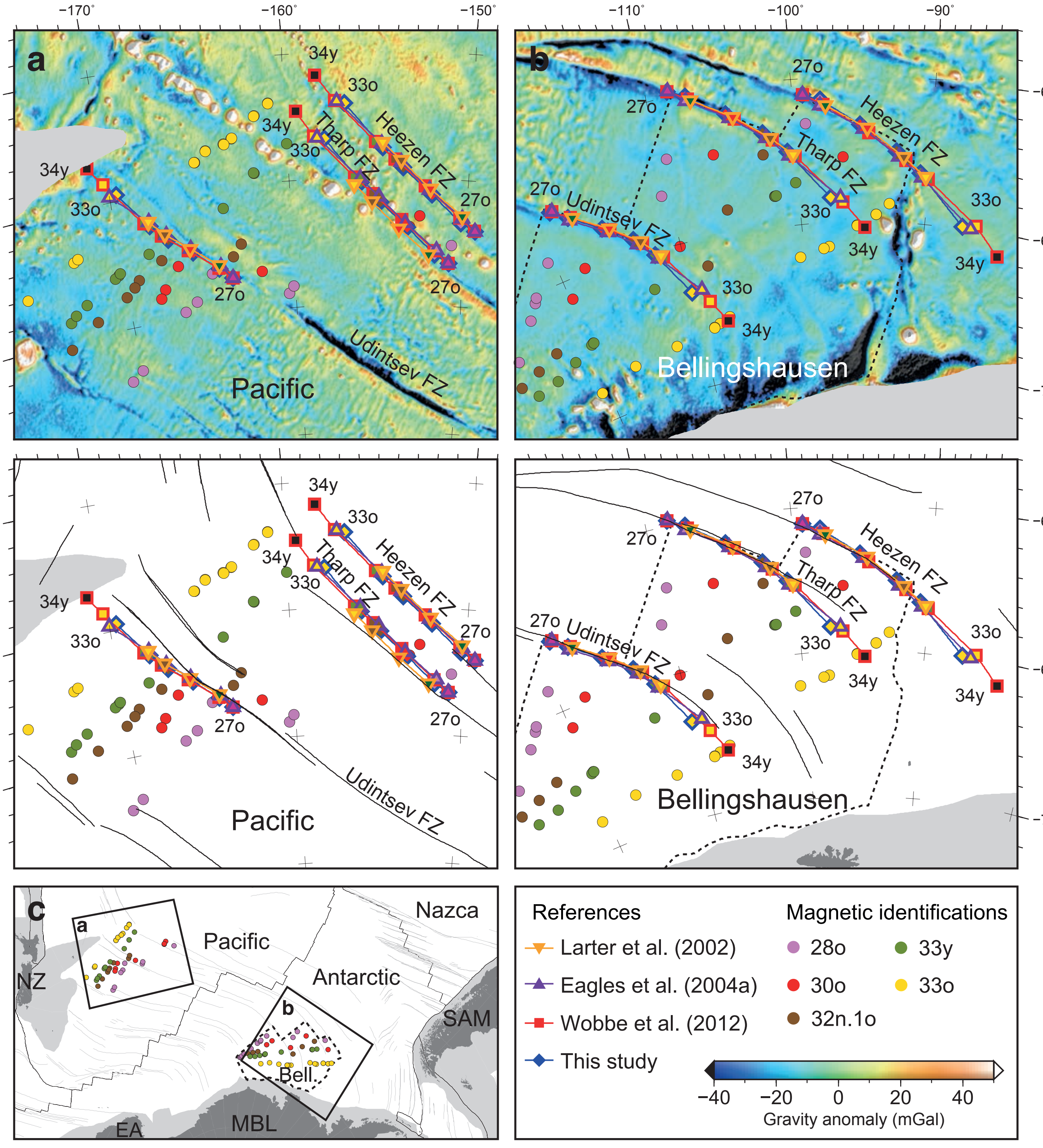

a
b
c
-170° -160° -150° -110° -100° -90°
-40° -45° -50° -60° -65° -70°
34y
33o
27o
Heezen FZ
Tharp FZ
Udintsev FZ
Pacific
Bellingshausen
Nazca
Antarctic
NZ
SAM
EA
MBL
Bell.
References
Larter et al. (2002)
Eagles et al. (2004a)
Wobbe et al. (2012)
This study
Magnetic identifications
28o
30o
32n.1o
33y
33o
-40 -20 0 20 40
Gravity anomaly (mGal)

Figure 12

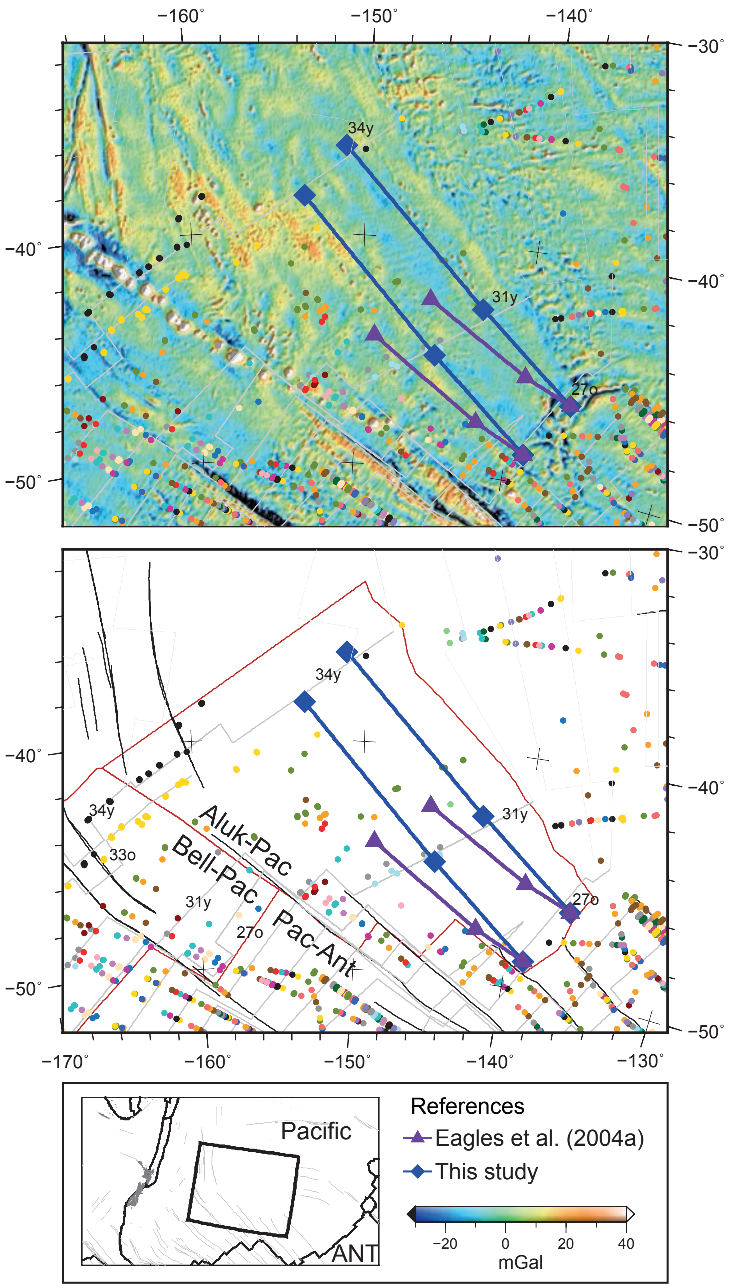

−160˚
−150˚
−140˚
−30˚
−40˚
−40˚
−50˚
−50˚
34y
31y
27o
−30˚
−40˚
−40˚
−50˚
−50˚
34y
34y
33o
31y
27o
31y
27o
Aluk-Pac
Bell-Pac
Pac-Ant
−170˚
−160˚
−150˚
−140˚
−130˚
Pacific
ANT
References
Eagles et al. (2004a)
This study
−20
0
20
40
mGal

Figure 13

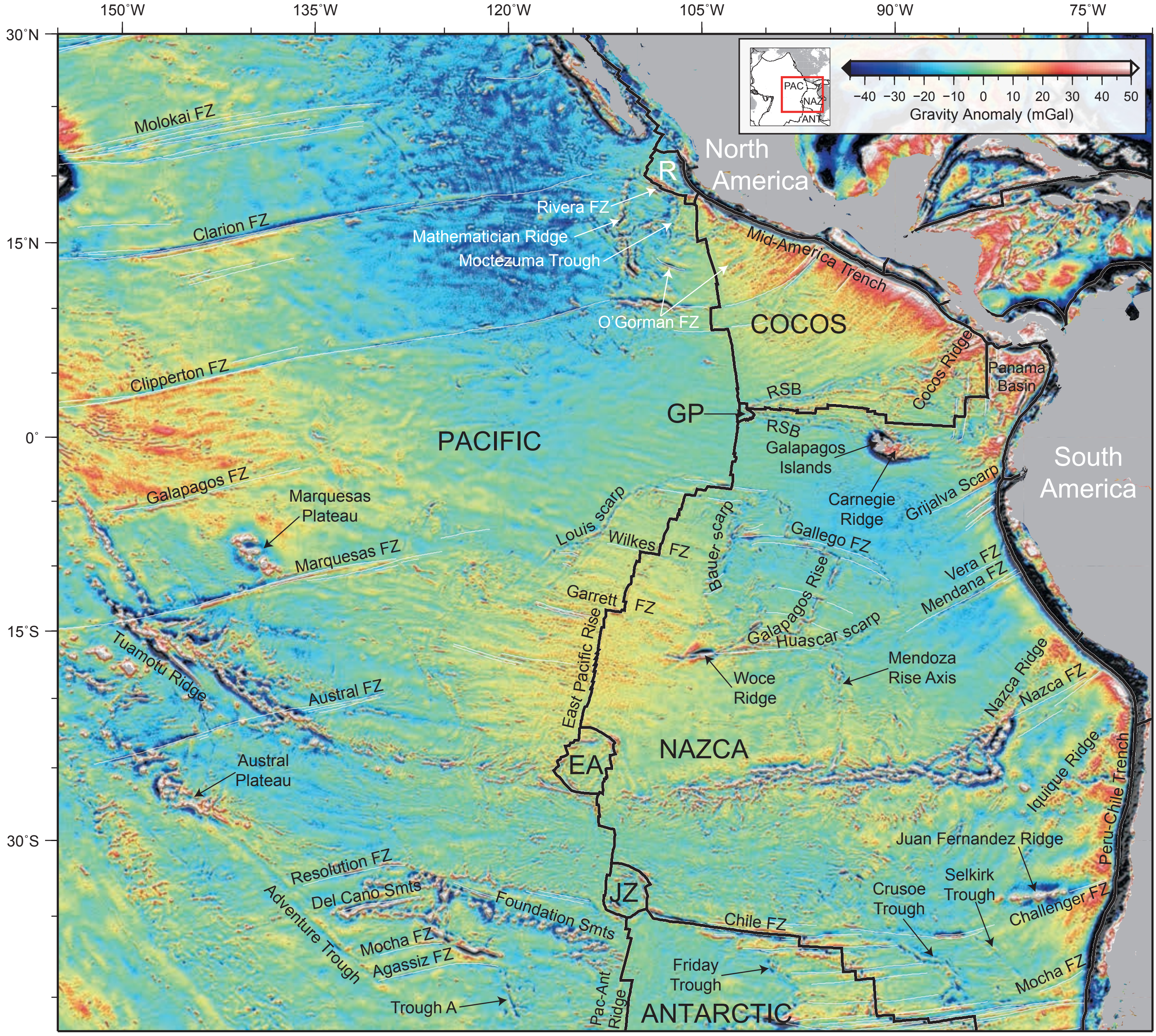

150°W
135°W
120°W
105°W
90°W
75°W
30°N
15°N
0°
15°S
30°S
PAC
NAZ
ANT
−40 −30 −20 −10 0 10 20 30 40 50
Gravity Anomaly (mGal)
North America
South America
R
Molokai FZ
Clarion FZ
Rivera FZ
Mathematician Ridge
Moctezuma Trough
O'Gorman FZ
Mid-America Trench
COCOS
Clipperton FZ
Cocos Ridge
Panama Basin
RSB
GP
RSB
PACIFIC
Galapagos Islands
Carnegie Ridge
Grijalva Scarp
Galapagos FZ
Marquesas Plateau
Louis scarp
Wilkes FZ
Bauer scarp
Gallego FZ
Marquesas FZ
Vera FZ
Mendana FZ
Garrett FZ
Galapagos Rise
Huascar scarp
Mendoza Rise Axis
East Pacific Rise
Woce Ridge
Tuamotu Ridge
Austral FZ
Nazca Ridge
Nazca FZ
EA
NAZCA
Austral Plateau
Iquique Ridge
Peru-Chile Trench
Juan Fernandez Ridge
Resolution FZ
Del Cano Smts
Adventure Trough
Foundation Smts
JZ
Crusoe Trough
Selkirk Trough
Challenger FZ
Chile FZ
Mocha FZ
Agassiz FZ
Friday Trough
Mocha FZ
Trough A
Pac-Ant Ridge
ANTARCTIC

Figure 14

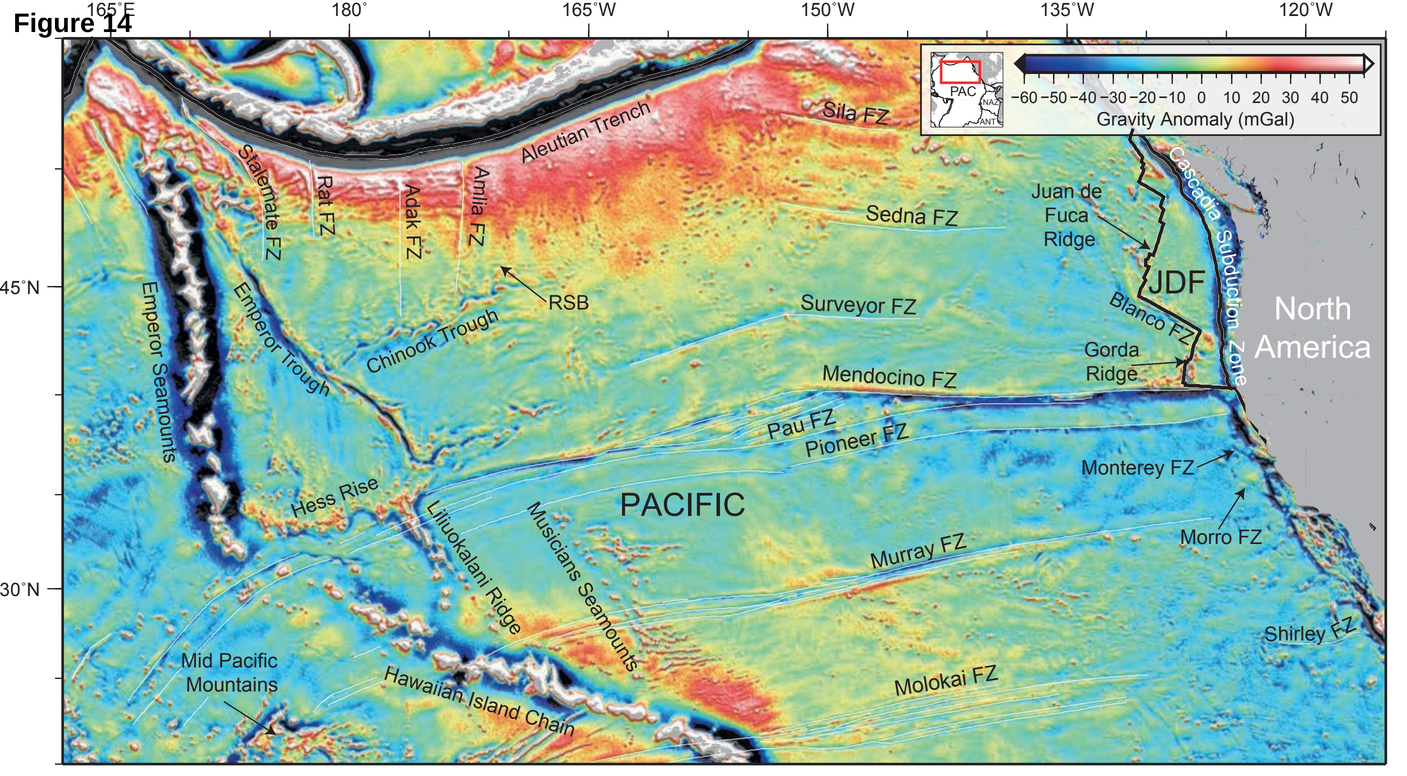

165°E
180°
165°W
150°W
135°W
120°W
45°N
30°N
PAC
NAZ
ANT
−60 −50 −40 −30 −20 −10 0 10 20 30 40 50
Gravity Anomaly (mGal)
Aleutian Trench
Sila FZ
Stalemate FZ
Rat FZ
Adak FZ
Amlia FZ
Sedna FZ
Juan de Fuca Ridge
Cascadia Subduction Zone
JDF
RSB
Surveyor FZ
Blanco FZ
North America
Emperor Seamounts
Emperor Trough
Chinook Trough
Gorda Ridge
Mendocino FZ
Pau FZ
Pioneer FZ
Monterey FZ
Hess Rise
PACIFIC
Liliuokalani Ridge
Musicians Seamounts
Morro FZ
Murray FZ
Shirley FZ
Mid Pacific Mountains
Hawaiian Island Chain
Molokai FZ

Figure 15

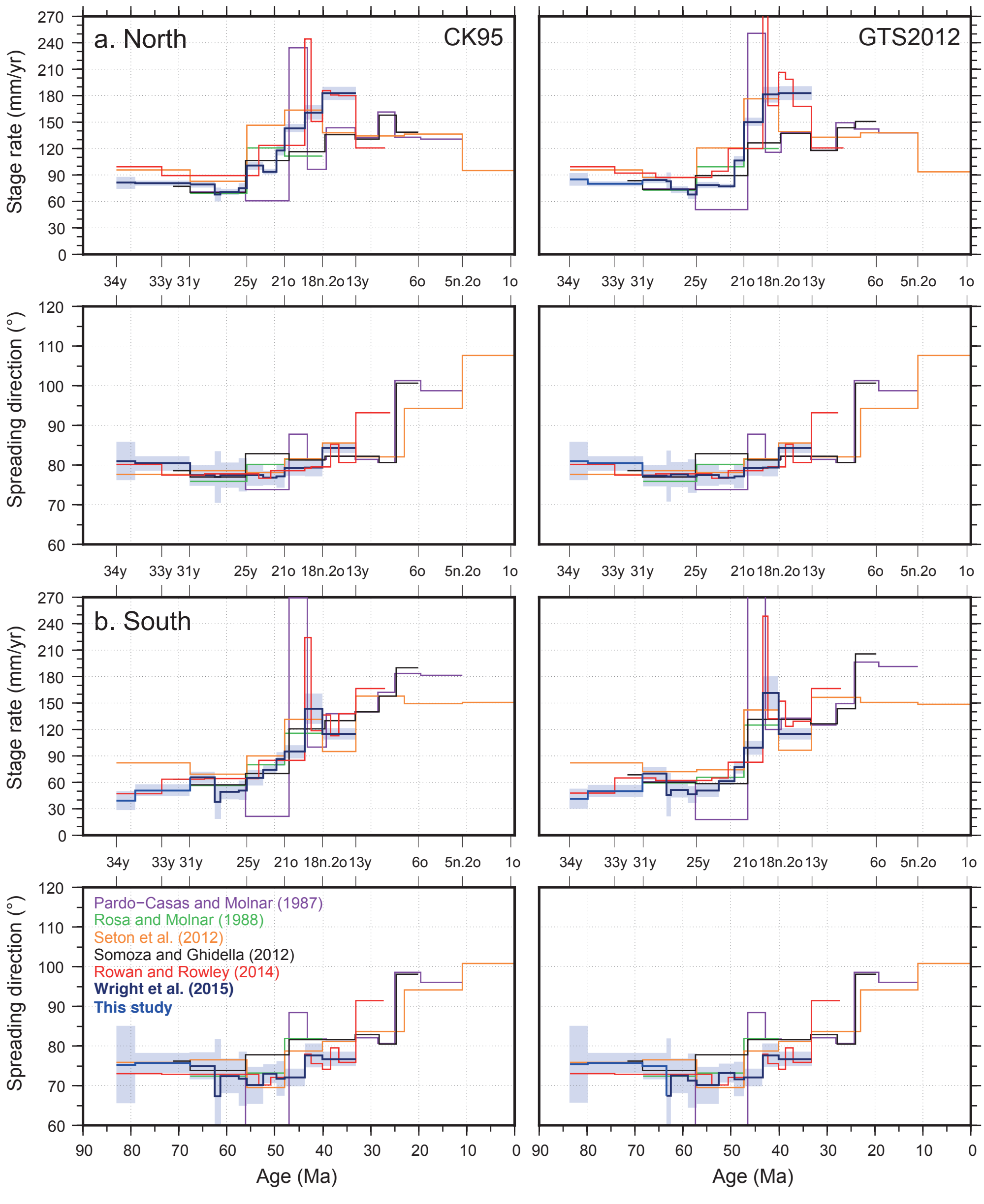

a. North
CK95
GTS2012
b. South
Stage rate (mm/yr)
Spreading direction (°)
Age (Ma)
34y 33y 31y 25y 21o 18n.2o 13y 6o 5n.2o 1o
Pardo−Casas and Molnar (1987)
Rosa and Molnar (1988)
Seton et al. (2012)
Somoza and Ghidella (2012)
Rowan and Rowley (2014)
Wright et al. (2015)
This study

Figure 16

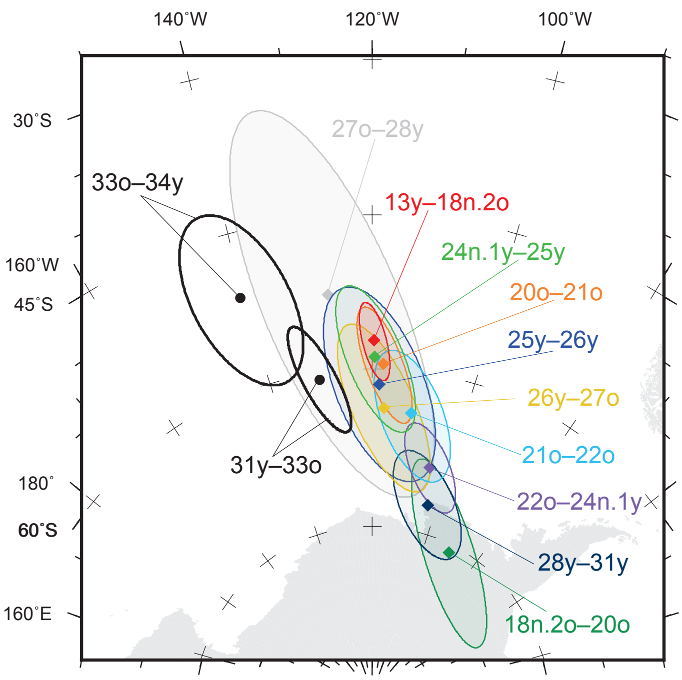
140°W
120°W
100°W
30°S
160°W
45°S
180°
60°S
160°E
27o–28y
33o–34y
13y–18n.2o
24n.1y–25y
20o–21o
25y–26y
26y–27o
21o–22o
22o–24n.1y
28y–31y
18n.2o–20o
31y–33o

Figure 17

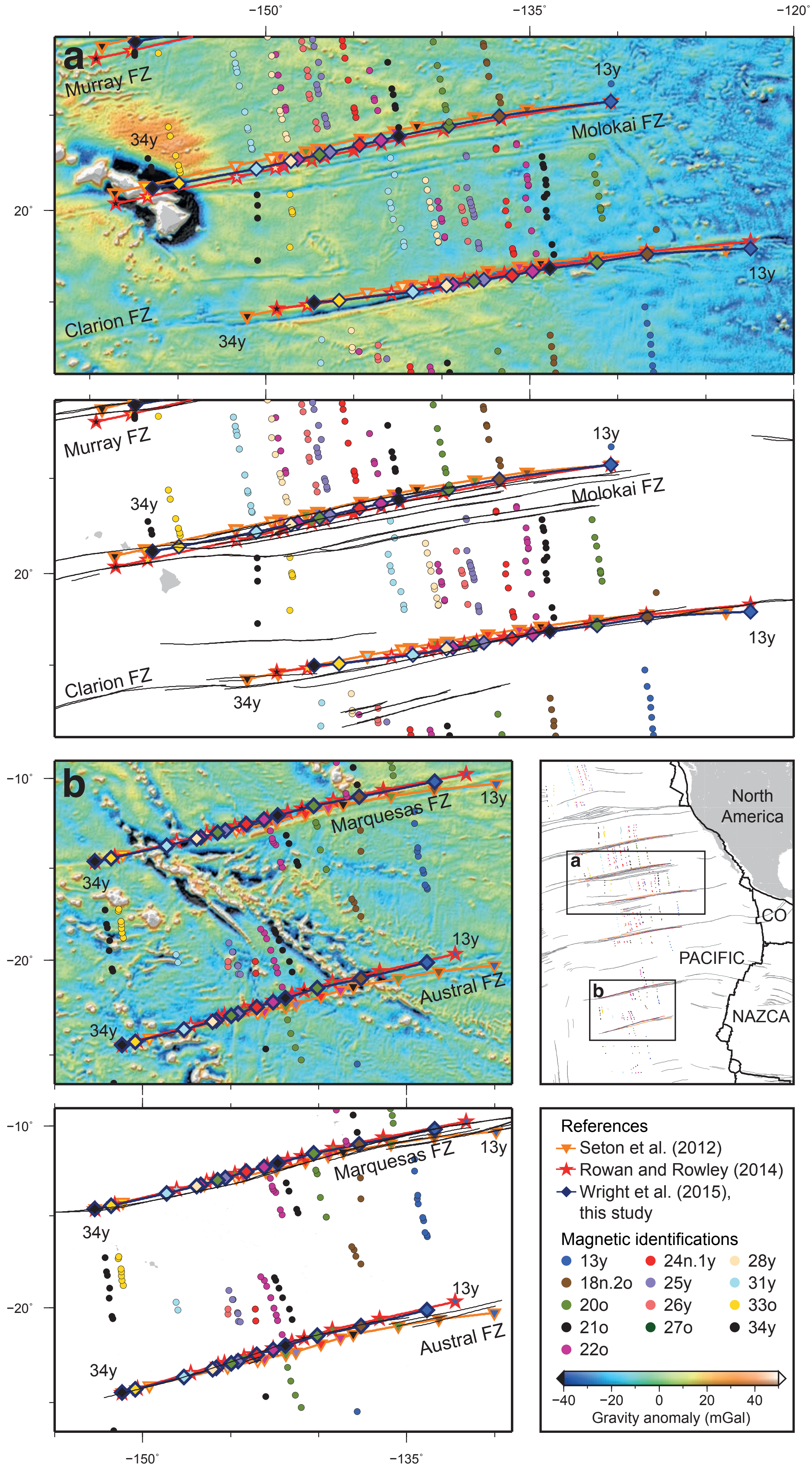

−150˚
−135˚
−120˚
20˚
a
Murray FZ
Molokai FZ
Clarion FZ
13y
34y
−10˚
−20˚
b
Marquesas FZ
Austral FZ
North America
CO
PACIFIC
NAZCA
References
Seton et al. (2012)
Rowan and Rowley (2014)
Wright et al. (2015), this study
Magnetic identifications
13y
18n.2o
20o
21o
22o
24n.1y
25y
26y
27o
28y
31y
33o
34y
−40
−20
0
20
40
Gravity anomaly (mGal)

Figure 18

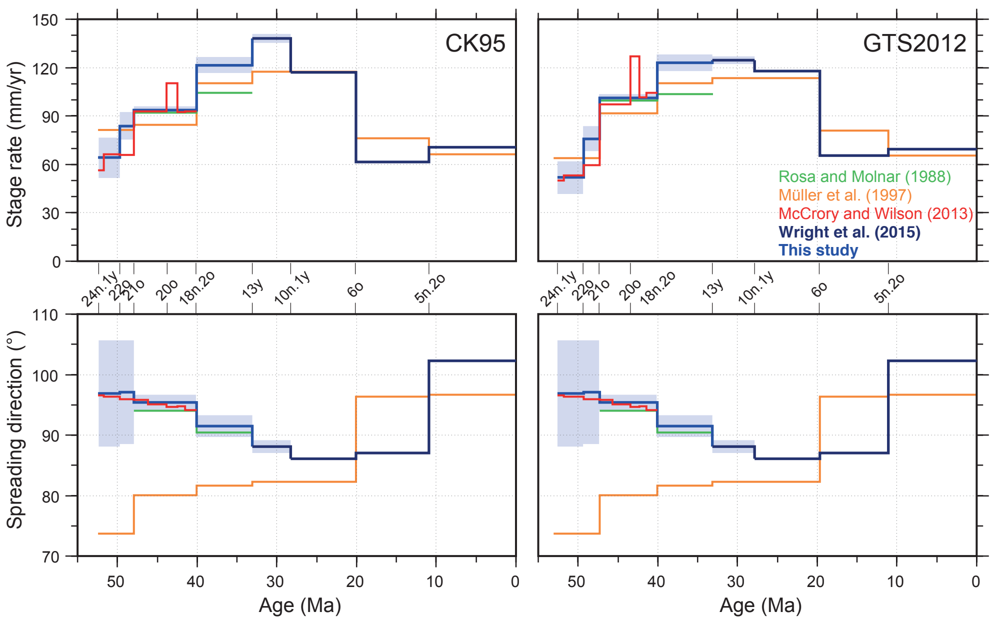
CK95
GTS2012
Stage rate (mm/yr)
Spreading direction (°)
Age (Ma)
24n.1y
22o
21o
20o
18n.2o
13y
10n.1y
6o
5n.2o
Rosa and Molnar (1988)
Müller et al. (1997)
McCrory and Wilson (2013)
Wright et al. (2015)
This study

Figure 19

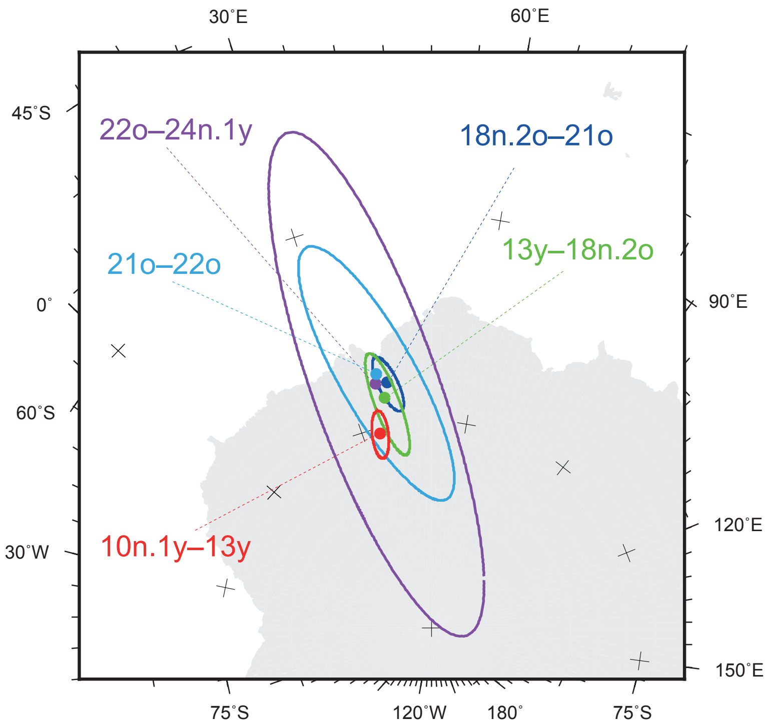

30°E
60°E
45°S
0°
60°S
30°W
90°E
120°E
150°E
75°S
120°W
180°
75°S
22o–24n.1y
18n.2o–21o
21o–22o
13y–18n.2o
10n.1y–13y

Figure 20

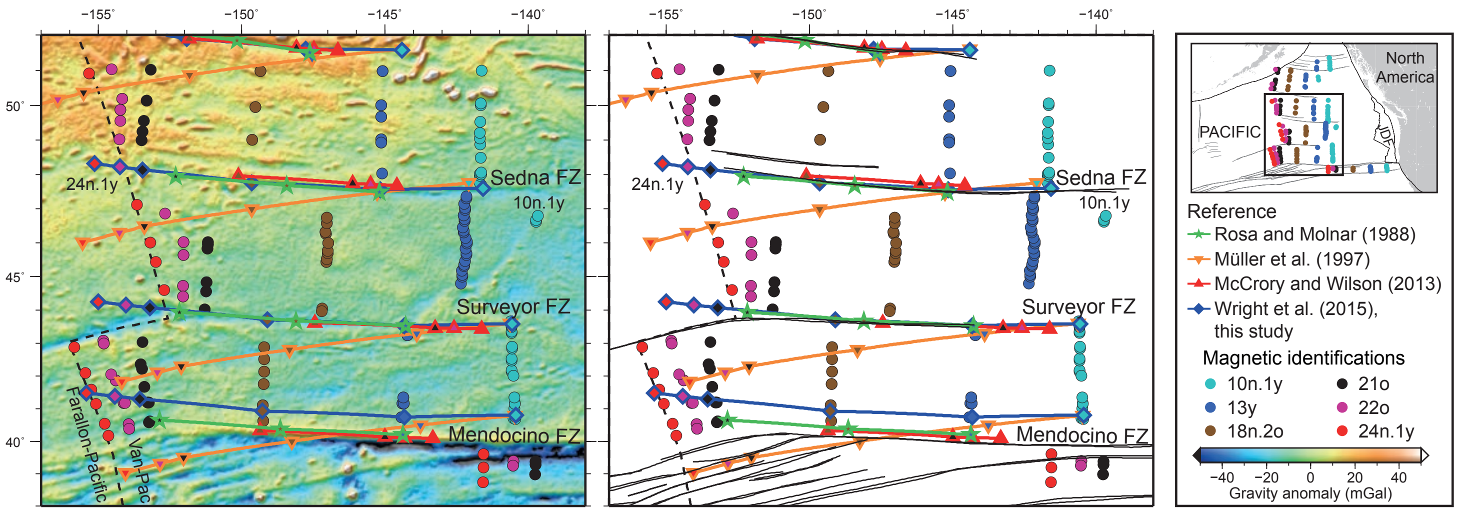

−155°
−150°
−145°
−140°
50°
45°
40°
Sedna FZ
24n.1y
10n.1y
Surveyor FZ
Mendocino FZ
Farallon-Pacific
Van-Pac
North America
PACIFIC
JdF
Reference
Rosa and Molnar (1988)
Müller et al. (1997)
McCrory and Wilson (2013)
Wright et al. (2015), this study
Magnetic identifications
10n.1y
13y
18n.2o
21o
22o
24n.1y
−40
−20
0
20
40
Gravity anomaly (mGal)

Figure 21

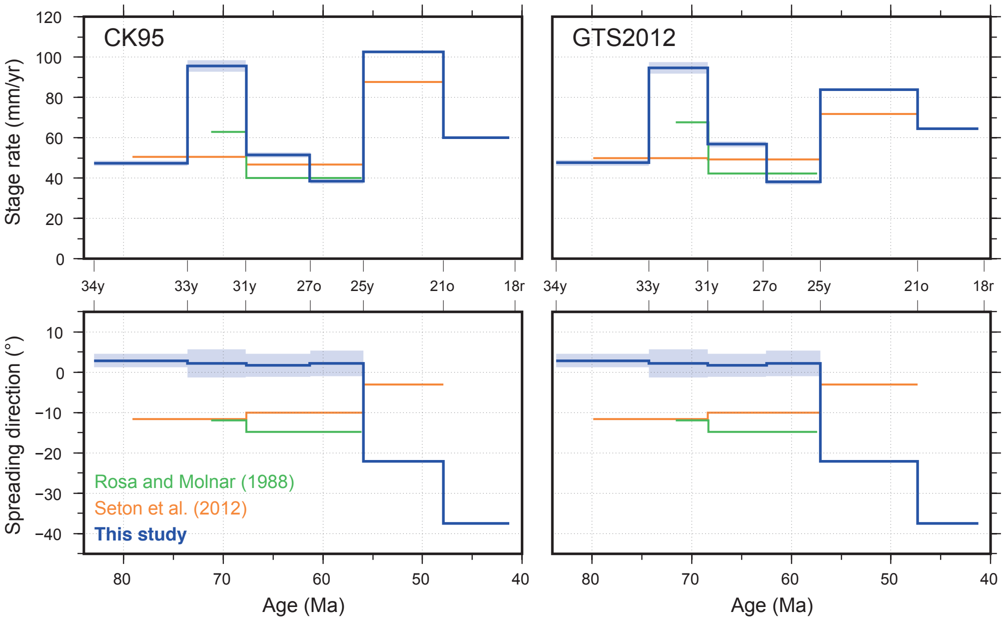
CK95
GTS2012
Stage rate (mm/yr)
Spreading direction (°)
34y
33y
31y
27o
25y
21o
18r
Rosa and Molnar (1988)
Seton et al. (2012)
This study
Age (Ma)
Age (Ma)

Figure 22

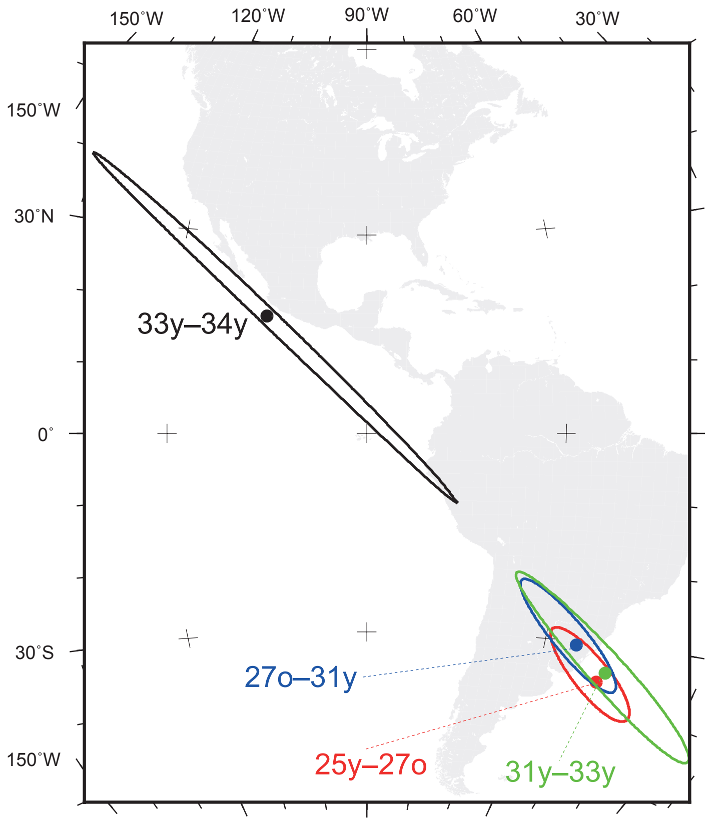

150˚W
120˚W
90˚W
60˚W
30˚W
150˚W
30˚N
0˚
30˚S
150˚W
33y–34y
27o–31y
25y–27o
31y–33y

Figure 23

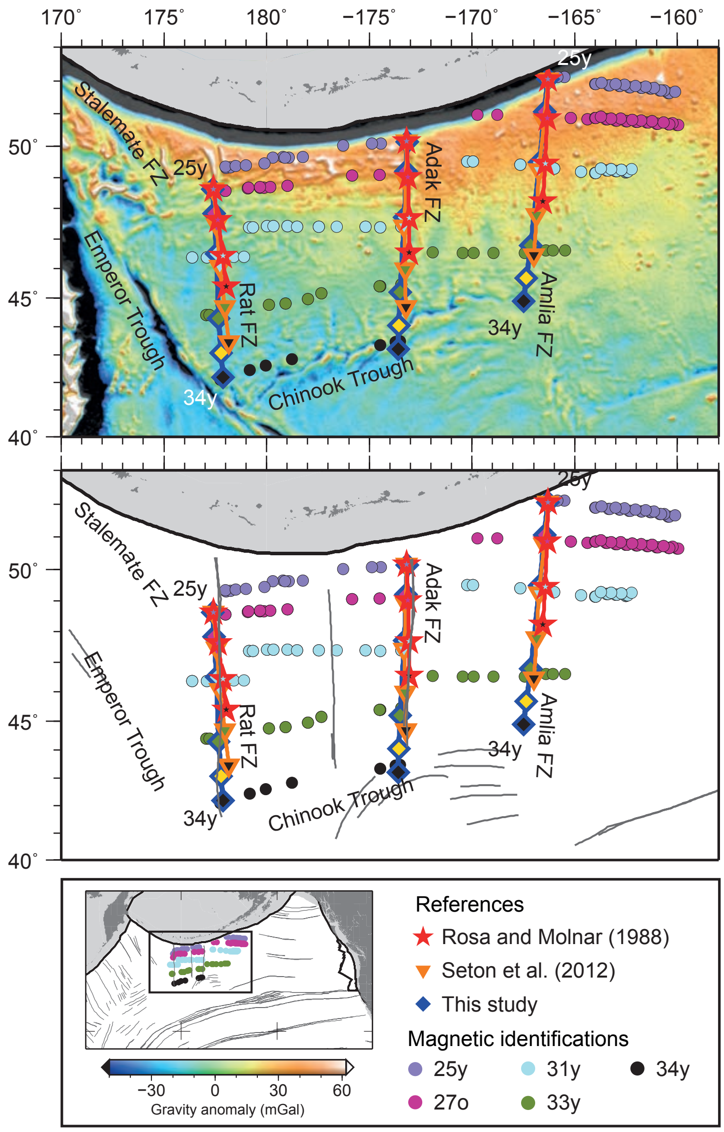

170˚
175˚
180˚
−175˚
−170˚
−165˚
−160˚
50˚
45˚
40˚
Stalemate FZ
Emperor Trough
Rat FZ
Adak FZ
Amlia FZ
Chinook Trough
25y
34y
References
Rosa and Molnar (1988)
Seton et al. (2012)
This study
Magnetic identifications
25y
31y
34y
27o
33y
−30
0
30
60
Gravity anomaly (mGal)

Figure 24

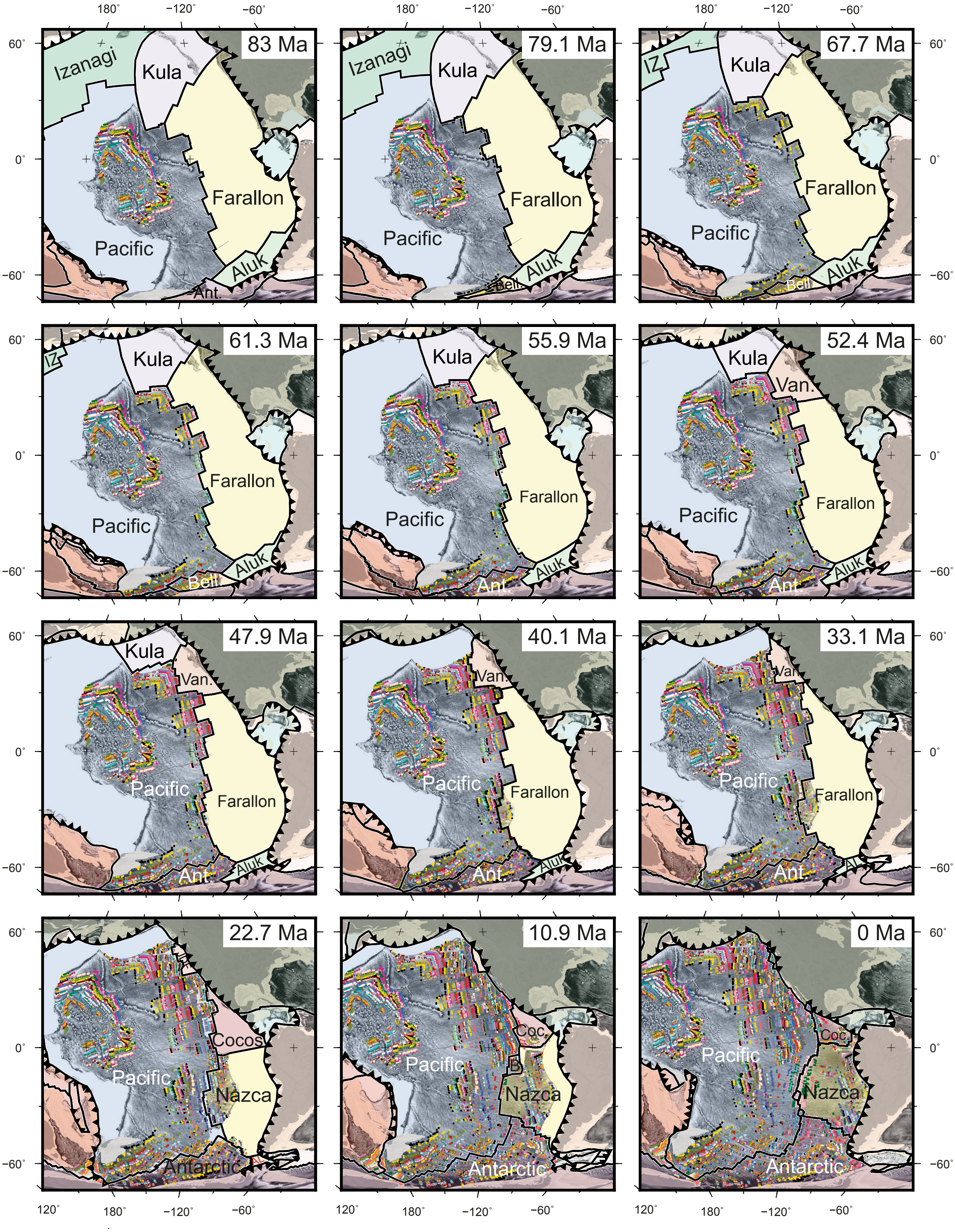
83 Ma
Izanagi
Kula
Farallon
Pacific
Aluk
Ant.
79.1 Ma
Bell.
67.7 Ma
IZ
61.3 Ma
55.9 Ma
52.4 Ma
Van.
47.9 Ma
40.1 Ma
33.1 Ma
22.7 Ma
Cocos
Nazca
Antarctic
10.9 Ma
Coc.
B
0 Ma
180°
−120°
−60°
120°
60°
0°
−60°

Figure 25

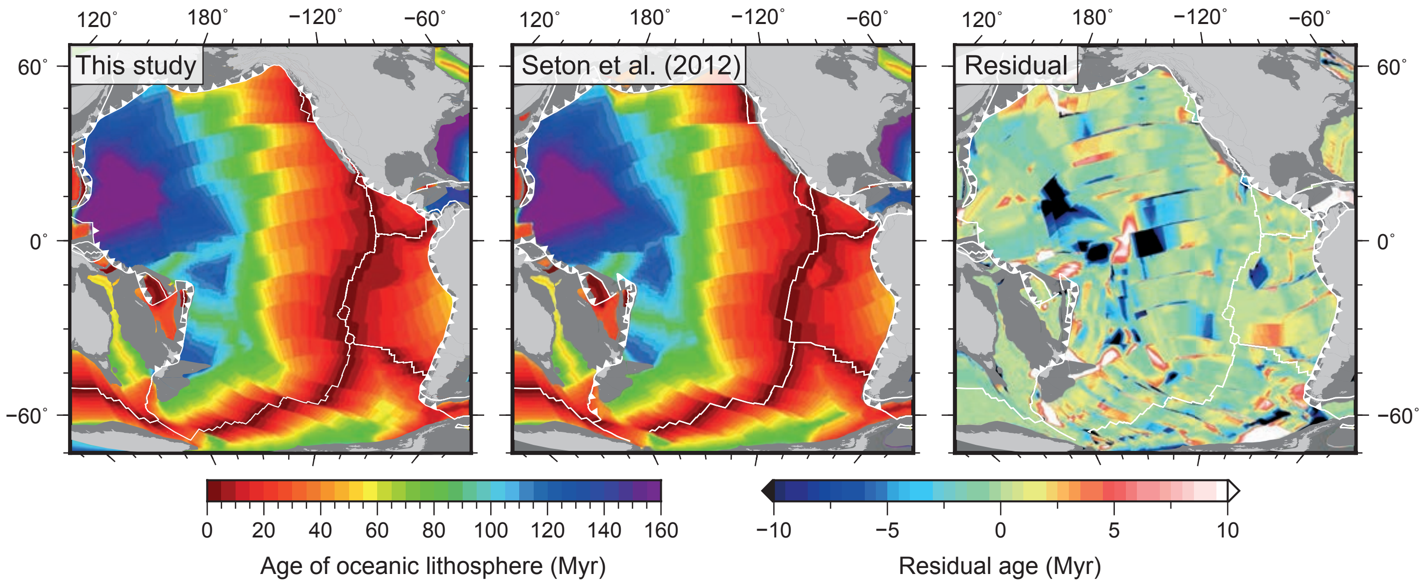

This study
Seton et al. (2012)
Residual
120°
180°
−120°
−60°
60°
0°
−60°
0
20
40
60
80
100
120
140
160
Age of oceanic lithosphere (Myr)
−10
−5
0
5
10
Residual age (Myr)

Figure 26

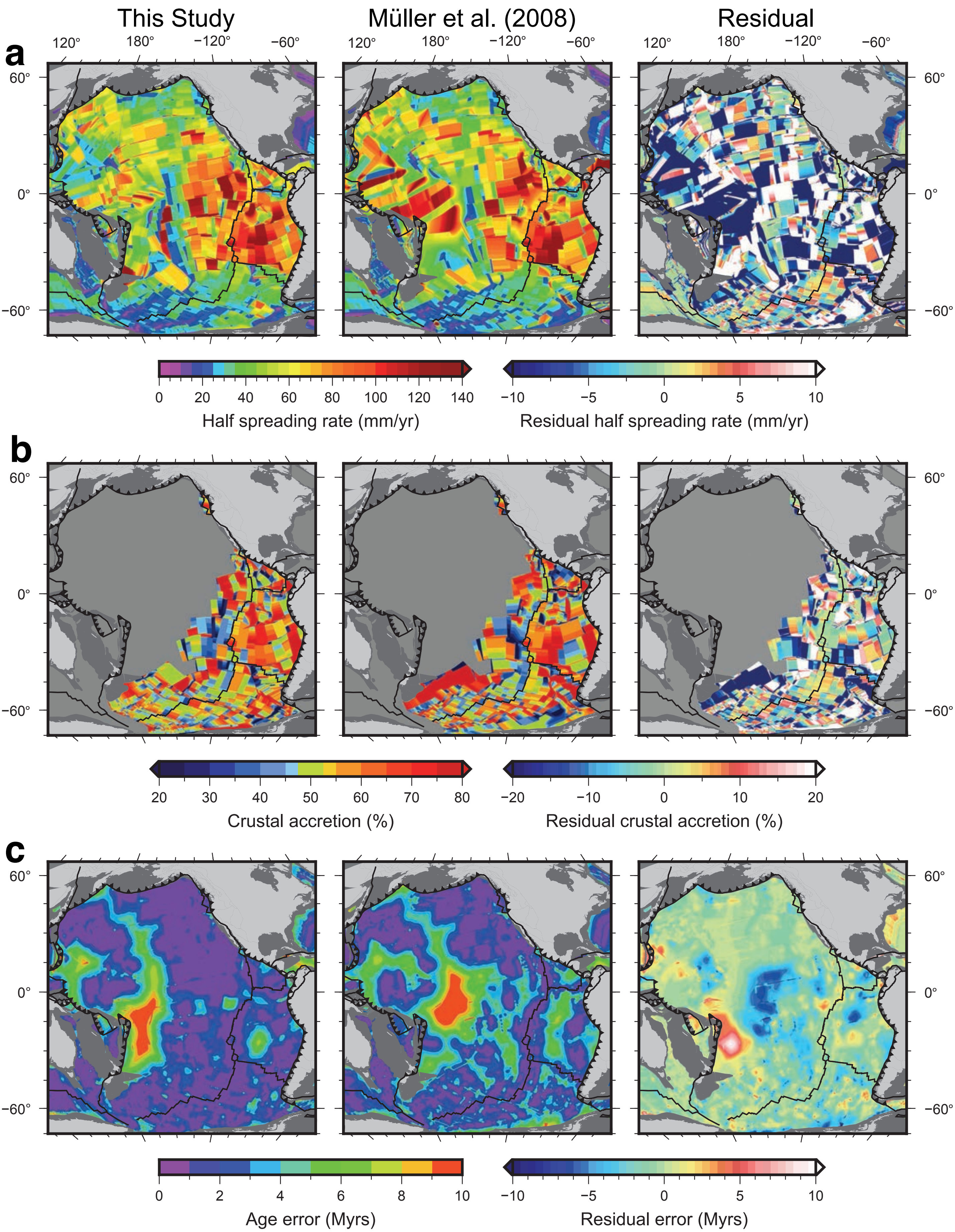
This Study
Müller et al. (2008)
Residual
a
b
c
120°
180°
−120°
−60°
60°
0°
−60°
0
20
40
60
80
100
120
140
Half spreading rate (mm/yr)
−10
−5
0
5
10
Residual half spreading rate (mm/yr)
20
30
40
50
60
70
80
Crustal accretion (%)
−20
−10
0
10
20
Residual crustal accretion (%)
0
2
4
6
8
10
Age error (Myrs)
−10
−5
0
5
10
Residual error (Myrs)

Figure 27, pg 1

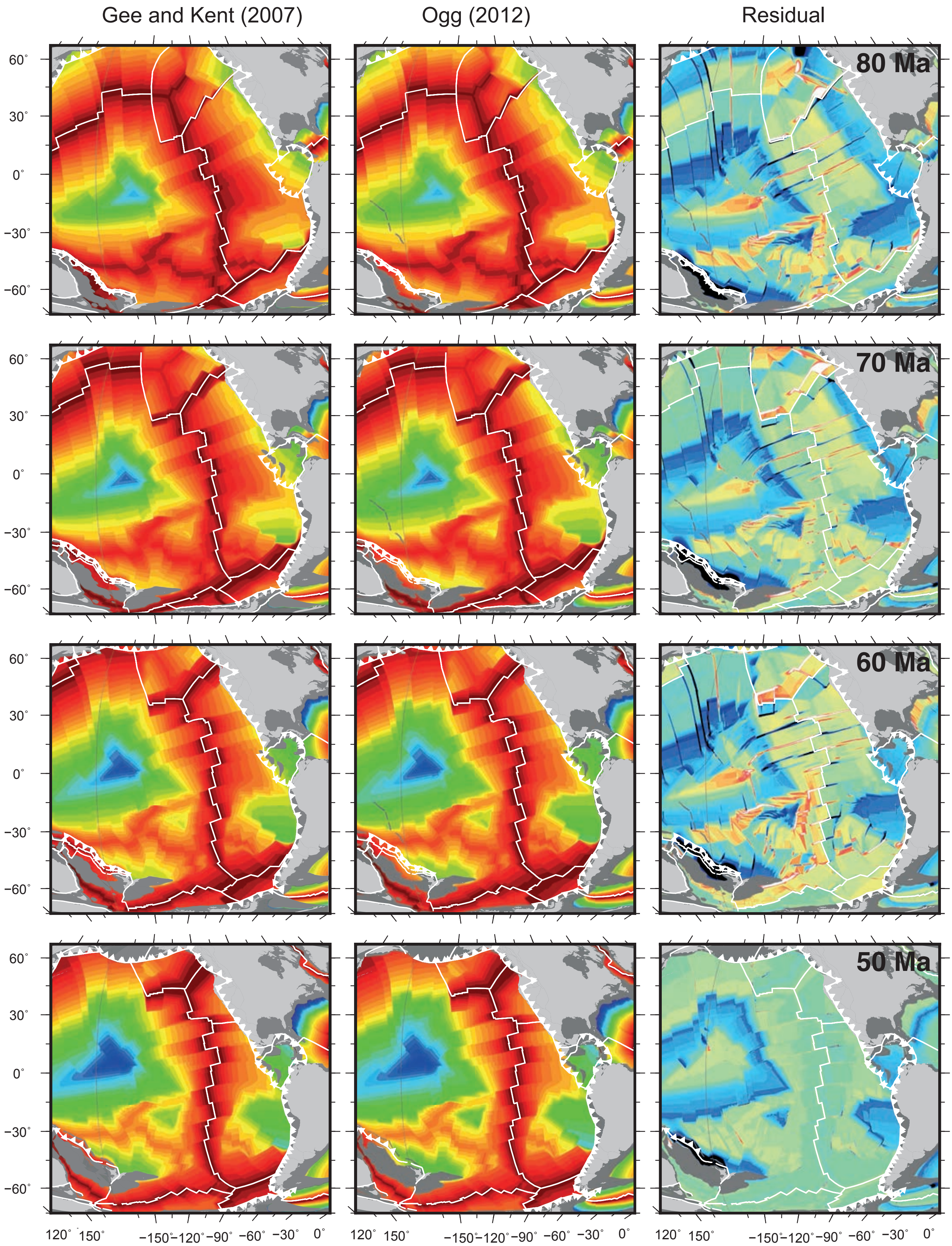

Figure 27, pg 2

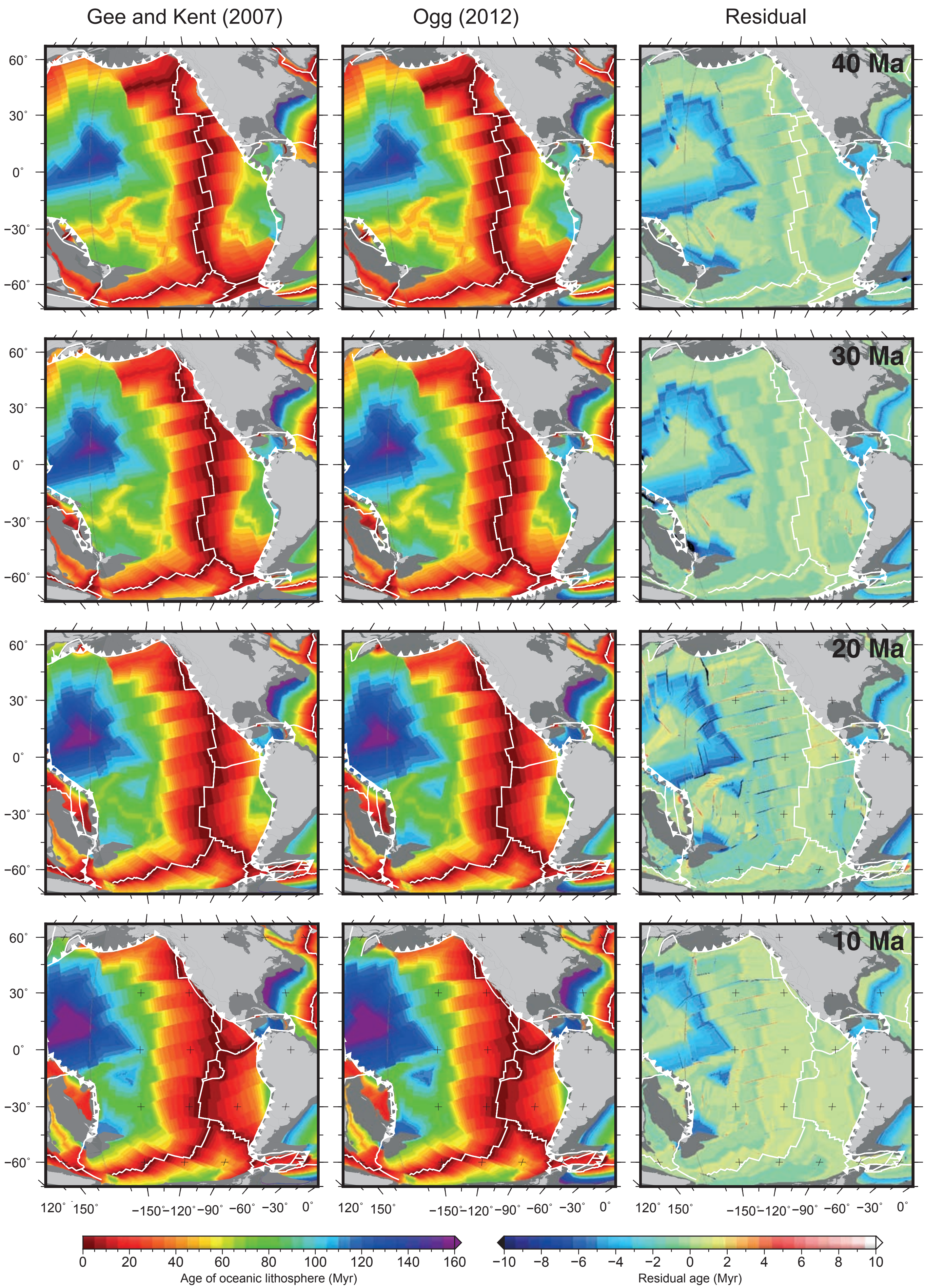

Figure 28

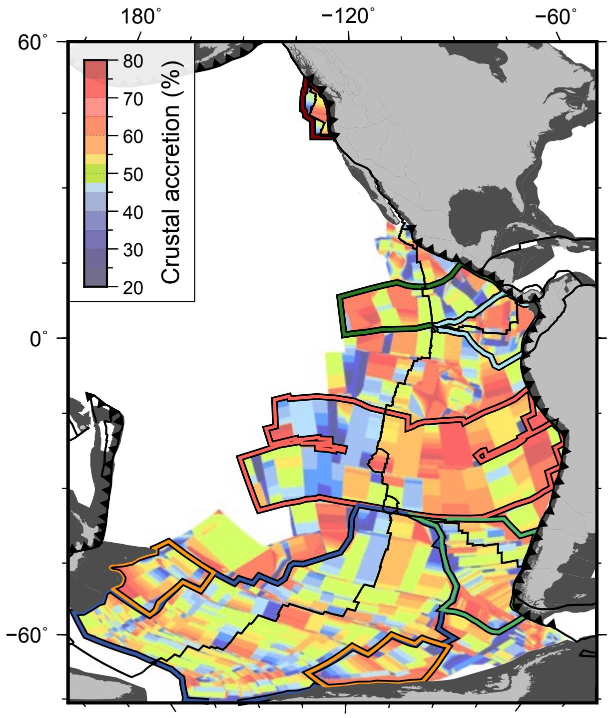

Figure 29

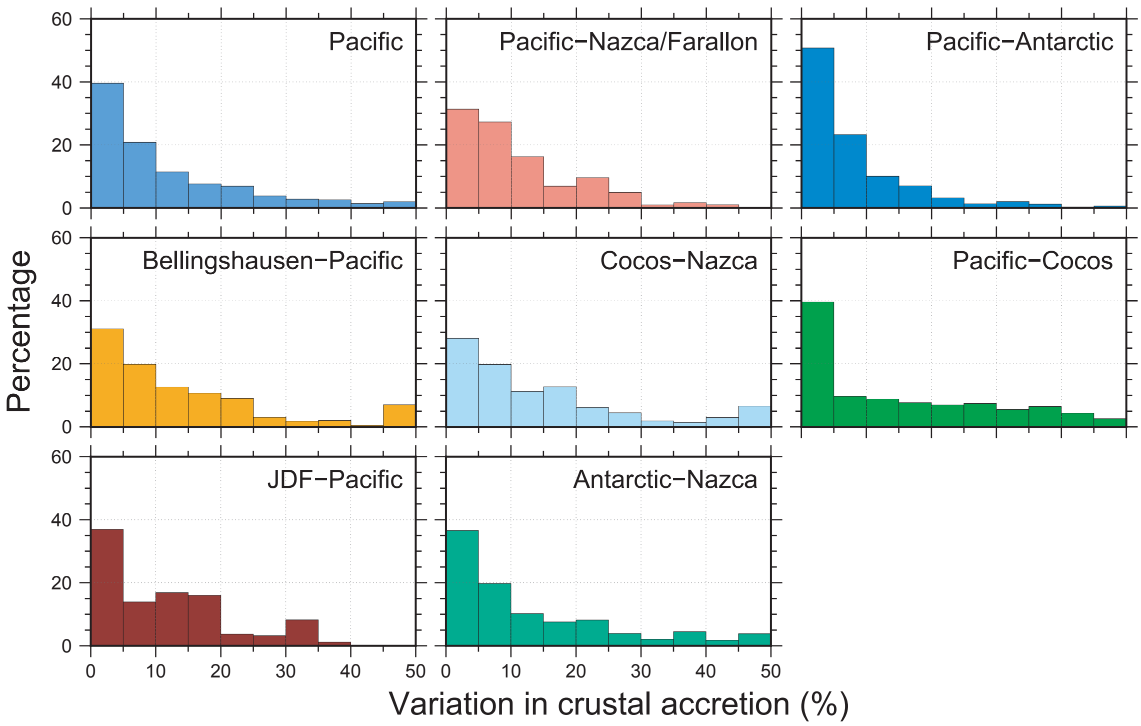

Pacific
Pacific−Nazca/Farallon
Pacific−Antarctic
Bellingshausen−Pacific
Cocos−Nazca
Pacific−Cocos
JDF−Pacific
Antarctic−Nazca
Percentage
Variation in crustal accretion (%)
0
20
40
60
0
10
20
30
40
50

Figure 30

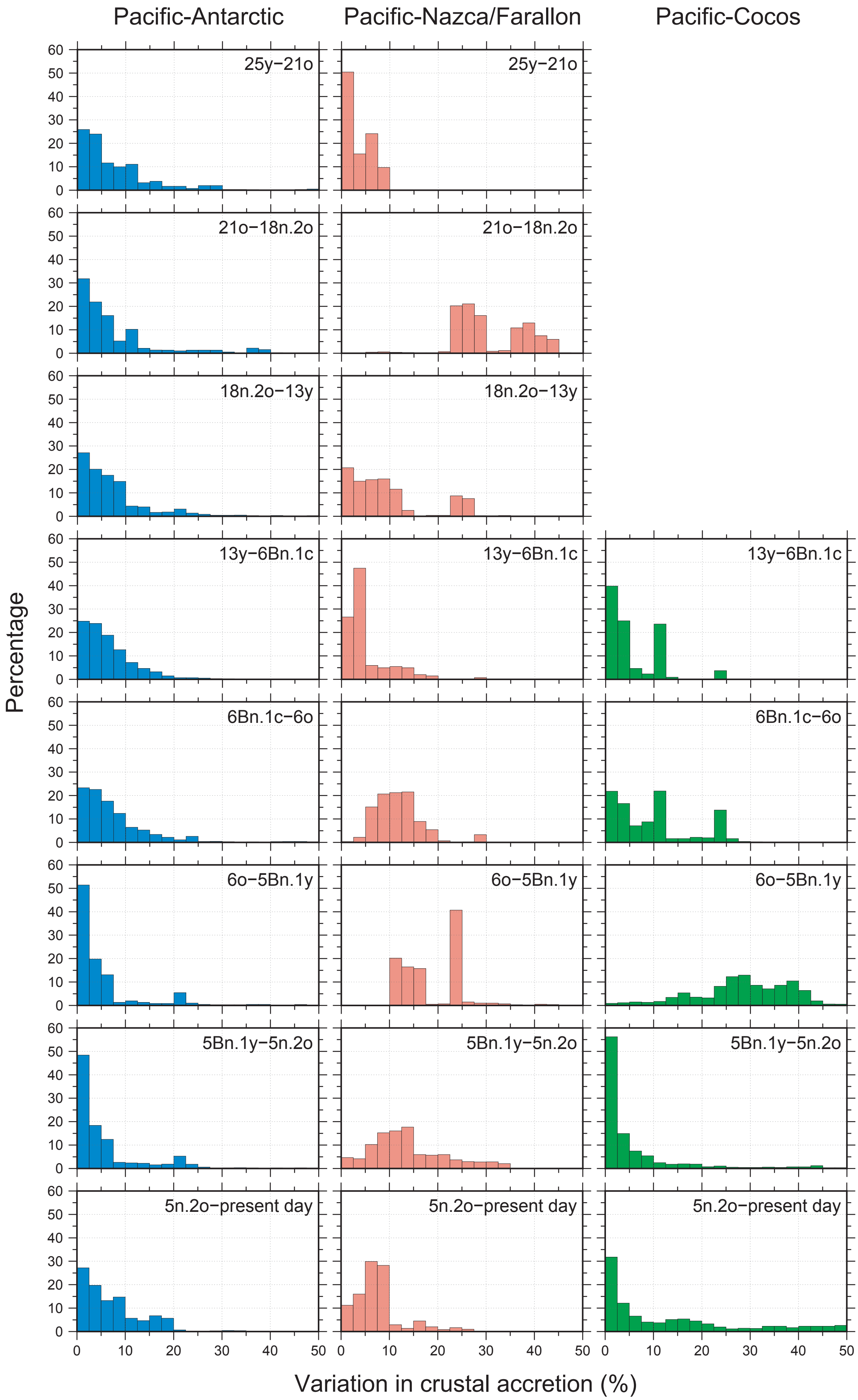

Pacific-Antarctic
Pacific-Nazca/Farallon
Pacific-Cocos
25y−21o
21o−18n.2o
18n.2o−13y
13y−6Bn.1c
6Bn.1c−6o
6o−5Bn.1y
5Bn.1y−5n.2o
5n.2o−present day
Percentage
Variation in crustal accretion (%)

Figure 31

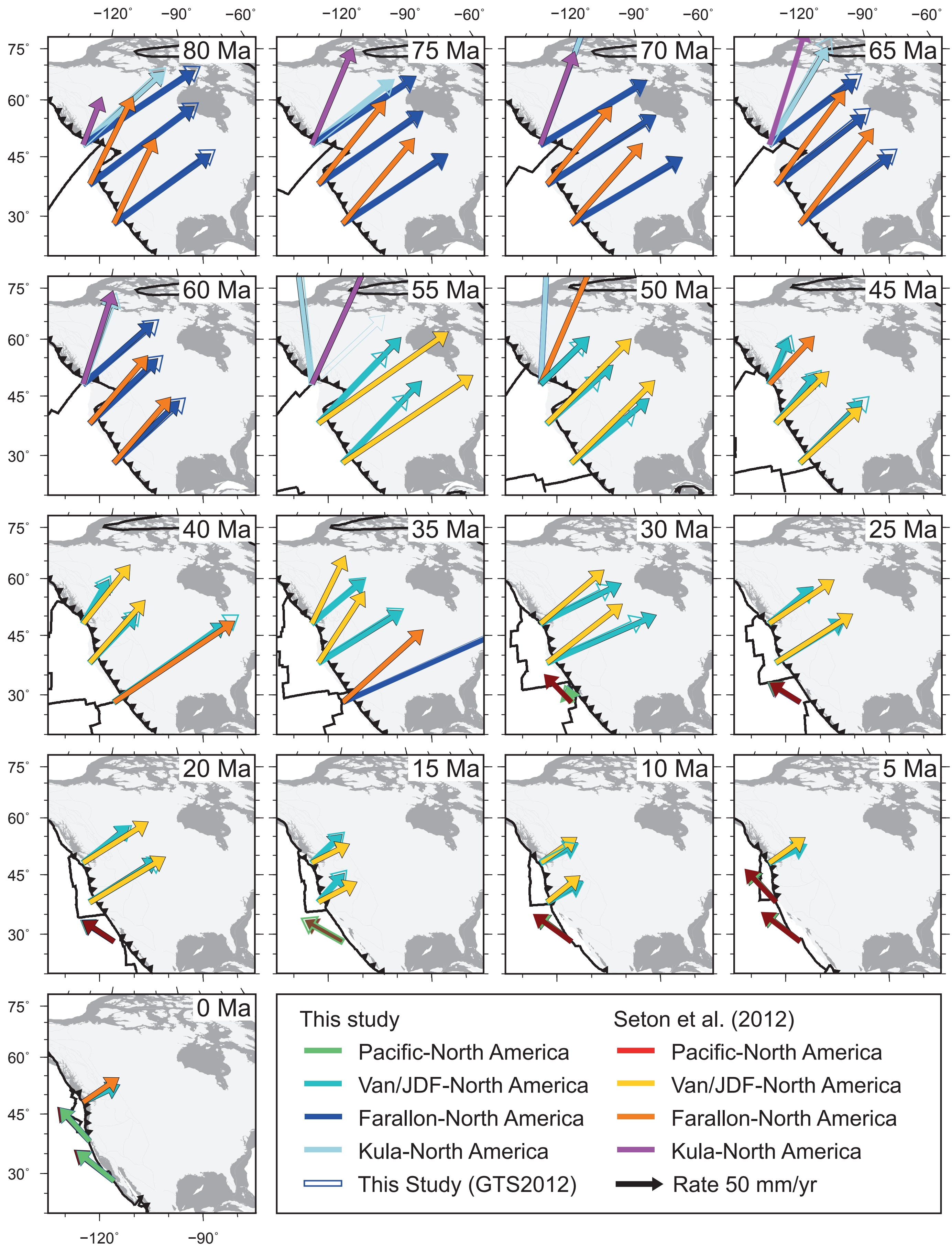

80 Ma
75 Ma
70 Ma
65 Ma
60 Ma
55 Ma
50 Ma
45 Ma
40 Ma
35 Ma
30 Ma
25 Ma
20 Ma
15 Ma
10 Ma
5 Ma
0 Ma
−120˚
−90˚
−60˚
75˚
60˚
45˚
30˚
This study
Pacific-North America
Van/JDF-North America
Farallon-North America
Kula-North America
This Study (GTS2012)
Seton et al. (2012)
Pacific-North America
Van/JDF-North America
Farallon-North America
Kula-North America
Rate 50 mm/yr

Figure 32

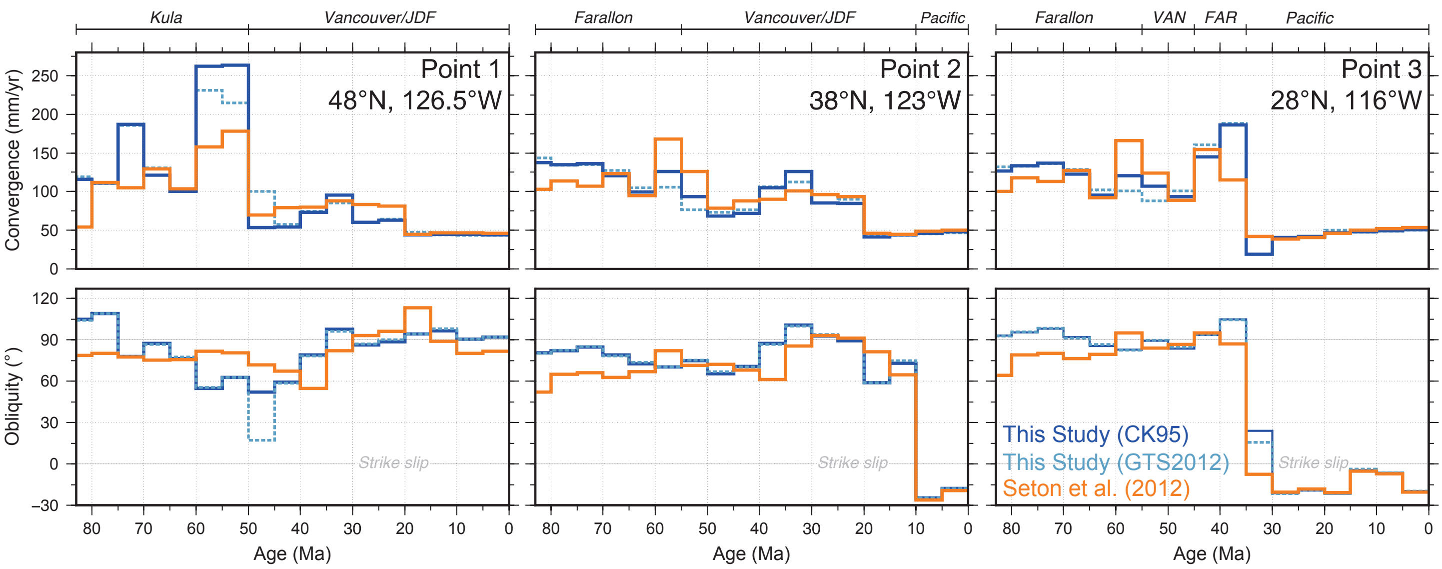

Kula
Vancouver/JDF
Farallon
Vancouver/JDF
Pacific
Farallon
VAN
FAR
Pacific
Point 1
48°N, 126.5°W
Point 2
38°N, 123°W
Point 3
28°N, 116°W
Convergence (mm/yr)
Obliquity (°)
Strike slip
Strike slip
Strike slip
This Study (CK95)
This Study (GTS2012)
Seton et al. (2012)
Age (Ma)
Age (Ma)
Age (Ma)

Figure 33

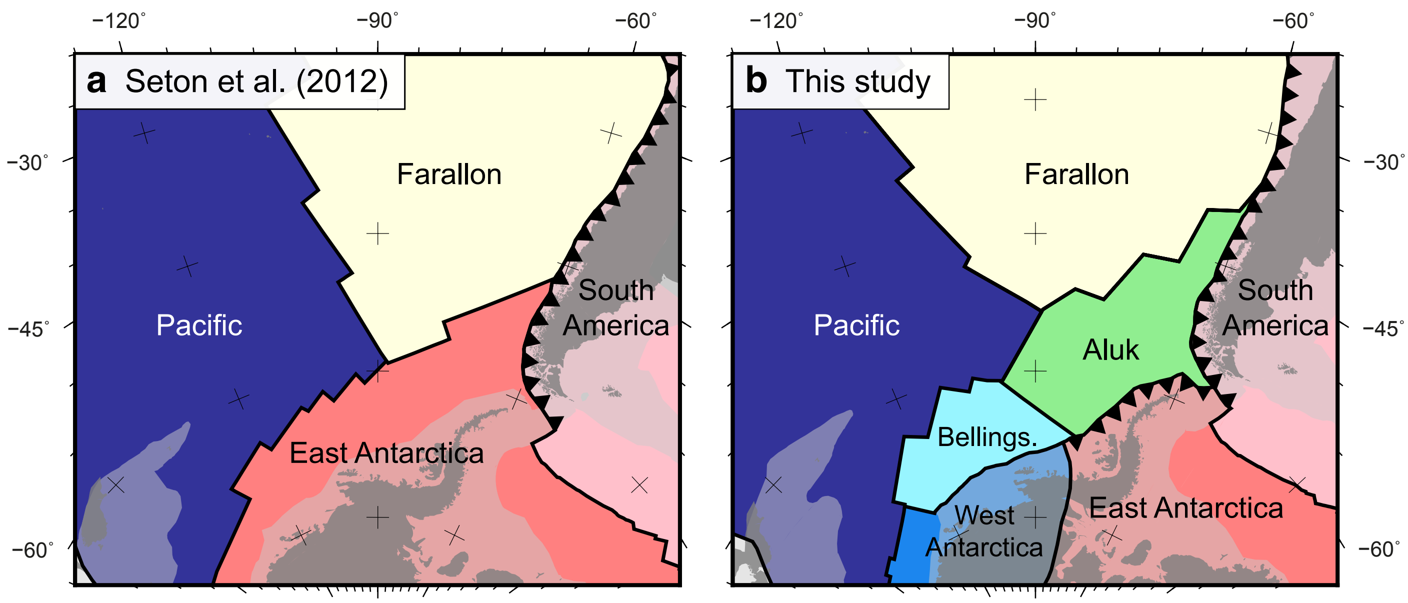

−120˚
−90˚
−60˚
−30˚
−45˚
−60˚
a Seton et al. (2012)
Farallon
Pacific
South America
East Antarctica
b This study
Farallon
Pacific
South America
Aluk
Bellings.
West Antarctica
East Antarctica

Figure 34

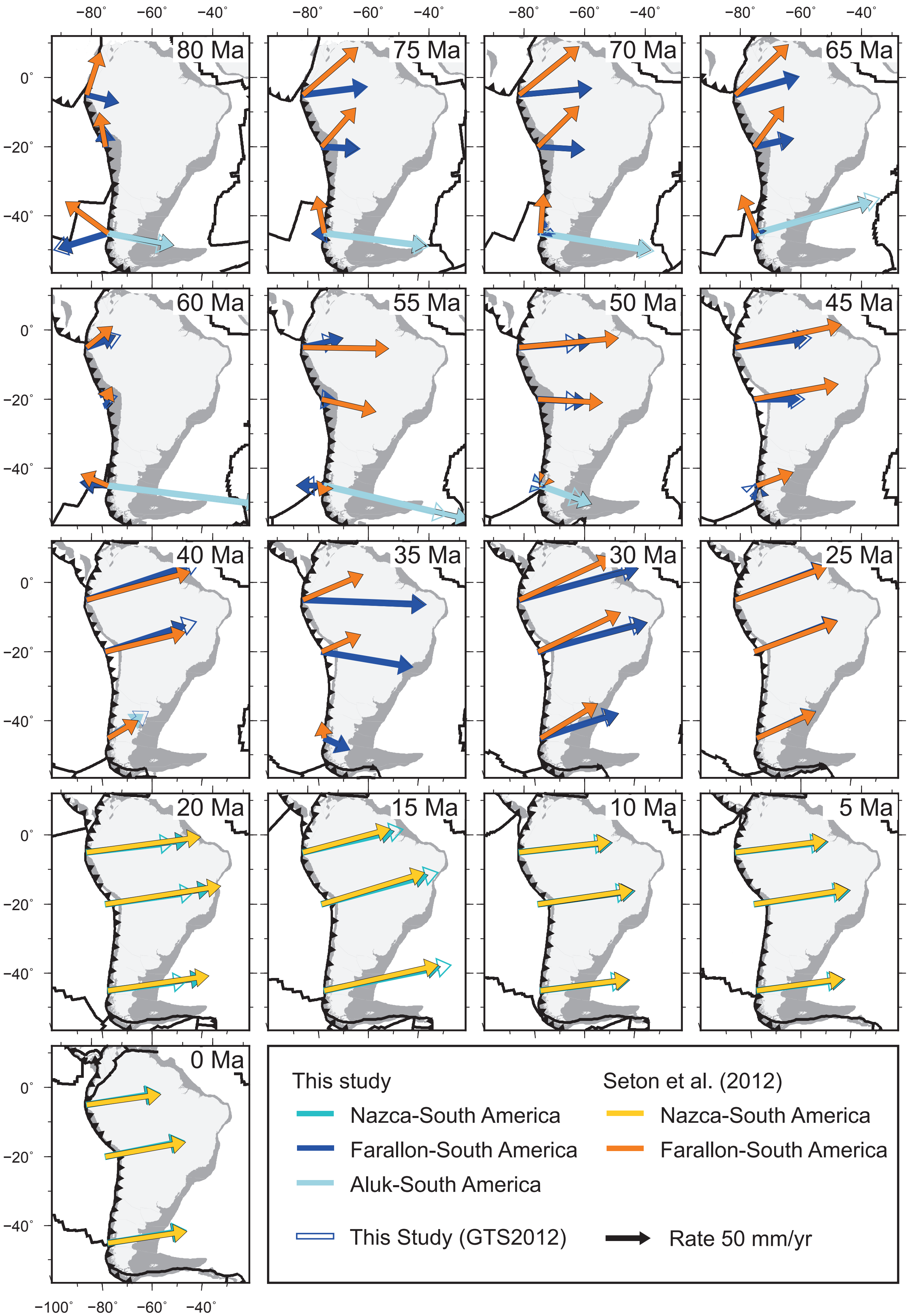
80 Ma
75 Ma
70 Ma
65 Ma
60 Ma
55 Ma
50 Ma
45 Ma
40 Ma
35 Ma
30 Ma
25 Ma
20 Ma
15 Ma
10 Ma
5 Ma
0 Ma
-100°
-80°
-60°
-40°
0°
-20°
-40°
This study
Nazca-South America
Farallon-South America
Aluk-South America
This Study (GTS2012)
Seton et al. (2012)
Nazca-South America
Farallon-South America
Rate 50 mm/yr

Figure 35

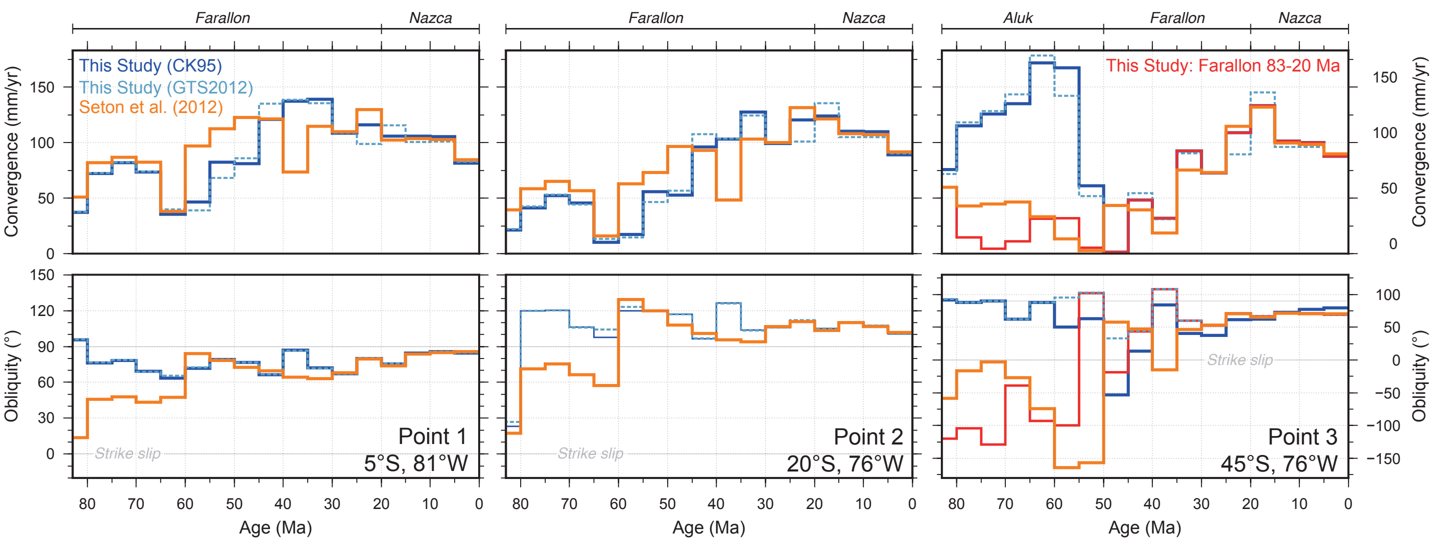

Farallon
Nazca
This Study (CK95)
This Study (GTS2012)
Seton et al. (2012)
Convergence (mm/yr)
Obliquity (°)
Strike slip
Point 1
5°S, 81°W
Point 2
20°S, 76°W
Aluk
This Study: Farallon 83-20 Ma
Point 3
45°S, 76°W
Age (Ma)

Figure 36

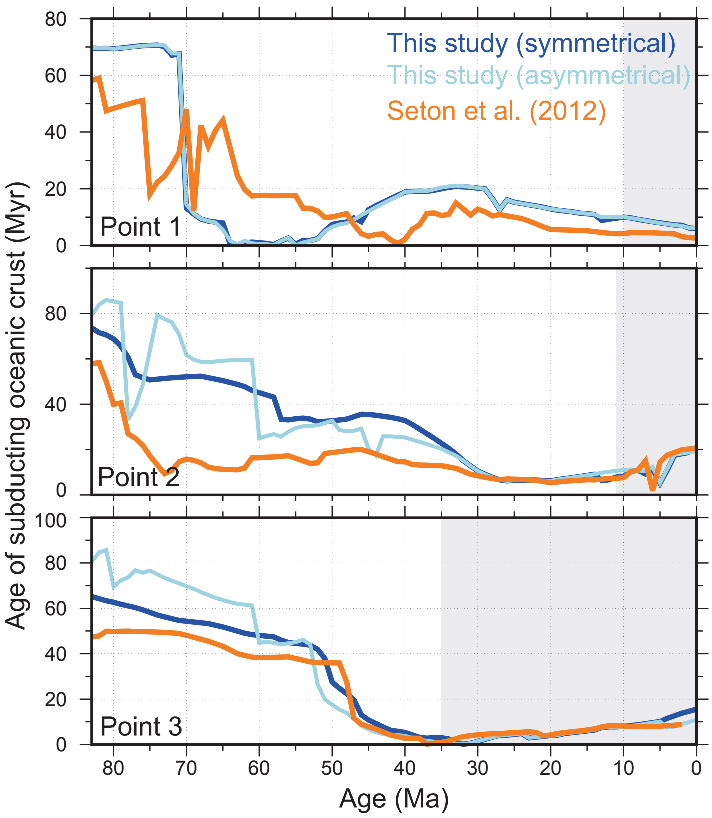

This study (symmetrical)
This study (asymmetrical)
Seton et al. (2012)
Point 1
Point 2
Point 3
Age of subducting oceanic crust (Myr)
Age (Ma)
80
60
40
20
0
80
40
0
100
80
60
40
20
0
80
70
60
50
40
30
20
10
0

Figure 37

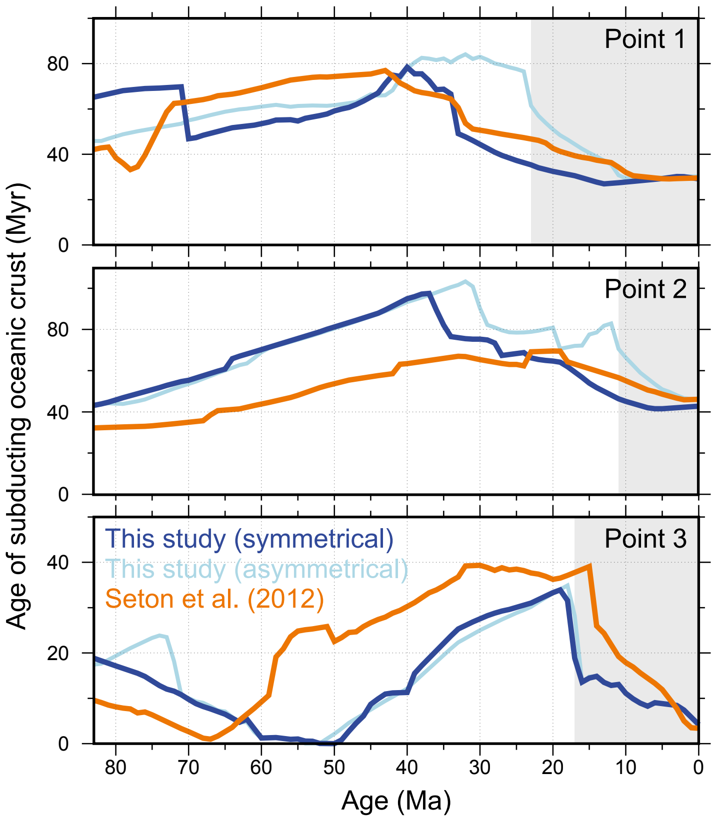

Point 1
Point 2
Point 3
This study (symmetrical)
This study (asymmetrical)
Seton et al. (2012)
Age of subducting oceanic crust (Myr)
Age (Ma)
80
40
0
80
40
0
40
20
0
80
70
60
50
40
30
20
10
0

The Late Cretaceous to recent tectonic history of the Pacific Ocean basin

Nicky M. Wright*, Maria Seton, Simon E. Williams, R. Dietmar Müller

EarthByte Group, School of Geosciences, University of Sydney, NSW 2006, Sydney, Australia

* Corresponding author: nicky.wright@sydney.edu.au

Keywords: Pacific, relative plate motions, seafloor spreading, plate reconstruction, tectonics

Abstract

A vast ocean basin has spanned the region between the Americas, Asia and Australasia for well over 100 Myr, represented today by the Pacific Ocean. Its evolution includes a number of plate fragmentation and plate capture events, such as the formation of the Vancouver, Nazca, and Cocos plates from the break-up of the Farallon plate, and the incorporation of the Bellingshausen, Kula, and Aluk (Phoenix) plates, which have studied individually, but never been synthesised into one coherent model of ocean basin evolution. Previous regional tectonic models of the Pacific typically restrict their scope to either the North or South Pacific, and global kinematic models fail to incorporate some of the complexities in the Pacific plate evolution (e.g. Bellingshausen and Aluk independent motion), thereby limiting their usefulness for understanding tectonic events and processes occurring in the Pacific Ocean perimeter. We derive relative plate motions (with 95% uncertainties) for the Pacific-Farallon/Vancouver, Kula-Pacific, Bellingshausen-Pacific, and early Pacific-West Antarctic spreading systems, based on recent data including marine gravity anomalies, well-constrained fracture zone traces and a large compilation of magnetic anomaly identifications. We find our well-constrained relative plate motions result in a good match to the fracture zone traces and magnetic anomaly identifications in both the North and South Pacific. In conjunction with recently published and well-constrained relative plate motions for other Pacific spreading systems (e.g. Aluk-West Antarctic, Cocos-Pacific, recent Pacific-West Antarctic spreading), we explore variations in the age of the oceanic crust, seafloor spreading rates and crustal accretion and find considerable refinements have been made in the central and southern Pacific. Asymmetries in crustal accretion within the overall Pacific basin (where both flanks of the spreading system are preserved) have typically deviated less than 5% from symmetry, and large variations in crustal accretion along the southern East Pacific Rise (i.e. Pacific-Nazca/Farallon spreading) appear to be unique to this spreading corridor. Through a relative plate motion circuit, we explore the implied convergence history along the North and South Americas, where we find that the inclusion of small

tectonic plate fragments such as the Aluk plate along South America are critical for reconciling the history of convergence with onshore geological evidence.

1 Introduction

The circum-Pacific is the most geologically active region in the world with a long, episodic history of subduction, arc volcanism, continental and back-arc extension. The interpretation of these geological processes along the margins of the Pacific relies on a detailed plate tectonic history of the adjacent ocean floor to relate the onshore geological record with the offshore seafloor spreading record. The present day seafloor spreading record of the Pacific basin involves the Pacific, Antarctic, Nazca, Cocos and Juan De Fuca plates and the smaller Rivera, Galapagos, Easter and Juan Fernandez micro-plates along the East Pacific Rise (Bird, 2003) (Figure 1; Figure 2). Additionally, the Pacific basin preserves clear evidence in the seafloor spreading record and seafloor fabric that several now extinct plates (e.g. Farallon, Phoenix, Izanagi, Kula, Aluk, Mathematician and Bauer plates; Figure 2) operated within this area, revealing that the Pacific Ocean basin has undergone a complex fragmentation and subduction history throughout its Mesozoic-Cenozoic history.

Previous plate tectonic models of the Pacific Ocean basin have either focussed on identifying magnetic lineations and deriving relative plate motions between presently active plates (e.g. Juan De Fuca-Pacific, Pacific-(West) Antarctic, Pacific-Nazca, and Cocos-Nazca), or on identifying magnetic lineations in those areas where conjugate magnetic lineations no longer exist due to subduction (e.g. Kula-Pacific, Izanagi-Pacific, Pacific-Farallon and Phoenix-Pacific spreading). Another suite of plate tectonic models are regional in nature (e.g. Engebretson et al., 1985; Atwater, 1989), combining the seafloor spreading histories of the majority of these plates into one coherent study. These studies are hugely beneficial for deciphering the evolution of the largely continental circum-Pacific plates, including the subduction histories along these margins; the deep mantle structure beneath the Pacific and its margins; the evolution of the Hawaiian-Emperor Bend (HEB); and the effect of changing plate circuits on the motion of the Pacific plate. In addition, these models allow us to assess the validity of relative plate motion models of individual plate pairs by ensuring that the motion they imply is consistent with the geological evidence from the surrounding regions.

Several recent advances, such as the development of high-resolution satellite altimetry data (e.g. Sandwell et al., 2014); the establishment of a repository of magnetic anomaly identifications (Seton et al., 2014); and the development of plate reconstruction software *GPlates* (Boyden et al. 2011) have prompted a re-analysis of the seafloor spreading history of the Pacific Ocean basin. In particular, the recent satellite gravity anomaly data have greatly improved kinematic models by providing tight constraints on the direction of plate motion through the identification (with spatial confidence) of fracture zones and related features throughout the world's ocean basins (Matthews et al., 2011; Wessel et al., 2015).

Here, we revise the plate tectonic history of the Late Cretaceous (83 Ma) to present day Pacific Ocean in order to investigate the differences in the tectonic history of the Pacific basin (e.g. Pacific-West Antarctic, Pacific-Nazca/Farallon, Pacific-Vancouver/Farallon) and its influence on spreading rate and asymmetry and the implied convergence history along the North and South America margins. We provide relative plate motions with 95% uncertainties for the Pacific-West Antarctic, Bellingshausen-Pacific, Pacific-Farallon, and Kula-Pacific, based on recent fracture zone traces (Matthews et al., 2011) and a compilation of magnetic identifications (Seton et al., 2014). We refine the tectonic plate configuration of the plates in the Pacific basin since the Late Cretaceous (chron 34y; 83 Ma), to include tectonic plates omitted in Seton et al. (2012) and Müller et al. (2008) (e.g. Aluk and Bellingshausen plates) and to refine the extent and timing of tectonic plates (e.g. Kula, Vancouver, Rivera).

2 Methodology

2.1 Magnetic anomaly and fracture zone data

We utilise a synthesis of 481 published magnetic anomaly identifications (‘picks’) from the following studies: Atwater and Severinghaus (1989), Cande et al. (1995), Elvers et al. (1967), Granot et al. (2009), Larter et al. (2002), Lonsdale (1988), Munschy et al. (1996), Wobbe et al. (2012). These magnetic anomaly identifications were downloaded from the Global Seafloor Fabric and Magnetic Lineation (GSFML) repository (Seton et al., 2014). Metadata associated with the magnetic picks are preserved, including reference, chron, anomaly end (old [‘o’], young [‘y’], or center [‘c’]) and the confidence of the magnetic anomaly end assignment. Throughout our paper we cite the normal polarity of chrons, and ages assigned to magnetic identifications are given in the timescale of Cande and Kent (1995), except where noted. Full magnetic pick coverage of the south Pacific, southeast Pacific, and northeast Pacific used in this study can be seen in Figure 3. We rely on digitized fracture zone traces from the GSFML repository (Matthews et al., 2011; Wessel et al., 2015). These fracture zone traces are updated as new data, such as new marine gravity data (Sandwell et al., 2014) are available. The magnetic anomaly identifications and fracture zone traces are the primary constraints in refining the relative plate motions in our study region.

2.2 Relative plate motions

Relative plate motions were computed as finite rotations in regions where both flanks of the spreading system are preserved (Figure 4a). We calculate finite rotation parameters for the Pacific-West Antarctic (chron 34y–33y) and Bellingshausen-Pacific (chron 33o–28o) spreading systems, and rely on published finite rotation parameters for later times (Croon et al., 2008; Wright et al., 2015). In cases where the conjugate flank has been subducted, we derive half-stage rotation parameters by reconstructing the younger chron to the older (‘fixed) chron on the preserved spreading flank (Figure 4b). Stage rotations and finite rotations were subsequently calculated, based on assumed symmetrical spreading. We calculate half-stage rotations for Pacific-Farallon (chron

34y–31y), Kula-Pacific (chron 34y–25y), Vancouver-Pacific (chron 13y–4Ac), and Pacific-Aluk (chron 34y–27o) spreading systems, and use published rotations from Wright et al. (2015) and Müller et al. (2008) for other times. Relative plate motions and uncertainties were revised using magnetic picks and fracture zone identifications and the best fitting criteria of Hellinger (1981), as implemented using the methods described in Chang (1987); Chang (1988) and Royer and Chang (1991).

Uncertainties for magnetic anomaly identifications are primarily navigational uncertainties (Kirkwood et al., 1999), and dispersion analysis of data obtained through different navigation methods (e.g. celestial navigation, Transit, Global Positioning System [GPS]) suggests these errors range from 3.0 to 5.2 km (Royer et al., 1997). Since our magnetic identification compilation includes data from different navigation methods, we obtain our magnetic identification uncertainty using the method outlined in Gaina et al. (1998). We assign the 1-sigma standard error (σ) of the magnetic data as our magnetic uncertainty, based on $\sigma = \hat{\sigma}/\sqrt{\hat{\kappa}_{\text{avg}}}$, where $\hat{\sigma}$ is the estimated uncertainty (10 km), and $\hat{\kappa}_{\text{avg}}$ is the harmonic mean of the quality factor ($\hat{\kappa}$) for each magnetic anomaly crossing. For Pacific-West Antarctic/Bellingshausen finite rotations, we obtain $\hat{\kappa}_{\text{avg}}$ of 2.1 and σ of 6.9 km. For Pacific-Farallon/Vancouver/Kula rotations, we find $\hat{\kappa}_{\text{avg}}$ of 1.6 and σ of 7.8 km. We assign a 5 km uncertainty to fracture zone identifications, based on the average horizontal mismatch between topographic and gravity lows in the central North Atlantic (Müller et al., 1991). The quality factor $\hat{\kappa}$ indicates how well uncertainties have been estimated: uncertainties are closely estimated when $\hat{\kappa} \approx 1$, whilst when $\hat{\kappa} \ll 1$ errors are underestimated, and errors are overestimated when $\hat{\kappa} \gg 1$.

We derive rotations at times broadly similar to commonly identified seafloor spreading isochrons, e.g. chrons 21o, 25y, 31y, 34y. We rely on synthetic flowlines to assess our derived rotations, whereby our rotation parameters are considered suitable if a good spatial and temporal match is obtained between the synthetic flowline and corresponding fracture zone segment. Synthetic flowlines were created at reconstructed times, to avoid propagating complexities from recent spreading, such as known asymmetric spreading (e.g. Nazca-Pacific).

We embed our relative rotation parameters into a modified version of the Seton et al. (2012) global kinematic model. Key modifications to this kinematic model of relevance to the Pacific plate, include an update to the moving hotspot absolute reference frame to Torsvik et al. (2008); and an update to the relative motions of the West Antarctic Rift System (WARS) based on Matthews et al. (2015).

Seafloor spreading isochrons in the Pacific basin were created based on our rotation parameters and magnetic anomaly identifications. Seafloor spreading isochrons were constructed at chrons 5n.2o (10.9 Ma), 6o (20.1 Ma), 13y (33.1 Ma), 18n.2o (40.1 Ma), 21o (47.9 Ma), 25y (55.9 Ma), 31y (67.7 Ma), and 34y (83 Ma), in order to be consistent with the scheme developed by Müller et al. (2008) and to link the Pacific seafloor spreading history to the Atlantic and Indian Ocean realms. Additional isochrons were created at intermediate times to reflect major tectonic events, e.g. formation of the Bellingshausen plate at chron 33o (79.1 Ma), and formation and motion of the Bauer microplate. Through a set of seafloor spreading isochrons, seafloor spreading ridges (present day and extinct), and defined continent-ocean-boundaries (COB), grids showing the age-area distribution of oceanic crust were created between 83 Ma and present day, corresponding to the time period of revised rotation parameters.

2.3 Implied convergence history

We calculate the implied convergence history of the Pacific plates with respect to the Americas (North America, South America) between 83 Ma and present day. Points were chosen along the trench adjacent to North America (point 1: 48°N, 126.5°W; point 2: 38°N, 123.4°W; point 3: 28°N, 116°W) and South America (point 1: 5°S, 81°W; point 2: 20°S, 76°W, point 3: 45°S, 76°W) to capture differences in the plate configuration and tectonic regimes experienced by these margins. Convergence velocities were calculated orthogonal to the trench, whilst obliquity was calculated based on the difference between the strike of the trench and the true convergence angle (bearing from North), where an obliquity angle of 0° suggests strike slip motion. All convergence parameters were calculated in 5 Myr increments, except the stage from 80-83 Ma.

The convergence histories are calculated using a plate chain that involves relative rotations for North or South America-Africa, Africa-East Antarctica, East Antarctica-West Antarctica (from Matthews et al., 2015), and West Antarctica to the Pacific. We used the rotations from the compilation of Seton et al (2012) unless otherwise stated.

3 Pacific basin tectonics since chron 34y (83 Ma)

In the following section we describe the regional tectonic evolution of the Pacific basin. We present our derived relative rotation parameters within each section (section 3.1.1, section 3.1.2, section 3.1.3, section 3.2.1, section 3.2.2, section 3.2.3). For a comprehensive review of Pacific basin development prior to 83 Ma, see section 3.2 in Seton et al. (2012).

3.1 South Pacific spreading history

The evolution of the South Pacific is essential in reducing uncertainties in global circuit calculations, since the spreading history in this region links plate motions in the Pacific and Indo-Atlantic realms within the global plate circuit from the Late Cretaceous to present day (Cande et al., 1995; Larter et al., 2002; Matthews et al., 2015). The Antarctic and Pacific plates presently dominate spreading in this region, however the former Aluk plate (also known as the Phoenix or Drake plate), Bellingshausen, and Farallon plates have all contributed to the complex evolution of the region, observed in gravity anomalies and magnetic identifications (Figure 5). Prior to chron 34y (83 Ma), this region involved Aluk-Farallon, Pacific-Aluk and Pacific-Farallon spreading (Eagles et al., 2004a; Larter et al., 2002; Mayes et al., 1990; Weissel et al., 1977) and the early separation of Zealandia and West Antarctica (Larter et al., 2002).

The Aluk plate was initially named as a South Pacific analogue of the northern Pacific Kula Plate (Herron and Tucholke, 1976), however, it has since been noted that it is a fragment of the Mesozoic Phoenix plate (Barker, 1982). Although many publications describing the Late Cretaceous and Cenozoic history of the Aluk plate use the name 'Phoenix', we rely on the term 'Aluk' plate to distinguish this fragment's spreading history since chron 34y (83 Ma) from the preceding Phoenix plate evolution and break-up history in the Cretaceous (i.e. Seton et al., 2012).

The final stages of Gondwana breakup and early stages of Zealandia-West Antarctic separation are not fully understood, with ambiguities in the oldest age of seafloor spreading, in the timing of independent West Antarctic and Bellingshausen motion, and the formation history of the Bounty Trough and Bollons Seamounts. The separation of Zealandia and West Antarctica is thought to initiate with rifting and crustal extension between the Chatham Rise (Figure 5) and West Antarctica around ~90 Ma (Eagles et al., 2004a; Larter et al., 2002). Seafloor spreading is believed to have started at ~85 Ma near the Bounty Trough (Davy, 2006), although the earliest magnetic identification in this region is a tentative chron 34y (83 Ma). Early seafloor spreading was highly asymmetric and involved a number of ridge jumps, including a ridge jump of the Bounty Trough rift to the Marie Byrd Land margin (Davy, 2006), and the initiation of seafloor spreading between Campbell Plateau and West Antarctica, during chron 33r (83–79.1 Ma) (Larter et al., 2002).

Mismatch in magnetic anomalies southeast of Zealandia and inferred Pacific-West Antarctic spreading led to the proposition of the independent Bellingshausen plate (Stock and Molnar, 1987). The Bellingshausen plate experienced independent motion from chron 33o (79.1 Ma) (Eagles et al., 2004b), with Bellingshausen-Pacific spreading forming seafloor west of the Bellingshausen gravity anomaly (BGA) (Figure 5). An additional fragment of the Aluk plate has been inferred in this region, known as the Charcot plate (McCarron and Larter, 1998): this plate forms the present-day triangular region of oceanic crust near Peter I Island, bounded by the BGA, southern De Gerlache gravity anomaly (DGGA), and Marie Byrd Land continental margin (Larter et al., 2002) (Figure 5). The Charcot plate was captured by the West Antarctic plate during Zealandia-West Antarctic breakup (by chron 34y), as subduction of the Charcot plate stalled (Larter et al., 2002; Cunningham et al., 2002).

By chron 34y (83 Ma), the West Pacific-Aluk spreading system was already established. Since chron 34y, the fast spreading Pacific-Aluk ridge has been replaced by slower spreading Pacific-

Antarctic and Antarctic-Aluk ridges (Cande et al., 1982). These ridge reorganisations are proposed to have occurred at chron 29 (~64 Ma), chron 28 (~63 Ma) and chron 21 (~47 Ma) (Cande et al., 1982), and are evident by the sequences of South Pacific magnetic lineations. However, re-interpretation and additional collection of magnetic lineations between the Tharp and Heezen Fracture zones indicates a north-westward younging trend in this area (Larter et al., 2002; Wobbe et al., 2012), suggesting this segment formed from Bellingshausen-Pacific spreading, rather than an earlier initiation of Aluk-Antarctic spreading at chron 29 (Cande et al., 1982; McCarron and Larter, 1998).

At chron 27 (~61 Ma), a tectonic reorganisation in the south Pacific (Eagles, 2004; Eagles et al., 2004b), led to the incorporation of the Bellingshausen plate into the West Antarctic plate (Eagles et al., 2004b), the initiation of Aluk-West Antarctic spreading (Eagles et al., 2004b), and changes in Australia, Antarctica and Zealandia relative motions (Eagles et al., 2004b). The timing of Bellingshausen plate incorporation has previouly been suggested to be much later, at chron 18 (~39 Ma) (Stock and Molnar, 1987) or chron 24 (~53 Ma) (Mayes et al., 1990). At chron 27, Aluk-West Antarctic spreading initiated (Eagles and Scott, 2014), and was concurrently active with a Pacific-Aluk divergent boundary. The DGGA is thought to represent a ‘scar’ from the westward ridge jump of Bellingshausen-Aluk to West Antarctic-Aluk spreading at this time (Larter et al., 2002).

A number of right-stepping fracture zones developed at chron 27 along the Pacific-Antarctic ridge, including the right-stepping Pitman Fracture Zone (Cande et al., 1995). The trace of the Pacific-Farallon-Aluk triple junction between chron 27 and 21 is inferred by the Humboldt Fracture Zone (Cande et al., 1982), which formed as a transform fault connecting Pacific-Aluk and Farallon-Aluk spreading (Cande et al., 1982).

At chron 21 (~47 Ma), Pacific-Antarctic ridge propagation resulted in the Pacific flank of the final Pacific-Aluk spreading corridor (i.e. situated between the Tula and Humbuldt Fracture Zones) to be captured by the West Antarctic plate (Eagles, 2004). The propagation of the Pacific-Antarctic ridge is marked by the Hudson trough, a 'scar' on the West Antarctic plate as the ridge (Cande et al., 1982). The Henry Trough forms the conjugate feature on the Pacific plate (Cande et al., 1982). This propagating rift system led to the formation of the Menard Fracture Zone (Croon et al., 2008). At ~47 Ma, the West Antarctic-Aluk ridge replaced the former Pacific-Aluk ridge, as the Pacific-West Antarctic spreading center propagated eastward at chron 21 (Mayes et al., 1990).

Between chron 20 (~43 Ma) and chron 5, an overall 12° (Cande et al., 1995) to 15° (Lonsdale, 1986) counterclockwise change occurred in Pacific-West Antarctic spreading, based on observations along the Eltanin Fracture Zone. Additional changes in Pacific-West Antarctic spreading direction have been determined based on a detailed study of the Menard Fracture Zone, with a clockwise change at chron 13o (33.5 Ma) a counterclockwise change at chron 10y (28.3 Ma) (Croon et al., 2008). During this time period, the Pacific-Farallon ridge underwent a 5° clockwise change at chron 7 (~25 Ma), followed by Farallon plate fragmenation and Cocos and Nazca plate formation (see section 3.2) (Barckhausen et al., 2008). Since chron 5y (9.7 Ma), the Pacific-Antarctic ridge has undergone a clockwise change in spreading direction (Croon et al., 2008).

The Aluk plate was incorporated into the West Antarctic plate around chron 2A (~3.3 Ma) (Larter and Barker, 1991; Livermore et al., 2000), possibly as a result of ridge-trench collision SW of the Hero Fracture zone (along the Antarctic peninsular) (Larter and Barker, 1991) and the resultant reduction in slab width and slab pull (Livermore et al., 2000).

East-West Antarctic motion

Motion has been inferred between West and East Antarctica throughout the Cenozoic based on large misfits in southwest Pacific plate reconstructions (Cande et al., 2000), however reconstructions of the relative movement between East and West Antarctica (Marie Byrd Land) are generally poorly constrained. Anomalies from the Adare trough (a fossil rift valley) (Figure 5) indicate a former ridge-ridge-ridge triple junction in this area between chrons 20 and 8 (43–26 Ma) (Cande et al., 2000) and may be the site of the East-West Antarctic boundary during the Eocene and Oligocene (Cande et al., 2000; Müller et al., 2007). Due to the few data points useful for plate reconstructions that are confined to the short seafloor spreading portion of the East-West Antarctic plate boundary, most of which was a transform boundary straddling the Transantarctic Mountains, and ambiguities in magnetic anomaly identification (Cande et al., 2000), the few reconstructions of East Antarctica-West Antarctica result in uncertainties ranging from ~500 km (Granot et al., 2013) to ~5000 km (Cande et al., 2000). The type of motion described in East-West Antarctic models also differ: a recent study has indicated motion varied from east northeast-west southwest extension in the Adare Basin, to dextral transcurrent motion in the central parts of the rift zone, with predominant oblique convergence in the eastern parts of the West Antarctica Rift System (WARS) (Granot et al., 2013), whereas previous models indicated extensional motion throughout the WARS (Cande et al., 2000) and dextral transcurrent motion (Müller et al., 2007).

3.1.1 Relative Pacific-West Antarctic plate motion

Relative Pacific-West Antarctic plate rotations published within the last two decades are listed in Table 1.

Spreading velocities along the Pitman Fracture Zone suggest an increase in spreading rate between 83 Ma and ~70 Ma, followed by a ~40 mm/yr decrease in spreading rate until ~40 Ma (Figure 6). Little variation in spreading rate occurs until ~33 Ma, after which the spreading rate increases until present day. This is accompanied by a ~60° counterclockwise change in spreading direction between 83 Ma and 20 Ma, followed by a ~15° clockwise change until present day (Figure 6). We note differences arise between Eagles et al. (2004a) and Cande et al. (1995), due to a slight difference in anomaly end assignment. Whilst there is broad agreement in the Pacific-West Antarctic spreading velocities, notable variation is observed between Wobbe et al. (2012) and Cande et al. (1995), in particular, at 80 Ma and between 65–40 Ma. These variations can be attributed to the small stage intervals used in Wobbe et al. (2012) analysis, which increase rotation noise unless the rotations are smoothed (Iaffaldano et al., 2014). A large change in spreading velocity is observed in Eagles et al. (2004a) at 67 Ma, which may arise from merging the finite rotation parameters of Cande et al. (1995) and Stock et al (unpublished).

Our reconstruction of the Pacific-West Antarctic ridge since chron 34y (83 Ma) relies on a combination of published rotation parameters and derived finite rotations. We rely on the tightly constrained rotation parameters in Croon et al. (2008) between chrons 20o to 1o (43.79 Ma–0.78 Ma). Since kinematic models of the earlier Pacific-West Antarctic spreading history do not incorporate spatially constrained fracture zone identifications (e.g. Cande et al. 1995) or do not incorporate all available magnetic identifications (Wobbe et al., 2012), we derive finite rotations and uncertainties for chrons 33y to 21o (73.6–47.9 Ma) (Table 2; Figure 7). The rotation pole for chron 34y (83 Ma) is based on the spreading velocity of stage chron 33y–30o (73.6–67.7 Ma), due to the absence of reliable magnetic identifications for this time. Our $\hat{\kappa}$ values ranged between 0.87 and 4.94 (Table 2): chrons 27o and 30o have a high $\hat{\kappa}$ value (4.94 and 2.50, respectively), suggesting we overestimated the assigned magnetic identification or fracture zone uncertainties.

Our derived Pacific-West Antarctic rotations parameters exhibit a comparable trend to previous models (i.e. Cande et al., 1995; Eagles et al., 2004a; Müller et al., 2008; Wobbe et al., 2012) (Figure 8). The flowlines produced from this study demonstrate the best fit with the fracture zone interpretations (Matthews et al., 2011) and the marine gravity anomaly data (Figure 8), compared with other previously published models. For example, the relative plate motions from Wobbe et al. (2012) demonstrate a partial match with the fracture zone identifications during the earliest spreading history (83–75 Ma), and a large change in spreading direction between chrons 27–25, in contrast to the more gradual change during this time from this study (Figure 7). These differences may be attributed to the more limited dataset used in Wobbe et al. (2012) analysis.

3.1.2 Relative Bellingshausen-Pacific plate motion

Published rotations for the Bellingshausen-Pacific are listed in Table 3. Larter et al. (2002) and Eagles et al. (2004a) rely on common rotations, resulting in similar spreading velocities (Figure 9). Spreading rate and direction differs by up to 20 mm/yr and 10° between Wobbe et al. (2012) and other models of Bellingshausen-Pacific spreading, in particular, between chron 33o and chron 33y, and chron 31y-28o (Figure 9). There is little difference in the trend of spreading direction derived in the timescales of Cande and Kent (1995) and Ogg (2012), however, there is a difference in spreading rate: Cande and Kent (1995) results in a ~10 mm/yr larger increase in rate at chron 33y, whilst Ogg (2012) results in 5 mm/yr increase in spreading rate at chron 31y (Figure 9).

We reconstruct the Bellingshausen plate during its period of independent motion i.e. chron 33o to 27o. We derive well-constrained finite rotations, with up to 10° of uncertainty in the calculated 95% confidence ellipses (Figure 10). $\hat{\kappa}$ values ranged between 0.46 to 1.01 (Table 4), indicating the fracture zone and magnetic pick uncertainties were slightly underestimated.

Our Bellingshausen-Pacific rotations display similar spreading velocities to published models between chron 33y and chron 28o (Figure 9) and a good spatial match is observed between derived flowlines and preserved fracture zone geometries (Figure 11). A comparison of our Bellingshausen-Pacific flowlines and flowlines produced from Eagles et al. (2004a), Wobbe et al. (2012) and Larter et al. (2002) indicate a similar spreading history between all models for the period of 70–60 Ma

(Figure 11). Discrepancies arise in the modelled flowline and fracture zone geometries during the early Bellingshausen-Pacific spreading; whilst all models closely match the latter spreading history, our model results in a closer match to the early Bellingshausen-Pacific spreading history along the Udintsev Fracture Zone than Wobbe et al. (2012) and Eagles et al. (2004a). This is likely a result of different interpretation of the fracture zones in this area, which is hampered by magmatic overprinting (Gohl et al., 2007) present in the satellite gravity (Sandwell et al., 2014).

3.1.3 Relative Aluk (Phoenix)-West Antarctic plate motion

We rely on recently published Aluk-West Antarctic relative plate motions (Eagles and Scott, 2014) for the Aluk plate spreading history between chron 27o (61 Ma) and present day. Parameters describing Aluk spreading prior to the Aluk-West Antarctic ridge initiation at chron 27o suffer from great uncertainty, however we derive Pacific-Aluk rotations for chron 34y–27o (83–61 Ma) and compare our result to the Pacific-Aluk stage rotation parameter from Eagles et al., (2004a) (17.2°S, 126.5°W, 30.15°, for stage 34y–27o; Figure 12). The Pacific-Aluk ridge continued until chron 21o (47.9 Ma), inferred from trapped Pacific crust (formed from the Pacific-Aluk spreading system; Figure 2) on the West Antarctic plate. This latter portion of the Pacific-Aluk spreading system (chron 27o–21o; 61–47.9 Ma) can be derived from the better constrained Pacific-Antarctic (this study) and Antarctic-Aluk (Eagles and Scott, 2014) rotation parameters, as the limited magnetic identifications available (Cande et al., 1982) and lack of fracture zones preserving spreading direction (the Humboldt Fracture Zone is not indicative of Pacific-Aluk spreading direction; McCarron and Larter, 1998), greatly hinder independent kinematic analysis.

Due to the paucity of data available for the Pacific-Aluk spreading, we derive our half-stage rotation parameters based on a spatial fit of magnetic identifications and inferred fracture zone lineations in *GPlates* (Table 5). A major assumption to this approach is the age of the youngest preserved Pacific-Aluk crust on the Pacific plate, adjacent to the Henry Trough (Figure 5, Figure 12). Pacific-Aluk spreading is preserved on the Pacific plate (chron 34y–27o?) and the West

Antarctic plate (chron 27?–21o), and formed as a continuous segment (Cande et al., 1982; McCarron and Larter, 1998). At chron 21o (47.9 Ma), the younger portion of this spreading segment was captured onto the Antarctic plate by the propagation of the Pacific-Antarctic ridge, leading to the formation of the Henry Trough and Hudson Troughs (Cande et al., 1982; McCarron and Larter, 1998). Here, we assume the Henry Trough is approximately representative of chron 27 (~61 Ma) on the Pacific plate; however, there are little data available to validate this assumption.

Our synthetic flowline for Pacific-Aluk spreading suggest a relatively good match with the fabric observed in the gravity, and with some of the magnetic identifications in this region (Figure 12). Comparison of our flowline with one derived from Eagles et al. (2004a) demonstrates the large uncertainty in reconstructing the Pacific-Aluk spreading corridor, as there are little constraints (e.g. no clear fracture zones, ambiguous or conflicting magnetic identifications) to fully constrain this spreading. We also find our Pacific-Aluk rotation parameter allows for the derivation of a divergent Farallon-Aluk ridge in the Late Cretaceous, when combined with our Pacific-Farallon relative motion (see section 3.2.1). A Farallon-Aluk spreading ridge correlates with published schematics for this region (e.g. Cande et al., 1982), however the location of the Farallon-Aluk ridge is poorly constrained.

3.2 East Pacific spreading history

The eastern and northern Pacific basin formed from spreading between the Pacific and Farallon plates, including the Farallon subplates, e.g. Nazca, Cocos, and Vancouver. The seafloor spreading record suggests breakup and subduction of the Farallon plate since the Late Cretaceous. The present-day southeast Pacific basin is dominated by the Pacific, Nazca, and Cocos plates, which are separated by the north-south trending East Pacific Rise (i.e. Pacific and Nazca plates), and the east-west trending Galapagos Spreading Centre (i.e. Nazca and Cocos plates) (Hey, 1977; Mayes et al., 1990) (Figure 13). The northeast Pacific largely consists of the Pacific plate, with the Juan de Fuca plate subducting beneath North America (Figure 14). On the Pacific plate, C-sequence magnetic anomalies can be identified up to chron 34y (83 Ma) (Cande and Haxby, 1991; Munschy et al., 1996). Due to subduction along North and South America, no conjugate anomalies are available in the northern Pacific basin (Pacific plate), and conjugate magnetic anomalies on the Nazca plate are only available up to chron 23y (50.8 Ma) (Atwater, 1989; Cande and Haxby, 1991).

Prior to chron 34y (83 Ma), the East Pacific basin was dominated by spreading between the Pacific and Farallon plates, inferred from the Mesozoic sequence of magnetic anomalies (Nakanishi et al., 1989). During the Cretaceous Normal Superchron (CNS; M0-34y; 120.6–83 Ma), mismatches in fracture zone offsets suggest there was likely a number of ridge jumps (e.g. in the Murray-Mendocino segment) (Atwater, 1989), however due to the lack of magnetic anomalies, the timing of such events is hard to decipher.

The Kula plate, deceivingly named to mean “all gone” in Athapascan (Grow and Atwater, 1970), is presently preserved as a small fragment that was incorporated into the Pacific plate after Kula-Pacific spreading ceased during chron 18r (~41 Ma) (Lonsdale, 1988). However, it should be noted that this interpretation of a preserved Kula extinct ridge relies on a sparse dataset. Since the Kula plate has been mostly subducted into the Aleutian trench, its spreading history has been inferred from its conjugate spreading region on the Pacific plate. Consequently, many uncertainties remain in the tectonic history of the Kula plate, including its origin (e.g. whether it was originally part of Farallon or Izanagi), timing of independent spreading, paleoposition, and plate configuration with the Farallon and North American boundaries. The Kula plate is proposed to derive from the Farallon plate (Atwater, 1989; Mammerickx and Sharman, 1988; Woods and Davies, 1982) or the Izanagi plate (Hilde et al., 1977; Larson and Chase, 1972; Norton, 2007; Zonenshain et al., 1987). Reconstructions relying on an Izanagi plate derivative rely on a greatly different tectonic plate configuration in the Late Cretaceous. For example, Norton (2007) infer a Late Cretaceous subduction of the Pacific plate along Asia, however this scenario contrasts with the onshore geological record from east Asia and the preserved magnetic identifications from the NW Pacific basin, which suggest Izanagi-Pacific ridge subduction occurred at ~55 Ma (Whittaker et al., 2007; Seton et al., 2012). Additionally, there is no clear way to reconcile the M-sequence (and presumably CNS) spreading history of the Izanagi plate with the C-sequence spreading history of the Kula plate (Atwater, 1989), suggesting the Kula plate likely formed as a fragment of the Pacific or Farallon plate (Atwater, 1989; Rea and Dixon, 1983).

Magnetic lineations adjacent to the Chinook Trough (Figure 14) mark the first signs of the north-south Kula-Pacific spreading at chron 34y (83 Ma), where the Kula plate broke away from the Chinook Trough (Mammerickx and Sharman, 1988; Rea and Dixon, 1983; Woods and Davies, 1982). The initiation of Kula-Pacific spreading occurred progressively, propagating from west to east (Mammerickx and Sharman, 1988). Seafloor spreading accelerated during chron 33n (~75 Ma), inferred from a rough-smooth transition (Figure 14) in the seafloor topography near chron 33y (Mammerickx and Sharman, 1988), although Norton (2007) notes the rough-smooth transition may record ridge reorientation due to a change in spreading direction. The Emperor Trough (Figure 14) acts as a western boundary of the Kula plate, however its evolution is unclear: during the early stages of Kula plate formation, the Emperor Trough may have formed as a rift (Woods and Davies), although this feature has also been proposed to be a transform fault formed during the CNS (Hilde et al., 1977; Larson and Chase, 1972). An additional plate, the Chinook plate, has been proposed to have formed contemporaneously with the Kula plate during the Late Cretaceous (Mammerickx and Sharman, 1988; Rea and Dixon, 1983). This proposed plate is bounded by the Chinook Trough, Emperor Trough, and Mendocino Fracture Zone (Rea and Dixon, 1983) (Figure 14). However, based on their analysis of north Pacific fracture zones, Atwater et al. (1993) reject this idea as the proposed region of the Chinook plate implies the region north of the Mendocino Fracture Zone was not part of the Pacific plate, and this region does not contain any characteristics of a plate boundary reorganisation.

A counterclockwise change in Pacific-Farallon spreading occurred at chron 33r (~80 Ma), based on the distinct bends in the Mendocino, Pioneer, Murray, and Molokai fracture zones (Atwater et al., 1993; McCarthy et al., 1996) (Figure 14). This change in spreading direction is thought to be linked to the initiation of Kula-Pacific spreading, due to the removal of northward slab-pull forces on the Pacific plate (Atwater et al., 1993).

At chron 25y, a counterclockwise change in the Kula-Pacific spreading system occurred. This has previously been linked to a change in slab-pull forces at this time (Lonsdale, 1988) caused by the initiation of the Aleutian subduction zone at 55 Ma (Scholl et al., 1986), with recent radiometric dating suggesting fluctuating magmatism beginning at 45–50 Ma (Jicha et al., 2009). There is a mismatch in the spreading rate implied by the western and eastern Kula-Pacific magnetic identifications, between chron 25y (55.9 Ma) and chron 24n.3o (53.3 Ma): the eastern region of Kula-Pacific spreading implies spreading rates up to three times that of the western region, with only a very minor counterclockwise change in spreading direction. In the eastern region of the Kula-Pacific spreading, a three-armed chron 24r anomaly is observed ("T" anomaly) and is thought to represent a captured piece of the Pacific-Farallon-Kula triple junction (Atwater, 1989). Previously, this has been interpreted to indicate the cessation of Kula-Pacific spreading (Byrne, 1979), however it is conceivable that Kula-Pacific spreading underwent a counterclockwise change (Lonsdale, 1988) and reorganisation of the triple junction occurred at this time, considering that this coincides with the fragmentation of the Farallon plate to form the Vancouver plate.

Fragmentation of the Farallon plate occurred at chron 24 (52 Ma), based on magnetic identifications and the prominent bend in Pacific basin fracture zones (e.g. Surveyor, Mendocino, and Pioneer fracture zones) (Mayes et al., 1990). The northern fragment is known as the Vancouver plate (Menard, 1978; Rosa and Molnar, 1988), with the Vancouver-Farallon boundary occurring around the Murray Fracture Zone (McCarthy et al., 1996; Menard, 1978) or the Pioneer Fracture Zone (Rosa and Molnar, 1988) (Figure 14). During this break-up, the Pacific-Farallon spreading direction remained unchanged (Atwater, 1989) and the Vancouver-Pacific spreading diverged 20° south (Atwater, 1989; McCarthy et al., 1996) causing the former Mendocino transform fault (present-day Mendocino Fracture Zone) to break across and eliminate the former Pau transform fault (present-day Pau Fracture Zone) (Atwater and Severinghaus, 1989). By chron 21 (~48 Ma), this new system had 'settled' and spreading continued steadily until chron 15 (34 Ma): at this time a major propagator crossed the Surveyor Fracture Zone, and offsets of the Vancouver-Pacific ridge were reorganised by episodes of rift propagation (Atwater, 1989; Atwater and Severinghaus, 1989; McCarthy et al., 1996). The boundary for the Farallon and Vancouver plates varied between the Pioneer and Murray fracture zones, reflected in the set of 'toothlike disjunctures' between chrons 19 (41 Ma) to 13 (33 Ma) (Atwater, 1989). Since chron 22o, we have evidence (albeit sparse) of Kula-Pacific spreading asymmetry (Lonsdale, 1988; Vallier et al., 1996), roughly 35:65 per cent. At chron 18r (~41 Ma), the Pacific-Kula ridge ceased spreading and the Kula plate was incorporated into the Pacific plate (Lonsdale, 1988). The abrupt cessation of Pacific-Kula spreading was previously thought to be a consequence of the change in the absolute motion of the Pacific plate at 43 Ma (Atwater, 1989; Lonsdale, 1988), based on the previously thought timing of the Hawaiian-Emperor Bend (HEB) (Clague and Dalrymple, 1987) and the age of chron 18r in the timescale of Berggren et al. (1985) (~43 Ma). However, recent research does not support this interpretation: recent timescales place chron 18r at 40.13–41.257 Ma (Cande and Kent, 1995; Gee and Kent, 2007) or 40.145–41.154 Ma (Ogg, 2012), whilst the refined age of the HEB is now 47.5 Ma (O'Connor et al., 2013), and the change in hotspot and mantle dynamics is thought to play the major role in HEB formation (Tarduno et al., 2009).

Magnetic anomalies indicate many small ridge jumps or periods of large asymmetrical spreading throughout Farallon/Nazca-Pacific spreading history, in particular south of the Austral Fracture Zone between chron 20 (43 Ma) and 17 (37 Ma), based on the differences in the amount of preserved Pacific crust compared to Farallon crust and the resulting inconsistencies in reconstructions (Cande and Haxby, 1991). During this time, Pacific-Farallon spreading also underwent reorganisations: between chron 19 and 12 (~42 to 32 Ma), ridge jumps and/or propagating rifts caused several fragments of the Farallon plate to break off and be incorporated into the Pacific plate (Atwater, 1989).

A major reorganisation event occurred in the eastern Pacific during the Oligocene, after the first segment of the East Pacific Rise (Pacific-Farallon spreading centre) intersected with the North American subduction zone near Baja California. This is thought to have occurred as early as chron 13 (~33 Ma) (Engebretson et al., 1985), although more recent studies have placed it around chron 9 or 10y (~28 Ma) (Atwater, 1989). The Vancouver plate is referred to as the Juan de Fuca plate after the Farallon-Pacific spreading ridge reached the subduction zone along North America, around chron 10y (28 Ma), (Atwater and Stock, 1998). The Juan de Fuca plate moved in a more northerly direction to the former Vancouver plate (McCarthy et al., 1996), whilst the Pacific-Farallon ridge segments and Farallon spreading rotated clockwise. Magnetic lineations between the Pioneer and Murray fracture zones suggest Farallon plate fragmentation occurred at chron 10y (28 Ma), forming the Monterey and Arguello microplates (Atwater, 1989; Severinghaus and Atwater, 1990), although Stock and Lee (1994) suggest the independent motion of the Arguello plate began around ~20 Ma. Pacific-Monterey spreading was slower than Pacific-Arguello spreading, allowing for the formation of the right-lateral transform known as the Morro Fracture Zone (Nicholson et al., 1994) (Figure 14). The Arguello and Monterey plates experienced independent motion until after chron 6 (~18 Ma), when it was incorporated into the Pacific plate (Atwater, 1989; Lonsdale, 1991; Stock and Lee, 1994). The remnants of the Arguello plate have been subducted, and its spreading history is based on preserved lineations on the Pacific plate, however a remnant of the former Monterey plate is preserved between the Monterey and Morro fracture zones (Atwater, 1989).

Further south, the initial signs of a plate reorganisation began at chron 7 (~25 Ma), observed by a 5° clockwise change in the Pacific-Farallon ridge (Barckhausen et al., 2008). The break-up of the Farallon plate at chron 6B (22.7 Ma) (Barckhausen et al., 2001) resulted in the formation of the Nazca and Cocos plates (Barckhausen et al., 2008; Hey, 1977; Meschede and Barckhausen, 2000; Meschede et al., 2008) and the development of the Cocos-Nazca spreading system (Hey, 1977; Klitgord and Mammerickx, 1982; Mayes et al., 1990) (Figure 13). The break-up of the Farallon plate has been attributed to a combination of factors, including the changes in slab forces and plate strength, including increased northward pull after the earlier splits of the Farallon plate (from the Vancouver and Monterey plates) (Lonsdale, 2005), increased slab pull at the Middle America subduction zone due to the increased length of the Farallon plate, and a possible weakening of the plate along the break-up point due to the influence of the Galapagos Hotspot (Barckhausen et al., 2008; Hey, 1977; Lonsdale, 2005). The Farallon plate break-up is also attributed to changes in spreading direction, where the change in Pacific-Farallon to Pacific-Nazca motion can be observed in a 20° to 25° clockwise change in spreading direction (Eakins and Lonsdale, 2003; Lonsdale, 2005) and an increase in crustal accretion rates (Eakins and Lonsdale, 2003).

Spreading associated with the Cocos-Nazca ridge began at chron 6B (22.7 Ma), based on magnetic identifications near the Grijalva Scarp and its conjugate feature near Costa Rica (Barckhausen et al., 2001). Cocos-Nazca spreading can be divided into three systems: Cocos-Nazca spreading 1 (~23–19.5 Ma; NW-SE); Cocos-Nazca spreading 2 (19.5–14.7 Ma; ENE-WSW); and Cocos-Nazca spreading 3 (14.7 Ma–present; E-W) (Meschede and Barckhausen, 2000). Following this, a number of reorganisations can be observed, which are primarily associated with the evolution of microplates. By ~20 Ma, the Mendoza microplate was forming between the Mendana and Nazca fracture zones, however there is ambiguity in the timing of its incorporation into the Nazca plate, which varies from chron 5A (~12 Ma) (Liu, 1996) and chron 5Cn.2n (~16.3 Ma) (Eakins and Lonsdale, 2003). Around chron 5D and 5E (~18 Ma), the Bauer microplate formed near the Marquesas and Mendana fracture zones (Figure 13), and underwent independent motion until captured by the Nazca plate at 6 Ma (Eakins and Lonsdale, 2003). Around chron 5A (~12 Ma), the Mathematician microplate formed with dual spreading centers between the Mathematician Ridge and the East Pacific Rise, and transform boundaries at the Rivera and West O'Gorman fracture zones (Mammerickx et al., 1988) (Figure 13). This was followed by the formation of the Rivera plate above the Rivera Fracture Zone, at chron 5n.2n (~10 Ma) (DeMets and Traylen, 2000). The Mathematician paleoplate ceased with the failure of the Mathematician ridge around chron 2A (3.28 Ma) (DeMets and Traylen, 2000). A reorganisation at chron 3o (~5 Ma) resulted in the formation of the Juan Fernandez and Easter microplates (Tebbens and Cande, 1997).

3.2.1 Relative Pacific-Farallon plate motion

The Pacific-Farallon spreading history is crucial in understanding circum-Pacific tectonics and the events surrounding the formation of the HEB. The Nazca and Pacific plates preserve conjugate anomalies formed from Pacific-Nazca/Farallon spreading until chron 23y (50.8 Ma) (Atwater, 1989; Cande and Haxby, 1991), however no conjugate anomalies are available for earlier times due to the subduction of the Farallon plate. Since this hinders our ability to reconstruct the Farallon plate motion for earlier times, models of Pacific-Farallon seafloor spreading rely on the conjugate Pacific plate to derive 'half'-stage and 'full'-stage rotations by assuming spreading symmetry. This assumption is reasonable, as global present-day ocean crust displays <10% cumulative spreading asymmetry (Müller et al., 1998). It should be noted that there are limitations in this approach due to the observed Pacific-Nazca/Farallon asymmetries (e.g. Rowan and Rowley, 2014) (see Discussion).

Many published Pacific-Farallon rotations (Table 6) are limited in their extent, with the notable exception of Rowan and Rowley (2014), who cover the full Pacific-Farallon spreading history since chron 34y (end of the CNS) with accompanying 95% confidence ellipses. Pardo-Casas and Molnar (1987) and Rowan and Rowley (2014) suggest Pacific-Farallon seafloor spreading rates were over 200 mm/yr during the Eocene (Figure 15), though these fast speeds are likely model errors. Our models imply Pacific-Farallon spreading was around ~80–100 mm/yr during the Late Cretaceous and early Cenozoic, followed by an increase in spreading rate and clockwise change in spreading direction between chron 25y (~56 Ma) until chron 13y (~33 Ma) (Figure 15), regardless of the timescale used. However, the timing and magnitude of these events differs between all the models due to the stage intervals used and the dataset used in deriving stage intervals. For example, Wright et al. (2015) rely on relatively small (~1–2 Myr) stage intervals for the Paleocene, whereas all other models use larger (~7 Myr) stage intervals, resulting in large changes in spreading velocity between 66 and 33 Ma. Rowan and Rowley (2014) and Wright et al. (2015) both rely on magnetic identifications from the northern and southern Pacific plate, whereas Pardo-Casas and Molnar (1987) and Rosa and Molnar (1988) rely on magnetic identifications from the northern Pacific only, which further contributes to the variations in spreading velocity between the models.

We provide new relative Pacific-Farallon plate motions between chron 34y (83 Ma) and 31y (67.7 Ma). We combine these stages with the relative motions from Wright et al. (2015) to derive a Pacific-Farallon spreading history until chron 13y (33.1 Ma) (Table 7), which has well-constrained half-stage rotation parameters for all times (Figure 16). We incorporate a minor counterclockwise change in Pacific-Farallon spreading direction at chron 33o, as observed by Atwater et al. (1993). Following this change, spreading remained relatively constant until chron 28 in the North Pacific (Molokai Fracture Zone; Figure 15a). This was succeeded by a significant two-stage increase in Pacific-Farallon spreading rates, with an initial 26 mm/yr increase between chron 25y (55.9 Ma) and 24n.1y (52.4 Ma), followed by a 64 mm/yr increase between chron 22o (49.7 Ma) and chron

18n.2o (40.1 Ma) (Wright et al., 2015). The timing of the initial increase in spreading rate (i.e. at chron 25y) precedes the formation time of the Hawaiian-Emperor Bend (~47.5 Ma; O'Connor et al., 2013), and is thought to be a result of an increase in Farallon plate motion, rather than a change in the motion of the Pacific plate (Wright et al., 2015). We find a slightly different trend in spreading velocities in the South Pacific (Austral Fracture Zone; Figure 15b). Along the Austral Fracture Zone, there is an increase in spreading rate from chron 34y–31y (83–67.7 Ma), a significant 27 mm/yr decrease at chron 28y (62.5 Ma), and a further 93 mm/yr increase between chron 25y (55.9 Ma) and 20o (43.8 Ma).

The flowlines derived from Wright et al. (2015) and this study (Table 7) produce an overall good spatial fit to fracture zones in the North (e.g. Molokai Fracture Zone) and South (e.g. Marquesas Fracture Zone) Pacific and produces the best fit to the temporal progression suggested by the compilation of magnetic identifications (Atwater and Severginhause, 1989; Barckhausen et al., 2013; Cande and Haxby, 1991;; Munschy et al., 1996) (Figure 17). Since spreading varies within each fracture zone segment, e.g. due to rift propagation and/or changes in spreading direction, we do not expect all Pacific fracture zone corridors to match our flowlines for all stages. One example of this occurs within the Molokai-Clarion spreading segment, where a pseudofault results in an offset between chron 34y and 30o (Atwater and Severinghaus, 1989), and major propagating rifts have removed much of chron 18 and 19 (Atwater, 1989; Atwater and Severinghaus, 1989). Due to these events, our flowline within stage 31y–33o underestimates the spreading rate suggested by the magnetic identifications within the Molokai-Clarion segment, despite finding a good fit for this stage for other Pacific spreading corridors (e.g. Murray-Molokai, Marquesas-Austral) (Figure 17). Flowlines derived from the rotations of Rowan and Rowley (2014) demonstrate a good spatial fit to the fracture zones, and displays a good temporal fit for chron 34y–13y spreading within the Molokai-Clarion segment, however, they slightly overestimate the spreading within the Murray-Molokai and Marquesas-Austral fracture segments (Figure 17). Flowlines derived from Seton et al.

(2012) diverge from the Pacific fracture zones geometries, especially compared to Rowan and Rowley (2014), Wright et al. (2015) and this study. These flowlines also overestimate the total spreading between chron 34y and 13y for all fracture zone spreading segments (Figure 17).

3.2.2 Relative Juan de Fuca/Vancouver-Pacific plate motions

The reconstruction history of the former Vancouver plate has been poorly explored in the past, with published relative motions listed in Table 8. The half-stage rotation parameters in Rosa and Molnar (1988) were converted into stage and finite rotation parameters based on assumed symmetric spreading. Large differences arise in the clockwise spreading direction of Müller et al. (1997) and the counterclockwise motions suggested by all other models (Figure 18).

We derive Vancouver/Juan de Fuca-Pacific relative plate motions between chrons 24n.1y (52.4 Ma) and 5n.2y (9.9 Ma). An additional published Juan de Fuca-Pacific rotation pole is included at chron 4Ay (8.9 Ma), taken from Wilson (1993). However, we do not include the detailed spreading history of the Juan de Fuca ridge (e.g. Wilson, 1993) as incorporating the spreading history of a small plate at short time intervals is well beyond the scope of this study. We derive half-stage rotations for the Juan de Fuca-Pacific spreading history between chron 10.n1y (28.3 Ma) and chron 4Ac (8.9 Ma) (Table 9) using visual fitting in *GPlates* (Boyden et al., 2011).

We derive the Vancouver plate spreading history with uncertainties between chrons 24n.1y (52.4 Ma) and 10n.1y (28.3 Ma) as half-stage rotations (Table 10). We find a constrained uncertainty for all times (Figure 19), with slightly larger uncertainties for the early Vancouver-Pacific stages (e.g. chron 22o–24n.1y), likely due to the propagation of the Vancouver-Pacific ridge (Caress et al. 1988).

There is a large difference in Vancouver-Pacific relative plate motion between Müller et al. (1997) Rosa and Molnar (1988), and this study. There is a poor match between flowlines produced from Müller et al. (1997) and fracture zone identifications in the area (Figure 20). Flowlines derived from Rosa and Molnar (1988) suggests a similar geometry with the Surveyor Fracture Zone, however flowlines derived from this study closer resemble the geometries of the Sila and Sedna fracture zones (Figure 20). Vancouver-Pacific spreading rate is slightly overestimated by Wright et al. (2015), based on the spatial difference between chron 24n.1y (52.364 Ma) and the flowline endpoint (52.4 Ma).

3.2.3 Relative Kula-Pacific plate motion

The spreading history of the Kula plate has important implications for the northward transport of terranes across the Pacific basin (Atwater, 1989). However, there are few published rotation parameters for Kula-Pacific spreading (Table 11), despite the number of studies related to the formation and reconstruction history of the Kula plate. Nevertheless, we compare the spreading velocities of Rosa and Molnar (1988) and Seton et al. (2012) with derived rotation parameters and uncertainties from this study (Figure 21). Stage rates are calculated assuming symmetrical spreading. The stage rates are all broadly similar, however there is a large difference in spreading direction from chron 25y (55.9 Ma) between Seton et al. (2012) (counterclockwise change) and this study (clockwise change).

We derive Kula-Pacific half-stage rotation parameters and uncertaintaties between chron 34y (83 Ma) and chron 25y (55.9 Ma) (Table 12). We find well constrained half-stage rotation parameters, except for the stage 34y–33y (Figure 22), which is likely due to the sparse magnetic and fracture zone data for chron 34y, as the Kula-Pacific ridge propagated east. As the data for the remaining Kula-Pacific spreading history is sparse and the counterclockwise rotation at chron 25 has resulted in offsets and/or elimination of fracture zones (e.g. Rat and Adak fracture zone), we derive rotation parameters between chron 25y–19y based on visual fitting of magnetic identifications and fracutre zone traces using *GPlates*, where we implement a large counterclockwise change based on the Stalemate Fracture Zone. We calculate finite rotation parameters from chron 21y (47.9 Ma), as conjugate magnetic identifications are preserved on the remaining fragment of the Kula plate.

A comparison of flowlines depicting Kula-Pacific spreading before chron 25y (~56 Ma) demonstrates the misfit between the flowlines of Seton et al. (2012) and Rosa and Molnar (1988) and recognized fracture zones (e.g. Rat and Amlia fracture zones) (Figure 23), in particular, the slight counterclockwise change of Seton et al. (2012), compared to the clockwise change observed in this study between chron 34y and 25y. Rosa and Molnar (1988) and Seton et al. (2012) also underestimate the spreading rates, based on the mistmatch between the flowlines and magnetic identifications, in particular, during the stage chron 33y–31y.

3.3 Reconstruction Summary

We present reconstructions of the Pacific basin since chron 34y (83 Ma). Listed in Table 13 are the finite rotation parameters used in this study. As this is a rigid model focused on the seafloor spreading history of the Pacific basin, we do not incorporate any deformation of the West Antarctic margin, or the rifting history of the West Antarctic margin and Chatham rise.

Spreading between West Antarctica and Chatham plateau in the southern Pacific initially began at chron 34y (83 Ma), which was likely preceded by a period of continental rifting during east Gondwana break-up. This was contemporaneous with the initial stages of Kula plate formation in the northern-central Pacific. During this time, Aluk (Phoenix)-Pacific spreading was active including subduction along the Antarctic Peninsula and southern South American margin adjacent to the Aluk plate (Figure 24). Subduction of the Farallon plate was occurring along North and South America, whilst the newly formed Kula plate was subducting along the present-day Alaskan and

North American margin. Spreading between the West Antarctic and Pacific plates initiated with an almost north-south direction.

By chron 33o (79.1 Ma), Kula-Pacific spreading had established in the North Pacific, whilst northeast-southwest Bellingshausen-Pacific spreading initiation occurred in the South Pacific. By chron 27o (~61 Ma) the Bellingshausen plate had ceased independent motion and was incorporated into the West Antarctic plate, prompting the replacement of Bellingshausen-Aluk spreading with Aluk-West Antarctic spreading. As noted by Eagles et al. (2004b), this event correlates with a regional plate reorganisation. From chron 25y (55.9 Ma), there was a large counterclockwise change in Kula-Pacific spreading, and the beginning of a slow counterclockwise change in Pacific-West Antarctic spreading. This coincides with a large increase in Pacific-Farallon spreading rates and small clockwise change in Pacific-Farallon spreading. Following this change in Pacific-Farallon spreading, the Farallon plate fragmented at chron 24n1y to form the Vancouver plate in its north and this appears to correlate with the counterclockwise motion of the Kula plate at this time (Figure 24). At chron 21o (Figure 24), there was a further South Pacific reorganisation: a portion of the Pacific flank of Pacific-Aluk spreading was trapped onto the West Antarctic plate as the Pacific-Antarctic ridge propagated eastward. During chron 18r, the Kula-Pacific ridge ceased spreading, and the Kula plate was incorporated into the Pacific plate.

The initial arrival of the Pacific-Farallon ridge at the North American trench occurred at ~29 Ma, near the Pioneer Fracture Zone. Following this, the Farallon plate experienced a major fragmentation to form the Nazca and Cocos plates during chron 6B (22.7 Ma) (Figure 24). Further reorganisations occurred, including the formation of the Bauer microplate in the South Pacific around chron 5D, the Mathematician microplate at chron 5n.2o, and the Rivera microplate. As the Pacific-Farallon ridge was progressively subducted beneath North America, the extinct ridges and remnants of the paleoplates approached the margin.

4 Discussion

4.1 Age of the oceanic crust in the Pacific

Our refined tectonic model for the Pacific Ocean basin since chron 34y (83 Ma) allows for a comparison of the model-derived age of oceanic crust at present-day and throughout the Late Cretaceous and Cenozoic. Our refined present-day age grid (Figure 25) is largely similar to that of Seton et al. (2012), however we do find a number of differences. Throughout the Pacific basin, we find differences arising from recent magnetic anomaly identifications (i.e. Barckhausen et al., 2013; Wobbe et al., 2012) and the use of a large compilation of published magnetic identifications (Seton et al., 2014), resulting in over 10 Myr differences in the equatorial and south Pacific. The use of well-constrained fracture zone interpretations (Matthews et al., 2011) has also permitted the detailed mapping of oceanic crustal offsets (along fracture zone and small circles) that Seton et al. (2012) does not fully acknowledge, in particular, on the southern Pacific and West Antarctic plates. In the regions associated with Pacific, West Antarctic, and former Aluk and Bellingshausen spreading, we find variations over 10 Myr due to the incorporation of independent plates and their seafloor spreading isochrons (i.e. Bellingshausen, Aluk). Minor variations (up to 5 Myr) between our refined age grid and Seton et al. (2012) are found in the northeast Pacific (Figure 25), which is expected due to the dense coverage of magnetic interpretations in this region, and lack of conjugate spreading flank.

Our updated age grids of the Pacific allow us to derive half-spreading rate, crustal accretion, and age error grids. Comparison of our derived half-spreading rates (Figure 26a) and those from Müller et al. (2008) demonstrate large differences in estimates for the western Pacific. These reflect refinements to the Mesozoic spreading history of the Pacific basin made in Seton et al. (2012). Our spreading rate grid highlights the fast Pacific-Farallon spreading rates, in particular since ~50 Ma, compared to the remaining Pacific basin. Crustal accretion throughout the Pacific basin where both spreading flanks are preserved is largely more symmetric (50%) than Müller et al. (2008), who find a large area of excess accretion on the Pacific plate. We find a broadly similar trend in crustal accretion patterns along the East Pacific Rise, although our refined Cocos-Pacific seafloor isochrons suggest this system experienced more spreading symmetry than Müller et al. (2008) indicate. Our error grids, derived based on the difference between a compilation of magnetic identifications (Seton et al., 2014) and interpreted gridded age, indicate a large difference in error in the low-latitude Pacific and South Pacific, largely related to the improved coverage of these areas. Errors of ~10 Myr occur in regions where no magnetic identifications occur in both our study and Müller et al. (2008), due to the lack of coverage or the CNS.

We present new paleo-age grids in 10 Myr increments for the Pacific basin between 80 Ma and present day in the timescales of Gee and Kent (2007) and Ogg (2012) (Figure 27). There is little difference in the distribution of ocean floor age since 50 Ma, regardless of timescale used. This is expected, due to the similarity in C-sequence timescales (i.e. Gee and Kent, 2007; Ogg, 2012). A ~5–6 Myr difference is observed in oceanic crust produced prior to M0, due primarily to the large difference attributed to this chron (Gee and Kent, 2007: 120.6 Ma, vs. Ogg, 2012: 125.93 Ma).

4.2 Spreading asymmetry

Spreading asymmetry between the Pacific and Nazca plates can be determined based on the relative spacing of magnetic anomalies on conjugate ridge flanks and it has been suggested that since ~50 Ma the ridge crest has favoured accretion on the Nazca plate (56–60 per cent) over the Pacific plate (40–44 per cent) (Rowan and Rowley, 2014). The subduction of the Farallon plate makes it impossible to fully constrain Pacific-Farallon seafloor spreading (and hence, the history of crustal accretion) prior to ~50 Ma, with reconstructions of the Pacific-Farallon spreading derived from half-stage rotations (based on the Pacific plate) and assumed symmetric spreading. This assumption of symmetric spreading has been criticized, as observations of asymmetry since ~50 Ma suggests this approach underestimates the crustal accretion of the Farallon plate in the Mesozoic and early Cenozoic.

Recently, Rowan and Rowley (2014) highlighted the importance of asymmetric crustal accretion along the East Pacific Rise and inferred asymmetric crustal accretion along the entire Pacific-Farallon ridge until chron 34y (83 Ma) based on extrapolating their 'best-fit' crustal accretion fraction (Pacific:Farallon asymmetry of 44:56 per cent) for the past 50 Myr. However, this approach is still somewhat problematic. While there were likely minor asymmetries in Pacific-Farallon spreading prior to 50 Ma, it is arbitrary to infer continuous and systematic spreading asymmetry until chron 34y (83 Ma), and unreasonable to extrapolate such high values of spreading asymmetries to the entire Cenozoic-Mesozoic Pacific-Farallon spreading history. Further, the inferred Farallon Plate history in the Mesozoic and early Cenozoic (i.e. large Farallon plate, with the Pacific-Farallon ridge inferred to be much further from the North or South America subduction zones) differs greatly to its more recent history (i.e. multiple fragmentation events as the Pacific-Farallon ridge approached and intersected with the subduction zones).

We compare spreading crustal accretion for the major spreading systems in the Pacific basin with both spreading flanks preserved (Figure 28). We find the Pacific basin has largely experienced symmetric spreading, with over 60% of the oceanic crust experiencing less than 20% variation in crustal accretion, with asymmetries less than 5% most frequent (Figure 29). Crustal accretion has also varied from stages of symmetric spreading (e.g. 25y–21o; 55.9–47.9 Ma; 18n.2o–6Bn.1c; 40.1–23 Ma) to asymmetric spreading (i.e. 6o–present day; 20.1–0 Ma) along the southern East Pacific Rise (Challenger-Resolution fracture zone segment; Pacific-Nazca/Farallon spreading) (Figure 30). These large fluctuations in spreading asymmetry are not observed along any other major spreading system in the Pacific basin, including the Pacific-Antarctic ridge and northern East Pacific Rise (Clipperton-Galapagos fracture zone segment; Pacific-Cocos spreading) (Figure 30).

There are major differences in the mantle associated with regions of the Pacific basin. The South Pacific superswell (e.g. 10°N to 30°S; 130°W to 160°W; Adam et al., 2014) underlies the Pacific plate, and is associated with a large depth anomaly, that is the difference between the observed and theoretical oceanic basement depth based on thermal subsidence models. This mantle is hotter (Cochran, 1986), and has been found to have a lower resistivity to the mantle than that beneath the Nazca plate (Evans et al., 1999). Additionally, the mantle north and south of the Easter microplate (along the East Pacific Rise) can be divided into northern and southern domains due to the variation in axial depths (deep and shallow, respectively) and the distinct geochemical signatures of these domains (Vlastelic et al., 1999; Zhang et al., 2013). The southern East Pacific Rise has remained relatively "anchored' throughout the past 100 Myr, due to the interaction of deep plumes and the mid-ocean ridge (Whittaker et al., 2015). We observe asymmetry along the southern East Pacific Rise (Pacific-Nazca/Farallon spreading) from ~48 Ma (chron 21o), with the East Pacific Rise successively jumping westwards towards the mantle upwelling associated with the South Pacific superswell. This behaviour has previously been identified in the Pacific and equivalently along spreading ridges in the Atlantic and Indian Ocean basins (Müller et al., 1998). The northern East Pacific Rise (Pacific-Cocos) spreading does not display this same pattern of westward ridge jumps (Figure 28). Asymmetry associated with Pacific-Cocos spreading is strongly driven by ridge-subduction zone interactions, where the large curvature of the subduction zone may induce an intraplate stress field on plate regions proximal to the subduction zone, resulting in ridge jumps and plate fragmentation. Contrary to the behaviour of the East Pacific Rise, the Pacific-Antarctic ridge demonstrates no major asymmetry in crustal accretion (Figure 30). Major driving forces such as upwelling (as underneath the southern East Pacific Rise) or a nearby subduction zone (as in the northern East Pacific Rise) are not located proximal to the Pacific-Antarctic Ridge. Rather, the Pacific-Antarctic ridge is likely influenced by small-scale mantle flow, causing random minor spreading asymmetry that varies between segments (Rouzo et al., 1995).

The variations in mantle dynamics along the East Pacific Rise indicate that this ridge cannot be treated as a continuous feature. Based on the largely symmetrical behaviour of the Pacific-Antarctic ridge and the northern East Pacific Rise (Cocos-Pacific), and the fluctuations in Pacific-Farallon spreading behaviour, we propose that Pacific-Nazca/Farallon spreading asymmetries since ~48 Ma (chron 21o) do not reflect the long-term behaviour of the entire Pacific-Farallon ridge. Rowan and Rowley (2014) observe a correlation between periods of high spreading rates and high spreading asymmetries since 40 Ma, and imply both high periods of spreading rate and asymmetry are causally linked to anomalous mantle flow beneath a mid-ocean ridge flank. There is little reason to expect high spreading asymmetries during periods of much slower Pacific-Farallon spreading rates, as is observed before ~50 Ma, contrary to the inferences by Rowan and Rowley (2014) (Figure 15).

4.3 Subduction along North and South America

4.3.1 Implied convergence history

We use our tectonic reconstructions to derive the convergence history along the western North and South American margins, by determining the relative motion of the Pacific plates and North/South Americas through the use of a plate circuit based on the seafloor spreading record preserved in the Pacific, Atlantic, and Indian oceans. This approach is relatively sensitive to changes in the relative motion of plates within the circuit and to the configuration of tectonic plates, in particular, the location of the Kula-Farallon ridge along the North American margin, and the Aluk-Farallon ridge location along the South American margin. Such discrepancies in the computed convergence history between kinematic models, such as our refined model and Seton et al. (2012), emphasize how such inferences are dependent on the kinematic model used. Despite this, there are also many similarities in the implied convergence history derived from Seton et al. (2012) and our refined model (i.e. since ~50 Ma), suggesting a robust trend for these times. Nevertheless, our model provides insights into the evolution of the North and South American convergent margins, and can provide a useful tectonic context when considering the geochemical and topographic evolution of these margins, particularly in relation to ridge subduction and slab window formation.

North America

The North American margin has been shaped by the convergence of Pacific basin plates, such as the Farallon, Kula, Vancouver, and Pacific plate. However, there are uncertainties in the extent of the paleoplates (e.g. Kula and Farallon plates) that bordered North America during most of the Late Cretaceous and Cenozoic. We model the Farallon-Kula ridge to coincide with southern British Columbia, which is broadly consistent with the tectonic configuration of Seton et al. (2012). This location is also consistent with the location of a slab window near Vancouver Island at 50 Ma, based on geochemical analysis of lavas from the Eocene Challis-Kamloops volcanic belt (Breitsprecher et al., 2003). The tectonic plate adjacent to the North American margin significantly affects the implied convergence velocity: after 60 Ma, there is a rapid increase in the Kula plate convergence velocity at point 1 (Vancouver Island), while there is little change in velocity if the Farallon/Vancouver plates are converging here (Figure 31). We derive similar implied convergence rates in the timescales of Cande and Kent (1995) and Ogg (2012) (Figure 31, Figure 32), and find no major differences in convergence velocity, suggesting our results are not strongly dependent on choice of timescale. Refinements to Pacific basin relative plate motions, such as Vancouver-Pacific and Pacific-Farallon, have a minor influence on the derived convergence history, in particular, at points 2 (San Francisico) and 3 (Baja California). The observed differences between Seton et al. (2012) and this study are likely due to the major influence of East-West Antarctica relative motion.

South America

The South American margin has experienced long-lived subduction since the Early Jurassic (Somoza and Ghidella, 2012). The configuration of the tectonic plates along the South American margin greatly influences the implied convergence history, especially along the southern Andean margin (e.g. Patagonia). We infer the Farallon-Aluk ridge to coincide with northern Chile in the Late Cretaceous and early Cenozoic (Figure 33), consistent with Somoza and Ghidella (2012), and broadly consistent with simplified schematics presented in Scalabrino et al. (2009). We implement a southward migrating Farallon-Aluk ridge, resulting in ridge intersection with Patagonia during the Eocene: this is consistent with alkali basalts suggesting a slab window occurred in this region at ~50 Ma (Breitsprecher and Thorkelson, 2009) and the location of the Farallon-Aluk paleo-ridge suggested by Eagles and Scott (2014). However, this contrasts with the scenario proposed by Scalabrino et al. (2009). We propose ridge subduction occurred in the vicinity of our point 3 (45°S, 76°W) at 53 Ma, after which the Farallon plate was subducted within this region. This correlates with Eagles and Scott (2014), who suggest ridge subduction in this region at 54 Ma. Our configuration of tectonic plates in the Late Cretaceous and early Cenozoic differs greatly from Seton et al. (2012), as their reconstruction does not incorporate the Aluk plate, and infers a Farallon-East Antarctica ridge intersecting the southern Andean margin (Figure 33).

Comparison with the implied convergence derived from Seton et al. (2012) (and their plate tectonic configuration) demonstrates little difference in rate and obliquity since 30 Ma (Figure 34, Figure 35). Prior to 30 Ma, minor differences in the convergence rate and obliquity are calculated along northern Peru (Point 1) and northern Chile (point 2). As the plate adjacent to the southern Andean margin (i.e. Patagonia; point 3) prior to 45 Ma differs between Seton et al. (2012) (Farallon plate) and this study (Aluk or Phoenix plate), the implied convergence history demonstrates significant differences in this region, with up to 150 mm/yr difference in convergence rate, and ~250° difference in convergence obliquity. Seton et al. (2012) proposes the Farallon and South American plates were diverging in the Patagonian region prior to 50 Ma (Figure 34, Figure 35), however Cretaceous and Cenozoic calcic/calc-alkaline rocks indicates this region has been influenced by subduction dynamics (Ramos, 2005), casting doubt on this interpretation.

4.3.2 Age of the subducting crust

The geological evolution of continental margins is further influenced by the age of subducting lithosphere through time. Due to its buoyancy, young lithosphere (<50 Myr old; Cross and Pilger, 1982) generally subducts at a shallower angle, and does not penetrate into the mantle as deeply as cold, older oceanic lithosphere (England and Wortel, 1980). Subduction of very young (≤ 20 Myr old) and relatively warm oceanic crust, including ridge subduction, is thought to result in dehydration of the slab and the release of volatiles at shallow depths (Harry and Green, 1999). Consequently, we expect a correlation in tectonic regimes and the age of the subducting oceanic lithosphere, where subduction of young lithosphere is linked to back-arc and intra-arc compression (Cross and Pilger, 1982), and cordilleran tectonics (Molnar and Atwater, 1978), whilst subduction of old lithosphere generally results in back-arc and intra-arc extension (Cross and Pilger, 1982). These broad relationships are not observed in all regions, with inconsistencies arising when we consider subduction of the older (e.g. ~60 Myr) Farallon and Nazca plate along the South American margin. The time-dependence of the age of oceanic lithosphere subducted beneath South America has important consequences for understanding changing spreading rates in the South Atlantic ocean, as discussed by Müller et al (in press).

North America

We find broadly similar trends in the age of oceanic crust at the North American trench through time, derived from Seton et al. (2012) and this study (Figure 36). We derive the age of oceanic crust at the trench based on a symmetrical spreading and ‘best-fit’ Farallon-Pacific asymmetrical spreading until chron 34y (83 Ma), based on the ratio described in Rowan and Rowley (2014). We do not incorporate any asymmetrical spreading into Vancouver-Pacific and Kula-Pacific relative motion. The incorporation of spreading asymmetry makes little difference in the age of subducting oceanic crust (Figure 36), with up to 15 Myr difference in the Late Cretaceous. Rather, the relative plate motions impart a larger influence on the age of oceanic crust at the trench, where there is up to a 40 Myr difference in the Late Cretaceous and early Cenozoic between Seton et al. (2012) and this study at point 2 (Figure 36). Point 1 shows little difference in the age of subducting oceanic crust derived from our models. This trend is expected, as this location records the subduction of the Kula and Vancouver plates, where we do not incorporate any spreading asymmetry into the 'asymmetric' model. Point 1 also shows a large decrease in the age of subducting oceanic crust at ~70 Ma in our model, which arises from the close proximity of point 1 to our modelled Kula-Farallon ridge. At ~60 Ma, our model records the subduction of the Kula-Farallon/Vancouver ridge along point 1, while Seton et al. (2012) record this event ~20 Myr later. This discrepancy highlights the dependence of such results on the kinematic model used in analysis. In this case, the age variation between our model and Seton et al. (2012) results from the slight change in the intersection of the Kula-Farallon ridge with the North American margin at this time, and is a consequence of the difference in Kula-Farallon relative motion (derived from Kula-Pacific and Farallon-Pacific relative motions). Since ~30 Ma, there is little difference in the age of subducting lithosphere, regardless of model choice. This is not unexpected; as for times younger than chron 13y (33.1 Ma) we incorporate the Farallon-Pacific relative motion from Seton et al. (2012).

South America

Comparison of the age of oceanic crust at the South American trench based on Seton et al. (2012) and this study indicates a relatively consistent 10–20 Myr age difference at all points. Despite the long-lived subduction of the Farallon plate, we find little difference in the age of oceanic crust when spreading asymmetry is incorporated, except for along northern Peru (point 1), where we observe up to 40 Myr differences in ocean crust age, at 30 Ma (Figure 37). The small difference in the age of subducting oceanic crust between our asymmetric and symmetric model is due to the orientation of the magnetic lineations on the subducting (e.g. Farallon) plate, and is a reflection on the earlier (pre-chron 34y; 83 Ma) tectonic history of the Pacific basin (i.e. Seton et al., 2012). At ~50 Ma, we observe ridge subduction at point 3, which is consistent with the proposed slab window in this region by Breitsprecher and Thorkelson (2009). This contrasts with the age derived from Seton et al. (2012), who suggest the subduction of ~20 Myr old oceanic crust (Figure 37).

4.4 Limitations

Uncertainties remain in our reconstruction of the Pacific Ocean basin due to the limited availability of data from preserved regions (e.g. central Nazca plate) and the subduction of former plates along the North and South American margins. The present-day age of oceanic lithosphere remains poorly constrained in regions where there is limited magnetic anomaly data available, in particular, areas associated with the CNS, and within the central Nazca plate. The age of oceanic lithosphere across the CNS is interpolated based on assuming no change in Pacific-Farallon spreading rate between M0 (120.6 Ma) and chron 34y (84 Ma), and further refinements to this region are beyond the scope of this study. The central Nazca Plate exhibits a large (~6 Myr) age error (Figure 26c), and is a region of relatively few magnetic identifications (Figure 3). This region is thought to preserve the remnants of transient microplates such as the Mendoza microplate (between the Mendana and Nazca fracture zones); however, we do not incorporate such events into our kinematic history due to large ambiguities in the limited data available. Additionally, we do not incorporate the independent motion of the Monterey or Arguello microplates. Uncertainty in the age of oceanic lithosphere also remains along the Marie Byrd Land margin, such as the age of the Charcot plate (McCarron and Larter, 1998). The age of oceanic lithosphere in such regions may be refined with the collection and provision of additional data.

As much of the record of Pacific basin seafloor spreading has been subducted (e.g. Farallon, Vancouver, Kula plates), our tectonic reconstruction represents the ‘simplest’ scenario, based on the preserved geophysical data from the Pacific plate, and onshore geochemical and geological data (e.g. locations of slab windows to infer ridge-trench interactions). Uncertainties in the plate configuration history are greatest during the earlier Pacific basin history, such as in the Cretaceous and early Cenozoic. In particular, the spreading history of the Kula plate remains poorly constrained, with concerns surrounding the tectonic history of the “T” anomaly, which has been proposed to represent a captured Kula-Farallon-Pacific triple junction (Atwater, 1989). The presence of a large Eocene-Oligoence aged turbidite body on the Aleutian Abyssal Plain, known as the Zodiac Fan (Stevenson et al., 1983), further suggests a gap in our understanding of the reconstruction history of the North Pacific. The Zodiac turbidite fan consists of granitic and metamorphic rocks, which are inferred to originate from southeastern Alaska and western Canada (Steward, 1976), and is thought to have contributed material to accretionary prisms along the eastern Aleutian trench (Suess et al., 1998). Eocene tectonic reconstructions place the Zodiac fan over ~2000 km away from its inferred source, and highlight the large uncertainty in the plate configuration of the North Pacific basin in parts of the Cenozoic.

It is possible that additional oceanic plates existed along the North and South American margins during the Late Cretaceous and early Cenozoic, contrary to our inferred configuration of large oceanic plates (e.g. the Farallon plate). Large uncertainties in the implied convergence history remain along northern North America, where the existence of an additional plate has been proposed (the Resurrection plate; Haeussler et al., 2003) based on the onshore geological record. We do not incorporate this plate into our model as there is little data to constrain its relative plate motion and plate boundary geometry and the geological evidence used to support a ridge-trench intersection event may be from an extinct rather than active mid-ocean ridge. The incorporation of the Resurrection plate, or any other tectonic plate within this region, would greatly alter the implied convergence history along northern North America and Alaska. The Late Cretaceous and early Cenozoic implied convergence history along central South America also has a large uncertainty, where variations in the age of subducting oceanic lithosphere are directly linked to the preceding events of the Farallon and Phoenix plates (e.g. Seton et al., 2012).

5 Conclusion

We have refined the plate tectonic model of the Pacific Ocean from the Late Cretaceous to present day, based on recent data including satellite marine gravity anomalies (Sandwell et al., 2014), well-constrained fracture zone traces (Matthews et al., 2011; Wessel et al., 2015) and a large compilation of magnetic anomaly identifications (Seton et al., 2014). Unlike many regional Pacific reviews that limit their scope to either the North (Atwater, 1989) or South Pacific (Mayes et al., 1990), we assess the seafloor spreading history for the entire Pacific basin and incorporate previously recognised tectonic plates, such as the Aluk (Phoenix) and Bellingshausen, which have so far been limited to regional studies. This approach allows for a comprehensive analysis of the Pacific-Farallon relative plate motion since the Late Cretaceous, as many previous studies have derived northern Farallon plate motions and extrapolated these to the entire Farallon plate. Our results show that this can result in skewed spreading velocities.

Where possible, we present 95% uncertainties for our relative plate motions, based on the best-fitting criteria of Hellinger (1981), allowing for the assessment of significance in tectonic changes. To eliminate any timescale bias in significant spreading events, we present all results in the timescale of Cande and Kent (1995) and Ogg (2012), and find similar trends regardless of timescale. Our relative plate motions result in a good match to both the fracture zone traces and magnetic pick data in both the North and South Pacific.

A comparison of our relative plate motions and published regional models demonstrates that while there are clear overall trends in spreading velocities, many publications do not conform with fracture zone traces observed in recent data (e.g. Vancouver-Pacific spreading based Seton et al. 2012), or do not incorporate changes in spreading rate indicated by the temporal progression of magnetic picks (e.g. Farallon-Pacific spreading based on Rowan and Rowley, 2014). Additionally, many regional studies do not provide any indication of uncertainties, or only provide spreading parameters for small portions of the spreading history of a plate (e.g. Rosa and Molnar, 1988).

Our refined reconstruction history of the Pacific allows for a comparison of Pacific basin oceanic age, spreading rates and asymmetries. Analysis of the error associated in the age grid demonstrates ~8 Myr errors between our refined age grids and Müller et al. (2008), in areas such as the central Pacific, where there is now improved magnetic pick coverage. Comparison of crustal accretion associated with the East Pacific Rise (i.e. Pacific-Farallon/Nazca and Pacific-Cocos) highlights how these systems have oscillated through periods of symmetrical and highly asymmetrical spreading, and varies greatly from the symmetrically spreading Pacific-Antarctic ridge. We attribute these differences to major differences in the Pacific mantle: the southern East Pacific Rise (Pacific-Farallon/Nazca) shows signs of successive westward ridge jumps towards mantle upwelling associated with the South Pacific superswell, however the northern East Pacific Rise (Pacific-Cocos) is strongly driven by the adjacent subduction zone, and underwent eastward ridge jumps. The Pacific-Antarctic ridge is not located near either of these major driving forces of asymmetry, and shows evidence of minor asymmetry due to small-scale changes in mantle flow. These regional differences in the Pacific mantle suggests that long-term Farallon-Pacific crustal accretion ratios cannot be extrapolated based on the ~50 Myr record of Farallon/Nazca-Pacific asymmetries.

Comparison of the implied convergence history of the Pacific plates along the western North and South American plates based on our refined model and Seton et al. (2012) highlights the importance of the Pacific plate tectonic configuration. In particular, the addition of the Aluk plate in the south Pacific significantly improves the implied convergence history in the Patagonian region of South America and correlates with a proposed ~50 Ma ridge subduction event (Breitsprecher and Thorkelson, 2009). Further, the incorporation of Farallon-Pacific spreading asymmetry (based on the ‘best-fit’ ratios of Rowan and Rowley, 2014) does not significantly influence the age of subducting oceanic lithosphere along the North and South American margin.

Our reconstruction provides a framework for understanding circum-Pacific tectonics, plate reorganisation events, and the evolution of seafloor spreading and asymmetry in the Pacific basin.

6 Acknowledgements

We thank Graeme Eagles and an anonymous reviewer for their detailed reviews, which greatly improved the manuscript. N.M.W. was supported by an Australian Postgraduate Award, M.S. by ARC grant FT130101564 and S.E.W. and R.D.M. by ARC grant FL0992245. Figures were constructed using Generic Mapping Tools.

Figure 1: Bathymetry (ETOPO1; Amante and Eakins (2009) of the present-day Pacific basin, showing the major tectonic plates and fracture zones. Plate boundaries (black) are from Bird (2003), and fracture zone (FZ) identifications (blue) are from Wessel et al. (2015). Coastlines (Wessel and Smith, 1996) are shown in grey. EA: Easter microplate; JDF: Juan de Fuca plate; JZ: Juan Fernandez microplate; R: Rivera microplate.

Figure 2: Overview of major spreading systems in the Pacific basin since chron 34y (83 Ma). The western Pacific basin formed prior to chron 34y. Uncertainties in the boundaries of spreading systems, including the Vancouver-Farallon boundary and the extinct of Pacific-Farallon spreading in the equatorial Pacific, are denoted with a "?". Plate boundaries (black) are modified from Bird (2003) to denote subduction zones (toothed), and fracture zone (FZ) identifications (blue) are from Wessel et al. (2015). Present-day coastlines (Wessel and Smith, 1996) are in dark-grey, and non-oceanic regions are in light grey. Bellings.: Bellingshausen; EA: Easter microplate; JDF: Juan de Fuca plate; JZ: Juan Fernandez microplate; Math.: Mathematician microplate; MP: Microplate; R: Rivera microplate; Van.: Vancouver.

Figure 3: Overview of magnetic anomaly identifications in the Pacific basin, downloaded from the Global Seafloor Fabric and Magnetic Lineation (GSFML) repository (Seton et al. 2014) in April, 2015. C-sequence magnetic identifications are colored based on their age in Cande and Kent (1995), while M-sequence magnetic identifications are hollow. Plate boundaries (black) are modified from Bird (2003) to denote subduction zones (triangles), and fracture zone (FZ) identifications (blue) are from Wessel et al. (2015). Present-day coastlines (Wessel and Smith, 1996) are in dark-grey, and non-oceanic regions are in light grey. Legend for spreading regions as in Figure 2.

Figure 4: Schematic of Hellinger (1981)'s method. (a) Method to determine finite rotations, when both spreading flanks are preserved. The best-fit rotation pole is found by matching conjugate magnetic anomaly (black) and fracture zones (grey) of the same age (t_1) on both plates. (b) Method to determine half-stage rotations, when one of the plates has been subducted. The best-fit half-stage rotation pole is found by reconstructing a younger (t_1) magnetic anomaly and fracture zones segment onto an older (t_2) time. t_0 represents the present-day ridge. Modified from Rowan and Rowley (2014).

Figure 5: Overview of seafloor features in the South Pacific, observed in marine gravity anomalies (Sandwell et al., 2014). Plate boundaries (black) are from Bird (2003), fracture zones (FZ; white) are from Wessel et al. (2015) and coastlines (grey) are from Wessel and Smith (1996). Dashed outline refers to the region associated with Bellingshausen (BELL) independent motion. BGA: Bellingshausen gravity anomaly; DGGA: De Gerlache gravity anomaly; EA: East Antarctica; MBS: Marie Byrd Seamounts; NZ: New Zealand; SAM: South America.

Figure 6: Comparison of Pacific-West Antarctic spreading velocities in the timescales of Cande and Kent (1995) (CK95; left) and Ogg (2012) (GTS2012; right), with selected chrons labelled. 95% uncertainties (shaded blue) are for Wright et al. (2015) and this study. Full stage rates (mm/yr) and spreading directions (°) are calculated along the Pitman Fracture Zone.

Figure 7: Comparison of finite pole locations and 95% confidence ellipses from Wright et al. (2015) and this study. Finite rotation parameters are labelled based on their chron and reference (color).

Figure 8: Comparison of synthetic flowlines for Pacific-West Antarctic relative motion between chron 34y and 21y and the Erebus, Pitman and IX fracture zones (FZ) observed in the marine gravity anomaly (top; Sandwell et al., 2014) and in a cartoon schematic with fracture zone

identifications (black lines; Wessel et al., 2015; bottom) on the (a) Pacific plate and (b) Antarctic plate. Flowlines are colored based on reference (line, symbol outline). Wright et al. (2015) and this study have been combined into one flowline. Symbols along each flowline correspond to the age of plotted magnetic identifications (symbol fill). Magnetic identifications used in Hellinger's analysis in Wright et al. (2015) and this study are shown. Region associated with Bellingshausen (Bell.) spreading shown in dotted outline. EA: East Antarctica; MBL: Marie Byrd Land; NZ: New Zealand.

Figure 9: Comparison of Bellingshausen-Pacific spreading velocities in the timescales of Cande and Kent (1995) (CK95; left), and Ogg (2012) (GTS2012; right), with selected chrons labelled. 95% uncertainties (shaded blue) refer to this study only. Full stage rates (mm/yr) and spreading directions (°) are calculated along the Udintsev Fracture Zone.

Figure 10: Comparison of Bellingshausen-Pacific finite rotation pole locations and 95% confidence ellipses from this study. Finite rotation parameters are labelled based on their chron and reference (color).

Figure 11: Comparison of derived flowlines for Bellingshausen-Pacific relative motion and fracture zones observed in the marine gravity anomaly (Sandwell et al., 2014) (top) and as a cartoon schematic with fracture zone identifications (black lines; Wessel et al., 2015; middle). (a) Pacific plate. (b) Antarctic plate (former Bellingshausen region). Flowlines are colored based on reference, with divisions corresponding to chron times (labeled along the (a) Tharp and (b) Udintsev Fracture Zones [FZ]). Magnetic identifications used in this study's Hellinger analysis are shown (colored). EA: East Antarctica; MBL: Marie Byrd Land; NZ: New Zealand; SAM: South America

Figure 12: Comparison of synthetic flowlines for Pacific-Aluk (Phoenix) spreading observed in the marine gravity anomaly (Sandwell et al., 2014) (top) and as a cartoon schematic with fracture zone identifications (black lines; Wessel et al., 2015; middle panel). Interpreted isochrons (thin grey) and a compilation of magnetic identifications (Cande et al., 1995; Cande and Haxby, 1991; Croon et al., 2008; Eagles et al., 2004b; Larter et al., 2002; Wobbe et al., 2012) since chron 34y (colored circles) are shown. Regions of Aluk (Phoenix)-Pacific (Aluk-Pac), Bellingshausen-Pacific (Bell-Pac), and Pacific-Antarctic (Pac-Ant) are outlined. ANT: Antarctica

Figure 13: Overview of seafloor features in the south-central eastern Pacific, observed in marine gravity anomalies (Sandwell et al., 2014). Plate boundaries (black) are from Bird (2003), fracture zones (FZ; white) are from Matthews et al. (2011) and coastlines (grey) are from Wessel and Smith (1996). EA: Easter microplate; GP: Galapagos plate; JZ: Juan Fernandez microplate; R: Rivera plate; RSB: Rough-smooth boundary

Figure 14: Overview of seafloor features in the north-east Pacific, observed in marine gravity anomalies (Sandwell et al., 2014). Plate boundaries (black) are from Bird (2003), fracture zones (FZ; white) are from Wessel et al. (2015) and coastlines (grey) are from Wessel and Smith (1996). JDF: Juan de Fuca plate; RSB: Rough-smooth boundary

Figure 15: Comparison of Pacific-Farallon spreading velocities in Cande and Kent (1995) (left); and Ogg (2012) (right), with selected chrons labeled. 95% uncertainties (shaded blue) are for Wright et al. (2015) and this study. Large increases in spreading rate during ~50–40 Ma are likely artefacts of timescale conversion, rather than an actual increase in stage rates. Full stage rates (mm/yr) and spreading directions (°) are calculated along the (a) Molokai Fracture Zone (‘North Pacific’) and (b) Austral Fracture Zone (‘South Pacific).

Figure 16: 95% uncertainties for Pacific-Farallon half-stage rotations from Wright et al. (2015) (colored diamonds) and this study (black circles)

Figure 17: Comparison of synthetic flowlines for Pacific-Farallon spreading and fracture zones observed in the marine gravity anomaly (Sandwell et al., 2014) and as a cartoon schematic with fracture zone identifications (black lines; Wessel et al., 2015). A: North Pacific, with the Molokai and Clarion fracture zones (FZ). B: South Pacific, with the Marquesas and Austral FZs. Magnetic identifications (colored circles) on figure and inset are those used in the Hellinger's method for Wright et al. (2015) and this study. References compared include Seton et al. (2012) (inverted triangle, orange), Rowan and Rowley (2014) (star, red), and Wright et al. (2015) and this study (diamond, navy), where symbols along the flowlines are colored to match the timing of magnetic identifications used in Hellinger's analysis. Flowlines were constructed based on a common point, corresponding to chron 13y (Molokai FZ), chron 18n.2o (Clarion FZ), and chron 34y (Austral and Marquesas fracture zones). These chrons were chosen for easy comparison, as rift propagation has disturbed some regions within spreading corridors. CO: Cocos

Figure 18: Comparison of Vancouver-Pacific spreading velocities, in the timescales of Cande and Kent (1995) (left) and Ogg (2012) (right), with selected chrons labelled. 95% uncertainties (shaded blue) are for Wright et al. (2015) and this study. Full stage rates (mm/yr) and spreading direction (°) are calculated along the Mendocino Fracture Zone.

Figure 19: 95% uncertainty ellipses from Wright et al. (2015) and this study for Vancouver-Pacific spreading

Figure 20: Comparison of Vancouver-Pacific synthetic flowlines and North Pacific fracture zones, observed in marine gravity anomalies (left; Sandwell et al., 2014) and in a cartoon schematic

(middle), with fracture zone identifications (black lines; Wessel et al., 2015). References compared include Rosa and Molnar (1988) (star, green), Müller et al (1997) (inverted triangle, orange), McCrory and Wilson (triangle, red), Wright et al. (2015) (triangle: navy), and this study (diamond, blue), where symbols along the flowlines are colored to match the timing of magnetic identifications used in Hellinger's analysis (magnetic identifications shown). Flowlines for Müller et al. (1997) and this study were constructed based on a common point corresponding to chron 10n.1y, whereas other synthetic flowlines match the available rotations in each reference.

Figure 21: Comparison of Kula-Pacific spreading velocities in the timescales of Cande and Kent (1995) (CK95; left) and Ogg (2012) (GTS2012; right), with selected chrons labelled. 95% uncertainties (shaded blue) are for this study only. Full stage rates (mm/yr) and spreading directions (°N) are calculated along the Amlia Fracture Zone.

Figure 22: 95% confidence ellipses for Kula-Pacific half-stage rotation parameters

Figure 23: Comparison of Kula-Pacific synthetic flowlines observed in marine gravity anomalies (left; Sandwell et al., 2014) and in a cartoon schematic (middle), with fracture zone identifications (black lines; Wessel et al., 2015). Both Rosa and Molnar (1988) and Seton et al. (2012) have a poor geometric match with the Amlia and Rat fracture zones.

Figure 24: Reconstruction of the Pacific basin since chron 34y, shown at times corresponding to major seafloor spreading isochrons or major reorganization events within the Pacific basin. These ages are 83 Ma (34y), 79.1 Ma (33o), 67.7 Ma (31y), 55.9 Ma (25y), 52.4 Ma (24n.1y), 47.9 Ma (21o), 40.1 Ma (18n.2o), 33.1 Ma (13y), 22.7 Ma (6Bn.1c), 10.9 Ma (5n.2o), and present-day (0 Ma). Ages are in the timescale of Cande and Kent (1995). Marine gravity anomalies (Sandwell et al., 2014) are reconstructed, to highlight presently preserved oceanic crust. The compilation of

magnetic identifications from the GSFML repository (Seton et al., 2014) is shown as colored circles. Ant: Antarctica; B: Bauer microplate; Bell.: Bellingshausen; Coc: Cocos; IZ: Izanagi; JDF: Juan de Fuca; Van: Vancouver.

Figure 25: Refined present-day age grid and comparison with those from Seton et al. (2012). Residual age of the oceanic lithosphere is from the difference between our refined age grid and Seton et al. (2012).). Plate boundaries (white) for this study and residual are modified from Bird (2003), while those for Seton et al. (2012) are from their study. Coastlines (light grey) and non-oceanic regions (dark grey) are also shown.

Figure 26: Comparison of (a) half-spreading rate, (b) crustal accretion, and (c) error grids, based on this study and Müller et al. (2008). Residual is based on the difference between this study and Müller et al. (2008).

Figure 27: Paleo-age grid in 10 Myr increments. Left: Age grid in Gee and Kent (2007); Middle: Age grid in Ogg (2012); Left: Age difference between Gee and Kent (2007) and Ogg (2012).

Figure 28: Regions used in crustal accretion analysis within the Pacific basin. Some regions were excluded from analysis due to microplate formation (e.g. Bauer microplate). Regions that do not have a preserved conjugate flank are in white. Spreading regions used include Pacific-Nazca/Farallon (pink); Cocos-Pacific (dark green); Cocos-Nazca (light blue); Pacific-West Antarctic (blue); Bellingshausen-Pacific (gold); Antarctic-Nazca (light green); and Juan de Fuca-Pacific (maroon).

Figure 29: Variation in symmetric crustal accretion for the Pacific basin with preserved conjugate flanks (blue), and for spreading regions Pacific-Nazca/Farallon (pink), Pacific-West Antarctic (dark

blue), Bellingshausen-Pacific (gold), Cocos-Nazca (light blue), Cocos-Pacific (dark green); Juan de Fuca (JDF)-Pacific (maroon), and West Antarctic-Nazca (light green). Percentage (y-axes) refers to the percentage of the binned range of crustal asymmetry compared to all data points available for the spreading corridor.

Figure 30: Stage comparison of variations in crustal accretion for the Pacific-West Antarctic (blue; since chron 25y, 55.9 Ma), Pacific-Farallon/Nazca (pink) and Cocos-Pacific (green) spreading systems. Percentage (y-axes) refers to the percentage of the binned range of crustal asymmetry compared to all data points available for the spreading corridor.

Figure 31: Comparison of the implied convergence velocities along the North American margin, based on this study (filled: Cande and Kent, 1995; hollow: Ogg, 2012) and Seton et al. (2012). Van/JDF: Vancouver or Juan de Fuca plate.

Figure 32: Comparison of the implied convergence rate and obliquity from this study, in the timescales of Cande and Kent (1995; blue) and Ogg (2012; light blue), and Seton et al. (2012; orange) derived at three points along the North American margin. Convergence velocities are calculated in 5 Myr increments (except for the stage 83–80 Ma) based on the active plate at the time (labeled).

Figure 33: South Pacific plate configuration in the Early Cenozoic (~65 Ma). A: Plate boundaries from Seton et al. (2012). B: Plate boundaries from this study. Bellings: Bellingshausen

Figure 34: Comparison of the implied convergence velocities along the South American margin, based on this study (filled: Cande and Kent, 1995; hollow: Ogg, 2012) and Seton et al. (2012).

Figure 35: Comparison of the implied convergence rate and obliquity from this study, in the timescales of Cande and Kent (1995; blue) and Ogg (2012; light blue), and Seton et al. (2012; orange) derived at three points along the South American margin. Convergence velocities are calculated in 5 Myr increments (except for the stage 83–80 Ma) based on the active plate at the time (labeled). Since Seton et al. (2012) do not incorporate an Aluk plate, velocities between 83–20 Ma are based on their Farallon plate, and are compared with Farallon-South America relative motion derived from this model (red).

Figure 36: Age of the subducting oceanic crust at point 1 (48°N, 126.5°W), point 2 (38°N, 123°W), and point 3 (28°N, 116°W) along the North American trench. We derive the age of the subducting oceanic crust based on Farallon-Pacific symmetrical spreading (dark blue) and asymmetrical Farallon-Pacific spreading (light blue), based on the 'best-fit' ratio of Rowan and Rowley (2014). Age derived from Seton et al. (2012) is in orange. Grey regions refer to times where we rely on finite rotations for the down going plate (e.g. Pacific, Juan de Fuca).

Figure 37: Age of the subducting oceanic crust at point 1 (5°S, 81°W), point 2 (20°S, 76°W), and point 3 (45°S, 76°W) along the South American trench. We derive the age of the subducting oceanic crust based on Farallon-Pacific symmetrical spreading (dark blue) and asymmetrical Farallon-Pacific spreading (light blue), based on the 'best-fit' ratio of Rowan and Rowley (2014). Age of oceanic crust derived from Seton et al. (2012) is in orange. Grey regions refer to times where we rely on finite rotations for the down going plate (e.g. Nazca).

Table 1: Publications (with rotation parameters) for the Pacific plate relative to the West Antarctic plate. CNS: Cretaceous Normal Superchron

Source	Chrons	Age (Ma)	Comment
Cande et al. (1995)	31y–1o	67.7–0.8	Provides 95% confidence ellipses
Larter et al. (2002)	CNS–30r	90–67.7	Chrons 33y–30r are from Stock et al. (unpublished)
Eagles et al. (2004a)	33y–1c	73.6–0.4	Chron 31o and chrons 27o-1c are from Cande et al. (1995); chrons 33y, 32n1y, 30r, and 28r are from Stock et al. (unpublished)
Croon et al. (2008)	20o–1o	43.8–0.8	Provides 95% confidence ellipses
Müller et al. (2008)	34y–1o	83–0.8	Relies on the combination of Larter et al. (2002) (chrons 34y–31y) and Cande et al. (1995) (chrons 31y–1o)
Seton et al. (2012)	34y–1o	83–0.8	Same as Müller et al. (2008)
Wobbe et al. (2012)	CNS–20o	90–43.79	Relies only on new magnetic identifications presented within the study no uncertainties given
Wright et al. (2015)	30o–21o	67.6–47.9	Provides 95% confidence ellipses

Table 2: Finite rotations and covariance matrix for the Pacific plate relative to the West Antarctic plate

Chron	Age (Ma)	Lat (°N)	Lon (°E)	Angle (deg)	$\hat{\kappa}$	*dF*	*N*	*s*	*r*	*a*	*b*	*c*	*d*	*e*	*f*	*g*	Source
21o	47.9	74.431	-48.544	38.176	0.37	37	56	8	100.11	0.24	0.05	0.37	0.02	0.08	0.62	10^{-5}	(1)
24n.3o	53.3	73.474	-52.081	40.105	0.21	19	38	8	92.60	0.49	0.06	0.79	0.03	0.09	1.34	10^{-5}	(1)
25m	56.1	72.627	-54.727	41.142	0.36	18	35	7	49.40	0.87	0.16	1.21	0.06	0.22	1.76	10^{-5}	(1)
26o	57.9	72.317	-54.189	42.531	0.67	23	48	11	34.20	0.35	0.02	0.55	0.02	0.02	0.93	10^{-5}	(1)
27o	61.3	71.348	-54.157	45.498	1.25	31	44	5	24.78	1.84	-0.21	3.00	0.04	-0.33	5.00	10^{-5}	(1)
30o	67.6	68.941	-56.694	49.007	2.76	16	31	6	5.79	4.95	-0.26	7.47	0.06	-0.40	11.39	10^{-5}	(1)
33y	73.6	66.631	-57.357	52.776	0.35	39	52	5	112.32	1.67	0.00	2.24	0.02	0.02	3.09	10^{-5}	(2)

$\hat{\kappa}$ is the estimated quality factor, dF is the number of degrees of freedom, N is the number of datapoints, s is the number of great circle segments, and r is the total misfit. Variables $\hat{\kappa}, a, b, c, d, e$ and f are in radians. The covariance matrix is defined as: $Cov(u) = \frac{g}{\hat{\kappa}} \begin{pmatrix} a & b & c \\ b & d & e \\ c & e & f \end{pmatrix}$ Sources: (1) Wright et al. (2015), (2) This study.

Table 3: Publications (with rotation parameters) for the Bellingshausen plate relative to the Pacific plate.

Source	Chrons	Age (Ma)	Comment
Stock and Molnar (1988)	30r–25c	67.7–56.1	Provides partial uncertainties
Larter et al. (2002)	33y–28r	73.6–63.8	Relies on Stock et al. (unpublished)
Eagles et al. (2004a)	33o–27o	79.08–61.3	Chrons 33y–28r are from Stock et al. (unpublished); chron 27o is from Cande et al. (2005)
Müller et al. (2008)	33y–27o	73.6–61.3	Same as Larter et al. (2002)
Seton et al. (2012)	33y–27o	73.6–61.2	Same as Müller et al. (2008)
Wobbe et al. (2012)	34y–27o	83–61.2	Relies only on new magnetic identifications presented within the study, and no uncertainties given

Table 4: Finite rotations and covariance matrix for the Bellingshausen plate relative to the Pacific plate.

Chron	Age (Ma)	Lat (°N)	Lon (°E)	Angle (deg)	$\hat{\kappa}$	*dF*	*N*	*s*	*r*	*a*	*b*	*c*	*d*	*e*	*f*	*g*
28o	63.63	-70.386	122.257	46.152	0.46	15	28	5	32.53	0.39	0.66	1.81	1.27	3.35	9.14	10^{-5}
30o	67.60	-71.101	129.504	52.623	1.01	7	20	5	6.94	0.18	0.43	0.98	1.35	2.92	6.60	10^{-5}
32n.1o	71.34	-71.655	137.499	59.611	0.55	9	18	3	16.29	0.51	0.91	2.41	1.87	4.80	12.84	10^{-5}
33y	73.60	-71.207	139.406	63.208	0.63	17	26	3	27.18	0.14	0.27	0.60	0.65	1.51	3.76	10^{-5}
33o	79.08	-70.107	144.208	70.971	0.54	27	36	3	49.98	0.07	0.16	0.32	0.74	1.56	3.65	10^{-5}

$\hat{\kappa}$ is the estimated quality factor, dF is the number of degrees of freedom, N is the number of datapoints, s is the number of great circle segments, and r is the total misfit. Variables $\hat{\kappa}, a, b, c, d, e$ and f are in radians. The covariance matrix is defined as: $Cov(u) = \frac{g}{\hat{\kappa}} \begin{pmatrix} a & b & c \\ b & d & e \\ c & e & f \end{pmatrix}$

Table 5: Pacific-Aluk spreading between chron 34y and 27o (83–61.3 Ma)

Stage		Half-stage			Full stage		
Chrons	Age (Ma)	Lat (°N)	Lon (°E)	Angle (°)	Lat (°N)	Lon (°E)	Angle (°)
27o–31y	61.3–67.7	-12.5	76.3	-6.13	-12.5	-76.3	-12.26
31y–34y	67.7–83	-53.9	132.0	-11.64	-53.9	132.0	-23.28

Table 6: Publications (with rotation parameters) for the Farallon plate relative to the Pacific plate between chron 34y and present-day

Source	Chrons	Age (Ma)	Comment
Pardo-Casas and Molnar (1987)	30r–5c	67.7–10.9	Finite rotations only
Rosa and Molnar (1988)	30r–13o	67.7–33.5	Half-stage rotations. Provides partial uncertainties
Stock and Molnar (1988)	30r–13o	67.7–33.5	From Rosa and Molnar (1988)
Müller et al. (2008)	34y–5n.2o	83–10.9	Finite rotations only. Provides rotations from 170 Ma
Seton et al. (2012)	34y–5n.2o	83–10.9	Same as Müller et al. (2008)
Rowan and Rowley (2014)	34y–10y	83–28.3	Half-stage rotations and finite rotations incorporating spreading asymmetry. Provides 95% confidence ellipses
Wright et al. (2015)	31y–13y	67.7–33.1	Half-stage rotations. Provides 95% confidence ellipses

Table 7: Half-stage rotations and covariance matrix for Farallon plate relative to the Pacific plate motion between chron 34y and 13y

Chron	Lat (°N)	Lon (°E)	Angle (deg.)	$\hat{\kappa}$	dF	*N*	*s*	*r*	*a*	*b*	*c*	*d*	*e*	*f*	*g*	Source
13y–18n.2o	-57.206	-119.683	5.796	0.24	51	76	11	208.82	8.49	8.83	0.24	11.90	0.27	1.90	10-^{7}	(1)

18n.2o–20o	-75.751	-90.302	2.765	0.30	51	74	10	172.34	10.45	9.08	-3.62	10.32	-3.58	2.94	10^{-7}	(1)
20o–21o	-59.482	-117.813	2.653	0.35	76	107	14	215.39	6.08	4.57	-1.72	4.95	-1.51	1.52	10^{-7}	(1)
21o–22o	-64.069	-111.485	0.954	0.99	105	138	15	105.87	3.20	2.11	-0.15	2.81	-0.24	0.68	10^{-7}	(1)
22o–24n.1y	-68.840	-104.776	1.147	3.19	57	80	10	17.86	6.18	3.79	-1.45	4.61	-1.30	1.61	10^{-7}	(1)
24n.1y–25y	-58.818	-119.609	1.591	0.60	71	96	11	118.99	6.58	4.17	-1.88	4.50	-1.51	1.65	10^{-7}	(1)
25y–26y	-61.494	-118.605	0.571	1.49	118	151	15	79.16	3.32	1.62	-1.70	2.15	-1.30	1.74	10^{-6}	(1)
26y–27o	-63.787	-117.523	1.177	0.87	87	114	12	99.97	6.28	3.34	-3.36	3.46	-2.31	2.87	10^{-7}	(1)
27o–28y	-52.581	-127.173	0.374	1.51	89	118	13	58.90	6.26	3.48	-3.34	3.36	-2.26	2.81	10^{-7}	(1)
28y–31y	-72.402	-102.630	1.881	0.61	122	145	10	198.70	4.84	2.05	-2.95	2.81	-2.01	2.82	10^{-7}	(1)
31y–33o	-60.674	-130.481	4.167	0.26	73	100	12	277.75	10.13	4.85	-6.11	3.98	-3.32	5.40	10^{-7}	(2)
33o–34y	-51.276	-140.757	1.493	0.28	77	102	11	271.81	4.45	1.47	-1.80	2.31	-0.87	1.79	10^{-7}	(2)

$\hat{\kappa}$ is the estimated quality factor, dF is the number of degrees of freedom, N is the number of datapoints, s is the number of great circle segments, and r is the total misfit. Variables $\hat{\kappa}, a, b, c, d, e$ and f are in radians. The covariance matrix is defined as: $Cov(u) = \frac{g}{\hat{\kappa}} \begin{pmatrix} a & b & c \\ b & d & e \\ c & e & f \end{pmatrix}$ Sources: (1) Wright et al. (2015), (2) This study.

Table 8: Publications (with rotation parameters) for the Vancouver plate relative to the Pacific plate

Source	Chrons	Age (Ma)	Comment
Rosa and Molnar (1988)	21y–13o	47.9–33.5	Half-stage rotations, includes partial uncertainties
Stock and Molnar (1988)	25c–13c	56.1–33.3	From Rosa and Molnar (1988), except for chron 21–25
Müller et al. (1997)	M21–5n.2o	147.7–10.9	Finite rotations
Seton et al. (2012)	24n.1y–5n.2o	52.4–10.9	Same as Müller et al. (1997)
McCrory and Wilson (2013)	24n.1y–18n.2o	52.4–40.1	Given as finite rotations
Wright et al. (2015)	24n.1y–13y	52.4–33.1	Half-stage rotations, includes 95% confidence ellipses

Table 9: Half-stage rotations for the Juan de Fuca plate relative to the Pacific plate between chron 10n.1y and 4Ac

Chron	Age (Ma)	Lat (+ °N)	Lon (+ °E)	Angle (deg)
4Ac–5n.2y	8.9–9.9	-65.32	50.03	1.91
5n.2y–6o	9.9–20.1	74.17	58.19	-3.11
6o–10n.1y	20.1–28.3	-70.34	39.23	8.58

Table 10: Half-stage rotations and covariance matrix for the Vancouver plate relative to the Pacific plate between 24n.1y and 10n.1y

Chron	Lat	Lon	Angle	$\hat{\kappa}$	*dF*	*N*	*s*	*r*	*a*	*b*	*c*	*d*	*e*	*f*	*g*	Source

	(°N)	(°E)	(deg.)													
10n.1y–13y	-75.414	35.037	5.135	1.92	79	100	9	41.14	1.96	1.59	-2.57	1.65	-2.33	3.76	10^{-6}	(2)
13y–18n.2o	-72.935	38.385	7.125	0.44	66	85	8	149.22	6.23	4.18	-8.02	3.10	-5.55	10.64	10^{-6}	(1)
18n.2o–21o	-71.865	39.600	6.217	1.41	49	66	7	34.78	5.06	2.94	-6.00	2.13	-3.72	7.50	10^{-6}	(1)
21o–22o	-71.145	37.555	1.319	2.32	35	52	7	15.06	7.80	3.91	-8.96	2.35	-4.72	10.72	10^{-6}	(1)
22o–24n.1y	-71.810	36.938	1.454	0.91	25	40	6	27.34	8.22	5.11	-9.40	3.65	-6.20	11.42	10^{-6}	(1)

$\hat{\kappa}$ is the estimated quality factor, dF is the number of degrees of freedom, N is the number of datapoints, s is the number of great circle segments, and r is the total misfit. Variables $\hat{\kappa}, a, b, c, d, e$ and f are in radians. The covariance matrix is defined as: $Cov(u) = \frac{g}{\hat{\kappa}}\begin{pmatrix} a & b & c \\ b & d & e \\ c & e & f \end{pmatrix}$ Sources: (1) Wright et al. (2015), (2) This study.

Table 11: Publications (with rotation parameters) for the Kula plate relative to the Pacific plate

Source	Chrons	Age (Ma)	Comment
Rosa and Molnar (1988)	30o–25m	67.6–56.1	Half-stage rotations. Provides partial uncertainties
Stock and Molnar (1988)	30o–25m	67.6–56.1	From Rosa and Molnar (1988)
Müller et al. (2008)	33o–18r	79.1–41	Finite rotations only
Seton et al. (2012)	33o–18r	79.1–41	From Müller et al. (2008)

Table 12: Half-stage rotation parameters and covariance matrix for the Kula plate relative to the Pacific plate motion.

Chron	Lat (°N)	Lon (°E)	Angle (deg.)	$\hat{\kappa}$	dF	N	s	r	a	b	c	d	e	f	g
25y–27o	-35.641	-48.924	1.373	2.65	75	90	6	28.26	4.15	0.89	-4.66	0.28	-1.02	5.94	10^{-6}
27o–31y	-30.598	-54.473	1.977	1.42	65	80	6	45.83	5.60	1.11	-6.29	0.32	-1.27	7.78	10^{-6}
31y–33y	-34.237	-47.824	3.744	0.25	41	58	7	162.27	1.37	0.15	-1.52	0.04	-0.17	1.73	10^{-5}
33y–34y	17.454	-105.400	2.253	3.39	13	28	6	3.84	16.55	0.98	-16.89	0.12	-0.99	17.28	10^{-5}

$\hat{\kappa}$ is the estimated quality factor, dF is the number of degrees of freedom, N is the number of datapoints, s is the number of great circle segments, and r is the total misfit. Variables $\hat{\kappa}, a, b, c, d, e$ and f are in radians. The covariance matrix is defined as: $Cov(u) = \frac{g}{\hat{\kappa}}\begin{pmatrix} a & b & c \\ b & d & e \\ c & e & f \end{pmatrix}$

Table 13: Summary of finite rotation parameters for the Pacifc basin since chron 34y

Chron	Age	Latitude	Longitude	Angle	Source
Pacific plate with respect to the West Antarctic plate					
5n.2o	10.9	70.36	-77.81	9.48	Croon et al. (2008)
6o	20.1	74.0	-70.16	16.73	Croon et al. (2008)
13y	33.1	74.5	-64.6	26.97	Derived from Croon et al. (2008)
18n.2o	40.1	74.87	-54.46	32.62	Croon et al. (2008)
21o	47.9	74.43	-48.54	38.18	Wright et al. (2015)

25y	55.9	73.0	-51.4	42.26	Derived from Wright et al. (2015)
31y	67.7	68.9	-56.7	49.07	Derived from Wright et al. (2015)
34y	83	63.6	-58.1	58.8	This study
Bellingshausen plate with respect to the Pacific plate					
27o	61.3	71.35	-54.16	-45.50	Crossover
31y	67.7	-71.07	129.93	52.72	This study
33o	79.1	-70.0441	144.3016	70.8871	This study
Aluk plate with respect to the West Antarctic plate					
5n.2o	10.9	-69.46	-89.6	12.4	Eagles and Scott (2014)
6o	20.1	-68.43	-89.45	32.3	Eagles and Scott (2014)
13y	33.1	-70.28	-106.31	40.72	Derived from Eagles and Scott (2014)
18n.2o	40.1	-70.77	-110.04	45.54	Eagles and Scott (2014)
21o	47.9	-71.67	-110.33	62.69	Derived from Eagles and Scott (2014)
25y	55.9	-71.82	-115.41	70.75	Derived from Eagles and Scott (2014)
27o	61.3	-71.48	-123.18	79.06	Eagles and Scott (2014)
Aluk plate with respect to the Pacific plate					
27o	61.3	70.3037	16.2941	-120.1011	Crossover
31y	67.7	66.2195	0.688	-120.9605	This study
34y	83	61.2364	-4.1952	-142.0441	This study
Farallon plate with respect to the Pacific plate					
5n.2o	10.9	60.11	-89.75	-14.88	Müller et al. (2008)
	23	73.53	-92.61	-31.08	Müller et al. (2008)
13y	33.1	76.1	-110.7	-45.27	Derived from Tebbens and Cande (1997)
18n.2o	40.1	84.45	-138.06	-53.87	Wright et al. (2015)
21o	47.9	85.5	168.93	-63.57	Wright et al. (2015)
25y	55.9	84.14	138.7	-70.14	Wright et al. (2015)
31y	67.7	82.43	124.34	-77.55	Wright et al. (2015)
33o	79.1	80.29	111.03	-84.97	This study
34y	83.0	79.29	106.41	-87.38	This study
Nazca plate with respect to the Pacific plate					
	5.0	60.08	-91.23	-7.13	Derived from Tebbens and Cande (1997) and Croon et al. (2008)
5n.2o	10.9	63.42	-91.82	-16.54	Derived from Tebbens and Cande (1997) and Croon et al. (2008)
	15.0	64.98	-91.73	-22.83	Derived from Tebbens and Cande (1997) and Croon et al. (2008)
6o	20.1	62.38	-93.02	-31.01	Tebbens and Cande (1997)
6Bn.1c	22.7	63.42	-94.11	-35.51	Derived from Tebbens and Cande (1997) and Croon et al. (2008)
Cocos plate with respect to the Pacific plate					
	5	39.13	-108.6	-10.25	Müller et al. (2008)
	10.0	35.3	-105.6	-25.08	Müller et al. (2008)
	11.9	36.0	-107.7	-30.27	Wilson (1996)
	13.0	36.7	-109.1	-32.66	Wilson (1996)
	14.8	38.3	-111.8	-36.33	Wilson (1996)
	17.3	39.3	-114.9	-42.45	Wilson (1996)
	20.0	40.42	-117.81	-47.44	Müller et al. (2008)
6Bn.1c	22.7	39.8	-119.7	-54.29	Müller et al. (2008)
Juan de Fuca/Vancouver plate with respect to the Pacific plate					
5n.2o	10.9	80.5	-38.8	-8.92	This study
6o	20.1	82.6	12.21	-14.34	This study
10n.1y	28.3	81.35	-117.91	-30.67	This study
13y	33.1	79.74	-125.38	-40.87	Wright et al. (2015)
18n.2o	40.1	77.74	-128.25	-55.02	Wright et al. (2015)
21o	47.9	76.45	-128.91	-67.38	Wright et al. (2015)
22o	49.7	76.2	-129.07	-70.0	Wright et al. (2015)
24n.1y	52.4	75.96	-129.3	-72.9	Wright et al. (2015)
Kula plate with respect to the Pacific plate					
19y	41.3	28.06	-56.8	0.11	This study

21o	47.9	27.14	-58.12	3.74	This study
25y	55.9	37.5205	153.3348	-24.1859	This study
27o	61.3	37.141	151.0921	-26.8115	This study
31y	67.7	35.9891	147.8721	-30.5089	This study
33y	73.6	35.1337	144.8728	-37.8426	This study
34y	83.0	30.2191	139.2524	-38.5042	This study
Bauer microplate with respect to the Pacific plate					
4n.1y	7.4	-28.0	-103.0	-3.9	Seton et al. (2012)
5n.2o	10.9	-27.25	-101.3	-19.3	Seton et al. (2012)
15.2	15.2	-24.86	-98.5	-40.63	Seton et al. (2012)
Mathematician microplate with respect to the Pacific plate					
3n.4c	5.1	27.7	-109.7	-6.29	DeMets and Traylen (2000)
5n.2o	10.9	-16.7	-115.6	9.39	DeMets and Traylen (2000)
Rivera microplate with respect to the Pacific plate					
1o	0.8	26.7	-105.2	-3.66	DeMets and Traylen (2000)
3n.4c	5.1	28.0	-105.7	-19.5	DeMets and Traylen (2000)
5n.2y	9.9	31.9	-106.0	-27.2	DeMets and Traylen (2000)

7 References

Adam, C., Yoshida, M., Suetsugu, D., Fakao, T. and Cadio, C., 2014. Geodynamic modeling of the South Pacific superswell. Physics of the Earth and Planetary Interiors, 229: 24-39

Amante, C. and Eakins, B., 2009. Arc-minute global relief model: procedures, data sources and analysis (ETOPO1). NOAA, National Geophysical Data Center, Colorado, USA.

Atwater, T., 1989. Plate tectonic history of the northeast Pacific and western North America. The eastern Pacific Ocean and Hawaii: Boulder, Colorado, Geological Society of America, Geology of North America, v. N: 21-72.

Atwater, T., Sclater, J., Sandwell, D., Severinghaus, J. and Marlow, M.S., 1993. Fracture zone traces across the North Pacific Cretaceous Quiet Zone and their tectonic implications. The Mesozoic Pacific: Geology, Tectonics, and Volcanism: 137-154.

Atwater, T. and Severinghaus, J., 1989. Tectonic maps of the northeast Pacific. The Geology of North America: 15-20.

Atwater, T. and Stock, J., 1998. Pacific-North America plate tectonics of the Neogene southwestern United States: an update. International Geology Review, 40(5): 375-402.

Barckhausen, U., Bagge, M. and Wilson, D.S., 2013. Seafloor spreading anomalies and crustal ages of the Clarion-Clipperton Zone. Marine Geophysical Research: 1-10.

Barckhausen, U., Ranero, C.R., Cande, S.C., Engels, M. and Weinrebe, W., 2008. Birth of an intraoceanic spreading center. Geology, 36(10): 767-770.

Barckhausen, U., Ranero, C.R., Huene, R.v., Cande, S.C. and Roeser, H.A., 2001. Revised tectonic boundaries in the Cocos Plate off Costa Rica: Implications for the segmentation of the convergent margin and for plate tectonic models. Journal of Geophysical Research: Solid Earth (1978–2012), 106(B9): 19207-19220.

Barker, P., 1982. The Cenozoic subduction history of the Pacific margin of the Antarctic Peninsula: ridge crest–trench interactions. Journal of the Geological Society, 139(6): 787-801.

Berggren, W.A., Kent, D.V., Flynn, J.J. and Van Couvering, J.A., 1985. Cenozoic geochronology.

Geological Society of America Bulletin, 96(11): 1407-1418.

Bird, P., 2003. An updated digital model of plate boundaries. Geochemistry, Geophysics, Geosystems, 4(3).

Bohannon, R.G. and Parsons, T., 1995. Tectonic implications of post–30 Ma Pacific and North American relative plate motions. Geological Society of America Bulletin, 107(8): 937-959.

Boyden, J.A., Müller, R.D., Gurnis, M., Torsvik, T.H., Clark, J.A., Turner, M., Ivey-Law, H., Watson, R.J. and Cannon, J.S., 2011. Next-generation plate-tectonic reconstructions using GPlates. Geoinformatics: cyberinfrastructure for the solid earth sciences: 95-114.

Breitsprecher, K., Thorkelson, D., Groome, W. and Dostal, J., 2003. Geochemical confirmation of the Kula-Farallon slab window beneath the Pacific Northwest in Eocene time. Geology, 31(4): 351-354.

Breitsprecher, K. and Thorkelson, D.J., 2009. Neogene kinematic history of Nazca–Antarctic–Phoenix slab windows beneath Patagonia and the Antarctic Peninsula. Tectonophysics, 464(1): 10-20.

Byrne, T., 1979. Late Paleocene demise of the Kula-Pacific spreading center. Geology, 7(7): 341-344.

Cande, S., Herron, E. and Hall, B., 1982. The early Cenozoic tectonic history of the southeast Pacific. Earth and Planetary Science Letters, 57(1): 63-74.

Cande, S.C. and Haxby, W.F., 1991. Eocene propagating rifts in the southwest Pacific and their conjugate features on the Nazca plate. Journal of Geophysical Research: Solid Earth (1978–2012), 96(B12): 19609-19622.

Cande, S.C. and Kent, D.V., 1995. Revised calibration of the geomagnetic polarity timescale for the Late Cretaceous and Cenozoic. Journal of Geophysical Research: Solid Earth, 100(B4): 6093-6095.

Cande, S.C., Raymond, C.A., Stock, J. and Haxby, W.F., 1995. Geophysics of the Pitman Fracture Zone and Pacific-Antarctic Plate. Science, 270: 10.

Cande, S.C., Stock, J.M., Müller, R.D. and Ishihara, T., 2000. Cenozoic motion between east and west Antarctica. Nature, 404(6774): 145-150.

Chang, T., 1987. On the statistical properties of estimated rotations. Journal of Geophysical Research: Solid Earth (1978–2012), 92(B7): 6319-6329.

Chang, T., 1988. Estimating the relative rotation of two tectonic plates from boundary crossings. Journal of the American Statistical Association, 83(404): 1178-1183.

Clague, D.A. and Dalrymple, G.B., 1987. The Hawaiian-Emperor volcanic chain. Part I. Geologic evolution. Volcanism in Hawaii, 1: 5-54.

Cochran, J.R., 1986. Variations in subsidence rates along intermediate and fast spreading mid-ocean ridges. Geophysical Journal International, 87(2): 421-454.

Conder, J.A., Forsyth, D.W. and Parmentier, E., 2002. Asthenospheric flow and asymmetry of the East Pacific Rise, MELT area. Journal of Geophysical Research: Solid Earth (1978–2012), 107(B12): ETG 8-1-ETG 8-13.

Croon, M.B., Cande, S.C. and Stock, J.M., 2008. Revised Pacific - Antarctic plate motions and geophysics of the Menard Fracture Zone. Geochemistry, Geophysics, Geosystems, 9(7).

Cross, T.A. and Pilger, R.H., 1982. Controls of subduction geometry, location of magmatic arcs, and tectonics of arc and back-arc regions. Geological Society of America Bulletin, 93(6): 545-562.

Cunningham, A.P., Larter, R.D., Barker, P.F., Gohl, K. and Nitsche, F.O., 2002. Tectonic evolution of the Pacific margin of Antarctica 2. Structure of Late Cretaceous–early Tertiary plate boundaries in the Bellingshausen Sea from seismic reflection and gravity data. Journal of Geophysical Research: Solid Earth (1978–2012), 107(B12): EPM 6-1-EPM 6-20.

Davy, B., 2006. Bollons Seamount and early New Zealand–Antarctic seafloor spreading. Geochemistry, Geophysics, Geosystems, 7(6).

DeMets, C. and Traylen, S., 2000. Motion of the Rivera plate since 10 Ma relative to the Pacific and North American plates and the mantle. Tectonophysics, 318(1): 119-159.

Eagles, G., 2004. Tectonic evolution of the Antarctic–Phoenix plate system since 15 Ma. Earth and Planetary Science Letters, 217(1): 97-109.

Eagles, G., Gohl, K. and Larter, R.D., 2004a. High-resolution animated tectonic reconstruction of the South Pacific and West Antarctic margin. Geochemistry Geophysics Geosystems, 5(7): Q07002.

Eagles, G., Gohl, K. and Larter, R.D., 2004b. Life of the Bellingshausen plate. Geophysical research letters, 31(7).

Eagles, G. and Scott, B.G., 2014. Plate convergence west of Patagonia and the Antarctic Peninsula since 61Ma. Global and Planetary Change, 123: 189-198.

Eakins, B.W. and Lonsdale, P.F., 2003. Structural patterns and tectonic history of the Bauer microplate, Eastern Tropical Pacific. Marine Geophysical Researches, 24(3-4): 171-205.

Elvers, D., Peter, G. and Moses, R., 1967. Analysis of magnetic lineations in the North Pacific. Eos Trans. AGU, 48: 89.

Engebretson, D.C., Cox, A. and Gordon, R.G., 1985. Relative motions between oceanic and continental plates in the Pacific basin. Geological Society of America Special Papers, 206: 1-60.

England, P. and Wortel, R., 1980. Some consequences of the subduction of young slabs. Earth and Planetary Science Letters, 47(3): 403-415.

Evans, R., Tarits, P., Chave, A., White, A., Heinson, G., Filloux, J., Toh, H., Seama, N., Utada, H. and Booker, J., 1999. Asymmetric electrical structure in the mantle beneath the East Pacific Rise at 17 S. Science, 286(5440): 752-756.

Gaina, C., Müller, D.R., Royer, J.Y., Stock, J., Hardebeck, J. and Symonds, P., 1998. The tectonic history of the Tasman Sea: a puzzle with 13 pieces. Journal of Geophysical Research: Solid Earth (1978–2012), 103(B6): 12413-12433.

Gee, J.S. and Kent, D.V., 2007. Source of oceanic magnetic anomalies and the geomagnetic polarity timescale. Treatise on Geophysics, Vol. 5: Geomagnetism: 455-507.

Gohl, K., Teterin, D., Eagles, G., Netzeband, G., Grobys, J., Parsiegla, N., Schlüter, P., Leinweber, V.T., Larter, R.D. and Uenzelmann-Neben, G., 2007. Geophysical survey reveals tectonic structures in the Amundsen Sea embayment, West Antarctica. US Geological Survey Open-File Report, 2007-1047

Granot, R., Cande, S., Stock, J. and Damaske, D., 2013. Revised Eocene ‐ Oligocene kinematics for the West Antarctic rift system. Geophysical research letters: 1-6.

Granot, R., Cande, S.C. and Gee, J.S., 2009. The implications of long-lived asymmetry of remanent magnetization across the North Pacific fracture zones. Earth and Planetary Science Letters, 288(3): 551-563.

Grow, J.A. and Atwater, T., 1970. Mid-Tertiary tectonic transition in the Aleutian Arc. Geological Society of America Bulletin, 81(12): 3715-3722.

Harry, D.L. and Green, N.L., 1999. Slab dehydration and basalt petrogenesis in subduction systems involving very young oceanic lithosphere. Chemical Geology, 160(4): 309-333.

Haeussler, P.J, Bradley, D.C., Wells, R.E. & Miller, M.L. 2003. 'Life and death of the Resurrection plate: Evidence for its existence and subduction in the northeastern Pacific in Paleocene–Eocene time.' Geological Society of America Bulletin, 115(7): 867-880.

Hellinger, S., 1981. The uncertainties of finite rotations in plate tectonics. Journal of Geophysical Research: Solid Earth (1978–2012), 86(B10): 9312-9318.

Herron, E. and Tucholke, B., 1976. Sea-floor magnetic patterns and basement structure in the southeastern Pacific. Initial Reports of the Deep Sea Drilling Project, 35: 263-278.

Hey, R., 1977. Tectonic evolution of the Cocos-Nazca spreading center. Geological Society of America Bulletin, 88(10): 1404-1420.

Hilde, T.W., Uyeda, S. and Kroenke, L., 1977. Evolution of the western Pacific and its margin. Tectonophysics, 38(1): 145-165.

Iaffaldano, G., Hawkins, R., Bodin, T., Sambridge, M., 2014. REDBACK: open-source software for efficient noise-reduction in plate kinematic reconstructions. Geochemistry Geophysics

Geosystems, v. 15, p. 1663-1670

Jicha, B. R., Scholl, D. W., and Rea, D. K. 2009. Circum-Pacific arc flare-ups and global cooling near the Eocene-Oligocene boundary. Geology, 37(4), 303-306.

Kirkwood, B.H., Royer, J.-Y., Chang, T.C. and Gordon, R.G., 1999. Statistical tools for estimating and combining finite rotations and their uncertainties. Geophysical Journal International, 137(2): 408-428.

Klitgord, K.D. and Mammerickx, J., 1982. Northern East Pacific Rise: magnetic anomaly and bathymetric framework. Journal of Geophysical Research: Solid Earth (1978–2012), 87(B8): 6725-6750.

Larson, R.L. and Chase, C.G., 1972. Late Mesozoic evolution of the western Pacific Ocean. Geological Society of America Bulletin, 83(12): 3627-3644.

Larter, R.D. and Barker, P.F., 1991. Effects of ridge crest ‐ trench interaction on Antarctic ‐ Phoenix Spreading: Forces on a young subducting plate. Journal of Geophysical Research: Solid Earth (1978ety of America Bulletin, 83(1

Larter, R.D., Cunningham, A.P., Barker, P.F., Gohl, K. and Nitsche, F.O., 2002. Tectonic evolution of the Pacific margin of Antarctica 1. Late Cretaceous tectonic reconstructions. Journal of Geophysical Research, 107(B12): 2345.

Liu, Z., 1996, The Origin and Evolution of the Easter Seamount Chain, Doctoral thesis, University of South Florida, St. Petersburg, 266 pp.

Livermore, R., Balanyá, J.C., Maldonado, A., Martínez, J.M., Rodríguez-Fernández, J., de Galdeano, C.S., Zaldívar, J.G., Jabaloy, A., Barnolas, A. and Somoza, L., 2000. Autopsy on a dead spreading center: the Phoenix Ridge, Drake Passage, Antarctica. Geology, 28(7): 607-610.

Lonsdale, P., 1986. Tectonic and magmatic ridges in the Eltanin fault system, South Pacific. Marine geophysical researches, 8(3): 203-242.

Lonsdale, P., 1988. Paleogene history of the Kula plate: Offshore evidence and onshore implications. Geological Society of America Bulletin, 100(5): 733-754.

Lonsdale, P., 1991. Structural patterns of the Pacific floor offshore of peninsular California. The gulf and peninsular province of the Californias, 47: 87-125.

Lonsdale, P., 2005. Creation of the Cocos and Nazca plates by fission of the Farallon plate. Tectonophysics, 404(3): 237-264.

Mammerickx, J., Naar, D. and Tyce, R., 1988. The mathematician paleoplate. Journal of Geophysical Research: Solid Earth (1978–2012), 93(B4): 3025-3040.

Mammerickx, J. and Sharman, G., 1988. Tectonic evolution of the North Pacific during the Cretaceous quiet period. Journal of Geophysical Research: Solid Earth (1978–2012), 93(B4): 3009-3024.

Matthews, K.J., Müller, R.D., Wessel, P. and Whittaker, J.M., 2011. The tectonic fabric of the ocean basins. Journal of Geophysical Research: Solid Earth (1978–2012), 116(B12).

Matthews, K.J., Williams, S.E., Whittaker, J.M., Müller, R.D., Seton, M. and Clarke, G.L., 2015. Geologic and kinematic constraints on Late Cretaceous to mid Eocene plate boundaries in the southwest Pacific. Earth-Science Reviews, 140: 72-107.

Mayes, C.L., Lawver, L.A. and Sandwell, D.T., 1990. Tectonic history and new isochron chart of the South Pacific. Journal of Geophysical Research: Solid Earth (1978–2012), 95(B6): 8543-8567.

McCarron, J.J. and Larter, R.D., 1998. Late Cretaceous to early Tertiary subduction history of the Antarctic Peninsula. Journal of the Geological Society, 155(2): 255-268.

McCarthy, M.C., Kruse, S.E., Brudzinski, M.R. and Ranieri, M.E., 1996. Changes in plate motions and the shape of Pacific fracture zones. Journal of Geophysical Research: Solid Earth (1978–2012), 101(B6): 13715-13730.

McCrory, P.A. and Wilson, D.S., 2013. A kinematic model for the formation of the Siletz ‐ Crescent forearc terrane by capture of coherent fragments of the Farallon and Resurrection plates. Tectonics, 32(3): 718-736.

Menard, H., 1978. Fragmentation of the Farallon plate by pivoting subduction. The Journal of Geology: 99-110.

Meschede, M. and Barckhausen, U., 2000. 7. Plate Tectonic Evolution of the Cocos-Nazca Spreading Center.

Meschede, M., Barckhausen, U., Engels, M. and Weinrebe, W., 2008. The trace of the Pacific ‐ Cocos ‐ Nazca triple junction in the Central Pacific and the formation of an overlapping spreading centre. Terra Nova, 20(3): 246-251.

Molnar, P. and Atwater, T., 1978. Interarc spreading and Cordilleran tectonics as alternates related to the age of subducted oceanic lithosphere. Earth and Planetary Science Letters, 41(3): 330-340.

Molnar, P., Atwater, T., Mammerickx, J. and Smith, S.M., 1975. Magnetic anomalies, bathymetry and the tectonic evolution of the South Pacific since the Late Cretaceous. Geophysical Journal International, 40(3): 383-420.

Müller, R.D, Gohl, K., Cande, S., Goncharov, A. and Golynsky, A., 2007. Eocene to Miocene geometry of the West Antarctic rift system. Australian Journal of Earth Sciences, 54(8): 1033-1045.

Müller, R.D., Roest, W.R. and Royer, J.-Y., 1998. Asymmetric sea-floor spreading caused by ridge–plume interactions. Nature, 396(6710): 455-459.

Müller, R.D., Roest, W.R., Royer, J.Y., Gahagan, L.M. and Sclater, J.G., 1997. Digital isochrons of the world's ocean floor. Journal of Geophysical Research: Solid Earth (1978–2012), 102(B2): 3211-3214.

Müller, R.D., Sandwell, D.T., Tucholke, B.E., Sclater, J.G. and Shaw, P.R., 1991. Depth to basement and geoid expression of the Kane Fracture Zone: A comparison. Marine geophysical researches, 13(2): 105-129.

Müller, R.D., Sdrolias, M., Gaina, C. and Roest, W.R., 2008. Age, spreading rates, and spreading asymmetry of the world's ocean crust. Geochemistry, Geophysics, Geosystems, 9(4).

Müller, R.D., Seton, M., Zahirovic, S., Williams, S.E., Matthews, K.J., Wright, N.M., Shephard, G.E., Maloney, K.T., Barnett-Moore, N., Hosseinpour, M., Bower, D.J., and Cannon, J. In press. Ocean basin evolution and global-scale plate reorganization events since Pangea breakup. Annual Review of Earth and Planetary Sciences.

Munschy, M., Antoine, C. and Gachon, A., 1996. Evolution tectonique de la région des Tuamotu, océan Pacifique Central. Comptes rendus de l'Académie des sciences. Série 2. Sciences de la terre et des planètes, 323(11): 941-948.

Nakanishi, M., Tamaki, K. and Kobayashi, K., 1989. Mesozoic magnetic anomaly lineations and seafloor spreading history of the northwestern Pacific. Journal of Geophysical Research: Solid Earth (1978–2012), 94(B11): 15437-15462.

Nicholson, C., Sorlien, C.C., Atwater, T., Crowell, J.C. and Luyendyk, B.P., 1994. Microplate capture, rotation of the western Transverse Ranges, and initiation of the San Andreas transform as a low-angle fault system. Geology, 22(6): 491-495.

Norton, I.O., 2007. Speculations on Cretaceous tectonic history of the northwest Pacific and a tectonic origin for the Hawaii hotspot. Geological Society of America Special Papers, 430: 451-470.

O'Connor, J.M., Steinberger, B., Regelous, M., Koppers, A.A., Wijbrans, J.R., Haase, K.M., Stoffers, P., Jokat, W. and Garbe-Schönberg, D., 2013. Constraints on past plate and mantle motion from new ages for the Hawaiian-Emperor Seamount Chain. Geochemistry, Geophysics, Geosystems, 14(10): 4564-4584.

Ogg, J.G., 2012. Chapter 5 - Geomagnetic Polarity Time Scale. In: F.M. Gradstein, J.G.O.D. Schmitz and G.M. Ogg (Editors), The Geologic Time Scale. Elsevier, Boston, pp. 85-113.

Pardo-Casas, F. and Molnar, P., 1987. Relative motion of the Nazca (Farallon) and South American plates since Late Cretaceous time. Tectonics, 6(3): 233-248.

Pitman, W.C., Herron, E. and Heirtzler, J., 1968. Magnetic anomalies in the Pacific and sea floor spreading. Journal of Geophysical Research, 73(6): 2069-2085.

Ramos, V.A., 2005. Seismic ridge subduction and topography: Foreland deformation in the Patagonian Andes. Tectonophysics, 399(1): 73-86.

Rea, D.K. and Dixon, J.M., 1983. Late Cretaceous and Paleogene tectonic evolution of the north Pacific Ocean. Earth and Planetary Science Letters, 65(1): 145-166.

Rosa, J.W.C. and Molnar, P., 1988. Uncertainties in reconstructions of the Pacific, Farallon, Vancouver, and Kula plates and constraints on the rigidity of the Pacific and Farallon (and Vancouver) plates between 72 and 35 Ma. Journal of Geophysical Research: Solid Earth (1978–2012), 93(B4): 2997-3008.

Rouzo, S., Rabinowicz, M. and Briais, A., 1995. Segmentation of mid-ocean ridges with an axial valley induced by small-scale mantle convection. Nature, 374(6525): 795–798.

Rowan, C.J. and Rowley, D.B., 2014. Spreading behaviour of the Pacific-Farallon ridge system since 83 Ma. Geophysical Journal International: ggu056.

Royer, J.-Y., Gordon, R.G., DeMets, C. and Vogt, P., 1997. New limits on India/Australia motion since Chron5 (11 Ma) and implications for the lithospheric deformation in the Equatorial Indian Ocean. Geophysical Journal International, 128: 41-74.

Royer, J.Y. and Chang, T., 1991. Evidence for relative motions between the Indian and Australian plates during the last 20 my from plate tectonic reconstructions: Implications for the deformation of the Indo‐Australian plate. Journal of Geophysical Research: Solid Earth (1978–2012), 96(B7): 11779-11802.

Sandwell, D.T., Müller, R.D., Smith, W.H., Garcia, E. and Francis, R., 2014. New global marine gravity model from CryoSat-2 and Jason-1 reveals buried tectonic structure. science, 346(6205): 65-67.

Sandwell, D.T. and Smith, W.H., 2009. Global marine gravity from retracked Geosat and ERS-1 altimetry: Ridge segmentation versus spreading rate. Journal of Geophysical Research: Solid Earth (1978del from CryoSat

Scalabrino, B., Lagabrielle, Y., de la Rupelle, A., Malavieille, J., Polvé, M., Espinoza, F., Morata,

D. and Suarez, M., 2009. Subduction of an active spreading ridge beneath southern South America: A review of the Cenozoic geological records from the Andean foreland, central Patagonia (46–47 S), Subduction Zone Geodynamics. Springer, pp. 227-246.

Scholl, D.W., Vallier, T.L. and Stevenson, A.J., 1986. Terrane accretion, production, and continental growth: A perspective based on the origin and tectonic fate of the Aleutian–Bering Sea region. Geology, 14(1): 43-47.

Seton, M., Müller, R.D., Zahirovic, S., Gaina, C., Torsvik, T., Shephard, G., Talsma, A., Gurnis, M., Turner, M. and Chandler, M., 2012. Global continental and ocean basin reconstructions since 200 Ma. Earth-Science Reviews.

Seton, M., Whittaker, J.M., Wessel, P., Müller, R.D., DeMets, C., Merkouriev, S., Cande, S., Gaina, C., Eagles, G., Granot, R., Stock, J., Wright, N. and Williams, S.E., 2014. Community infrastructure and repository for marine magnetic identifications. Geochemistry, Geophysics, Geosystems, 15(4): 1629-1641.

Severinghaus, J. and Atwater, T., 1990. Cenozoic geometry and thermal state of the subducting slabs beneath western North America. Geological Society of America Memoirs, 176: 1-22.

Somoza, R. and Ghidella, M.E., 2012. Late Cretaceous to recent plate motions in western South America revisited. Earth and Planetary Science Letters, 331: 152-163.

Stevenson, A.J., Scholl, D.W. and Vallier, T.L., 1983. Tectonic and geologic implications of the Zodiac fan, Aleutian Abyssal Plain, northeast Pacific. Geological Society of America Bulletin, 94(2): 259–273.

Stewart, R.J., 1976. Turbidites of the Aleutian abyssal plain: Mineralogy, provenance, and constraints for Cenozoic motion of the Pacific plate. Geological Society of America Bulletin, 87:793-808

Stock, J. and Lee, J., 1994. Do microplates in subduction zones leave a geological record? Tectonics, 13(6): 1472-1487

Stock, J. and Molnar, P., 1987. Revised history of early Tertiary plate motion in the south-west

Pacific. Nature, 325(6104): 495-499.

Stock, J. and Molnar, P., 1988. Uncertainties and implications of the Late Cretaceous and Tertiary position of North America relative to the Farallon, Kula, and Pacific plates. Tectonics, 7(6): 1339-1384.

Suess, E., Bohrmann, G., Huene, R., Linke, P., Wallmann, K., Lammers, S., ... & Orange, D. (1998). Fluid venting in the eastern Aleutian subduction zone. Journal of Geophysical Research: Solid Earth (1978–2012), 103(B2), 2597-2614.

Tarduno, J., Bunge, H.-P., Sleep, N. and Hansen, U., 2009. The bent Hawaiian-Emperor hotspot track: Inheriting the mantle wind. Science, 324(5923): 50-53.

Tebbens, S. and Cande, S., 1997. Southeast Pacific tectonic evolution from early Oligocene to Present. Journal of Geophysical Research, 102(B6): 12061-12,084.

Torsvik, T.H., Müller, R.D., Van der Voo, R., Steinberger, B. and Gaina, C., 2008. Global plate motion frames: toward a unified model. Reviews of Geophysics, 46(3).

Vallier, T.L., Mortera-Gutierrez, C.A., Karl, H.A., Masson, D.G., Prueher, L. and Chase, T.E., 1996. 18 Geology of the Kula Paleo-Plate, North Pacific Ocean. Geology of the United States' seafloor: the view from GLORIA: 333.

Vlastelic, I., Aslanian, D., Dosso, L., Bougault, H., Olivet, J. L., & Geli, L. (1999). Large-scale chemical and thermal division of the Pacific mantle. *Nature*, *399*(6734), 345-350.

Weissel, J.K., Hayes, D.E. and Herron, E.M., 1977. Plate tectonics synthesis: the displacements between Australia, New Zealand, and Antarctica since the Late Cretaceous. Marine geology, 25(1): 231-277.

Wessel, P., Matthews, K.J., Müller, R.D., Mazzoni, A., Whittaker, J.M., Myhill, R., and Chandler, M.T., 2015. Semiautomatic fracture zone tracking, Geochemistry, Geophysics, Geosystems, doi: 10.1002/2015GC005853

Wessel, P. and Smith, W.H., 1996. A global, self‐consistent, hierarchical, high-resolution shoreline database. Journal of Geophysical Research: Solid Earth (1978y, Geophysics, Geosystemsys

Whittaker, J.M., Afonso, J.C., Masterston, S., Müller, R.D. Wessel, P., Williams, S.E., and Seton, M. 2015. Long-term interaction between mid-ocean ridges and mantle plumes. Nature Geoscience, doi:10.1038/NGEO2437

Whittaker, J., Müller, R., Leitchenkov, G., Stagg, H., Sdrolias, M., Gaina, C. and Goncharov, A., 2007. Major Australian-Antarctic plate reorganization at Hawaiian-Emperor bend time. Science, 318(5847): 83-86.

Wilson, D.S., 1993. Confidence intervals for motion and deformation of the Juan de Fuca plate. Journal of Geophysical Research: Solid Earth (1978–2012), 98(B9): 16053-16071.

Wobbe, F., Gohl, K., Chambord, A. and Sutherland, R., 2012. Structure and breakup history of the rifted margin of West Antarctica in relation to Cretaceous separation from Zealandia and Bellingshausen plate motion. Geochemistry, Geophysics, Geosystems, 13(4).

Woods, M.T. and Davies, G.F., 1982. Late Cretaceous genesis of the Kula plate. Earth and Planetary Science Letters, 58(2): 161-166.

Wright, N.M., Müller, R.D., Seton, M. and Williams, S.E., 2015. Revision of Paleogene plate motions in the Pacific and implications for the Hawaiian-Emperor bend. Geology, 43(5): 455-458.

Zhang, G.-L., Chen, L.-H. and Li, S.-Z., 2013. Mantle dynamics and generation of a geochemical mantle boundary along the East Pacific Rise–Pacific/Antarctic ridge. Earth and Planetary Science Letters, 383: 153-163.

Zonenshain, L., Kononov, M. and Savostin, L., 1987. Pacific and Kula/Eurasia relative motions during the last 130 Ma and their bearing on orogenesis in northeast Asia. Circum-Pacific orogenic belts and evolution of the Pacific Ocean basin: 29-47.